Preparation and characterisation of biodegradable polymer nanocomposites with magnesium hydroxide ($Mg(OH)_2$) and functionalized titania (f-TiO_2) nanoparticles as fillers

By

LESLEY TSITSI MUKWADA (B.Sc. Hons.)

Submitted in accordance with the requirements for the degree

MASTER OF SCIENCE (M.Sc.) IN POLYMER SCIENCE

Department of Chemistry

Faculty of Natural and Agricultural Sciences

at the

UNIVERSITY OF THE FREE STATE

(QWAQWA CAMPUS)

SUPERVISOR: Dr. J.P. MOFOKENG

20 June 2018

Declaration

I, the undersigned, hereby declare that the research in this thesis is my own original work, which has not been submitted to any other University to obtain a degree. I furthermore cede copyright of the thesis in favour of the University of the Free State.

_____

Ms. L.T. Mukwada

Dedication

I would like to dedicate this thesis to my family: my father Professor Geofrey Mukwada, my mother Mrs Ester Mukwada, and my brothers Geoffrey and Brandon.

"An eclectic mural painted with the most sophisticated
technique and auspiciously crafted into a living wonder
If there was a ninth wonder, this would be it
A thought
A thought manifested into a zest of life, it breathes, it lives,
it breathes"

Abstract

Magnesium hydroxide ($Mg(OH)_2$) (1, 3, 5 and 10 wt.%) and (3-aminopropyl)-trimethoxysilane functionalized titania (APTMS-TiO_2) (1, 3 and 5 wt.%) nanoparticles were added to PLA, PCL and their blends (70/30, 50/50 and 30/70) to improve their morphology, thermal and thermomechanical properties. The nanocomposites were prepared via melt mixing, and various techniques were employed to investigate the effect of blending of the two polymers and the influence of the nanoparticles on those properties. The confirmation of the functionalization of titania was done using Fourier transform infrared (FTIR) and thermogravimetric analysis (TGA)-FTIR. The morphology of the blend nanocomposites, the dispersion and localization of the $Mg(OH)_2$ nanorods and APTMS-TiO_2 nanoparticles were investigated using scanning electron microscopy (SEM), transmission electron microscopy (TEM), with help of melt flow tester for viscosities (melt flow indices (MFI)) of the polymers, and surface energy properties by surface energy evaluation system (SEES). With differential scanning calorimetry (DSC), the glass transition, cold crystallization, melting temperatures, melting and crystallization enthalpies of all the samples were studied. The effectiveness of these fillers as nucleating agents for crystallization was assessed and any other changes with the presence of both $Mg(OH)_2$ and APTMS-TiO_2 nanoparticles were noted. Through TGA, the thermal stabilities of PLA, PCL, their blends and nanocomposites were obtained, and their thermal degradation volatilization was studied using TGA-FTIR. The thermomechanical properties (storage modulus, loss modulus and damping factor (tan δ)) of the materials were determined via dynamic mechanical analysis (DMA).

The functionalized TiO_2 nanoparticles showed presence of a Si-O-Ti stretching vibration band at 919 cm^{-1} on an FTIR spectrum which was absent in neat TiO_2 and the APTMS functionalizing agent, this indicated a newly formed bond between TiO_2 and APTMS. A degradation step between 480.39 and 600 °C which was absent in the neat TiO_2 was observed in functionalized TiO_2. This indicated that the TiO_2 nanoparticles were successfully functionalized, and the mass loss was due to the oxidative thermal decomposition of APTMS. A dispersion of $Mg(OH)_2$ nanoparticles in both polymers was observed. Cracks/crevices were present at the interface of the filler with both polymers and within the agglomerates. In the APTMS-TiO_2 nanocomposites, a good dispersion of the filler was seen, but agglomeration and a preferential location in the PLA phase was also observed. This was attributed to the surface

energy, viscosity and degree of crystallinities of the polymers and fillers. Both $Mg(OH)_2$ and APTMS-TiO_2 nanoparticles acted as nucleating agents in the individual polymers and in some blend ratios. Decreased degrees of crystallinity were experienced in some nanocomposites due to poor dispersion and/or agglomeration of the nanoparticles especially at a higher content with both fillers. PLA and PCL were determined to be immiscible and the presence of the nanoparticles improved their miscibility slightly.

$Mg(OH)_2$ had an autocatalytic effect on the degradation of PLA, PCL and their blends. At lower temperatures (below 300 ºC), the rate of degradation was faster and a shift to lower temperatures on the thermal degradation of the polymers was observed, due to the loss of water which is known to catalyse the thermal degradation of biodegradable polyesters. At temperatures above 300 ºC, where only the stable MgO of $Mg(OH)_2$ was left, the improvement in the degradation temperatures of the polymers was noticed. In the APTMS-TiO_2 nanocomposites, an increase in the thermal stability of all the samples was observed even at low temperatures. Both fillers suppressed the release of the degradation volatiles which was seen with reduced intensities of the peaks on the FTIR spectra at different temperatures. In both single and blend nanocomposites with $Mg(OH)_2$ and APTMS-TiO_2, there was generally a decrease in the highest thermal degradation volatilization of PLA and PCL. $Mg(OH)_2$ nanocomposites mostly had storage modulus between those of the neat polymers. However, a decrease was observed with the addition APTMS-TiO_2 to PLA, PCL and their blends. Miscibility was improved between PLA and PCL in the presence of both $Mg(OH)_2$ and APTMS-TiO_2 nanoparticles. This was seen with the decrease in the temperature difference between the glass transition temperatures in the loss modulus curves. The loss factor (tan δ) was decreased in the presence of $Mg(OH)_2$ nanorods and increased with APTMS-TiO_2 in the single and blend nanocomposites of both $Mg(OH)_2$ and APTMS-TiO_2. This indicated that APTMS-TiO_2 nanoparticles had a less restricting/stiffening effect than the $Mg(OH)_2$ nanorods.

Conference presentations

1. L. T. Mukwada, J. P. Mofokeng. Structure and properties of PLA/PCL blend nanocomposites with $Mg(OH)_2$ and APTMS-TiO_2. UNESCO/IUPAC Workshop and Conference on Macromolecules and Materials, 11-13 April 2017, Stellenbosch, South Africa (oral presentation).

Table of Contents

List of tables

List of figures

List of symbols and abbreviations

APS	3-Aminopropyl-triethoxysilane
APTMS	3-(Aminopropyl)trimethoxysilane
$Ca_3(PO_4)_2$	Calcium phosphate
$Ca_5(PO_4)_3(OH)$	Hydroxyapatite
$CaCO_3$	Calcium carbonate
CH_4	Methane
CNT	Carbon nanotubes
CO_2	Carbon dioxide
DMA	Dynamic mechanical analysis
DSC	Differential scanning calorimetry
E'	Storage modulus
E''	Loss modulus
ΔH_c	Crystallization enthalpy
ΔH_m	Melting enthalpy
ΔG_{mix}	Free energy of mixing
FTIR	Fourier transform infrared spectroscopy
γ	Surface energy
γ^d	Dispersive component of surface energy
γ^p	Polar component of surface energy
GPa	Gigapascal
ICTOS	3-Isocyanatopropyl-triethoxysilane
IPTMS	3-Isocyanatopropyl-trimethoxysilane
LDH	Layered double hydroxides
LTI	Lysine triisocyanate
$Mg(OH)_2$	Magnesium hydroxide
$MgCO_3$	Magnesium carbonate
MPa	Megapascal
MWCNT	Multi-walled carbon nanotubes
PCL	Poly(ε-caprolactone)
PDLA	Poly(D-lactide)
PDLLA	Poly(DL-lactide)
PEO	Poly(ethylene oxide)
PER	Pentaerythritol
PGA	Poly(glycolic acid)

PHB	Poly(hydroxyl butyrate)
PLA	Poly(lactic acid)
PLLA	Poly(L-lactide)
POSS	Polyhedral oligomeric silsesquioxanes
PTA	Poly(thiophene amide)
SEES	Surface energy evaluation system
SEM	Scanning electron microscopy
tan δ	Damping factor
T_c	Crystallization temperature
T_{cc}	Cold crystallization temperature
TEM	Transmission electron microscopy
T_g	Glass transition temperature
TGA	Thermogravimetric analysis
TGA-FTIR	TGA-Fourier-transform infrared spectroscopy
TiO_2	Titania, Titanium (IV) oxide, titanium dioxide
T_m	Melting temperature
X_c	Degree of crystallinity

Chapter 1

General introduction

1.1 Background

One of the biggest challenges the world is currently facing, is the threat of land and water pollution due to poor waste management from the plastic industry. For instance, in South Africa, in 2015, only 310,600 of the 1,800,600 metric tonnes of plastic used that year were recycled [1]. Most of the plastics which are not recycled are usually used for short shelf life purposes such as disposable food containers, shopping or refuse bags, and they result in waste as shown in Figure 1.1. Some of the factors contributing to this low rate of recycling include the difficulty of separation of plastic from other waste material as well as the fact that the recycled plastic normally have inferior properties than the original plastics (non-recycled plastic) [2].

Figure 1.1 Dump site at the University of the Free State (QwaQwa Campus)

The unfavourable conditions resulting from the above mentioned factors demand the use of more environmentally friendly plastics that do not necessarily need to be recycled. Such

plastics have been around for decades, and they are known as biodegradable polymers (bioplastics). These plastics can be decomposed by environmental factors (water, temperature, light) as well as microorganisms to give non-toxic degradation products (biomass, gases (carbon dioxide (CO_2), methane (CH_4)) and water) [2-4]. In the 1970's, the requirements to produce a photodegradable and biodegradable polymer included i) use of a non-toxic material which would result in non-toxic degradation products, ii) good mechanical properties for the intended use, iii) controlled rates of degradation, iv) economic viability and v) ease of processing [4]. These guidelines are still being allowed, and a lot of research has been done on biodegradable polymers with numerous publications and patents on biodegradable polymers have been cited [2, 3]. In 2013, a minimum of eighty-four different biodegradable polymers were reported to have been approved by the US Food and Drug Administration for use [2-13].

Biodegradable polymers are classified into two groups, namely natural and synthetic polymers. Natural biodegradable polymers include polysaccharides (alginate, chitin/chitosan, cellulose, hyaluronic acid and starch) and proteins (albumin, collagen, and gluten). These are mostly derived from plants and animal sources. Synthetic biodegradable polymers include, (i) polyesters: (a) aliphatic polyesters (poly(butylene succinate) (PBS), polybutyrate adipate terephthalate (PBAT), poly(ε-caprolactone) (PCL), poly(glycolic acid) (PGA), poly(lactic acid) (PLA)); (b) polyesters produced by microorganisms (polyhydroxyalkanoates: poly(trimethylene carbonate), poly(3-hydroxybutyrate-co-3-hydroxyvalerate) (PHBV), poly(hydroxyl butyrate) (PHB)) (ii) poly(ester amides): hybrane ® S1200; (iii) polyurethanes: degraPol®), (iv) polyanhydrides: poly[(carboxyphenoxy) propane-sebacic acid], (v) polyphosphoesters: (poly[bis(hydroxyethyl) terephthalate-ethyl orthophosphorylate/terephthaloyl chloride]) and (vi) polyethers: poly(ethylene glycol) (PEG) and poly(ethylene oxide) (PEO) [2-4]. Some of the synthetic biodegradable polymers like PLA and PHB are made from renewable resources such as plants (sugarcane and corn), though some (PCL and PBAT) are still being made from non-renewable sources such as crude oil [2-4].

Amongst the synthetic biodegradable polymers, the polyester family plays a major role as biodegradable polymers due to their potentially hydrolysable ester bonds. Polyesters are versatile in applications, they have good mechanical strength and their degradation products are completely non-toxic. They contain ester linkages and they have the general formula RCOOR'. In this case R may be a hydrogen atom, an alkyl group, or an aryl group, whereas R' may either be an alkyl group or an aryl group but not a hydrogen atom. The most commonly investigated biodegradable polyesters are: PCL, PGA, PLA and PHB [1-3]. This is mostly

because of their easy availability, biodegradability and also their applications from ranging household use to medical use.

PLA is a synthetic biopolymer, made from the monomer lactic acid (2-hydroxypropanoic acid). Lactic acid is extracted from natural carbohydrate feed stocks (sugarcane, corn starches) and through polymerization it is converted to PLA. The chemical structure of PLA consists of an ester linkage bonded to a carbon atom attached to a hydrogen atom and a methyl group (Figure 1.2). Three stereochemical forms of PLA exist: poly(L-lactic acid)(PLLA), poly(D-lactic acid)(PDLA) and poly(DL-lactic acid)(PDLLA) [2-4, 8-18]. The physical (density, electrical conductivity, thermal conductivity, weight) and mechanical (tensile strength, fracture toughness, and wear resistance) properties, as well as the degradation rates (thermal and biodegradation) of PLA depend on the composition (different stereochemical forms) and molecular weight. PLA has a glass transition temperature which ranges from 55 to 65 °C, a melting temperature from 120 to 180 °C and a density from 1.24 to 1.29 g/cm^3. A cold crystallisation transition is usually observed between the glass transition and melting transmission. PLA has a modulus which ranges from 3.2 to 3.7 GPa and a tensile strength in the range of 55 to 60 MPa. Its mechanical properties can vary from "soft, elastic plastic to stiff and high strength plastic", depending on the stereochemical composition. Increasing PLLA molecular weight increases the mechanical properties (flexural and tensile strength) of PLA [2, 4, 7-17]. PLA has good biocompatibility and processability. It is also recyclable, and can be modified to meet application requirements [2, 4, 8-18]. PLA is completely biodegradable, and normally requires 30 days to 20 months depending on the conditions (temperature, water, pH, presence of microorganisms) under which the composting is performed [13].

However, PLA is still reasonably expensive and has its shortcomings. It is characterized with a low heat distortion temperature, brittleness, and poor impact resistance. It is often combined with other materials (polymers, fillers, and compatibilizers) in order to compensate and improve its lacking properties [2-8, 12-18]. For instance, blending PLA with other polymers has been reported to overcome its brittleness, poor impact properties, and low heat distortion properties [12-18]. Some of the polymers which have been blended with PLA include polyvinyl acetate, poly (ε-caprolactone) (PCL), poly ethylene glycol (PEG), starch, polyvinyl alcohol, ethylene vinyl alcohol (EVOH), polycarbonate and poly ethylene glycidyl methacrylate (PEGMA) [12-18]. Even though most of these polymers used enforce some flexibility in PLA, PCL is outstanding since it has high thermal stability relative to PLA, and has been shown to result in blends that are easily processable [2, 4-6, 9, 13-17]. PCL improves the low distortion

temperature of PLA, which is one of its biggest limitations of PLA, allowing it to be used for a wide range of applications.

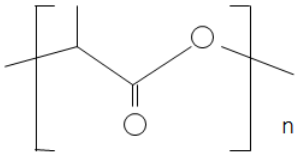

Figure 1.2 Chemical structure of polylactic acid (PLA)

PCL is amongst the common affordable biodegradable polyesters on the market. It is an oil derived semicrystalline biodegradable polyester, synthesized from the monomer cyclic ε-caprolactone through ring opening polymerization. PCL polymer chains contain ester linkages with five $–CH_2$ groups in their repeat units (Figure 1.3). PCL is characterized with good resistance to chlorine, oil, solvent and water, has low viscosity and is easy processability. It has a low melting temperature (T_m = 60 °C), and a low glass transition temperature (-61 °C). It has a high elongation at break (>700%), and a low tensile strength (~23 MPa). Its low melting temperature, tensile strength and longer biodegradation times relative to other biodegradable polymers are the major drawbacks for this polymer to be used as an individual matrix. PCL is also often combined with other materials (polymers, fillers, and compatibilizers) to make it ideal for various applications [2-8, 12-18]. Wang *et al.* [17] increased the enzymatic degradation rate of PLA/PCL blends by adding a reactive compatibilizer triphenyl phosphite. The compatibilized blends biodegraded faster than the neat polymers, PLA and PCL.

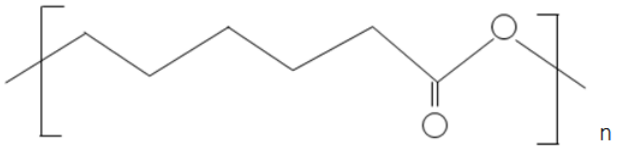

Figure 1.3 Chemical structure of polycaprolactone (PCL)

As mentioned above, the properties of individual polymers can be enhanced by mixing them with other polymers to prepare blends and also with the addition of fillers and compatibilizers. Blending, copolymerization, curing, grafting, and derivatization are some of the ways that are used to achieve this [2-4]. Blending is the most commonly used as it is a lot easier compared

to the other methods. Blending can be done via solution (solvent casting) and melt mixing. Solvent casting results in polymer blends that are well mixed. However, they require the use of solvents that are usually expensive and not environmentally friendly when disposed. Therefore, the use of expensive solvents on an industrial scale is not practical due to the large volumes of the solvents required. Industrially, melt blending is the most commonly used method for polymer mixing as it is more affordable. The materials used are melt-mixed together using a mechanical force. Melt-mixing is a simple method which also allows good control of the temperature, time and environment. However, its major disadvantage is that thermal degradation of the polymers can take place whilst they are still in their preparatory state, if the conditions for preparation are not chosen carefully [2-8, 12-18].

The blends between PLA and PCL have been moderately investigated and they have better properties in comparison to the constituent polymers [2-8, 12-18]. The brittleness of PLA has been reported to decrease and its thermal stability increased by blending it with a ductile, tough and thermally stable PCL. The biggest challenge with PCL's use is its very low melting temperature, which makes it very runny during processing at higher temperatures. However, the presence of PLA compensates for this, as it has a high melting temperature. PLA also increases the tensile strength of PCL by imparting its rigidity or brittleness [12]. An increase in fracture toughness of PLA/PCL blend compared to neat PLA has been reported [13]. PLA/PCL polymer blends are also favourable because of their reproducibility and the cost efficiency they offer.

Despite an improvement of properties in the polymer blend, PLA and PCL are immiscible and not completely compatible. The immiscibility of PLA and PCL can be attributed to the polymers having different properties (surface energies, polar characters, degrees of crystallinity and viscosities). Because of these differences in properties, multi-component systems that are immiscible are usually observed. If there is poor compatibility between these immiscible phases of the polymer blend, poor properties are usually observed such as poor flexural and tensile strength. A possible way to improve compatibility between the two or more phases that are incompatible, would be to introduce a third component into the system such as a compatibilizer, polymer, copolymer, filler or chemical modifier, which acts by reducing the surface interfacial tensions between the immiscible phases [2, 4-6].

Improvements in the morphological, mechanical and thermal properties of PLA/PCL blends have also been reported with the addition of compatibilizers to the blends [2, 3-8, 12-18]. Amongst the compatibilizers, fillers (especially inorganic nanoparticles) are preferable over

the other types. They are able to act as compatibilizers in polymer composites, and they can also improve toughness, thermal stability, flammability or gas barrier properties [13-17]. They have been shown to result in nanocomposites with good chemical resistance, improved mechanical properties and low permeability to gases, as well as good compatibility at the interface between different polymer phases. Inorganic nanoparticles act by filling in the cracks between the immiscible phases, and thereby acting as a compatibilizer as well. The smaller the particles are, the greater the surface area they will have to interact with the polymer matrix [18].

Several types of inorganic nanofillers that have already been used in other polymer blends include carbon derivatives (carbon nanofibers, carbon nanotubes (CNT), graphene), inorganic nanoparticles (aluminium hydroxide, aluminium trihydrate, ammonium borate, ammonium chlorides, ammonium phosphates, ammonium sulphate, antimony oxide, boric acid, calcium carbonate ($CaCO_3$) and phosphates ($Ca_3(PO_4)_2$), iron oxide (Fe_3O_4), layered silicates (montmorillonite, saponite), layer double hydroxides (LDH), magnesium carbonate ($MgCO_3$), polyhedral oligomeric silsesquioxanes (POSS), silica, pentaerythritol (PER), sodium borate, sodium dicyanodiamide, titania (TiO_2), zinc borate and zinc chloride and ceramics (organoclays such as hydroxyapatite ($Ca_5(PO_4)_3(OH)$)) [2, 4, 6, 13-17, 19-41]. Inorganic nanoparticles especially those that are naturally occurring and non-toxic ($Mg(OH)_2$ and TiO_2) are readily available and affordable. They have relatively higher degradation temperatures than those of the polymer matrices, making them more preferable. Unlike other compatibilizers, inorganic nanoparticles do not change the chemical structure of the polymers and only a small amount is required for them to be effective. Biodegradability of the polymer blends is also maintained as they are biodegradable as well.

One of the nanofillers which has mostly been used for non-biodegradable plastics is magnesium hydroxide ($Mg(OH)_2$), a naturally existing flame retardant, reinforcement and smoke suppressant [19-32]. It is often prepared using ammonia magnesium-deposition, bischofite pyrolysis, magnesite calcination hydration and sea water (brine-bittern) line cream magnesium-deposition methods [20, 27, 32]. It is commonly used as a filler in polymers because of its capability to increase the dimensional stability of the polymers, their rigidity as well as their strength. $Mg(OH)_2$ has an autocatalytic effect on the thermal stabilities of biodegradable polymers. At lower temperatures, $Mg(OH)_2$ releases water vapour during its decomposition, which will likely accelerate the decomposition of biodegradable polyester polymers as they are susceptible to degradation via hydrolysis [21, 25]. At higher temperatures, the MgO is formed after losing water vapour. Because of its high heat capacity, MgO will insulate the remaining

polymer chains forming a char and suppressing smoke generation [19-20, 30]. Its use has been reported in various applications, including fertilizer additives, flame retardancy, gas sensors, Li-cells, pharmaceuticals, photocatalysis, pulp, paper and wastewater treatments, and as a precursor for magnesium oxide [19-32].

Also, like $Mg(OH)_2$, titania (TiO_2) (nanoparticles) is an isotropic inorganic filler which has been fairly studied for non-biodegradable polymers. It is naturally occurring and abundant in nature, and therefore readily available for use. It can be synthesized via various methods, which include flame spray pyrolysis, hydrothermal, nonhydrolytic, reverse micelles, sol gel, solvothermal and sonochemical methods. It has a wide range of applications which include, biomedical, energy conversion (dye-sensitized solar cells, gas sensor, photo-catalysis) and waste water treatment (removal of inorganic and organic pollutants). This is because of its good antibacterial, biocompatibility, low cost, non-toxicity, high photo stability, photo catalytic effect, UV resistance and environmentally benign properties [33-34]. It is also reported to have high thermal stability. In its nanoparticle form, it tends to cluster and form agglomerates and to have poor dispersion [33, 35].

The nanoparticles dispersion, and reduced agglomeration can be improved through surface modification of these nanoparticles [33, 35]. Surface modification allows for introduction of organic functional groups on the surface of inorganic nanoparticles which are able to interact with the polymer matrix [36]. For titania, propionic acid, silanes (3-aminopropyltrimethoxysilane (APTMS), 3-aminopropyltriethoxysilane (APTES), 3-isocyanatopropyl-triethoxysilane (ICTOS)), glycidol, alkylamines and N-trimellitylimido-S-valine diacid have been reportedly used as surface modification [33-41]. The above mentioned silanes including alkylalkoxysilanes and aminopropylalkoxysilanes (3-aminopropyldimethylethoxysilane (APDMES)), and N-(6-aminohexyl) aminomethyltriethoxysilane (AHAMTES)) are normally used as coupling agents to improve compatibility between the surfaces of the fillers and the polymer matrix. Because of their functionality (presence of two or more functional groups), silanes have been used as self-assembling monolayers in adhesion, biocompatibility, catalysis, corrosion and lubrication applications [37-41]. In aminopropylalkoxysilanes, the presence of the amine and alkoxyl groups allows them to form hydrogen bonds and to interact with other organic molecules or chains [35, 37]. The amine group is also reported to catalyse the reaction between the silane molecules to form siloxane bonds [35]. Amongst the aminopropylalkoxysilanes, 3-aminopropyltrimethoxysilane (APTMS) is mostly used not only because of its functionality but also because of its low cost [40].

1.2 Aims and Objectives

The aim of this study was to prepare PLA and PCL polymer blends nanocomposites via melt mixing in the presence of two nanofillers (magnesium hydroxide ($Mg(OH)_2$ and APTMS silane functionalised titania (APTMS-TiO_2)), in order to improve morphology and thermal properties for short shelf application materials. $Mg(OH)_2$ and APTMS-TiO_2 were investigated to determine the most effective filler for various potential applications. The confirmation of functionalization of titania was investigated using Fourier-transform infrared (FTIR) and thermogravimetric analysis-Fourier transform infrared (TGA-FTIR). The morphology of the blends nanocomposites, the dispersion of $Mg(OH)_2$ and APTMS-TiO_2 nanoparticles, and localization of the fillers were investigated using scanning electron microscopy (SEM), transmission electron microscopy (TEM), contact angle measurements, and melt flow testing. Differential scanning calorimetry (DSC) was used to note any changes in crystallinity, melting, and enthalpies in the presence of APTMS-TiO_2 and $Mg(OH)_2$ nanoparticles, and to investigate if these fillers acted as effective nucleating agents for crystallization. The thermal degradation of all the nanocomposites were studied using thermogravimetric analysis (TGA). Degradation volatilization was studied using TGA-FTIR. Dynamic mechanical analysis (DMA) was used to determine the thermomechanical and rheological properties of materials.

1.3 Structure of the thesis

- Chapter 1: General introduction
- Chapter 2: Literature review
- Chapter 3: Material and methods (experimental)
- Chapter 4: Results and discussion
- Chapter 5: Conclusions

1.4 References

1. C. Verster, K. Minnaar, H. Bouwman. Marine and freshwater microplastic research in South Africa. Integrated Environmental Assessment and Management 2017; 13:533–535. DOI: 10.1002/ieam.1900
2. W. Amass, A. Amass, B. Tighe. A review of biodegradable polymers: uses, current developments in the synthesis and characterization of biodegradable polyesters, blends of biodegradable polymers and recent advances in biodegradation studies. Polymer International 1998; 47:89–144.

DOI: 10.1002/(SICI)1097-0126(1998100)47:2<89::AID-PI86>3.0.CO;2-F
3. E. Marin, M. I. Briceño, C. Caballero-George. Critical evaluation of biodegradable polymers used in nanodrugs. International Journal of Nanomedicine 2013; 8:3071–3091. DOI: 10.2147/IJN.S47186
4. G. E. Luckachan, C. K. S. Pillai. Biodegradable polymers - a review on recent trends and emerging perspectives. Journal of Polymers and the Environment 2011; 19:637–676. DOI: 10.1007/s10924-011-0317-1
5. I. Siró, D. Plackett. Microfibrillated cellulose and new nanocomposite materials: a review. Cellulose 2010; 17:459–494. DOI: 10.1007/s10570-010-9405-y
6. M. Abedalwafa, F. Wang, L. Wang, C. Li. Biodegradable poly-epsilon-caprolactone (PCL) for tissue engineering applications: a review. Reviews on Advanced Materials Science 2013; 34:123–140. (Published online)
7. J. M. Williams, A. Adewunmi, R. M. Scheka, C. L. Flanagana, P. H. Krebsbacha, S. E. Feinberg, S. J. Hollister, S. Das. Bone tissue engineering using polycaprolactone scaffolds fabricated via selective laser sintering. Biomaterials 2005; 26:4817–4827. DOI: 10.1016/j.biomaterials.2004.11.057
8. S. I. A. Razak, N. F. A. Sharif, W. A. W. Al Rahman. Biodegradable polymers and their bone applications: a review. International Journal of Basic and Applied Sciences IJBAS-IJENS 2012; 12:31–49. OAI: CiteSeerX.psu:10.1.1.418.8617
9. A. P. Gupta, V. Kumar. New emerging trends in synthetic biodegradable polymers – polylactide: a critique. European Polymer Journal 2007; 43:4053–4074. DOI: 10.1016/j.eurpolymj.2007.06.045
10. I. Harte, C. Birkinshaw, E. Jones, J. Kennedy, E. DeBarra. The effect of citrate ester plasticizers on the thermal and mechanical properties of poly(DL-lactide). Journal of Applied Polymer Science 2012; 127:1997–2003. DOI: 10.1002/app.37600
11. A. J. R. Lasprilla, G. A. R. Martinez, B. H. Lunelli, A. L. Jardini, R. M. Filho. Poly-lactic acid synthesis for application in biomedical devices - A review. Biotechnology Advances 2012; 30:321–328. DOI: 10.1016/j.biotechadv.2011.06.019
12. M. Jamshidian, E. A. Tehrany, M. Imran, M. Jacquot, S. Desobry. Poly-lactic acid: production, applications, nanocomposites, and release studies. Comprehensive Reviews in Food Science and Food Safety 2010; 9:552–571.

DOI: 10.1111/j.1541-4337.2010.00126.x
13. V. Siracusaa, P. Rocculi, S. Romani, M. D. Rosa. Biodegradable polymers for food packaging: a review. Trends in Food Science and Technology 2008; 19:634–643.
DOI: 10.1016/j.tifs.2008.07.003
14. E. Laredo, M. Grimau, A. Bello, D. F. Wu, Y. S. Zhang, D. P. Lin. AC conductivity of selectively located carbon nanotubes in poly(ε-caprolactone)/polylactide blend nanocomposites. Biomacromolecules 2010, 11, 1339–1347.
DOI: 10.1021/bm100135n
15. T. Takayama, M. Todo, H. Tsuji, K. Arakawa. Effect of LTI content on impact fracture property of PLA/PCL/LTI polymer blends. Journal of Materials Science 2006; 41:6501–6504.
DOI: 10.1007/s10853-006-0611-9
16. B. Imre, B. Pukánszky. Compatibilization in bio-based and biodegradable polymer blends. European Polymer Journal 2013; 49:1215–1233.
DOI: 10.1016/j.eurpolymj.2013.01.019
17. L. Wang, W. Ma, R. A. Gross, S. P. McCarthy. Reactive compatibilization of biodegradable blends of poly(lactic acid) and poly(ε-caprolactone). Polymer Degradation and Stability 1998; 59:161–168.
PII: SO141-3910(97)00196-l
18. J. P. Mofokeng, A. S. Luyt. Morphology and thermal degradation studies of melt-mixed poly(lactic acid) (PLA)/poly(ε-caprolactone) (PCL) biodegradable polymer blend nanocomposites with TiO_2 as filler. Polymer Testing 2015; 45:93–100.
DOI: 10.1016/j.polymertesting.2015.05.007
19. H. T. Oyama, M. Sekikawa, Y. Ikezawa. Influence of the polymer/inorganic filler interface on the mechanical, thermal, and flame retardant properties of polypropylene/magnesium hydroxide composites. Journal of Macromolecular Science Part B: Physics 2011; 50:463–483.
DOI: 10.1080/00222341003780996
20. M. Shabanian, D. Ghanbari. Synthesis of magnesium hydroxide nanofiller and its use for improving thermal properties of new poly(ether-amide). Journal of Applied Polymer Science 2013; 2004–2009.
DOI: 10.1002/app.37640
21. B. B. Marosfoi, S. Garas, B. Bodzay, F. Zubonyai, G. Marosi. Flame retardancy study on magnesium hydroxide associated with clays of different morphology in polypropylene matrix. Polymers for Advanced Technologies 2008; 19:693–700.

DOI: 10.1002/pat.1153

22. J. Wang, J. F. Tung, M. Y. Ahmad Fuad, P. R. Hornsby. Microstructure and mechanical properties of ternary phase polypropylene/elastomer/magnesium hydroxide fire-retardant compositions. Journal of Applied Polymer Science 1996; 60:1425–1437.
    CCC 0021-8995/96/091425-13
23. A. Kausar. Study on physical properties of poly(methyl methacrylate)/poly(thiophene amide)–silica–titaniagrafted multiwalled carbon nanotube based nanofiber composites. High Performance Polymers 2014; 26:961–969.
    DOI: 10.1177/0954008314536213
24. J. I. Velasco, C. Morhain, A. B. Martinez, M. A. Rodriguez-Perez, J. A. de Saj. The effect of filler type, morphology and coating on the anisotropy and microstructure heterogeneity of injection-moulded discs of polypropylene filled with aluminium and magnesium hydroxides. Part 1. A wide-angle X-ray diffraction study. Polymer 2002; 43:6805–6811.
    PII: S0032-3861(02)00668-7
25. Y. Wang, X. Yang, H. Peng, F. Wang, X. Liu, Y. Yang, J. Hao. Layer-by-layer assembly of multifunctional flame retardant based on brucite, 3-aminopropyltriethoxysilane and alginate and its applications in ethylene-vinyl acetate resin. ACS Applied, Materials and Interfaces 2016; 8:9925−9935.
    DOI: 10.1021/acsami.6b00998
26. H. Cheraghi, F. A. Ghasemi, G. Payganeh. Morphology and mechanical properties of PP/LLDPE blends and ternary PP/LLDPE/nano-$CaCO_3$ composites. Strength of Materials 2013; 45:730–738.
    DOI: 10.1007/s11223-013-9508-4
27. S. Mishra, S. H. Sonawane, R. P. Singh, A. Bendale, K. Patil. Effect of nano-$Mg(OH)_2$ on the mechanical and flame-retarding properties of polypropylene composites. Journal of Applied Polymer Sciences 2004; 94:116–122.
    DOI: 10.1002/app.20750
28. J. W. Bae, T. U. Yang, G. J. Nam, G. J. Lee, B. Nam, J. Y. Jho. Dispersion and flame retardancy of ethylene vinylacetate/layered silicate nanocomposites using the masterbatch approach for cable insulating material. Polymer Bulletin 2011; 67:729–740.
    DOI: 10.1007/s00289-011-0498-8
29. Y. Arao. Flame retardants: polymer blends, composites and nanocomposites. Cham: Springer International Publishing (2015) pp 15-44.
    ISBN: 978-3-319-03466-9

30. B. Dittrich, K. Wartig, R. Mülhaupt, B. Schartel. Flame-retardancy properties of intumescent ammonium poly(phosphate) and mineral filler magnesium hydroxide in combination with graphene. Polymers 2014; 6:2875-2895.
DOI: 10.3390/polym6112875
31. C. Gérard, G. Fontaine, S. Bourbigot. New trends in reaction and resistance to fire of fire-retardant epoxies. Materials 2010; 3:4476-4499.
DOI: 10.3390/ma3084476
32. D. Zhang, P. Zhang , S. Song, Q. Yuan, P. Yang, X. Ren. Simulation of magnesium hydroxide surface and interface. Journal of Alloys and Compounds 2014; 612:315–322.
DOI: 10.1016/j.jallcom.2014.05.198
33. A. Buzarovska. PLA nanocomposites with functionalized TiO_2 nanoparticles. Polymer-Plastics Technology and Engineering 2013; 52: 280–286.
DOI: 10.1080/03602559.2012.751411
34. Y. Luo, W. Li, X. Wang, D. Xu, Y. Wang. Preparation and properties of nanocomposites based on poly(lactic acid) and functionalized TiO_2. Acta Materialia 2009; 57:3182–3191.
DOI: 10.1016/j.actamat.2009.03.022
35. S. Mallakpour, M. Madani. Effect of functionalized TiO_2 on mechanical, thermal and swelling properties of chitosan-based nanocomposite films. Polymer-Plastics Technology and Engineering 2015; 54:1035–1042.
DOI: 10.1080/03602559.2014.974194
36. Z. Shi, G. Xueping, S. Deying, Y. Zhou, D. Yan. Preparation of poly(ε-caprolactone) grafted titanate nanotubes. Polymer 2007; 48:7516–7522.
DOI: 10.1016/j.polymer.2007.10.037
37. J. Raquez, Y. Habibi, M. Murariu, P. Dubois. Polylactide (PLA)-based nanocomposites. Progress in Polymer Science 2013; 38:1504–1542.
DOI: 10.1016/j.progpolymsci.2013.05.014
38. D. Pasqui, R. Barbucci. Synthesis, characterization and self-cleaning properties of titania nanoparticles grafted on polyester fabrics. Journal of Photochemistry and Photobiology A: Chemistry 2014; 274:1–6.
DOI: 10.1016/j.jphotochem.2013.08.017
39. S. Kango, S. Kalia, A. Celli, J. Njuguna, Y. Habibi, R. Kumar. Surface modification of inorganic nanoparticles for development of organic–inorganic nanocomposites-a review. Progress in Polymer Science 2013; 38:1232–1261.
DOI: 10.1016/j.progpolymsci.2013.02.003

40. J. Zhao, M. Milanova, M. M. C. G. Warmoeskerken, V. Dutschk. Surface modification of TiO_2 nanoparticles with silane coupling agents. Colloids and Surfaces A: Physicochemical and Engineering Aspects 2012; 413:273–279.
DOI: 10.1016/j.colsurfa.2011.11.033
41. E. A. Smith, W. Chen. How to prevent the loss of surface functionality derived from aminosilanes. Langmuir 2008; 24:12405–12409.
DOI: 10.1021/la802234x

Chapter 2

Literature review

2.1 Introduction

In this chapter, the interest is directed towards the understanding of biodegradable polymers particularly PLA and PCL. A brief explanation of their origin and synthesis are given. Also, the literature on various studies performed on their blends and blend nanocomposites to understand their morphology, thermal and thermomechanical properties are reported. The use of fillers and the effect of functionalization of the fillers are discussed briefly. A further interest is shown to the potential applications that these biodegradable polyesters hold.

2.2 Biodegradable polymers

Biodegradation is a process of the disintegration of matter through the action of microorganism (bacteria and fungi) and abiotic reactions (hydrolysis, oxidation and photodegradation) into natural occurring by-products (carbon dioxide (CO_2), methane (CH_4), biomass, water). It can take place in the absence or presence of oxygen and it occurs in two stages: i) depolymerisation and ii) mineralization. During depolymerisation, long polymer chains are broken, and converted into shorter chains through various degradation processes (enzymatic, hydrolysis and oxidation reactions). This takes place outside microorganisms where extra-cellular enzymes and abiotic reactions facilitate depolymerisation. As the size of polymeric chains decreases, there is an increase in the interaction surface between the polymer chains and microorganisms. The short polymer chains are assimilated into the microorganisms where the second stage takes place, mineralization (Figure 2.1). During mineralization, the short polymer chains are converted to naturally occurring molecules (CO_2, CH_4, monomer units) and biomass [1-4].

Biodegradable polymers can be defined as materials which can be disintegrated through the above-mentioned processes. They can be grouped into two types based on their origins; natural or synthetic. Naturally occurring biodegradable polymers are mostly obtained from resources like vegetables (alginate, cellulose, gluten, and starch) and animals (albumin, chitin/chitosan, collagen, and hyaluronic acid) [2, 3]. The naturally occurring biodegradable polymers are easily hydrolysed and oxidized when subjected to various environmental degradation factors (water, oxygen and heat) [2, 3]. Some synthetic biodegradable polymers are still being derived from oil based resources, although renewable resources such as vegetables are now widely

used. Synthetic biodegradable polymers also have a hydrolysable backbone which makes them susceptible to hydrolysis. They can be classified based on the functional groups in the backbone of their chains. The common synthetic biodegradable polymers include polyamides, polyanhydrides, aliphatic polyesters, poly(orthoesters), polyphosphoesters, poly(ester amides), polyethers, polyureas, polyurethanes and vinyl polymers [1-3]. Synthetic biodegradable polymers are one way which has been used in the management of packaging waste [1].

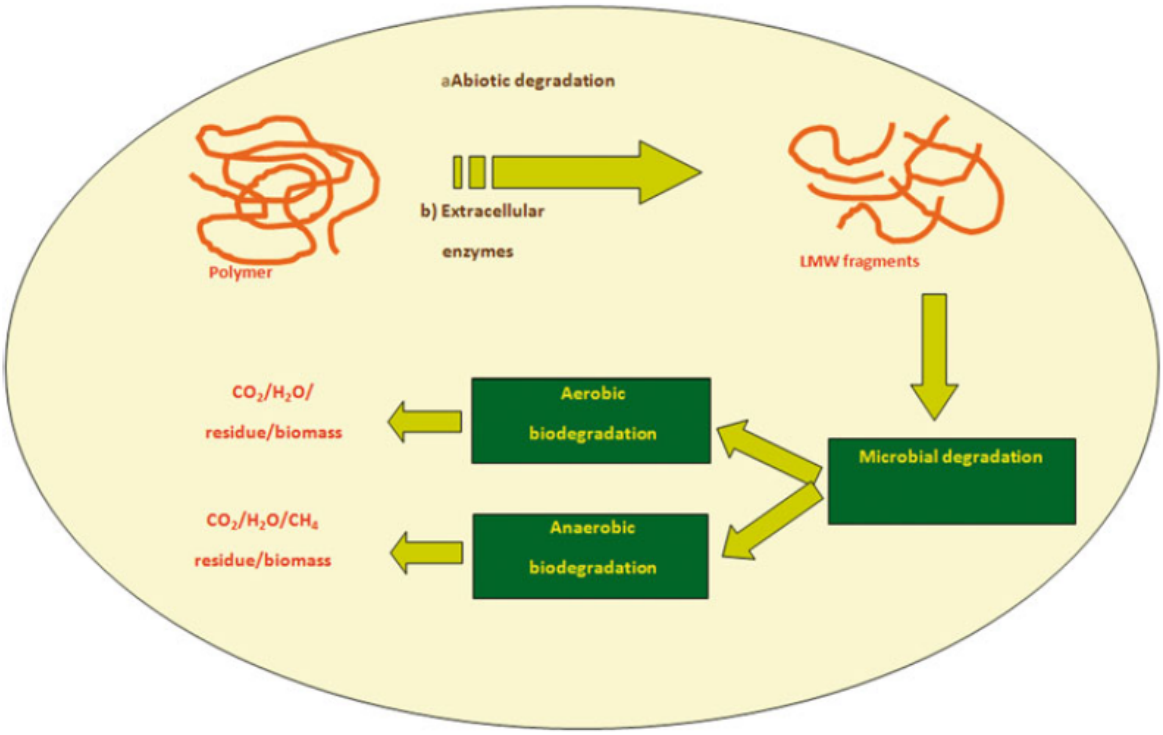

Figure 2.1 Diagrammatic representation of the chemistry of biodegradation [3]

Aliphatic polyesters are amongst the most widely used synthetic biodegradable polymers, because of their environmentally friendly degradation products and available renewable resources. The synthesis of polyesters is normally performed through ring opening polymerization and polycondensation reactions. Monomers used in these reactions are environmentally friendly, and some of them are made through the fermentation of renewable resources such as corn and sugarcane. These include adipic acid, 1,4-butane diol, γ-butyrolactone, lactic acid, n-methylpyrrolidone, 1,3-propanediol and succinic acid [1-6]. Polyesters are able to break down into their respective monomers during biodegradation. Their biodegradation can take place on the surface of the polymer or within the polymer. For polyesters, degradation occurs mainly through enzymatic, hydrolysis and oxidation depolymerisation reactions, and result in non-toxic degradation products. The biodegradation

mechanism often depends on a number of factors which include: (i) the nature of the polyester (its chemistry, degree of crystallinity, glass transition, hydrophilicity/hydrophobicity, molecular weight, morphology, stability (photo, thermal, oxidative)), (ii) additives (fillers, plasticizers and other polymers) and (iii) environmental factors (pH and temperature) [1-3].

A wide range of properties have been reported for biodegradable polymers and these include: barrier, biodegradability, chemical resistance, conductivity, morphology, mechanical, optical, structural, thermal, thermomechanical and rheological properties [7-11]. Studying polymer morphology allows for understanding of the interaction of the components of polymer blends and the interactions fillers have in the polymer matrices on both the surface and internal parts of the composites [12-16]. Observations made from surface and internal morphology studies often help to understand the thermal as well as the thermomechanical properties unique to the specific compositions. Also, to better understand the morphology, surface energy (polar and dispersive characters) and viscosity properties of the individual polymers and the fillers are often investigated [10, 13, 17]. These will give a clear indication of certain behaviours like preferential location of a filler in one phase or at the interface between two polymers, or even in both phases. As for thermal properties (glass transitions, melting temperatures, thermal degradation and thermal stabilities), they can reveal the miscibility of polymers, the highest temperatures they can be used for processing to avoid premature degradation, and the influence of additives, compatibilizers and fillers [13-15]. The thermal degradation volatiles released during degradation can also be analysed to determine the products coming out at different temperatures, and also to confirm if they are toxic or nontoxic. The thermal degradation volatilization can also reveal the effectiveness of a filler in the insulation of the polymers to degrade at higher temperatures. Also, the thermomechanical properties are important as they reveal the strength of the material as a function of temperature and the ability of a material to absorb and dissipate energy. Miscibility of polymer blends or composites, and the effect of the fillers on storage modulus (E'), loss modulus (E"), and tan δ can also be seen [16].

2.3 Polylactic acid (PLA) and poly(ε-caprolactone) (PCL)

In 1932, Carothers discovered the ring opening polymerization of polylactic acid (PLA) using the monomer lactic acid (2-hydroxy propanoic acid) [4]. Lactic acid is obtained from renewable carbohydrate sources. Ever since its discovery, some of the carbohydrates that have been used include artichokes (helianthus tuberosus), carrot processing waste, cassava, cellulose (lignocellulose/hemicellulose hydrolysates), corn (cobs, stalks, and fiber hydrolysates), cottonseed hulls, molasses (beet, spent wash), rye flour, starch (barley, cassava), sweet

sorghum and wheat bran. These carbohydrate resources (feedstocks) are often chosen based on their availability, purity and price. Of the three, price is the most important as PLA is still relatively expensive to produce. Lactic acid is optically active and exists in D and L enantiomeric forms. When synthesized through bacteria, only the L-form is obtained, but when synthesized chemically, a racemic mixture is usually obtained. PLA is characterized by a high sensitivity to relative humidity and temperature [4, 7, 18-20]. Because of its sensitivity, precautions such drying its pellets at 50 °C for at least 24 hours before processing are usually observed. Blow moulding, extrusion, fibre spinning, injection moulding and thermoformation processing of PLA have been reported [4]. The mechanical properties of PLA are also influenced by its crystallinity, the method used for production and the processing conditions. PLA is so versatile because it can be tailor-made to meet the required properties of the intended application. It has a considerable number of applications in agriculture, building, electric appliance and electronics, furniture, houseware, medical, packaging, pharmaceuticals, textiles and transportation industries [2-4, 7-12, 19-21].

To make PLA, lactic acid can be polymerized through direct polycondensation (azeotropic, solid state) or ring opening (anionic, cationic, coordination–insertion mechanisms using metal alkoxide, enzymatic, solid state) polymerizations [2-4, 7-12, 19-21]. A monomer of high purity is a requirement, since impurities would interfere with the polymerization reactions and result in a poorer quality of the polymer. Depending on the enantiomeric precursors used, three stereochemical forms of PLA are possible; Poly(L-lactic acid) (PLLA), poly(D-lactic acid) (PDLA) and poly(DL-lactic acid) (PDLLA). Properties such biodegradability, crystallinity, and mechanical properties of PLA are dependent on the stereochemical forms that are present. For instance, the biodegradation of PDLPLA is a lot faster than PLLA which can take up to two years before complete assimilation takes place. Bulk erosion mechanism (random chain scission on the linkage of ester bonds) is the main pathway in which biodegradation of PLA takes place. Hydrolytic degradation occurs much more slowly. This is because of the presence of the methyl substituent, which has a shielding effect on the ester linkages, and therefore hindering hydrolytic degradation [2-4, 7-12, 19-21].

PCL is also a semicrystalline thermoplastic polymer, and classified as a biodegradable aliphatic polyester. Unlike PLA, the monomers used in the synthesis of PCL are obtained from crude oil, a non-renewable raw material. Both 6-hydroxycaproic (6-hydroxyhexanoic) acid and cyclic ε-caprolactone are monomers used in the synthesis of PCL. They are both intermediate products during the synthesis of hexanedioic (adipic) acid, which is the monomer used in the synthesis of nylon. 6-Hydroxycaproic acid is converted to PCL through condensation

polymerization and cyclic ε-caprolactone via ring opening polymerisation (ROP). The ROP is the most commonly used method at industrial scales. The molecular weight and degree of crystallinity of PCL determine the biodegradability, mechanical, physical, and thermal properties that are observed [5, 6, 22-31]. The biodegradation of PCL occurs slowly through the abiotic hydrolytic cleavage of ester linkages and a bulk random chain scission mechanisms. Some studies have shown that PCL can take up to 3-4 years to completely degrade. This is because of the $–CH_2$ moieties present within its chains which impart a hydrophobic nature and slows down the hydrolytic degradation [5-6, 29, 30].

Both PLA and PCL have good processability, biocompatibility, recyclability, and biodegradability which make them appealing for use. However, they both have shortcomings which limit their applications as individual polymers [29]. For instance, PLA is very brittle and breaks easily [8, 31-35]. In one study [8], it was reported that PLA was brittle, and in order to improve its ductility, it had to be blended with a less brittle polymer like PCL. As for PCL, the major drawback has been mentioned to be its low melting temperature [29]. In another study [7], it was mentioned that the limitations for use of PCL were because of its poor gas barrier properties. It is therefore necessary to modify them using various methods. Some of the methods which have already been used are blending, copolymerization (block, statistical, random), use of fillers, chemical modifiers and physical treatments (aging, annealing, drawing, orientation, solid-state extrusion techniques and vacuum compression-molding). Formulations such as films, fibres, scaffolds, hydrogels, and nanoparticles of PLA and PCL have been reported [1-6, 18]. In literature, both PLA and PCL have been reportedly blended with various natural polymers (cellulose, chitosan, silk fibroin, spider silk, collagen, elastin and gelatine) and synthetic polymers (polyurethane (PU), poly(lactic-co-glycolic acid) (PLGA), polystyrene (PS) and PGA) [1-6, 18]. These polymers can improve the mechanical and thermal properties of PLA and PCL, as well as reduce production cost. However, a loss in other valuable properties (biodegradability, biocompatibility, hydrophobicity, clarity, mechanical strength and processability) is usually observed, especially if there is poor compatibility. For instance, Liao *et al.* [15] studied the influence of starch on PLA/PCL blends. They noticed that the cost of production was reduced. However, a loss in mechanical strength (tensile and elongation at break) was also apparent with increase in starch content. This was attributed to the large starch phases which were present, as well as poor wetting of the starch with the PLA/PCL blends.

2.3.1 Morphology of neat polymers and their composites/nanocomposites

Studying the morphology of PLA and PCL (especially when combined with other materials) helps to understand or predict their other property behaviour. This has been seen in several studies [19, 24] including one by Yang *et al.* [19] where they investigated the effect of modified starches (epoxidized cardanol grafted starch and maleic anhydride grafted starch) in PLA/thermoplastic starch blends. In their morphology study of the blends using SEM, they observed gaps at the interfaces between PLA and starch. This poor compatibility resulted in a loss in the mechanical strength (tensile, flexural, impact strength and elongation at break) of PLA. When the starch was modified with epoxidized cardanol, the starch was better dispersed and no gaps were observed at the interface of PLA/Starch blends. This resulted in improved mechanical properties. However, poor properties were observed when maleic anhydride was used in the modification. There was poor compatibility between the maleic anhydride and the PLA and the starch. It is important to note that PLA and PCL interact differently with different substances. Fukushima *et al.* [24] studied the morphology of PLA and PCL composites with montmorillonite (CLOSITE 30B and NANOFIL 804) and sepiolite (PANGEL S9) fillers using SEM and TEM. With the addition of CLOSITE 30B and PANGEL S9 to PLA, they did not observe any aggregates in the micron scale. However, with NANOFIL 804, the aggregates ranged from 5 to 10 μm. When these fillers were added to PCL, similar observations were made. Both CLOSITE 30B and PANGEL S9 had a good degree of dispersion and NANOFIL 804 had larger aggregates in micron scale.

2.3.2 Thermal properties of neat polymers and their composites/nanocomposites

2.3.2.1 Glass transition, cold crystallization, melting, and enthalpies of the neat polymers and their composites/nanocomposites

Thermal properties such as glass transition (T_g), cold crystallization (T_{cc}) and melting temperatures (T_m) are usually studied to give a better understanding of polymer behaviour and limitations of their applications. Mohamed *et al.* [13] studied the thermal properties of PCL/gluten bioblends prepared through extrusion and injection-moulding. In their DSC study, they found the T_g and T_m of neat PCL to be -67.8 ºC and 56.9 ºC, respectively. Muñoz-Bonilla *et al.* [22] investigated the preparation, characterization and antimicrobial properties of biodegradable polycaprolactone (PCL)-titania (TiO_2) nanocomposites. On their thermal properties by DSC they investigated the glass transition (T_g), melting (T_m), and crystallization (T_c) temperatures, as well as the degree of crystallinity. It was noted that noticed that TiO_2 nanoparticles had a little or no influence on T_g (-60 ºC) of PCL since the temperatures at

different content did not show any significant change. Thus it was concluded that the presence of TiO_2 in the amorphous regions did not affect the mobility of the polymer chains. For the melting transition of neat PCL, they found the melting temperature was around 55 ºC and there were multiple melting stages observed due to possible successive melting-recrystallization processes. This was explained in that at lower temperatures, the smallest and thinnest crystals melted and the molten polymer underwent a recrystallization-melting phenomena forming larger and thicker lamellae which melted at higher temperatures. It was also mentioned that this process could have resulted in the presence of dual lamellar populations or the presence of two or more polymorphs of PCL. When TiO_2 nanoparticles were added, a slight increase in the T_m was observed. This was attributed to the nucleating effect of TiO_2, which was also seen with the increase in the crystallization temperature.

The crystalline structure of a polymer influences its mechanical, as well as rheological behaviour. For instance, in semi-crystalline polymers, the crystalline parts increase the toughness and thermal stability of the polymer whilst the amorphous parts are likely to improve the elasticity and impact resistance properties. The crystallinity of polymers can be affected by temperature and mechanical force during processing. Wu *et al.* [37] examined the crystallization behaviour of PLA/PCL blend systems filled with CNTs using DSC. The authors mentioned that the properties of PLA and PCL are controlled by their super molecular structures, which are dependent on the crystallization processes involved. Using DSC, they observed three transitions for pristine semicrystalline PLA, a T_g between 55-65 °C, a T_m between 140-160 °C and a T_{cc} (100-140 ºC) occurring between them. For neat PCL, a melting temperature which occurred around 56.4 °C was observed and a degree of crystallinity around 53%. It was observed that these transitions were highly dependent on the various heating rates used in the study. In a different study, Kweon *et al.* [26] investigated the preparation of PCL networks through photopolymerization of the PCL macromer. It was found that the starting material (PCL macromere) had a melting temperature of 51.9 ºC and its degree of crystallinity was around 50.36%. From all these studies of the neat polymers and their composites/nanocomposites, variations in the glass transition, cold crystallization, melting, and enthalpies properties were observed. It was not mentioned why PLA or PCL had such different properties, but it is probably due to the different polymer grades used, as well as the different processing techniques and conditions involved in each study.

2.3.2.2 Thermal degradation and stabilities of the neat polymers and their composites/nanocomposites

The thermal stability of polymers and their composites determine their applications and suitable processing conditions. The data obtained from TGA analysis shows the degradation steps involved, as well as reveal information about the miscibility in blends and effect of fillers on the thermal stabilities of polymer matrices [10, 13, 21, 28]. PLA has been reported to have one-step degradation at a temperature around 365 °C. Its degradation mechanism occurs via a back-biting ester interchange reaction at the -OH chain ends. PCL is much more thermally stable than PLA and decomposes in two steps around 415 and 520 °C. The first step (415 ºC) has been said to be as a result of polymer chain cleavage via cis elimination and the second step (520 ºC) is attributed to unzipping depolymerization from the hydroxyl end of the polymer chain [10]. Other studies report PCL having only a single degradation step [13, 31]. Mohamed *et al.* [13] studied the thermal degradation of PCL/Gluten blends using TGA, and they reported PCL having only a single degradation step which took place from 342 to 489 ºC. Su *et al.* [31] studied the thermal stabilities and degradation kinetics of PCL. They also observed a single degradation step with maximum degradation taking place around 432 ºC from the TGA and its derivative curves. However, from the thermal degradation kinetics analysis they performed using the Flynn-Wall-Ozawa (FWO) method, they found that the degradation actually involved two mechanisms. Muñoz-Bonilla *et al.* [22] prepared polycaprolactone-titania nanocomposites and characterized their morphology, thermal and anti-microbial properties. They studied the thermal stability of the nanocomposites using TGA study under inert (nitrogen atmosphere) and oxidant conditions. It was found that under inert conditions the degradability of the nanocomposites was mostly unaffected and a decrease in the degradation onset was seen. Under an oxidant conditions, they found that the degradation followed a complex mechanism which took place in several steps. Despite a decrease in the maximum degradation, an increase in the onset temperature by 20 ºC was seen. Fukushima *et al.* [24] studied nanocomposites of PLA and PCL containing clay (montmorillonite and sepiolites). When they investigated the thermal stability of PLA under nitrogen conditions, they found that it was improved with the presence of the clays. The improved thermal stability was attributed to the ability of the clay to act as a barrier to the release of volatile degradation products, and this resulted in an increase in the onset and maximum degradation temperatures. As for PCL, they also observed an increase in thermal stability with the presence of montmorillonite. A decrease was however seen with the presence of sepiolites due to the presence of Lewis acidic sites in the sepiolites, which are capable of catalysing the thermal degradation of PCL. The authors also suggested

that dispersion could have played a role in the difference between PLA and PCL, as the clay was more dispersed in PLA than PCL. Raquez *et al.* [14] reviewed polylactide (PLA)-based nanocomposites. In their summary they reported that clay-based (layered silicates, sepiolite, halloysite), carbonaceous-based (carbon nanotubes, graphene derivates), metal and metallic oxide/hydroxide-based (Ag, ZnO, TiO_2, Layered double hydroxide) and silicon based (silica, polyhedral oligomeric silsesquioxanes (POSS)) nanofillers improved the thermal stability of PLA.

2.3.2.3 Thermal degradation volatilization of the neat polymers and their composites/nanocomposites.

The study of thermal degradation volatiles produced during thermal degradation can be indicative of the chemical composition of the evolved gases, as well as the thermal stability of polymers and their nanocomposite. Mofokeng *et al.* [10] conducted a study on the thermal degradation studies of PLA/PCL blend nanocomposites filled with TiO_2 nanoparticles using TGA-Fourier-transform infrared (FTIR) spectroscopy. For neat PLA, they observed bands at 2400-2300 (CO_2) and 1792 (-C=O) cm^{-1}. The FTIR spectra showed presence of the typical degradation products (acetaldehydes, carbon monoxide, lactide molecules and oligomeric rings) of PLA. At temperatures round 350 °C, addition of TiO_2 resulted in a shift in its FTIR peaks to the left and a decrease in the intensity of the carbonyl bands. They attributed this to the possibility of the nanoparticles interacting with the degradation products thereby slowing their diffusion from the molten polymer. Also, in the same study, in their thermal degradation volatilization investigation of PCL, the FTIR spectra showed bands at 3577 (-OH), 2400-2300 (CO_2), 1756 (-C=O) and 1400-1100 (overlapped C-O-C, C=O, CH, CH_2). It was mentioned that the FTIR spectra were typically indicative of the presence of 5-hexanoic acid (ε-caprolactone), carbon dioxide, water and methyl pentanoate. In the presence of TiO_2, the intensity of the peaks were reported to have decreased and an increase in degradation temperature was observed. This could have been due to the TiO_2 nanoparticles absorbing more thermal energy than any of the polymers, therefore increasing the thermal stability of the polymers. They also attributed the increase to the titania nanoparticles retarding the diffusion of the volatile degradation products, which then increased the onset of degradation to higher temperatures. Persenaire *et al.* [30] investigated the mechanisms and kinetics of the degradation of PCL. From the TGA and DTGA curves, one major degradation step was observed around 420 ºC, which had a shoulder peak around 360 ºC. And from the FTIR spectra of the gases evolved, around 360 ºC, the degradation peaks were indicative of the presence of water, carbon dioxide and hexanoic acid. They reported that the first step occurred via ester pyrolysis

reaction. Around 420 ºC, the FTIR spectra were attributed to the presence of carbon dioxide, water, carboxylic acid and ε-caprolactone monomer. The mechanism followed an unzipping depolymerization process.

2.3.3 Thermomechanical studies of the neat polymers and their composites/nanocomposites.

Thermomechanical properties of PLA and PCL have been fairly studied [12, 16, 21, 29, 38]. As mentioned earlier, the glass transition (T_g) can also be determined using DMA. T_g is a kinetic process, it can be affected by the rate of heating and technique used, different time responses in the motions of side and main chain polar groups and mechanical or thermal stimulation of the motion [21]. Harte *et al.* [21] investigated the thermomechanical properties of amorphous PDLLA containing citrate esters (triethyl citrate, tributyl citrate and acetyl tributyl citrate) as plasticizers. From the tan δ curves, at temperatures above a glass transition of PLA, a decrease in the T_g peak was observed when the citrate plasticizers were added. The peaks became broadened and further decreased with an increase in the plasticizer content. From the storage modulus curves, at temperatures above and below the T_g, a decrease in the storage modulus was observed with increasing plasticizer content. This was attributed to the plasticizers ability to increase chain mobility. Jain *et al.* [32] studied the effect of micro-talc on poly(lactic acid)/poly(ε -caprolactone) blends. In their investigation of the thermomechanical properties, they found that the storage modulus of neat PLA was high (3819 MPa at 25 ºC). The storage modulus of PCL was low (359 MPa at room temperature) compared to that of the neat PLA (3819 MPa).

2.4 PLA/PCL blends, composites and nanocomposites with inorganic nanomaterials

Blending PLA with PCL has been reported to lower the brittleness of PLA whilst maintaining its biocompatibility, biodegradability and processability characteristics [7-12]. In a certain study [7], they improved the poor gas properties of PCL using the good gas barrier properties of PLA. In the same study, they reported increased thermal stability properties of PLA with an increase in the PCL content. Despite having improved properties, PLA and PCL are not completely miscible and often have poor mechanical properties [18]. Compatibilizers, chemical modifiers, fillers or plasticizers can be added to improve the interaction between the polymers [25, 28, 29, 33, 36]. Na *et al.* [33] used PCL-b-PEG as a compatibilizer in PLA/PCL blends. They observed improved mechanical properties and synergism for certain compositions.

Use of inorganic (ceramics, titania, layered silicates (montmorillonite, saponite), layer double hydroxides, metal hydroxide and oxides (magnesium hydroxide ($Mg(OH)_2$) and carbon based (carbon nanofibers, carbon nanotubes (CNT), graphene)) fillers has been reported for mostly non-biodegradable polymers [1-6]. The challenge; however, with the use of inorganic nanoparticles is that they tend to cluster resulting in poor dispersibility in polymer matrices. The agglomeration can be attributed to the large interparticle forces (electrostatic forces, magnetic attraction, and van der Waals forces) which limit their uniform dispersion in polymer matrices. Agglomeration limits the improvement of desired properties and the amount of filler which can be used [10, 11, 34, 35].

One way to avoid the agglomeration of the fillers would be to increase the interaction between the fillers and the polymer matrices. This can be achieved by functionalizing (chemically modifying) the surface of the fillers. Functionalization brings affinity between the filler and the polymers in the composites, and therefore lowers the interfacial tension between the multiple phases in the blend [11, 35]. The lower the interfacial/surface tension between the filler and the polymer components, the better the dispersion of the filler in the polymer matrices. This has been seen through other studies which have already been done [8, 11].

2.4.1 Morphology of the polymer blends and their composites/nanocomposites

Some studies have been conducted on the morphology of PLA/PCL blend composites and nanocomposites, prepared mostly via melt mixing. Phase separation is normally seen because PLA and PCL are immiscible. The polymer with the higher content constituted the major phase, having the other polymer dispersed as globules (inclusions) making up the minor phase [12, 13, 15, 16, 27]. In one study, Sarazin *et al.* [16] investigated the morphology of PLA/PCL polymer blends using SEM. It was found that PLA and PCL were immiscible and the dispersed phase had a coarse appearance. In other studies, the addition of fillers, compatibilizers, additives and plasticizers has been reported to reduce the size of the inclusions and improve the interfacial adhesion between PLA and PCL [8-10, 29]. One such study was performed by Laredo *et al.* [8]. They reported on the use of functionalized and non-functionalised multiwalled carbon nanotubes (MWCNT) in a 70/30 PCL/PLA blend. The PCL constituted the major phase while the PLA was dispersed as inclusions. Addition of the non-functionalised nanofiller from 0.2 to 2% reduced the sizes of the PLA inclusions and improved the interfacial adhesion between PLA and PCL. This behaviour was attributed to the fair dispersion of the filler, and its ability to act as a compatibilizer between the two polymer phases. Further improvements were observed when the nanofiller was functionalized using carboxylic acid

groups (–COOH). The MWCNT preferentially located in the PCL phase and at the PCL/PLA interface. The preferential location of MWCNT was attributed to the low viscosity of PCL. A polymer with a low viscosity has more disordered chains allowing easier penetration of the nanofiller. Fillers; however, offer more benefits in comparison to the other methods mentioned, especially because they are effective at improving interfacial adhesion of the blend components and therefore acting as compatibilizers [8].

2.4.2 Thermal properties of the polymer blends and their composites/nanocomposites

2.4.2.1 Glass transition, cold crystallization, melting, and enthalpies of the polymer blends and their composites/nanocomposites

When PLA and PCL are blended together, two separate glass transitions and melting peaks are usually observed, because these two polymers are immiscible [26, 29]. Miscibility of the two can be studied by assessing the temperature difference between their glass transition or melting temperatures. Improvement in miscibility is said to have taken place if only one transition is achieved, that represents both components in the blend or the difference/distance between the two temperatures becomes smaller, and enclosed within the transitions of the individual components [1, 17, 38]. However, if the two polymers are immiscible, two glass transitions and two melting transitions are observed. Mohamed *et al.* [13] studied the thermal properties of PCL/gluten bioblends prepared through extrusion and injection moulding. In their DSC study, they found the T_g temperatures of neat PCL and gluten to be -67.8 ºC and 63.0 ºC, respectively. In the polymer blends, a single glass transition (~67 ºC) was present at all blend compositions, they concluded that PCL and gluten were miscible. The glass transition of the blends occurred around the T_g of the neat PCL, they attributed this to the domination of PCL molecular mobility over that of the gluten chains. Even though they were miscible, PCL and gluten seemed to have physical interactions rather than chemical interaction, which they confirmed using fourier-transform infrared spectroscopy (FTIR). In their FTIR analysis they observed no major chemical changes for the blends. From the melting peaks of PCL in some of the blends, they observed a decrease in the onset of the T_m and a decrease in the enthalpy as well with the addition of gluten. In the composites where they observed an increase in the melting temperature, they attributed it to interactions between PCL and gluten.

In the polymer blends of PLA and PCL, the PLA glass transition coexists with the PCL melting temperature but it is usually overshadowed and not clearly observable [15]. Miscibility of PLA and PCL, as well as the degree of crystallinities of the blends, are often dependant on the grades of the polymers used. Tuba *et al.* [36] studied the blend composites of PCL/PLA with a

compatibilizer (L-lysine-diisocyanate (LDI) and L-lysine-triisocyanate (LTI)). Neat PCL had a T_m of 65.2 ºC and a degree of crystallinity of 54.2 %. For neat PLA, T_{cc} and T_m peaks were seen at 124 ºC and 168.7 ºC, respectively, and a degree of crystallinity of 7.9% was observed. A decrease in the melting temperature of PCL was observed with the addition of PLA as the minor phase. Also, the degree of crystallinity of PCL decreased with the presence and increase in PLA content. The decrease was as a result of the PLA limiting molecular mobility of the PCL chains. However, the presence of a compatibilizer in the blends did not result in any further decrease in the melting temperature, but, a further decrease in the degree of crystallinity. This was attributed to the grafting reactions between PLA, PCL and the LDI. These grafting reactions therefore resulted in restricted segment-motion, organization and densification of PCL molecules. The PLA melting temperature remained unchanged with the presence of PCL or compatibilizer. An increase in the crystallinity of PLA in the blends and composites was observed, and this was attributed to the promotion of slow crystallization of PLA. The nucleating of PLA in the presence of a second phase (PCL) and the compatibilizer was seen with the decrease in the cold crystallization temperatures as well as the narrowing of the crystallization ranges. Carmona *et al.* [25] prepared ternary composites with thermoplastic starch (TPS), PLA and PCL, using citric acid and maleic anhydride as compatibilizers. In this study, it was found that the PLA and TPS reduced the crystallinity of PCL due to restricted mobility of the PCL chains. The presence of PLA had a different effect; the PLA behaved as a nucleating agent for PCL, and an increase in the degree of crystallinity was observed. The degree of crystallinity of PLA was increased with the presence of both PCL and TPS. This was attributed to the low viscosity of both polymers which provided mobility to the PLA chains, resulting in an increase in PLA crystallinity.

Addition of fillers also has an influence on the crystallinity properties of polymers in the blends. Wu *et al.* [37] reported the preparation of 70:30 and 30:70 w/w PLA/PCL composites with clay or CNTs through melt compounding. They found that selective localization of the fillers influenced the crystallization of the constituent polymers differently. Contrary to what other researchers observed, the presence of PLA in the PCL polymer matrix increased the crystallinity of PCL. A preferential location of the CNT in the PCL phase, despite the CNT having a heterogeneous nucleating effect, they reduced the overall crystallization rate of PCL, they acted as a physical hindrance to the growth of spherulites. In the PLA phase, the cold crystallization temperature of PLA was decreased, as the PCL is already in its molten state. Also, the addition of CNT or clay resulted in a greater decrease of the cold crystallization temperature. The filler effectively acted as a nucleating agent, lowering the temperature at

which crystallization was taking place. An increase in the degree of crystallinity of PLA was observed and this was attributed to the heterogeneous nucleating effect of the fillers. It is important to note that all these different researchers used different grades of PLA, which explains the disparities observed in their studies.

2.4.2.2 Thermal degradation and stabilities of the polymer blends and their composites/nanocomposites

PLA and PCL in their blends show separate degradation steps for each polymer, and they are proportional to the amount of each polymer present [10]. Mofokeng *et al.* [10] investigated the morphology and thermal degradation properties of melt-mixed poly(lactic acid) (PLA)/poly(ε-caprolactone) (PCL) biodegradable polymer blend nanocomposites with TiO_2 as filler. They observed a decrease in the thermal stability of both PCL and PLA with increasing the amount of the other polymer, for instance increasing PLA content decreased the thermal stability of PCL and vice versa. This decrease was attributed to the incompatibility between the two polymers. However, with the addition of titania nanoparticles, an increase in the mass loss temperature with increasing filler content was observed, and this was interpreted as an increase in thermal stability. This was observed for both polymers, individually and in the blend nanocomposites. This increase in thermal stability was attributed to the titania nanoparticles absorbing more energy than the polymers and also to the retardation of the diffusion of volatile degradation products. A char residue from the presence of the filler was observed in all the nanocomposites, and this was attributed to the fair dispersion of TiO_2 as observed in the morphology study. Carmona *et al.* [25] studied ternary composites with thermoplastic starch (TPS), PLA and PCL. In this study, two separate degradation steps were observed for the PLA and PCL in the blends. Compared to the neat polymers, a decrease in the onset temperature of degradation was seen for both PLA and PCL. For the degradation of PCL, it took place in two stages, they attributed the first step to polymer chain cleavage via cis-elimination and the second step to unzipping depolymerisation from the hydroxyl end of the polymer chain. The degradation of PLA, they mentioned it occurred through cleavage of main and side-chains of macromolecules. They mentioned that its mechanism was way more complicated as it was influenced by the presence of hydrolysed monomers and oligomers, moisture, molecular weight and residual metals. When they added TPS, a decrease in thermal stability of the PLA/PCL blend was observed. A decrease in the onset of degradation by 24 ºC was seen. This was attributed to the low thermal stability of TPS. The mass loss from TPS was mostly due to evaporation of volatile compounds, glycerol and water which were present in the TPS.

2.4.2.3 Thermal degradation volatilization of the polymer blends and their composites/nanocomposites

Analysing the volatile degradation products helps to understand the thermal stabilities of polymers. Mofokeng *et al.* [10] performed thermal degradation volatilization studies for PLA/PCL blend nanocomposites filled with TiO_2 nanoparticles using TGA-Fourier-transform infrared (FTIR) spectroscopy. In the polymer blends, the degradation products which were observed in the constituent polymers were also observed. Also, because the two polymers were immiscible, the degradation products were produced at different times. In the 50/50 w/w PLA/PCL blend, they observed a maximum degradation for PLA around 343.1 ºC and that of PCL was around 402.0 ºC. When titania nanoparticles were added to the blends, they observed a decrease in intensity in the FTIR spectra and a shift of the maximum degradation temperature by 2 ºC to higher temperatures were observed. They attributed this to a probable retardation of the volatile degradation volatiles due to interaction with the nanoparticles. The FTIR spectra of the volatile degradation products of PLA and PCL were very similar. The degradation volatiles of PLA were emitted first, and those of PCL were released whilst those of PLA were still being emitted. For that reason, they observed multiple peak for the same chemical bonds (indicating a certain degradation product). For example, for carbon dioxide, two different wavenumbers at 2375 and 2309 cm^{-1}were observed. Mngomezulu *et al.* [34] studied the effect of expandable graphite on thermal and flammability properties of poly(lactic acid)-starch/poly(ε-caprolactone) blend systems prepared via melt mixing. From the TGA analysis, it was found that PCL improved the thermal stability of PLA-starch in the blend due to its better thermal stability. The presence of expandable graphite resulted in more thermally stable composites. There was an increase in the temperature at which the maximum mass loss rate was seen. This was attributed to the shielding effect of the flake-like structure of expandable graphite, which hindered the escape of the degradation volatiles by increasing the diffusion pathway. The FTIR spectra of the TGA-FTIR curves showed that the degradation products were indicative of the presence of water, CO_2 and CO from both polymers. Additional degradation products unique to the individual polymers were also observed. Aldehyde, lactide, and methane were observed for PLA, and 5-hexenoic acid and ε-caprolactone were produced from the PCL.

2.4.3 Thermomechanical studies of the polymer blends and their composites/nanocomposites

Thermomechanical studies reveal miscibility as well as filler effectiveness. Wu *et al.* [38] evaluated the compatibility effect of PCL/PLA blend with carboxylic acid functionalized

MWCNTs using a dynamic thermal mechanical analyzer. From the tan δ curves, the glass transitions of PLA and PCL moved closer to each other when the functionalized MWCNTs were added. This indicated improved compatibility between the two phases. This was attributed to the thermodynamic interface stabilization as a result of the filler acting as an emulsifier at the phase interface. Mofokeng *et al.* [29] studied the dynamic mechanical properties of PLA/PHBV, PLA/PCL, PHBV/PCL blends and their nanocomposites with TiO_2 as nanofiller. From the storage modulus curves, it was reported that PLA/PCL polymer blends had average properties of the constituent polymers. At temperatures between the glass transition of the two polymers, a decrease in storage modulus was observed with increasing PCL content. They attributed this to blends having average properties of the constituent polymers. From the loss modulus curves, they noticed little change in the glass transition temperatures of PLA and PCL in the blends. This revealed the immiscibility of the two polymers. The little changes that they observed were not elaborated. They also mentioned that they could not accurately determine the glass transition temperature of PLA because it occurred in the same temperature region with the PCL melting transition. From their tan δ curves, they observed a glass transition for PCL and a glass transition for PLA. Using titania as a filler, no clear trends were observed with its presence or increase in content. Jain *et al.* [32] investigated poly(lactic acid)/poly(ε - caprolactone) blends filled with micro-talc at temperature around the room temperature. They found neat PLA had a higher storage modulus than PCL, and when they were blended together, PCL lowered the storage modulus of PLA. When talc was added to the polymer blend, an increase in the storage modulus was observed. They attributed this to the stiffness of talc, and ability to introduce a rigid interface in the PLA/PCL blend which allowed better stress transfer. The increase in storage modulus was proportional to the amount of filler content. When they added 1, 3 and 5 wt. % filler content increases in storage modulus with up to 14, 27 and 58% respectively were observed. From the tan δ curves, they observed a decrease in the peaks with increases in the talc content. They attributed this to reduced molecular mobility of the polymer chains and also to the reduction of the mechanical loss which was required to overcome intermolecular chain friction.

2.5 Magnesium hydroxide

Flame retardants are materials which are able to disrupt the burning process. The burning process consists of five stages, which are: heating, decomposition, ignition, combustion and propagation. Flame retardants act by disrupting the burning process during any of the five stages involved [39]. Metal hydroxides like magnesium hydroxide ($Mg(OH)_2$ have been known to: i) release water vapour which dilutes the amount of fuel available for combustion, ii)

withdraw heat from the combustion zone and iii) produce a metal oxide residue which behaves as an insulating layer and as a smoke suppressant [39-49]. Magnesium hydroxide is readily available, toxic-free, environmentally benign and friendly. It has a low cost, good thermal stability (high decomposition temperature) and smoke suppressing properties, and has an ability to neutralize acidic volatile products from polymer combustion. It is halogen-free, it does not result in any corrosive, gaseous or toxic substances when it thermally degrades [39, 40, 44, 47]. Its use as a flame retardant has been examined comparatively especially for non-biodegradable petroleum based polymers [50-56]. $Mg(OH)_2$ nanoparticles can have various morphologies (nanoflower-like, nanolamellar (or nanoplate), nanoneedle or nanorod crystals) depending on the synthesis conditions. Nanocomposites of $Mg(OH)_2$ with polymers such as polyamides (poly(ether-amide) (PEA)), polypropylene (PP), ethylene-propylene copolymer (EPR), poly(ethylene-vinyl acetate) copolymers (EVA), polyethylene terephthalate (PET) and polyethylene (PE) have been reported [41-43, 45, 46, 48, 49, 53, 54].

$Mg(OH)_2$ nanoparticles provides heat insulation to the polymer matrix as temperature increases, it achieves this by redirecting the heat as it accumulates on the surface of the polymer. Above 300 °C, $Mg(OH)_2$ is decomposed into MgO, and gaseous water is released. The water which is released reduces the temperature and also dilutes the combustible gases. Dilution of combustible gases limits the fuel available for the burning process to take place. As the water is released, the MgO generated forms a coat and acts as a protective insulating layer; the char that is formed will result in further flame retardant protection and less smoke generation. During the burning process, $Mg(OH)_2$ inhibits polymer ignition and also acts as a smoke suppressant. It also absorbs heat from the combustion zone and therefore reduces the possibility of the burning process to continue [38-40, 49, 50-52, 56].

$$Mg(OH)_2(s) \xrightarrow{\Delta} MgO(s) + H_2O(g) \uparrow$$ Equation 2.1 [51]

Some studies have found that the flame retardance effect of $Mg(OH)_2$ can be improved by using very large amounts of the filler. However, this often results in loss of valuable properties such as mechanical strength, as the compatibility between the filler and polymer matrix is compromised. To prevent this, $Mg(OH)_2$ is used in its nano scale form where a lesser amount of the $Mg(OH)_2$ will be required, in comparison to larger particles, whilst maintaining the same level of flame retardancy. The nanoparticles have a larger surface area to volume ratio and homogeneously disperse in the polymer matrix allowing for formation of a more compact char during burning [39-41, 46, 51, 56].

2.5.1 Morphology of $Mg(OH)_2$

Zhang *et al.* [51] did simulations of the magnesium hydroxide surface and interface. Through various methods, they successfully synthesized $Mg(OH)_2$ (MH) nanoparticles with different morphologies were synthesized successfully. SEM images showed mono-dispersed, flower-like MH and vertically aligned nanosheets. Each of these different morphologies had different thermal degradation peaks from the TG and DTA curves obtained during thermo-gravimetric analysis. Peaks at 341, 378 and 381 °C were observed for flower-like $Mg(OH)_2$, vertically aligned $Mg(OH)_2$ nanosheets and mono-disperse $Mg(OH)_2$ respectively. Zhang *et al.* [53] studied the synergistic effects of layered double hydroxide with hyperfine magnesium hydroxide in halogen-free flame retardant EVA/HFMH/LDH nanocomposites. The magnesium hydroxide nanoparticles were seen as dark platelets during TEM analysis. Shen *et al.* [57] worked on an *in situ* synthesis of hydrophobic magnesium hydroxide nanoparticles in a novel impinging stream-rotating packed bed reactor. Through field-emission scanning electron microscope (FESEM), they found that unmodified $Mg(OH)_2$ nanoparticles showed a more irregular morphology and had nanoparticles which had a mean diameter larger than 30 nm. Wang *et al.* [41], studied the addition of $Mg(OH)_2$ nanoparticles to polypropylene using SEM. The extensive particle pull-out of $Mg(OH)_2$ from the fracture surface of polypropylene were observed. They attributed this to the large difference in surface energy between the polymer matrix and the $Mg(OH)_2$ filler, which they determined using melt flow index measurements. The addition of $Mg(OH)_2$ as a filler in polymers or blends has been shown to result in agglomeration. $Mg(OH)_2$ usually clusters and has irregular morphology (irregularly shaped large particles) [44, 57]. Increasing the content of the nanoparticles usually results in more agglomerates [50]. Using TEM, Zhang *et al.* [53] found that the addition of $Mg(OH)_2$ nanoparticles to ethylene-vinyl acetate resulted in large agglomerates.

2.5.2 The effect of $Mg(OH)_2$ on thermal properties of polymers

2.5.2.1 Glass transition, cold crystallization, melting, and enthalpies of $Mg(OH)_2$

$Mg(OH)_2$ does influence the thermal properties of polymers and particle size also affects the efficiency of a filler. Oyama *et al.* [42] investigated the influence of the polymer/inorganic filler interface on the mechanical, thermal, and flame retardant properties of polypropylene/magnesium hydroxide composites. In this study, the $Mg(OH)_2$ micro particles were used as a filler in isotactic polypropylene (iPP). They found that the $Mg(OH)_2$ micro particles decreased the glass transition of iPP. This they attributed to the presence of a non-wetted interface formed due a lack of attractive interactions between the iPP and $Mg(OH)_2$.

Mishra *et al.* [46] studied the effect of nano-$Mg(OH)_2$ on the mechanical and flame-retarding properties of polypropylene composite. From the DSC analysis, it was observed that there is a smooth onset for the melting peak. This was attributed to the variation in heat absorption of the $Mg(OH)_2$ nanoparticles, which was more pronounced at higher filler content.

2.5.2.2 Thermal degradation and stabilities of $Mg(OH)_2$

$Mg(OH)_2$ is mostly used as a flame retardant because of its thermal properties (heat insulation at high temperatures and thermal stability) and environmentally friendly degradation volatiles. Shen *et al.* [47] coupled DSC with TGA when analysing $Mg(OH)_2$ nanoparticles which had been synthesized using a stream-rotating packed bed (IS-RPB) reactor. It was reported that the thermal degradation of $Mg(OH)_2$ was composed of two steps and took place from 89 to 376.2 °C. The first step was a small mass loss at lower temperatures (89 °C to 250 °C) and it was attributed to the desorption of water absorbed on the surface of $Mg(OH)_2$. The second step took place from 340.2 to 376.2 °C. They observed an endothermic peak at 368.2 °C, which they attributed to the degradation of $Mg(OH)_2$ to MgO. Sometimes a third step can be observed and that can be attributed to the complete dehydroxylation of the $Mg(OH)_2$ [48]. Oyama *et al.* [42], found that addition of the $Mg(OH)_2$ to isotactic propylene increased its thermal stability when burning in air. However, under a nitrogen atmosphere, Dittrich *et al.* [49] found that $Mg(OH)_2$ had no significant effect on the thermal stability of polypropylene. Pyrolysis of PP/$Mg(OH)_2$ nanocomposites still occurred in the same temperature when compared with neat PP. In another study, Zhang *et al.* [52] investigated addition of aromatic boronic acid derivative 2,4,6-tris(4-boronic-2-thiophene)-1,3,5-triazine (3TT-3BA) and $Mg(OH)_2$ to an epoxy resin (EP) polymer matrix. After pyrolysis, the epoxy resin which had $Mg(OH)_2$ nanoparticles only, had a rugged appearance because the MgO formed an uneven protective layer on its surface. Yang *et al.* [54] studied the effect of $Mg(OH)_2$ and carbon microspheres coated magnesium hydroxide on the flame retardancy properties of polyethylene terephthalate (PET). Contrary to what has been observed in other studies [42, 49], presence of $Mg(OH)_2$ nanoparticles lowered the maximum degradation temperature of PET indicating that it promoted its degradation. After degradation, the charring effect of $Mg(OH)_2$ was observed in all composites using SEM. The morphology of the PET/$Mg(OH)_2$ showed a char which was described as a "dense, smooth and continuous residue" [54]. It was mentioned that the MgO particles were embedded in the residue, and therefore improving the continuity and compactness of residual char.

2.5.2.3 Thermal degradation volatilization of $Mg(OH)_2$

Changes in thermal stability with the addition of $Mg(OH)_2$ have been studied by analysing thermal degradation volatiles released during its thermal degradation, in order to see its effectiveness as a flame retardant, and insulator in polymers. Wang *et al.* [45] studied the thermal degradation of polyethylene composites filled with magnesium hydroxide and red phosphorus using thermogravimetric analysis (TGA), real time Fourier transform infrared (FTIR) and pyrolysis gas chromatography mass spectrometry (Py-GC/MS). During pyrolysis in the absence of a purge gas, changes in the relative intensities of C–H absorption peaks (2920 and 2850 cm^{-1}) occur as the temperature increased. In neat polyethylene, these peaks disappeared around 350 °C. When $Mg(OH)_2$ nanoparticles were added, the peaks were still present at temperatures around 400 °C. This showed that presence of $Mg(OH)_2$ nanoparticles increased the thermo-oxidative stability of polyethylene. Also, another peak around 3690 cm^{-1} which was attributed to the –OH of the $Mg(OH)_2$, decreased gradually with an increase in temperature. This was due to the decrease in content of the $Mg(OH)_2$ as the temperature increased.

2.5.3 The effect of $Mg(OH)_2$ on thermomechanical properties of polymers composites

The addition of fillers to polymers has been reported to have an anti-plasticizing effect. Wang *et al.* [41], studied microstructure and mechanical properties of polypropylene/elastomer/magnesium hydroxide fire-retardant compositions. In their thermomechanical study using a rheometric analyser, an increase in the storage modulus of polypropylene with the addition of $Mg(OH)_2$ was observed. Oyama *et al.* [42] investigated the influence of the polymer/inorganic filler interface on the mechanical, thermal, and flame retardant properties of polypropylene/magnesium hydroxide composites. In their study of dynamic viscoelastic properties using dynamic mechanical analysis, they also observed an increase in storage modulus with an increase in $Mg(OH)_2$ content in polypropylene. This increase was attributed to the higher stiffness of the particles, alignment of the $Mg(OH)_2$ platelets along the film surface and also the higher degree of orientation of the polymer in the composites. From the tan δ curves of 70/30 w/w iPP/$Mg(OH)_2$ composites, two relaxation transitions, α and β were observed. The α relaxation was attributed to the relaxation of restricted iPP amorphous chains found in the crystalline phase. The β relaxation was the T_g of the unrestricted amorphous iPP, which tended to decrease upon the addition of $Mg(OH)_2$.

2.6 Titania and its functionalization

Titania (TiO_2) is one of the inorganic nanofillers that has been researched for non-biodegradable thermoplastics such as polypropylene and polyethylene [10-14, 29, 57-58]. It is naturally occurring and it is found in various forms, such as anatase, brookite, ilmenite, octahedrite, and rutile. Anatase is one of the most used forms, because its crystal structure allows it to have the most surface reactivity. It is often used in its nanosize in its different shapes such as mesoporous and nanoporous TiO_2 nanoparticles, nanorods, nanotubes and nanowires [61]. Titania nanoparticles are often found in various applications such as chemical decontamination, environmental purification (air and water purification), self-cleaning coatings, inks in solar cells and photocatalysts. The applications often capitalize on the low price and non-toxicity TiO_2, as well as its anti-corrosion, anti-microbial, good photostability, photocatalytic activity and UV resistance properties. Nanocomposites of TiO_2 with various polymers such as cellulose, chitosan, polyaniline, polyacrylate, poly (methyl methacrylate), polycarbonate, polycaprolactone, epoxy resins, polyester, polyethylenes, poly(hydroxybutyrate-co-hydroxyvalerate), polyimide, poly(lactic acid), polypropylene, polypyrrole, polystyrene, polyurethanes, polyvinyl alcohol and polyvinyl chloride have been reported [10, 29, 60, 61-66]. These nanocomposites often have improved gas barrier, biodegradable, dielectric, thermal or mechanical properties. However, the challenge in its use is agglomeration and poor dispersion in polymer blends. This can be improved by surface modification.

The chemical modification of TiO_2 has become a topic of relevance because of the influence it has on improving the dispersion of TiO_2 in the polymer matrices and colloids (gels, sols and emulsions). TiO_2 has been functionalized using acids (dodecylbenzenesulfonic acid, propionic acid, N-trimellitylimido-S-valine diacid, pentadecylbenzenesulfonic acid), alkylamines, glycidol, polyethylene glycol, silanes (3-aminopropyltrimethoxysilane (APTMS), 3-isocyanatopropyl-triethoxysilane (ICTOS), hexadecyltrimethoxysilane, vinyltrimethoxysilane (VTMS)) and Silwet L-7280 (a copolymer of silicone, ethylene oxide, and propylene oxide) [10-14, 57, 62, 65, 67]. Looking at the silane coupling agents as surface modifiers for titania nanoparticles, they allow interactions between the polymer matrix and the titania nanoparticles, and therefore improve their dispersion. Silane functionalization can be performed using environmentally friendly solvents such as water and ethanol [67]. 3-aminopropyltrimethoxysilane (APTMS) is one of the simplest silanes that is mostly used because of its low cost and results in improved photodegradation, thermal degradation, mechanical and UV protective properties [67-70]. The functionalization of TiO_2 using APTMS

is shown in in Figures 2.2 [67]. APTMS has two functional groups (-OH and $–NH_2$ groups) that allow them to interact with the polymer matrices and the fillers. The –OH groups of the silane react with the –OH groups on the surface of titania nanoparticles through a dehydration reaction. This allows for the attachment of the coupling agent through the formation of Si-O-Ti chemical bonds. The $–NH_2$ group is capable of hydrogen bonding and transesterification reactions with the -C=O of the ester linkages in the polymer backbone.

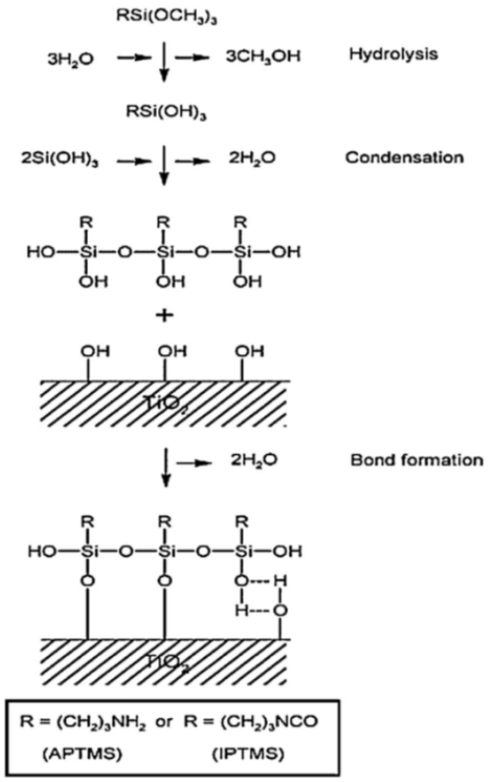

Figure 2.2 Scheme of chemical grafting of organosilanes onto TiO_2 nanoparticles surface [68]

Titania functionalized nanoparticles are expected to graft onto the ester bonds in the polyester chains (PCL or PLA). The primary amine groups of the functionalized TiO_2 nanoparticles are covalently bonded to the polyesters through the breaking of ester linkages followed by the formation of an amide linkages. The unreacted amine groups on the coupling agent are capable to form hydrogen bonding with the –C=O group of the ester linkages on the backbone of the polymer chains [67-70]. According to my knowledge the use of functionalized titania inorganic nanoparticles in PCL/PLA blends has not been explored yet. It would be a topic of significance to investigate the influence of the functionalisation on the dispersion of titania in the PLA and PCL blends.

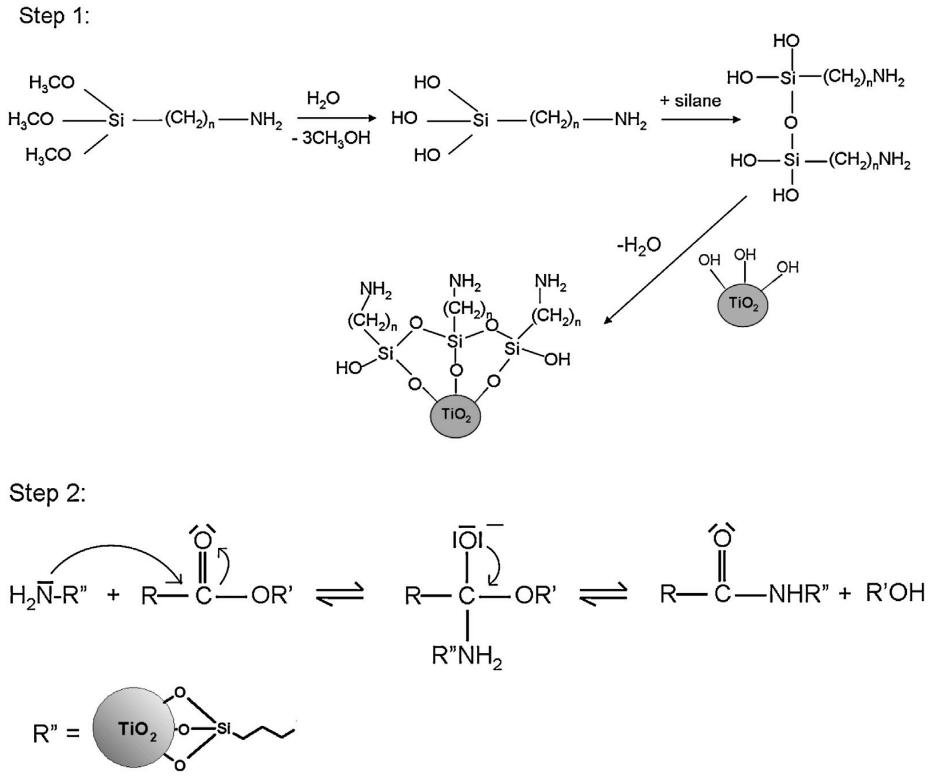

Figure 2.3 Scheme of surface functionalization of TiO_2 nanoparticles by APTMS (step 1) and surface binding of amino functionalized TiO_2 nanoparticles on to the polymer chains (step 2) [67].

2.6.1 Morphology of TiO_2

The morphology of unfunctionalized and functionalized titania with PLA, PCL and their blends has been reported. Mofokeng *et al.* [10, 29] investigated the addition of small amounts of unfunctionalized TiO_2 nanofiller to PLA/PCL blends using TEM. They observed a preferential location of the TiO_2 nanoparticles in PLA and at the PLA/PCL interface instead of PCL. This was attributed to the lower interfacial tension between PLA and the nanofiller. Also, they observed occurrence of agglomerates in both polymer phases. These occurred as a result of a large difference between the polar characters of the polymers and the nanofiller, which was determined using contact angle measurements. The nanoparticles still aggregated together because they were still strongly attracted to each other. The authors concluded that the dispersion of nanoparticles is not only dependant on PCL having a lower viscosity than PLA, but also on other factors such as molecular weight, degree of crystallinity and surface energies [10, 29, 38]. Muñoz-Bonilla *et al.* [22] analysed the interaction of unfunctionalised TiO_2 anatase with PCL using TEM. On the morphology of these nanocomposites, they noticed a

good dispersion of the filler. The TiO_2 nanoparticles were uniformly dispersed, however small agglomerates ranging from 10 to 180 nm were present.

In other studies, improvements in the dispersion of TiO_2 nanoparticles has been reported with surface modification. Buzarovska *et al.* [11] studied the morphology of nanocomposites of PLA with propionic acid functionalized TiO_2 nanoparticles using SEM. They observed poor dispersion and agglomeration of neat TiO_2 which they attributed to the van der Waals forces between the nanoparticles. However, functionalization of TiO_2 using propionic acid as a surface modifiers improved their dispersion and resulted in smaller and fewer agglomerates. This was because the functionalizing agent reduced the interparticle forces which allowed the nanoparticles to disperse easily in the polymer matrix. The functionalizing agent also reduced the surface energy of nanoparticles and acted as a compatibilizer between the polymer matrix and the filler [11-12]. Luo *et al.* [12] worked on the morphology of PLA nanocomposites containing lactic acid functionalized titania using SEM and TEM. They observed an improvement in the dispersion of TiO_2 in PLA after functionalization was done using lactic acid. They mentioned that the improvements in dispersion highlighted the role grafting had in achieving good dispersion.

2.6.2 The effect of TiO_2 on the thermal properties of polymer nanocomposites

2.6.2.1 Glass transition, cold crystallization, melting, and enthalpies of TiO_2

Titania nanoparticles also has an influence on some of the thermal properties of polymers. Luo *et al.* [12] studied the influence of titania nanoparticles on the temperature transition in PLA. The PLA/TiO_2 nanocomposites with various filler content were prepared via melt mixing. During the DSC study, it was reported that the addition of the filler did not result in any significant changes in the T_g or T_{cc} especially at low content. However, at a higher filler content, the T_{cc} and the T_m were reported to have decreased. The decrease indicated that the filler resulted in a decreased crystalline phase. In the unfilled PLA, two peaks were observed for the T_m. These were attributed to the presence of two crystalline phases with one being less ordered and melting at a lower temperature, and the other one being more ordered and melting at a higher temperature. Increasing content of the filler in the nanocomposites resulted in disappearance of the first peak and also decrease in the T_m. This behaviour was attributed to a decrease in sizes of the PLA crystalline phase because of the presence of nanoparticles. An increase in the degree of crystallinity with the increase in titania content was reported. The increase in the degree of crystallinity was attributed to the accelerated rate of crystallization due to the nucleating effect of the titania nanoparticles in PLA. They also functionalized the

titiania nanoparticles with lactic acid, and the increase in the crystallinity was also observed with the presence of the functionalized filler. The functionalized filler acted as a heterogeneous nucleating agent, increasing the number of primary nucleation sites and rate of crystallization. They confirmed this by further studying the effect of the filler on the size and shape of the spherulites using polar optical microscopy. They reported that the unfilled PLA had larger and fewer spherulites but the filled one had smaller and more spherulites. This could therefore possibly reduce the brittleness of the PLA as smaller spherulites make a polymer less brittleness [15]. Nguyen *et al.* [59] studied the degree of crystallinity of polyethylene/TiO_2 nanocomposites using DSC. Contrary to the afore mentioned study, they reported a relative decrease in the intensities of the melting peaks of polyethylene in the presence of titania. They attributed this to the hindering of the spherulite growth stage by the titania nanoparticles due to immiscibility with the polymer matrix and possibly resulting in a larger surface energy difference. They reported that the TiO_2 nanoparticles might have reduced the bulk crystallization rate and the sizes of the crystal domain, therefore lowering the degree of crystallinity. When they used vinyltrimethoxysilane, they observed a smaller decrease in the degree of crystallinity compared to the unfunctionalised titania. They also cautioned that the degree of crystallinity is influenced by the method used for sample preparation (melt mixing) as well as the characterization technique.

2.6.2.2 Thermal degradation and stabilities of TiO_2

Functionalizing agents do have an influence on the thermal stability of fillers. Zhao *et al.* [69] studied the functionalization of titania nanoparticles using silane coupling agents 3-aminopropyltrimethoxysilane (APTMS) and 3-isocyanatopropyltrimethoxysilane (IPTMS) using TGA. For the non-functionalized titania, a mass loss between 100 and 160 °C was observed as a result of the vaporization of water adsorbed on the surface of the titania nanoparticles. A second mass loss between 340 and 420 °C was attributed to the condensation of the –OH groups found on the surface of titania nanoparticles. In the silane functionalized nanoparticles, the second step was also due to the condensation of the silane molecules. From 300 °C till 670 °C, the silane functionalizing agents were reported to undergo oxidative thermal decomposition. Mallakpour *et al.* [71] prepared chitosan nanocomposites containing N-trimellitylimido-S-valine diacid functionalized TiO_2 through solution casting. Presence of the functionalized titania nanoparticles was reported to increase the thermal stability of chitosan and was proportional to the amount of filler used. Demétrio da Silva *et al.* [60] studied the polyurethane/titanium dioxide nanocomposites prepared through *in situ* polymerization. They reported an increase in the degradation temperature of the polymer with increasing TiO_2

content. They attributed the increase in the degradation temperature to the ability of titania acting as a thermal insulator and also acting as a barrier to the escape of the degradation volatile products.

2.6.2.3 Thermal degradation volatilization of TiO_2

Thermal degradation volatilization can be used as a tool to measure the effectiveness of fillers in thermal degradation volatile suppression. The ability of titania to influence thermal stabilities of polymers has been investigated also through thermal degradation volatilization studies. Motaung *et al.* [74] studied the morphology, mechanical properties, and thermal degradation of polycarbonate-titania nanocomposites. In their degradation volatilization studies using TGA-FTIR, they found that presence of titania did not result in shifts or new peaks in the spectra of the degradation volatiles. They however mentioned that the volatilization of the polycarbonate nanocomposites was slower when compared to the pristine polymer. They attributed this to various possible interactions between the titania nanoparticles with (i) the polymer chains (ii) the free radicals formed during degradation, and (iii) the volatile degradation products. Mofokeng *et al.* [10, 29, 72, 73] performed various studies on the thermal degradation volatilization of biodegradable polymers. In one study, they investigated the morphology and thermal degradation properties of poly(hydroxybutyrate-co-valerate) (PHBV)/poly(ε-caprolactone) (PCL) blend nanocomposites with TiO_2 as a filler [72]. In their investigation of the degradation kinetics by TGA, they reported that TiO_2 lowered the activation energy of PHBV in the PHBV/TiO_2 nanocomposites, which indicated a loss in thermal stability. This was attributed to the nanoparticles acting as catalysts for the initiation of degradation. Even though a decrease in the activation was observed for PHBV, it was also observed that there was a retardation in the emission of the thermal degradation volatile products TiO_2 increased the temperature at which the degradation volatile peak was observed on the FTIR spectra. It was mentioned that this did not indicate an increase in thermal stability but rather masked the lower thermal stability of the polymer. In PCL/TiO_2 nanocomposites, the activation energy for degradation was increased in the presence of TiO_2. Also, a decrease in intensity and a shift of some of the FTIR spectra of the volatiles was observed. In both cases, the increase in activation energy and changes in the FTIR spectra indicated a retardation of the thermal degradation volatiles and increased thermal stability. In another study, Mofokeng *et al.* [73] investigated the morphology and thermal degradation studies of melt-mixed PLA/PHBV polymer blend nanocomposites with titania nanoparticles. In this paper, it was reported that TiO_2 had an autocatalytic effect on PLA. At lower temperatures TiO_2 decreased the activation energy and increased the rate at which polymer degraded, but as the temperature

increased, the high heat capacity TiO_2 insulated the polymers to degrade at much higher temperatures. TiO_2 decreased the intensities and shifted some peaks of the FTIR spectra of the degradation volatiles. It was concluded that this indicated interaction between the nanoparticles and the degradation products which resulted in their retardation.

2.6.3 The effect of TiO_2 on thermomechanical properties of polymers composites

Little effects on thermomechanical properties have been observed with the addition of TiO_2 to polymer matrix. Mofokeng *et al.* [29] studied the influence of titania on the thermomechanical properties of PLA/PCL blends. No clear trends were observed in the storage modulus values and tan δ with an increase in content of the TiO_2 nanoparticles. They attributed this to the preferential dispersion of the titania in the PLA phase and also to the large agglomerates unevenly distributed in both the PLA and PCL phases. From the loss modulus curves, TiO_2 was found to have little effect on the glass transition of PCL. This was attributed to the preferential dispersion in the PLA phase. However, the glass transition temperature of PLA could not be accurately determined in the blends. This was because it occurred in the same temperature range as the melting point of PCL. Luo *et al.* [12] have mentioned that titania nanoparticles had very little influence on the chain dynamics of the polymer used. From the loss modulus curves, very little changes were observed on the T_g of the polymers, indicating immiscibility. The presence of a filler had little effect on the T_g as well. Because the melting temperature of PCL and the glass transition of PLA occur around the same temperature ranges, the glass transition temperature of PLA could not be determined accurately in both the blends and the nanocomposites. From the tan δ curves, three transitions were observed, the glass transition of PCL, the glass transition of PLA and the cold crystallization of PLA. The maximum values observed for these peaks are usually dependant on a number of factors which include polymer properties (molecular weight, crosslink density), filler properties (content, morphology, type and distribution), and the interactions between the polymer and the filler (interfacial properties, void content). The intensity as well as the area of the peaks, when it changes, indicates changes in the chain dynamics (mobility of the polymer chain). The presence and increase in amount of filler had very little effect on the maximum peaks obtained for PCL. PCL is often used as a plasticizer and is known to have very low damping because of its high chain mobility. When it is added to PLA, an increase in the intensity of the PLA peaks was observed with increase in PCL content. This was attributed to the high mobility of the PCL chains.

2.7 Potential applications

Based on the properties of PLA/PCL blends and nanocomposites with anisotropic fillers, some of the potential applications include: (i) agricultural uses (planting containers and controlled release systems (polymer nanocomposite/insecticide pellet)), (ii) denitrifying bacteria in water purification, (iii) decorations, (iv) disposable outdoor goods (plates, cutlery), (v) textiles and fabrics (industrial wipes and filters, geotextiles (for erosion control and landscaping), personal hygiene products (disposable diapers with a biodegradable plastic liner or tampon applicators)), and (vi) packaging. With the presence of $Mg(OH)_2$ nanoparticles, the PLA/PCL could be used effectively as planting containers, geotextiles and flame-retardant packaging. With the addition of APTMS functionalized titania, the PLA/PCL nanocomposites would mostly be suited for packaging. In both cases, they will have the appropriate mechanical strength and thermal stability [7-12].

2.8 References

1. W. Amass, A. Amass, B. Tighe. A review of biodegradable polymers: uses, current developments in the synthesis and characterization of biodegradable polyesters, blends of biodegradable polymers and recent advances in biodegradation studies. Polymer International 1998; 47:89–144.
   DOI: 10.1002/(SICI)1097-0126(1998100)47:2<89::AID-PI86>3.0.CO;2-F
2. E. Marin, M. I. Briceño, C. Caballero-George. Critical evaluation of biodegradable polymers used in nanodrugs. International Journal of Nanomedicine 2013; 8:3071–3091.
   DOI: 10.2147/IJN.S47186
3. G. E. Luckachan, C. K. S. Pillai. Biodegradable polymers - a review on recent trends and emerging perspectives. Journal of Polymers and the Environment 2011; 19:637–676.
   DOI: 10.1007/s10924-011-0317-1
4. A. P. Gupta, V. Kumar. New emerging trends in synthetic biodegradable polymers – polylactide: A critique. European Polymer Journal 2007; 43:4053–4074.
   DOI: 10.1016/j.eurpolymj.2007.06.045
5. M. Abedalwafa, F. Wang, L. Wang, C. Li. Biodegradable poly-epsilon-caprolactone (PCL) for tissue engineering applications: a review. Reviews on Advanced Materials Science 2013; 34:123–140.
   ISSN: 16065131

6. J. M. Williams, A. Adewunmi, R. M. Scheka, C. L. Flanagana, P. H. Krebsbacha, S. E. Feinberg, S. J. Hollister, S. Das. Bone tissue engineering using polycaprolactone scaffolds fabricated via selective laser sintering. Biomaterials 2005; 26:4817–4827. DOI:10.1016/j.biomaterials.2004.11.057
7. V. Siracusaa, P. Rocculi, S. Romani, M. D. Rosa. Biodegradable polymers for food packaging: a review. Trends in Food Science and Technology 2008; 19:634–643. DOI: 10.1016/j.tifs.2008.07.003
8. E. Laredo, M. Grimau, A. Bello, D. F. Wu, Y. S. Zhang, D. P. Lin. AC conductivity of selectively located carbon nanotubes in poly(ε-caprolactone)/polylactide blend nanocomposites. Biomacromolecules 2010, 11, 1339–1347. DOI: 10.1021/bm100135n
9. T. Takayama, M. Todo, H. Tsuji, K. Arakawa. Effect of LTI content on impact fracture property of PLA/PCL/LTI polymer blends. Journal of Materials Science 2006; 41:6501–6504. DOI: 10.1007/s10853-006-0611-9
10. J. P. Mofokeng, A. S. Luyt. Morphology and thermal degradation studies of melt-mixed poly(lactic acid) (PLA)/poly(ε-caprolactone) (PCL) biodegradable polymer blend nanocomposites with TiO_2 as filler. Polymer Testing 2015; 45:93–100. DOI: 10.1016/j.polymertesting.2015.05.007
11. A. Buzarovska. PLA nanocomposites with functionalized TiO_2 nanoparticles. Polymer-Plastics Technology and Engineering 2013; 52: 280–286. DOI: 10.1080/03602559.2012.751411
12. Y. Luo, W. Li, X. Wang, D. Xu, Y. Wang. Preparation and properties of nanocomposites based on poly(lactic acid) and functionalized TiO_2. Acta Materialia 2009; 57:3182–3191. DOI:10.1016/j.actamat.2009.03.022
13. A. Mohamed, V. L. Finkenstadt, S. H. Gordon, G. Biresaw, P. Debra E., P. Rayas-Duarte. Thermal properties of PCL/Gluten bioblends characterized by TGA, DSC, SEM, and Infrared-PAS. Journal of Applied Polymer Science 2008; 110:3256–3266. DOI: 10.1002/app.28914
14. J. Raquez, Y. Habibi, M. Murariu, P. Dubois. Polylactide (PLA)-based nanocomposites. Progress in Polymer Science 2013; 38:1504–1542. DOI: 10.1016/j.progpolymsci.2013.05.014
15. H. Liao, C. Wu. Preparation and characterization of ternary blends composed of polylactide, poly(ε-caprolactone) and starch. Materials Science and Engineering A 2009; 515:207–214.

DOI: 10.1016/j.msea.2009.03.003
16. P. Sarazin, G. Li, W. J. Orts, B. D. Favis. Binary and ternary blends of polylactide, polycaprolactone and thermoplastic starch. Polymer 2008; 49:599-609.
DOI: 10.1016/j.polymer.2007.11.029
17. B. Imre, B. Pukánszky. Compatibilization in bio-based and biodegradable polymer Blends. European Polymer Journal 2013; 49:1215–1233.
DOI: 10.1016/j.eurpolymj.2013.01.019
18. S. I. A. Razak, N. F. A. Sharif, W.A.W. Al Rahman. Biodegradable polymers and their bone applications: A review. International Journal of Basic and Applied Sciences IJBAS-IJENS 2012; 12:31–49.
OAI: CiteSeerX.psu:10.1.1.418.8617 1.
19. Y. Yang, Z. Tang, Z. Xiong, J. Zhu. Preparation and characterization of thermoplastic starches and their blends with poly(lactic acid). International Journal of Biological Macromolecules 2015; 77:273–279.
DOI: 10.1016/j.ijbiomac.2015.03.053 1.
20. A. J. R. Lasprilla, G. A. R. Martinez, B. H. Lunelli, A. L. Jardini, R. M. Filho. Poly-lactic acid synthesis for application in biomedical devices - A review. Biotechnology Advances 2012; 30:321–328.
DOI: 10.1016/j.biotechadv.2011.06.019
21. I. Harte, C. Birkinshaw, E. Jones, J. Kennedy, E. DeBarra. The effect of citrate ester plasticizers on the thermal and mechanical properties of poly(DL-lactide). Journal of Applied Polymer Science 2012; 127:1997–2003.
DOI: 10.1002/app.37600 1.
22. A. Muñoz-Bonilla, M. L. Cerrada, M. Fernández-García, A. Kubacka, M. Ferrer, M. Fernández-García. Biodegradable polycaprolactone-titania nanocomposites: preparation, characterization and antimicrobial properties. International Journal of Molecular Sciences 2013; 14:9249–9266.
DOI: 10.3390/ijms14059249 21.
23. T. K. Dash, V. B. Konkimalla. Poly-ϵ-caprolactone based formulations for drug delivery and tissue engineering: A review. Journal of Controlled Release 2012; 158:15–33.
DOI: 10.1016/j.jconrel.2011.09.064
24. K. Fukushima, D. Tabuani, G. Camino. Nanocomposites of PLA and PCL based on montmorillonite and sepiolite. Materials Science and Engineering C 2009; 29:1433–1441.
DOI: 10.1016/j.msec.2008.11.005

25. V. B. Carmona, A. C. Corrěa, J. M. Marconcini, L. H. C. Mattoso. Properties of a biodegradable ternary blend of thermoplastic starch (TPS), poly(ε-caprolactone) (PCL) and poly(lactic acid) (PLA). Journal of Polymers and the Environment 2015; 23:83–89.
DOI: 10.1007/s10924-014-0666-7
26. H. Kweon, M. K. Yoo, I. K. Park, T. H. Kim, H. C. Lee, H. Lee, J. Oh, T. Akaiked, C. Cho. A novel degradable polycaprolactone networks for tissue engineering. Biomaterials 2003; 24: 801–808.
PII: S 0 1 4 2 - 9 6 1 2 (0 2) 0 0 3 7 0 – 8
27. Z. Shi, G. Xueping, S. Deying, Y. Zhou, D. Yan. Preparation of poly(ε-caprolactone) grafted titanate nanotubes. Polymer 2007; 48:7516–7522.
DOI: 10.1016/j.polymer.2007.10.037 27.
28. A. Baji, S. Wong, T. S. Srivatsan, G. O. Njus, G. Mathur. Processing methodologies for polycaprolactone-hydroxyapatite composites: A review. Materials and Manufacturing Processes 2006; 20:211–218.
DOI: 10.1081/AMP-200068681
29. J. P. Mofokeng, A. S. Luyt. Dynamic mechanical properties of PLA/PHBV, PLA/PCL, PHBV/PCL blends and their nanocomposites with TiO_2 as nanofiller. Thermochimica Acta 2015; 613:41–53.
DOI: 10.1016/j.tca.2015.05.019
30. O. Persenaire, M. Alexandre, P. Degee, P. Dubois. Mechanisms and kinetics of thermal degradation of poly(ε-caprolactone). Biomacromolecules 2001; 2:288-294.
DOI: 10.1021/bm0056310
31. T. Su , H. Jiang, H. Gong. Thermal stabilities and the thermal degradation kinetics of poly(ε-caprolactone). Polymer-Plastics Technology and Engineering 2008; 47:398-403.
DOI: 10.1080/03602550801897695
32. S. Jain, M. M. Reddy, A. K. Mohanty, M. Misra, A. K. Ghosh. A new biodegradable flexible composite sheet from poly(lactic acid)/poly(ε -caprolactone) blends and micro-talc. Macromolecular Materials and Engineering 2010; 295: 750–762.
DOI: 10.1002/mame.201000063
33. Y. Na, Y. He, X. Shuai, Y. Kikkawa, Y. Doi, Y. Inoue. Compatibilization effect of poly(ε-caprolactone)-b-poly(ethylene glycol) block copolymers and phase morphology analysis in immiscible poly(lactide)/poly(ε-caprolactone) blends. Biomacromolecules 2002; 3:1179–1186.
DOI: 10.1021/bm020050r CCC: $22.00

34. M. E. Mngomezulu, A. S. Luyt , S. A. Chapple, M. J. John. Effect of expandable graphite on thermal and flammability properties of poly(lactic acid)-starch/poly(ε-caprolactone) blend systems. POLYMER ENGINEERING AND SCIENCE 2017; 0:1-11.
DOI: 10.1002/pen.24751
35. M. Jamshidian, E. A. Tehrany, M. Imran, M. Jacquot, S. Desobry. Poly-lactic acid: Production, applications, nanocomposites, and release studies. Comprehensive Reviews in Food Science and Food Safety 2010; 9:552–571.
DOI: 10.1111/j.1541-4337.2010.00126.x
36. F. Tuba, L. Oláh, P. Nagy. Characterization of reactively compatibilized poly(D,L-lactide)/poly(e-caprolactone) biodegradable blends by essential work of fracture method. Engineering Fracture Mechanics 2011; 78:3123–3133.
DOI: 10.1016/j.engfracmech.2011.09.010
37. D. Wu, D. Lin, J. Zhang, W. Zhou, M. Zhang, Y. Zhang, D. Wang, B. Lin. Selective localization of nanofillers: Effect on morphology and crystallization of PLA/PCL blends. Macromolecular Chemistry and Physics 2011; 212:613–626.
DOI: 10.1002/macp.201000579
38. D. Wu, Y. Zhang, M. Zhang, W. Yu. Selective localization of multiwalled carbon nanotubes in poly(ε-caprolactone)/polylactide blend. Biomacromolecules 2009; 10:417–424.
DOI: 10.1021/bm801183f
39. M. Sain, S. H. Park, F. Suhara, S. Law. Flame retardant and mechanical properties of natural fibre–PP composites containing magnesium hydroxide. Polymer Degradation and Stability 2004; 83:363–367.
DOI: 10.1016/S0141-3910(03)00280-5
40. B. B. Marosfoi, S. Garas, B. Bodzay, F. Zubonyai, G. Marosi. Flame retardancy study on magnesium hydroxide associated with clays of different morphology in polypropylene matrix. Polymers for Advanced Technologies 2008; 19:693–700.
DOI: 10.1002/pat.1153
41. J. Wang, J. F. Tung, M. Y. Ahmad Fuad, P. R. Hornsby. Microstructure and mechanical properties of ternary phase polypropylene/elastomer/magnesium hydroxide fire-retardant compositions. Journal of Applied Polymer Science 1996; 60:1425–1437.
CCC 0021-8995/96/091425-13
42. H. T. Oyama, M. Sekikawa, Y. Ikezawa. Influence of the polymer/inorganic filler interface on the mechanical, thermal, and flame retardant properties of polypropylene/magnesium

hydroxide composites. Journal of Macromolecular Science Part B: Physics 2011; 50:463–483.
DOI: 10.1080/00222341003780996 42.

43. J. I. Velasco, C. Morhain, A. B. Martinez, M. A. Rodriguez-Perez, J. A. de Saj. The effect of filler type, morphology and coating on the anisotropy and microstructure heterogeneity of injection-moulded discs of polypropylene filled with aluminium and magnesium hydroxides. Part 1. A wide-angle X-ray diffraction study. Polymer 2002; 43:6805–6811.
PII: S0032-3861(02)00668-7
44. Y. Wang, X. Yang, H. Peng, F. Wang, X. Liu, Y. Yang, J. Hao. Layer-by-layer assembly of multifunctional flame retardant based on brucite, 3-aminopropyltriethoxysilane and alginate and its applications in ethylene-vinyl acetate resin. ACS Applied Materials and Interfaces 2016; 8:9925−9935.
DOI: 10.1021/acsami.6b00998
45. Z. Wang, G. Wu, Y. Hu, Y. Ding, K. Hu, W. Fan. Thermal degradation of magnesium hydroxide and red phosphorus flame retarded polyethylene composites. Polymer Degradation and Stability 2002; 77:427–434.
PII: S0141-3910(02)00099-X
46. S. Mishra, S. H. Sonawane, R. P. Singh, A. Bendale, K. Patil. Effect of nano-$Mg(OH)_2$ on the mechanical and flame-retarding properties of polypropylene composites. Journal of Applied Polymer Sciences 2004; 94:116–122.
DOI: 10.1002/app.20750
47. H. Shen, Y. Liu. *In situ* synthesis of hydrophobic magnesium hydroxide nanoparticles in a novel impinging stream-rotating packed bed reactor. Chinese Journal of Chemical Engineering 2016; 24:1306–1312.
DOI: 10.1016/j.cjche.2016.07.012 1.
48. Sh. El Rafie and M. S. Mohamed. Precipitation of nano-magnesium hydroxide from bittern using ultrasound irradiation. Pelagia Research Library Der Chemica Sinica 2013; 4:69–81.
ISSN: 09768505
49. B. Dittrich, K. Wartig, R. Mülhaupt, B. Schartel. Flame-retardancy properties of intumescent ammonium poly(phosphate) and mineral filler magnesium hydroxide in combination with graphene. Polymers 2014; 6:2875–2895.
DOI: 10.3390/polym6112875
50. M. Shabanian, D. Ghanbari. Synthesis of magnesium hydroxide nanofiller and its use for improving thermal properties of new poly(ether-amide). Journal of Applied Polymer Science 2013; 127:2004–2009.

DOI: 10.1002/app.37640 59

51. D. Zhang, P. Zhang , S. Song, Q. Yuan, P. Yang, X. Ren. Simulation of magnesium hydroxide surface and interface. Journal of Alloys and Compounds 2014; 612:315–322. DOI: 10.1016/j.jallcom.2014.05.198
52. T. Zhang, W. Liu, M. Wang, P. Liu. Y, Pan, D. Liu. Synergistic effect of an aromatic boronic acid derivative and magnesium hydroxide on the flame retardancy of epoxy resin. Polymer Degradation and Stability 2016; 130:257–263. DOI: 10.1016/j.polymdegradstab.2016.06.011
53. G. Zhang, P. Ding, M. Zhang, B. Qu. Synergistic effects of layered double hydroxide with hyperfine magnesium hydroxide in halogen-free flame retardant EVA/HFMH/LDH nanocomposites. Polymer Degradation and Stability 2007; 92:1715–1720. DOI: 10.1016/j.polymdegradstab.2007.06.004
54. Y. Yang, M. Niu, J. Li, B. Xue, J. Dai. Preparation of carbon microspheres coated magnesium hydroxide and its application in polyethylene terephthalate as flame retardant. Polymer Degradation and Stability 2016; 134:1–9. DOI: 10.1016/j.polymdegradstab.2016.09.019
55. J. Wu, J. Du, Y. Gao. Crystal growth morphology of magnesium hydroxide. Turkish Journal of Chemistry 2014; 38:402–412. DOI: 10.3906/kim-1209-7
56. M. Yousefi. A fast method for synthesis magnesium hydroxide nanoparticles, thermal stable and flame retardant poly vinyl alcohol nanocomposite. Journal of Nanostructures 2014; 4: 383–388. DOI: 10.7508/jns.2014.03.015
57. G. Polizos, E. Tuncer, I. Sauers, K. L. More. Physical properties of epoxy resin/titanium dioxide nanocomposites. Polymer Engineering and Science 2011; 51:87-93. DOI: 10.1002/pen.21783
58. H. Xiu, H. W. Bai, C. M. Huang, C. L. Xu, X. Y. Li, Q. Fu. Selective localization of titanium dioxide nanoparticles at the interface and its effect on the impact toughness of poly(L-lactide)/poly(ether)urethane blends. Express Polymer Letters 2013; 7:261–271. DOI: 10.3144/expresspolymlett.2013.24
59. V. G. Nguyen, H. Thai, D. H. Mai, H. T. Tran, D. L.Tran, M. T. Vu. Effect of titanium dioxide on the properties of polyethylene/TiO_2 nanocomposites. Composites: Part B 2013; 45:1192–1198. DOI:10.1016/j.compositesb.2012.09.058

60. V. Demétrio da Silva, L. M. dos Santos. S. M. Subda, R. Ligabue, M. Seferin, C. L. P. Carone, S. Einloft. Synthesis and characterization of polyurethane/titanium dioxide nanocomposites obtained by *in situ* polymerization. Polymer Bulletin 2013; 70:1819–1833. DOI: 10.1007/s00289-013-0927-y
61. H. Arora, C. Doty, Y. Yuan, J. Boyle, K. Petras, B. Rabatic, T. Paunesku, G. Woloschak. Titanium dioxide nanocomposites. Nanomaterials for the life sciences nanocomposites 2012; 8:1-51.
DOI: 10.1002/9783527610419.ntls0217
ISBN: 978-3-527-32168-1
62. S. J. Su, N. Kuramoto. Processable polyaniline–titanium dioxide nanocomposites: effect of titanium dioxide on the conductivity. Synthetic Metals 2000; 147–153.
PII: S0379- 6779(00)00238-1
63. A. Buzarovska, A. Grozdanov, M. Avella, G. Gentile, M. Errico. Poly(hydroxybutyrate-co-hydroxyvalerate)/titanium dioxide nanocomposites: A degradation study. Journal of Applied Polymer Science 2009; 114:3118–3124.
DOI: 10.1002/app.30867
64. A. Chandra, L. Turng, S. Gong, D. C. Hall, D. F. Caulfield, H. Yang. Study of polystyrene/titanium dioxide nanocomposites via melt compounding for optical applications. Polymer Composites 2007; 28:241–250.
DOI: 10.1002/pc.20274
65. A. Zenteno, I. Lieberwirth, F. Catalina, T. Corrales, S. Guerrero, D. A. Vasco, P. A. Zapata. Study of the effect of the incorporation of TiO_2 nanotubes on the mechanical and photodegradation properties of polyethylenes. Composites Part B 2017; 112:66–73.
DOI: 10.1016/j.compositesb.2016.12.007
66. P. A. A. P. Marques, T. Trindade, C. P. Neto. Titanium dioxide/cellulose nanocomposites prepared by a controlled hydrolysis method. Composites Science and Technology 2006; 66:1038–1044.
DOI: 10.1016/j.compscitech.2005.07.029
67. D. Pasqui, R. Barbucci. Synthesis, characterization and self-cleaning properties of titania nanoparticles grafted on polyester fabrics. Journal of Photochemistry and Photobiology A: Chemistry 2014; 274:1–6.
DOI: 10.1016/j.jphotochem.2013.08.017 1.
68. S. Kango, S. Kalia, A. Celli, J. Njuguna, Y. Habibi, R. Kumar. Surface modification of inorganic nanoparticles for development of organic–inorganic nanocomposites - A review. Progress in Polymer Science 2013; 38:1232–1261.

DOI: 10.1016/j.progpolymsci.2013.02.003 1.

69. J. Zhao, M. Milanova, M. M. C. G. Warmoeskerken, V. Dutschk. Surface modification of TiO_2 nanoparticles with silane coupling agents. Colloids and Surfaces A: Physicochemical and Engineering Aspects 2012; 413:273–279.
DOI: 10.1016/j.colsurfa.2011.11.033
70. A. Kausar. Study on physical properties of poly(methyl methacrylate)/poly(thiophene amide)–silica–titaniagrafted multiwalled carbon nanotubebased nanofiber composites. High Performance Polymers 2014; 26:961–969.
DOI: 10.1177/0954008314536213
71. S. Mallakpour, M. Madani. Effect of functionalized TiO_2 on mechanical, thermal and swelling properties of chitosan-based nanocomposite films. Polymer-Plastics Technology and Engineering 2015; 54:1035–1042.
DOI: 10.1080/03602559.2014.974194
72. J. P. Mofokeng, A. S. Luyt. Morphology and thermal degradation studies of melt-mixed PLA/PHBV biodegradable polymer blend nanocomposites with TiO_2 as filler. Journal of Applied Polymer Science 2015; 132:1-11.
DOI: 10.1002/app.42138
73. J. P. Mofokeng, A. S. Luyt. Morphology and thermal degradation studies of melt-mixed poly(hydroxybutyrate-co-valerate) (PHBV)/poly(e-caprolactone) (PCL) biodegradable polymer blend nanocomposites with TiO_2 as filler. Journal of Material Science 2015; 50:3812–3824.
DOI: 10.1007/s10853-015-8950-z
74. T. E. Motaung, A. S. Luyt , M. L. Saladino, E. Caponetti. Study of morphology, mechanical properties, and thermal degradation of polycarbonate-titania nanocomposites as function of titania crystalline phase and content. Polymer Composites 2013; 34:164-172.
DOI: 10.1002/pc.22389

Chapter 3

Research design and methods (experimental)

3.1 Materials

Commercial grade polylactic acid (PLA 4043D) obtained from Natureworks, LLC (USA) has a density of 1.24 g cm^{-3}, glass transition temperature of 63.1 ºC, a melting temperature of 151 ºC and a degree of crystallinity of 17.7 %. CapaTM 6500 poly(caprolactone) (PCL) was purchased from Southern Chemicals in Johannesburg, South Africa. It has a density of 1.1 g cm^{-3}, a glass transition temperature of -61 ºC, a melting temperature 58 ºC and a degree of crystallinity of 33.4 %. Titanium(IV) oxide (Anatase) with a particle size < 25 nm and a 99.7% purity, magnesium hydroxide nanoparticles with a molecular weight of 58.32 g/mol, a particle size <100 nm, and a purity of 99.8%, as well as 3-aminopropyltrimethoxysilane (APTMS) with a purity of 97% and a relative density of 1.027 g/mL at 25 °C were used. The titania, magnesium hydroxide and silane coupling agent were purchased from Sigma-Aldrich, South Africa.

3.2 Functionalization of TiO_2 using 3-aminopropyltrimethoxysilane

Commercial TiO_2 nanoparticles (10 g) were dispersed in 1000 ml deionised water by ultrasonication for 10 min. Then a 100 ml of the silane coupling agent (APTMS) was added to the dispersion. The mixture was kept under reflux at 80 °C for 4.5 hours. The dispersed particles were then separated from solvent by a centrifuge (10 min at 10,000 rpm) followed by washing with ethanol and water alternatively for 2 cycles to remove excessive silanes. The centrifuged particles were re-dispersed in an ethanol and water mixture (90:10) and then they were put in an ultrasonic bath for more than 10 min to ensure a visually well dispersed suspension was regained before filtering. Once the process was finished, the modified particles were dried in an oven at 100 °C for 24 hours, then cooled to room temperature and used as a filler in biodegradable polymers and their blends. This procedure was repeated three times in order to acquire enough APTMS-TiO_2 to prepare the polymer nanocomposites.

3.3 Blend and nanocomposite preparation

The samples were prepared *via* melt-mixing using a Brabender Plastograph. All the materials were dried in an oven at 50 °C for 24 hours prior to mixing. The 30/70, 50/50, and 70/30 w/w PLA/PCL blends ratios and their nanocomposites with APTMS functionalized TiO_2 (1, 3, and 5 wt.%) and $Mg(OH)_2$ (1, 3, 5 and 10 wt.%) nanoparticles were mixed at 190 ºC for ten minutes. The samples were compression moulded into 2 mm thick sheets at the same temperature for 5 minutes using a hydraulic press at a pressure of 50 bar, after which they were removed and cooled under ambient conditions. The thermal history of all samples was kept identical, and all the samples compositions are shown in Table 3.1.

Table 3.1 Blend and nanocomposite composition

Samples with functionalized titania (f-TiO_2) nanoparticles	**Samples with magnesium hydroxide nanoparticles ($Mg(OH)_2$)**
Neat PLA	Neat PLA
99.0/1.0 w/w PLA/f-TiO_2	99.0/1.0 w/w PLA/$Mg(OH)_2$
97.0/3.0 w/w PLA/ f-TiO_2	97.0/3.0 w/w PLA/ $Mg(OH)_2$
95.0/5.0 w/w PLA/ f-TiO_2	95.0/5.0 w/w PLA/ $Mg(OH)_2$
-	90.0/10.0 w/w PLA/ $Mg(OH)_2$
Neat PCL	Neat PCL
99.0/1.0 w/w PCL/ f-TiO_2	99.0/1.0 w/w PCL/ $Mg(OH)_2$
97.0/3.0 w/w PCL/ f-TiO_2	97.0/3.0 w/w PCL/ $Mg(OH)_2$
95.0/5.0 w/w PCL/ f-TiO_2	95.0/5.0 w/w PCL/ $Mg(OH)_2$
-	90.0/10.0 w/w PCL/ $Mg(OH)_2$
70/30 w/w PLA/PCL	70/30 w/w PLA/PCL
69.3/29.3/1.0 w/w PLA/PCL/ f-TiO_2	69.3/29.3/1.0 w/w PLA/PCL/ $Mg(OH)_2$
67.9/29.1/3.0 w/w PLA/PCL/ f-TiO_2	67.9/29.1/3.0 w/w PLA/PCL/ $Mg(OH)_2$
66.5/28.5/5.0 w/w PLA/PCL/ f-TiO_2	66.5/28.5/5.0 w/w PLA/PCL/ $Mg(OH)_2$
-	63.0/27.0/10.0 w/w PLA/PCL/ $Mg(OH)_2$
50/50 w/w PLA/PCL	50/50 w/w PLA/PCL
49.5/49.5/1.0 w/w PLA/PCL/ f-TiO_2	49.5/49.5/1.0 w/w PLA/PCL/ $Mg(OH)_2$
48.5/48.5/3.0 w/w PLA/PCL/ f-TiO_2	48.5/48.5/3.0 w/w PLA/PCL/ $Mg(OH)_2$
47.5/47.5/5.0 w/w PLA/PCL/ f-TiO_2	47.5/47.5/5.0 w/w PLA/PCL/ $Mg(OH)_2$
-	45.0/45.0/10.0 w/w PLA/PCL/ $Mg(OH)_2$
30/70 w/w PLA/PCL	30/70 w/w PLA/PCL
29.3/69.7/1.0 w/w PLA/PCL/ f-TiO_2	29.3/69.7/1.0 w/w PLA/PCL/ $Mg(OH)_2$
29.1/67.9/3.0 w/w PLA/PCL/ f-TiO_2	29.1/67.9/3.0 w/w PLA/PCL/ $Mg(OH)_2$
28.5/66.5/5.0 w/w PLA/PCL/ f-TiO_2	28.5/66.5/5.0 w/w PLA/PCL/ $Mg(OH)_2$
-	27.0/63.0/10.0 w/w PLA/PCL/ $Mg(OH)_2$

3.4 Characterization

3.4.1 Attenuated total reflectance-Fourier-transform infrared (ATR-FTIR)

FTIR is a technique which is used to obtain the infrared absorption or emission spectra for solids, liquids or gases. Infrared radiation is passed through a polymer so as to excite its atoms in a molecule to a higher energy state. Some of the wavelengths of the infrared radiation are absorbed by the atoms in a molecule (dependant on the chemical structure of the sample) and those that are not absorbed will be detected and recorded on spectra. In the ATR mode, infrared light is passed through an ATR crystal such that the light beam is reflected on the surface of sample. The resultant reflection forms an evanescent wave which extends into the interior of the sample, and a detector can be used to measure the reflections which are then translated into spectra. The spectra obtained will give an indication of the chemical bonds or interactions in a sample [1-3]. The ATR mode allows the analysis of materials of varying physical states (powders and gases.).

A Perkin Elmer Spectrum 100 Fourier-transform infrared spectrophotometer was used to determine the surface chemical composition of samples. A spectrum of wave number (650-4000 cm^{-1}) vs. % Transmittance was obtained after 8 scans at a resolution of 4 cm^{-1} using an attenuated total reflectance (ATR) detector. In this study, FTIR was used to confirm the functionalization of TiO_2 nanoparticles using a silane functionalizing agent, APTMS.

3.4.2 Scanning electron microscope (SEM)

SEM is a technique which is used to produce images of a surface of a samples. It works by focusing a beam of electrons onto the surface of the sample to generate an image. Different atoms will interact with the electron beam differently and produce different signals; that will allow for understanding of the surface topology and composition [4-5].

A JSM-7800F Extreme-resolution analytical field emission scanning electron microscope (JEOL Tokyo, Japan) was used to study the surface morphologies of the PLA/PCL blends and nanocomposites at low (1600x) and high (8000x) magnifications. Liquid nitrogen was used to fracture the samples before mounting them onto aluminium pin stubs with a steel epoxy glue and coating with gold. The sputter coater: BIO-RAD (microscience division) coating system (London, UK) Au/Ar sputter of 50-60nm was used. The analysis was performed at different magnifications. The dispersion of $Mg(OH)_2$ and APTMS functionalized TiO_2 nanoparticles in

the polymers matrices was studied. The influence of the nanoparticles on the miscibility of PLA and PCL was also investigated.

3.4.3 Transmission Electron Microscopy (TEM)

TEM is a technique which is used to obtain information of the composition and dispersion within a sample. A beam of electrons is transmitted through a very thin sample, as it passes through it interacts with the electrons allowing for capturing of an images at very high resolutions [5].

A Philips (FEI, The Netherlands) CM100 Transmission Electron Microscope was used to perform the analysis. The TEM samples were sectioned with a Leica ultramicrotome EM UC7 (Vienna, Austria). The morphologies within the PLA/PCL blend nanocomposites were investigated at 1950x and 13500x magnifications. The size, shape, dispersion and location of $Mg(OH)_2$ and functionalised TiO_2 nanoparticles in the nanocomposites (on an atomic scale) were analysed.

3.4.4 Contact angle measurements

Contact angle measurements system is a technique which measures angle formed between a liquid with known properties (such as density) with a gas, liquid or solid, at a specific temperature and pressure. The angle obtained will give an indication of the type of molecular interaction between the drop and the surface of the sample. Information such as contact angles, total surface energies, dispersive and polar surface energy components can be determined [6-8]. Whilst using a polar solvent, an angle below 90° indicates that the sample is hydrophilic and an angle above 90° is observed when the sample is hydrophobic [7]. Literature values of the contact angles and surface energies for fillers and solvents were obtained [6-8].

A surface energy evaluation system (SEES) was used to conduct the contact angle measurements using the sessile drop method. The analysis was done at room temperature, and 9 replicates were done for each sample. The contact angles, total surface energies, dispersive and polar components for PLA and PCL were determined. Polar and non-polar solvents with known surface energies were used. Distilled water (H_2O) was used as the polar solvent. From literature [7-8], water has a polar surface energy of 50.7 mJ m^{-2} and a dispersive surface energy of 22.1 mJ m^{-2}. As for the non-polar solvent, diiodomethane (CH_2I_2) was used. Diiodomethane

is known to have a polar surface energy of 6.7 mJ m^{-2} and a dispersive surface energy of 44.1 mJ m^{-2}. The Owens-Wendt method (Equation 3.1 and 3.2) was chosen to calculate the contact angles, total surface energies and the individual surface components (dispersive and polar surface components).

$$\gamma_s = \gamma_s^d + \gamma_s^p \qquad \text{Equation 3.1}$$

$$\gamma_1 = (1 + Cos\theta) = 2\sqrt{\gamma_s^d . \gamma_l^d + \gamma_s^p . \gamma_l^p} \qquad \text{Equation 3.2}$$

Where θ is the contact angle, γ is the surface energy, the subscripts 's' and 'l' indicate solid and liquid, respectively, the superscripts 'd' and 'p' indicate the dispersive and polar components, respectively. If the contact angle of at least two liquids, usually a polar and nonpolar with known γ_l^d and γ_l^p values, are measured on a solid surface, the γ_s^d and γ_s^p and the total surface energy (γ_s) of the solid can be calculated by combining Equations 3.1 and 3.2. The interfacial tensions between the components in a blend were calculated from the contact angle measurement results using the geometric mean equation (Equation 3.3) [8].

$$\gamma_{12} = \gamma_1 + \gamma_2 - 2\sqrt{\gamma_1^d . \gamma_2^d + \gamma_1^p . \gamma_2^p} \qquad \text{Equation 3.3}$$

where γ_{12} = interfacial tension between components 1 and 2 in the blend, γ_1 and γ_2 are the total surface energies of components 1 and 2, γ_1^d and γ_2^d are the dispersive surface energies of components 1 and 2, and γ_1^p and γ_2^p are the polar surface energies of the components in the nanocomposites.

3.4.5 Melt flow index measurements

Melt flow index (MFI) measurement is a technique which is used to understand how a polymer will flow when exposed to temperatures above its melting temperature. The MFI gives an indication of how much polymer will be released through a die in ten minutes, when the polymer is heated above its melting temperature. A weight with a known mass is used to apply a constant force to assist the flow of the molten polymer [9].

The melt flow index of neat PCL and PLA were determined using a CEAST Melt Flow Junior. Ten samples for each polymer were analysed at 190 °C. The amount of polymer which flowed through the die over a period of 10 min, under 2.16 kg weight was determined. For PCL, because of its low viscosity, the amount of polymer which flowed through the die over a period of 2 min was determined and repeated 5 times to have cumulative mass in 10 minutes.

3.4.6 Differential scanning calorimetry (DSC)

DSC is a technique in which the heat flow rate difference into a substance and a reference is measured as a function of temperature, while the sample is subjected to a controlled temperature program. Thermal transitions such as the glass transition, cold crystallization and melting temperatures together with their enthalpies (heat capacity, and heat of fusion), degrees of crystallinity and miscibility of polymers can be determined [10].

Perkin Elmer DSC 6000 was used to determine the above mentioned properties. The analyses were performed under nitrogen flow (20 ml min^{-1}) from 0 to 190 °C at 10 °C min^{-1}. Sample masses were kept around ~9 mg and repeated three times so as to obtain an average for accurate and comparable data. The melting enthalpies of the polymers were determined from the second heating scans, and Equation 3.4 and 3.5 were used to calculate the degree of crystallinities for neat polymers, their polymer blends and nanocomposites, respectively.

$$\mathcal{X}_c(\%) = \frac{\Delta H_m}{\Delta H_m^\theta} \times 100\% \qquad \text{Equation 3.4}$$

$$\mathcal{X}_c(\%) = \frac{\Delta H_m}{w\Delta H_m^\theta} \times 100\% \qquad \text{Equation 3.5}$$

where ΔH_m is the melting enthalpy of the polymer sample, ΔH_m^0 is the melting enthalpy of the 100 % crystalline polymer and W is the weight fraction of the polymer in the polymer blends or the nanocomposites. Values of 93.7 J g^{-1} and 139 J g^{-1} were used as the melting enthalpies for a 100 % crystalline polymer for PLA and PCL, respectively.

3.4.7 Thermogravimetric analysis (TGA)

TGA is a technique in which mass of a sample is measured as a function of either temperature or time while the sample is subjected to a controlled temperature program in a controlled

atmosphere. Studying the thermal degradation of samples provides an understanding of the temperature conditions under which a polymeric material can be used [11].

A Perkin-Elmer STA6000 thermogravimetric analyser (TGA) was used to analyse the thermal degradation behaviour of the samples. The extent of functionalization and the thermal stability of the samples were investigated. The analyses were done from 30 to 600 °C at a heating rate of 10 °C min^{-1} under nitrogen flow (20 ml min^{-1}). The sample masses were approximately 23 mg. The TGA was also connected to a Perkin-Elmer Spectrum 100 Fourier transform infrared (FTIR) spectrometer to analyse the thermal degradation volatiles. The same temperature range and heating rate were used, and the volatiles were transferred to FTIR by a Perkin-Elmer TL 8000 balanced flow FT-IR EGA system at 200 ºC and a flow rate of 150 ml min^{-1}. The spectra were collected at five different temperatures during the degradation process.

3.4.8 Dynamic mechanical analysis (DMA)

Dynamic mechanical analysis (DMA) is a technique which gives the thermo-mechanical and rheological properties of materials through measuring stress/strain caused by application of a small cyclic strain/stress on the sample. It is used to determine polymer properties such as dynamic fragility parameters, filler effectiveness, glass transition temperatures, interfacial compatibility of individual composite components, stress relaxation and miscibility in polymer blends [12].

The dynamic mechanical properties of the samples were tested using a Perkin Elmer Diamond DMA. The following specifications were used for the analysis:

Frequency	1 Hz
Temperature range	-90 to 140 °C
Temperature program mode	Ramp
Measurement mode	Bending mode
Heating rate	3 °C.min^{-1}
Sample length	50 mm
Sample width	~12.3 mm
Sample thickness	1.3 – 2.5 mm

The loss and storage moduli as well as the tan δ curves for the $Mg(OH)_2$ and APTMS-TiO_2 filled nanocomposites were analysed. For all the samples with only PCL as the polymer matrix, a maximum temperature of 65 °C was used because of the low melting temperature of PCL.

3.5 References

1. Z. Khoshhesab. Reflectance IR Spectroscopy. In: T. Theophanides (Editors), Infrared Spectroscopy - Materials Science, Engineering and Technology (2012).
   DOI: 10.5772/37180
2. D. Scarano, A. Zecchina, S. Bordiga, F. Geobaldo, G. Spoto, G. Petrini, G. Leofanti, M. Padovan, G. Tozzola. Fourier-transform infrared and Raman spectra of pure and Al-, B-, Ti- and Fe-substituted silicalites: stretching-mode region. Journal of the Chemical Society, Faraday Transactions 1993; 89:4123-4130.
   DOI: 10.1039/FT9938904123
3. S. Petrova, S. Miloshev, R. Mateva, I. Iliev. Synthesis of amphiphilic PEG-PCL-PEG triblock copolymers. Journal of the University of Chemical Technology and Metallurgy 2008; 43:199-204.
   ISSN 1314-3859
4. W. Denk, H. Horstmann. Serial block-face scanning electron microscopy to reconstruct three-dimensional tissue nanostructure. Public Library of Science Biology 2004; 2:1900-1909.
   DOI:10.1371/journal.pbio.0020329
5. S. Zhang, L. Li, A. Kumar. Transmission electron microscopy and scanning electron microscopy. In: S. Zhang, L. Li, A. Kumar. Material characterization techniques. CRC Press Taylor and Francis group: USA (2008).
   ISBN 9781420042948
6. C. Wang, H. Mao, C. Wang, S. Fu. Dispersibility and hydrophobicity analysis of titanium dioxide nanoparticles grafted with silane coupling agent. Journal of Industrial and Engineering Chemistry Research 2011; 50:11930–11934.
   DOI: 10.1021/ie200887x
7. H. Liu, J. Yi. Polystyrene/magnesium hydroxide nanocomposite particles prepared by surface-initiated in-situ polymerization. Applied Surface Science 2009; 255:5714–5720.
   DOI: 10.1016/j.apsusc.2008.12.073
8. J. P. Mofokeng, A. S. Luyt. Morphology and thermal degradation studies of melt-mixed poly(lactic acid) (PLA)/poly(ε-caprolactone) (PCL) biodegradable polymer blend nanocomposites with TiO_2 as filler. Polymer Testing 2015; 45:93–100.

DOI: 10.1016/j.polymertesting.2015.05.007

9. A. V. Shenoy, S. Chattopadhyay, V. M. Nadkarni. From melt flow index to rheogram. Rheologica Acta 1983; 22:90-101.
   DOI: 10.1007/BF01679833
10. J. D. Menczel, L. Judovits, R. B. Prime, H. E. Bair, M. Reading, S. Swier. Differential scanning calorimetry (DSC). In: J. D. Menczel, R. B. Prime. Thermal analysis of polymers fundamentals and applications. John Wiley and Sons: New York City (2009).
    ISBN 978-0-471-76917-0
11. R. B. Prime, H. E. Bair, S. Vyazovkin, P. K. Gallagher, A. Riga. Thermogravimetric analysis (TGA). In: J. D. Menczel, R. B. Prime. Thermal analysis of polymers fundamentals and applications. John Wiley and Sons: New York City (2009).
    ISBN 978-0-471-76917-0
12. R. P. Chartoff, J. D. Menczel, S. H. Dillman. Dynamic mechanical analysis (DMA). In: J. D. Menczel, R. B. Prime. Thermal analysis of polymers fundamentals and applications. John Wiley and Sons: New York City (2009).
    ISBN 978-0-471-76917-0

Chapter 4

Results and discussion

4.1 Morphology

4.1.1 FTIR analysis of unfunctionalised, and 3-aminopropyltrimethoxysilane (APTMS) functionalised titania

Chemical modification of nanoparticles creates an opportunity of improving their chemical interaction and dispersion within a polymer matrix. Titania was functionalised using 3-aminopropyltrimethoxysilane (APTMS), and the success of the functionalisation was confirmed by Fourier-transform infrared spectroscopy (FTIR). Studying the chemical interactions gave an indication that the surface modification of titania was achieved. Figure 4.1 shows the FTIR spectra of neat titania, APTMS functionalising agent, and functionalised titania. For neat/unfunctionalised titania (Figure 4.1 (a), Table 4.1), several peaks were observed. Peaks below 860 cm^{-1} were attributed to Ti-O and Ti-O-Ti stretching vibration bands [1-3]. The peak for the Ti-O vibration band was observed at 807 cm^{-1} and the peak for Ti-O-Ti stretching vibration band was observed at 732 cm^{-1} [3]. A broad band due to –OH on the surface of titania nanoparticles was observed, it had a peak around 3242 cm^{-1}. Another peak also belonging to the -OH stretching vibrations was observed around 1640 cm^{-1} [1-3].

For the silane functionalising agent, 3-aminopropyltrimethoxysilane (APTMS) (Figure 4.1(b), Table 4.1), a range of different peaks was observed. -OH stretching vibration were observed with a peak around 3385 cm^{-1}. The -N-H bending vibration was also observed as a broad band with a peak around 1599 cm^{-1}. For the –C-H band, the most clearly visible peaks were at 2940 and 2840 cm^{-1}, due to $–CH_3$ symmetrical stretching and $-CH_2$ from the propyl chain, respectively. A peak at 1222 cm^{-1} was observed overlapping with another peak (C-N stretching; 1190 cm^{-1}), and it was attributed to the $Si-CH_2-R$ stretching (where R is $-CH_2-CH_2-NH_2$). A peak was observed at 1074 cm^{-1} and it was attributed to Si-O-R bond deformation (where R is either $-CH_3$ or another APTMS molecule bonded via a covalent bond). Another peak was also observed at 809 cm^{-1} and was attributed to Si-C [4-5].

In the APTMS functionalised titania (Figure 4.1 (a), Table 4.1), peaks from both titania and APTMS were observed. Most of the peaks either had different intensities or shift in positions on the spectrum when compared to the neat components. Peaks for –OH stretching (3759 cm^{-1}); $-CH_2$ asymmetrical C-H stretching (2929 cm^{-1}); -N-H bending (1574 cm^{-1}), $-CH_3$ symmetric

bending and -CH_2 wagging (1315 cm^{-1}) were observed. Peaks for Si-CH_2-R (1201 cm^{-1}, where R is -CH_2-CH_2-NH_2)), C-N stretching (1194 cm^{-1}), Si-O-R (1128 cm^{-1}, where R is another APTMS molecule bonded via a covalent bond) and Si-O-R (where R is -CH_3) asymmetric stretching (1031 cm^{-1}) were also observed. Below 890 cm^{-1}, a band was observed, and it was attributed to Ti-O stretching and Si-C stretching. A new peak (919 cm^{-1}) which was absent in both titania and APTMS was observed in functionalised titania. This peak was attributed to Si-O-Ti bonds [4-5]. A decrease in the broadness and intensity of the –OH stretching peak (3640-3600 cm^{-1}) was observed. The other -OH peak, previously observed around 1639 cm^{-1} in neat TiO_2 disappeared completely. In comparison to neat APTMS, a shift for the amine peak was observed for functionalised titania. A shift from 1599 to 1574 cm^{-1} was observed for the –N-H bending vibration. There was also a shift to a lower wavenumber for the Si-O-R (where R is another APTMS molecule bonded via a Si-O-Si covalent bond), from 1074 to 1031 cm^{-1}; this could have been due to the formation of Si-O-Ti bonds (919 cm^{-1}). Any shifts on FTIR curves are indicative of occurrence of a chemical interaction [5, 6].

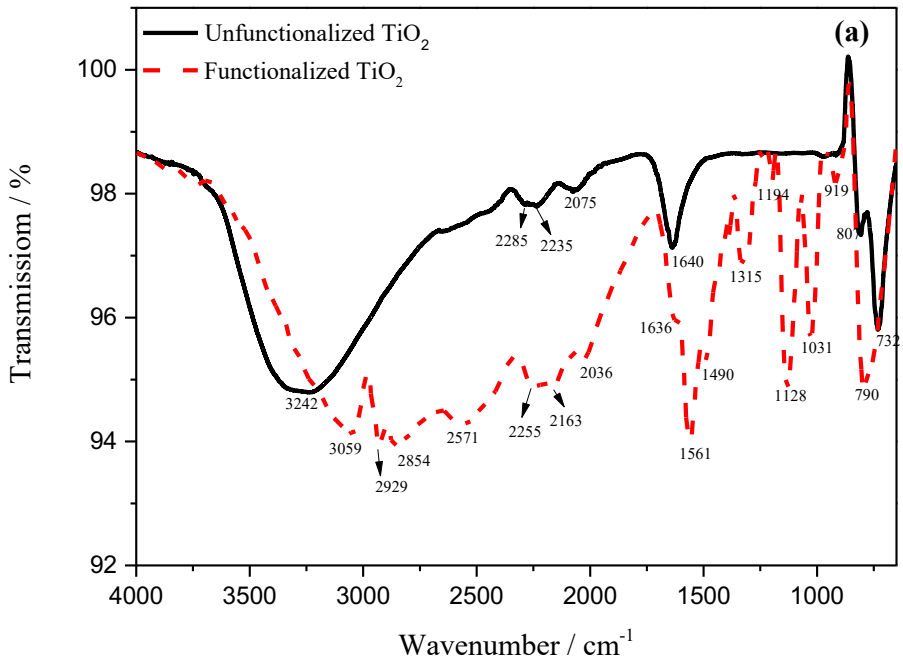

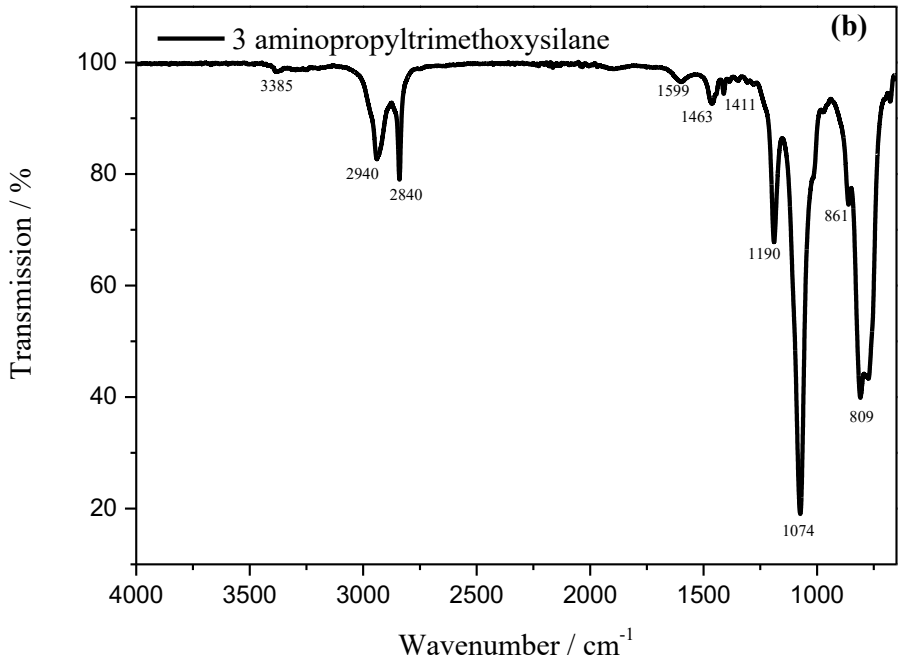

Figure 4.1 FTIR spectra of (a) unfunctionalised titania and APTMS functionalised titania and (b) APTMS silane functionalising agent

Table 4.1 FTIR spectra of neat titania, APTMS and APTMS functionalised titania

Peak / cm^{-1}	Chemical identification
Peaks of neat/unfunctionalised titania (TiO_2)	
3263	-OH (stretching vibration)
1640	-OH (stretching vibration)
860	Ti-O or Ti-O-Ti (stretching vibration)
Peaks of (3-aminopropyl)trimethoxysilane (APTMS)	
3385	-OH stretching
1599	-NH_2 deformation, N-H bending
1074	Si-O-C asymmetric stretching
Peaks of functionalised titania (APTMS-TiO_2)	
3759	-OH stretching
1574	-N-H bending
1031	Asymmetric Si-O-C stretching
919	Si-O-Ti (stretching vibration band)

4.1.2 Surface energy measurements and melt flow testing

Surface energy measurements are a good indicator of the behaviour and compatibility of components within a blend or composite. In polymer nanocomposites, if the difference between the polar components of the materials' surface free energies is too large, immiscibility and incompatibility increases. This often leads to a complete phase separation of the components in the blends, or agglomeration where the fillers are concerned [6]. The values obtained from surface energy measurements are summarized in Tables 4.2. Some of the values were obtained from literature as our lab is not fully equipped to determine the surface properties of the fillers, especially in their powder form in which they were used in. When conducting surface energy measurements, the contact angle of PLA (52.7º) with water was lower than that of PCL (61.9º). From literature [7], when using a hydrophilic solvent like water to perform the test, values that are below to 90º indicate that a material is hydrophilic and those that are above 90º are said to be hydrophobic. Both PLA and PCL were hydrophilic, with PCL being less hydrophilic than PLA. The interfacial tension between PLA and PCL was found to be 0.4 mN m^{-1}. For $Mg(OH)_2$ and neat TiO_2 nanoparticles, the contact angles (10º and 19.7º, respectively) and surface energies (95 and 80.7 mN m^{-1}) with water were obtained from literature and they indicated that they were very hydrophilic [6, 8, 9]. Because of the large difference in the surface properties between the individual polymers and the nanoparticles, the particle to particle interaction of the nanofiller might occur which would lead to nanoparticles clustering together in the nanocomposites. This is because of the van der Waals forces between the nanoparticles.

Melt flow testing of PLA and PCL was performed at 190 ºC. From the melt flow indexes (MFI) obtained, PCL had a value of 11.9 g/10 min and PLA of 1.6 g/10 min. A low MFI indicates that the polymer is highly viscous and a high value shows that a polymer is less viscous. At 190 ºC, PLA was therefore more viscous than PCL. The surface energy and MFI results will be used in the sections below to explain other results later in this chapter.

Table 4.2 Contact angle and surface energy values of PLA, PCL, TiO_2 and $Mg(OH)_2$ together with the melt flow index (MFI) of PLA and PCL

Contact angle/ °			Surface energy/ mN m^{-1}			MFI/(g/10min)
	H_2O	CH_2I_2	γ	γ^d	γ^p	
PCL	61.9 ± 0.3	28.7 ± 0.1	54.5	44.8	9.8	11.9
PLA	52.7 ± 0.4	26.2 ± 0.3	59.9	45.7	14.2	1.6
TiO_2 [6]	19.7	10.1	80.7	46.4	34.3	
$Mg(OH)_2$ [8, 9]	10.0		95.0			

γ = total surface energy, γ^d = dispersive component of surface energy, γ^p = polar component of surface energy, MFI = melt flow index

4.1.3 Scanning electron microscopy (SEM)

To have an understanding of the interaction of the components of the polymer nanocomposites, morphology was studied using SEM. The interaction amongst the constituent components of polymer nanocomposites influences their mechanical and thermal stability properties. Figure 4.2 shows the 70/30, 50/50, and 30/70 w/w PLA/PCL blends ratios, all with the 5 wt.% $Mg(OH)_2$ filler content at 1600 and 8000x magnifications. For the APTMS-TiO_2 containing nanocomposites with the same polymer ratios and amount of filler (5 wt.%), the SEM micrographs are illustrated in Figure 4.3. From Figure 4.2, the $Mg(OH)_2$ nanoparticles appeared as rod-like (needle-like) structures embedded randomly in the polymer matrix, which contained crevices (gaps) between them. This was clearly visible in the 66.5/28.5/5 w/w PLA/PCL/$Mg(OH)_2$ (Figure 4.2(a) and (b)) and 28.5/66.5/5 w/w PLA/PCL/$Mg(OH)_2$ (Figure 4.2(e) and (f)) samples**.** Large agglomerates of the nanoparticles were observed, and they were dispersed throughout the surface of the polymers. This is attributed to the large difference in surface energy properties of the polymers and the $Mg(OH)_2$ nanorods. The $Mg(OH)_2$ nanorods seemed to prefer coming together rather than dispersing in the polymer matrix. The polymer phases of the $Mg(OH)_2$ blend nanocomposites could not be seen clearly using SEM.

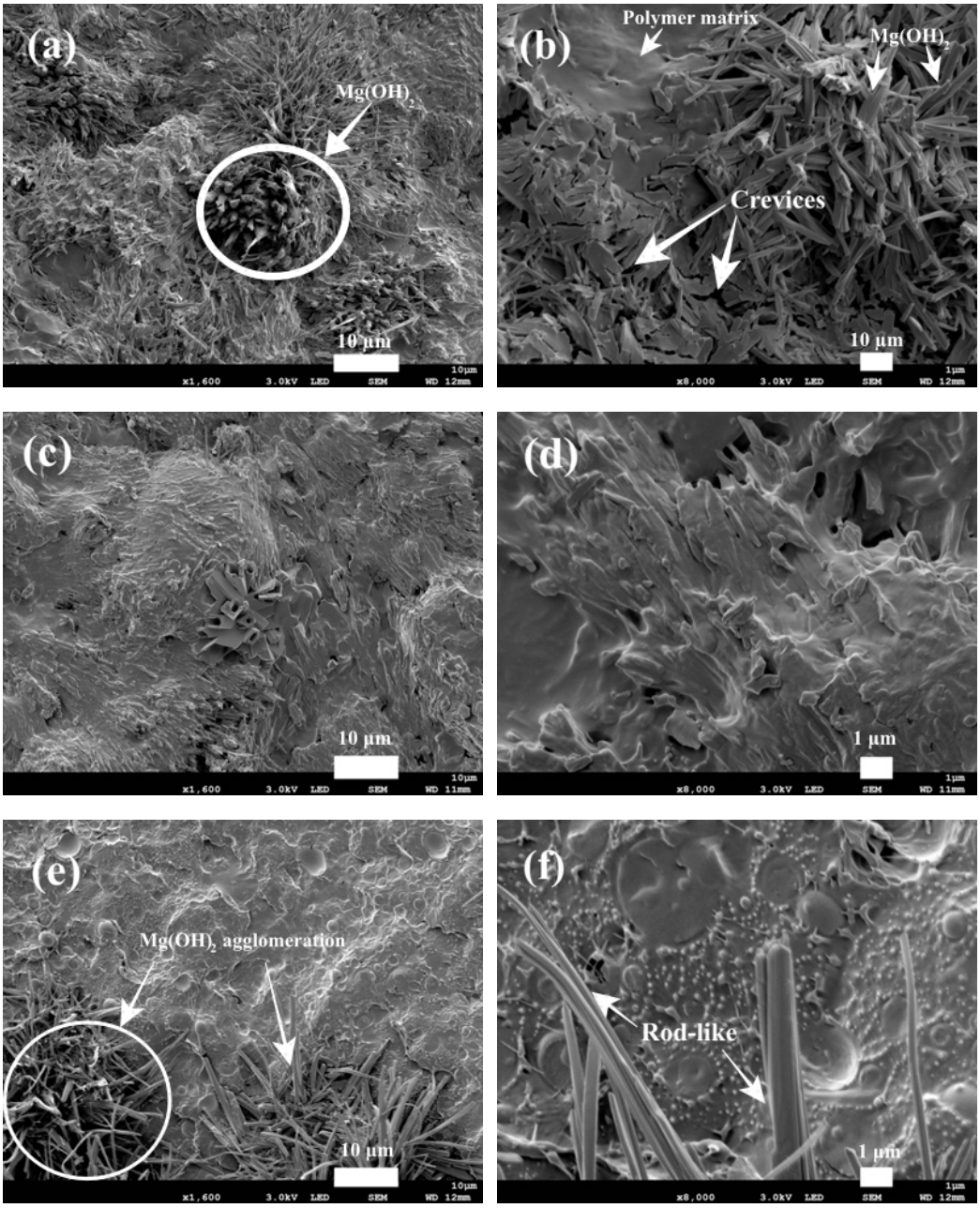

Figure 4.2 SEM micrographs of the fracture surfaces of (a, b) 66.5/28.5/5 w/w PLA/PCL/$Mg(OH)_2$, (c, d) 47.5/47.5/5 w/w PLA/PCL/$Mg(OH)_2$, (e, f) 28.5/66.5//5 w/w PLA/PCL/$Mg(OH)_2$ blend nanocomposites at 1600x and at 8000x magnification

For the samples that contain the silane functionalized titania (APTMS-TiO_2) (Figure 4.3), the nanoparticles were fairly well dispersed. A preferential location in one polymer phase and at the PLA/PCL interface was observed. In the 66.5/28.5/5 w/w PLA/PCL/APTMS-TiO_2 sample (Figure 4.3(a) and (b)), the nanoparticles seemed to be distributed in the major phase (PLA). Very few nanoparticles were present in the minor phase (PCL) and at the PLA/PCL interface. In the 28.5/66.5//5 w/w PLA/PCL/APTMS-TiO_2 sample (Figure 4.3(e) and (f)), the nanoparticles were mostly dispersed in the dispersed phase (i.e. PLA in this case). Though PCL had a lower viscosity (MFI of 11.9 g/10min) than PLA (MFI of 1.6 g/10min), but the degree of crystallinity (33.3%) of PCL was higher than that of PLA (17.7%). One would think that the nanoparticles might have found it easier to disperse in PCL which has a lower viscosity, but the APTMS-TiO_2 preferred to disperse in PLA which has a lower degree of crystallinity. A lower degree of crystallinity indicates presence of a larger amorphous phase (a high entropy phase), where easier dispersion of nanoparticles in the matrix can take place [10]. The dispersion of APTMS-TiO_2 was therefore influenced by a combination of thermodynamic (degree of crystallinity) and kinetic (viscosity) properties of the polymers. To have a better understanding of the observations made for both $Mg(OH)_2$ and APTMS-TiO_2 nanocomposites in SEM, the samples were further characterized using TEM.

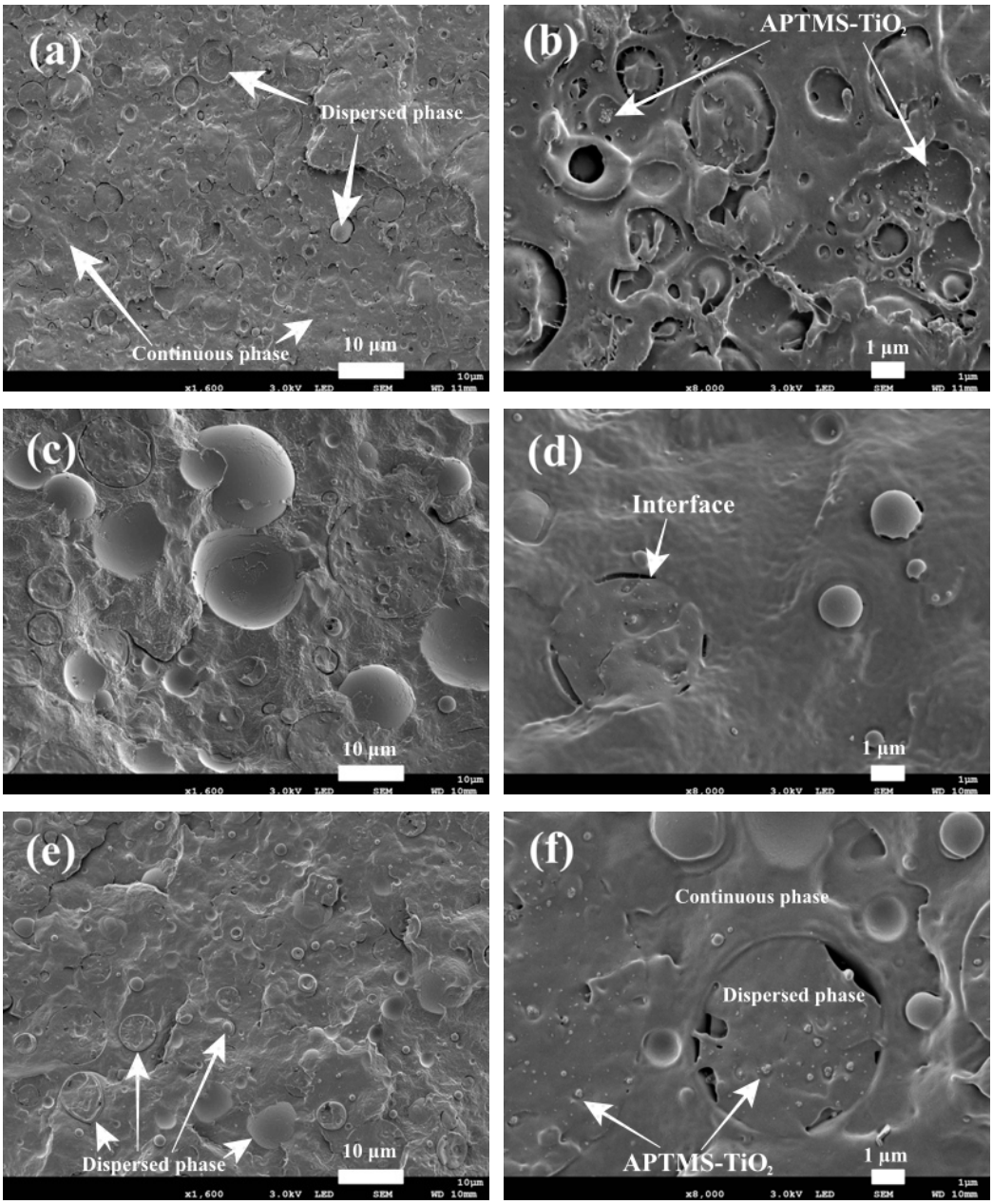

Figure 4.3 SEM micrographs of the fracture surfaces of (a, b) 66.5/28.5/5 w/w PLA/PCL/APTMS-TiO_2, (c, d) 47.5/47.5/5 w/w PLA/PCL/ APTMS-TiO_2, (e, f) 28.5/66.5//5 w/w PLA/PCL/ APTMS-TiO_2 blend nanocomposites at 1600x and at 8000x magnification

4.1.4 Transmission electron microscopy (TEM)

To further investigate the relationship between the filler and the polymer matrices, TEM analyses of the samples were performed. Figures 4.4 and 4.5 show the TEM images for $Mg(OH)_2$ and APTMS-TiO_2 at 5% filler content, respectively. For the $Mg(OH)_2$ samples, only two samples were sectioned successfully, i.e. 66.5/28.5/5 w/w PLA/PCL/$Mg(OH)_2$ and 47.5/47.5/5 w/w PLA/PCL/$Mg(OH)_2$ nanocomposites. The rest of the $Mg(OH)_2$ polymer blend nanocomposites disintegrated during sectioning. The TEM images for these $Mg(OH)_2$ samples (Figure 4.4) which disintegrated were difficult to analyse. There is therefore a possibility that the morphology has been distorted, holes were perforated on the sample whilst performing TEM analysis. This might be attributed to the gaps observed from SEM images found in the $Mg(OH)_2$ agglomerates (where no polymer was covering the $Mg(OH)_2$, and the $Mg(OH)_2$ rods were exposed), and on the interface of PLA and PCL, that could have caused the $Mg(OH)_2$ samples to be more brittle. These gaps are possibly the weak links where the defects propagated. In both 66.5/28.5/5 w/w PLA/PCL/$Mg(OH)_2$ and 47.5/47.5/5 w/w PLA/PCL/$Mg(OH)_2$ nanocomposites, a fairly well dispersion of $Mg(OH)_2$ was observed in both polymer phases. This was clearly visible in the 47.5/47.5/5 w/w PLA/PCL/$Mg(OH)_2$ (Figure 4.4 (b)) sample. Even though $Mg(OH)_2$ nanorods were dispersed throughout both polymer phases, agglomerates were present. This was also observed in our SEM results (see section 4.1.3). The fair dispersion of $Mg(OH)_2$ nanorods in both PLA and PCL was attributed to the surface energy, degree of crystallinities and viscosity of the polymers. Surfaces energy values of PLA (59.90 mN m^{-1}) and that of PCL (54.51 mN m^{-1}) were much closer, but both very far from that of $Mg(OH)_2$ (95 mN m^{-1}). In this case it is obvious that $Mg(OH)_2$ did not have preferential location in terms of these surface energies. This might be the reason it was dispersed in both the polymers, although most of the $Mg(OH)_2$ favoured agglomeration. Also, the degree of crystallinity of the polymers might have influenced the dispersion of the $Mg(OH)_2$ nanorods. From the DSC results, PLA and PCL had low degree of crystallinity of about 17.4 and 33.3%, respectively. The presence of a larger amorphous fractions (disordered phases) in polymers would therefore allow the nanoparticles to diffuse easily into the chains of matrices, in order to balance the properties. The assumption is with much effect in PCL, since PCL has lower viscosity (higher MFI) as seen from the melt flow results conducted. The MFI of PCL (11.9 g/10 min) was higher than that of PLA (1.6 g/ 10 min) indicating that PCL flowed much easily and quickly than PLA. During cooling after melt mixing, we assume that the PCL would have therefore allowed easy dispersion of the $Mg(OH)_2$ nanorods in its matrix. So, the presence

of $Mg(OH)_2$ in both PLA and PCL was due to a balance amongst the surface energy, degree of crystallinity and melt flow properties of the two polymers (PLA and PCL).

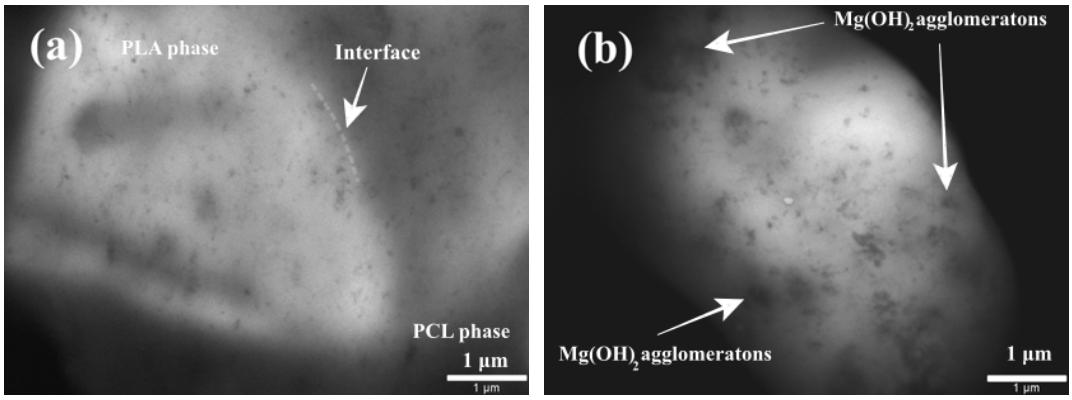

Figure 4.4 TEM images of (a) 66.5/28.5/5 w/w PLA/PCL/$Mg(OH)_2$ (b) 47.5/47.5/5 w/w PLA/PCL/$Mg(OH)_2$ at 13500x magnifications

For the APTMS-TiO_2 samples (Figure 4.5), a clear preference for the PLA/PCL interface and one polymer phase was observed. In the 66.5/28.5/5 w/w PLA/PCL/APTMS-TiO_2 (Figure 4.5 (a)), the nanoparticles were mostly distributed in the major phase, i.e. PLA. In the 28.5/66.5/5 w/w PLA/PCL/APTMS-TiO_2 ((Figure 4.5 (e)), the nanoparticles were mostly confined in the minor phase, i.e. PLA in this case. It is therefore clear that the APTMS-TiO_2 nanoparticles had a preferential location in the PLA phase. Since PLA (17.4%) was less crystalline than that of PCL (33.4%), the APTMS-TiO_2 nanoparticles would have preferred to disperse in the amorphous phase (more disordered), which was larger in PLA. Although PLA showed high viscosity and low MFI relative to PCL, its lower degree of crystallinity made it suitable for the APTMS-TiO_2 to preferentially disperse in its matrix. It was however not possible to determine how the surface energy properties of APTMS-TiO_2 might have played a role in their dispersion since no information was available due to a lack of resources. To summarize the observations made during morphology studies, APTMS-TiO_2 had a better dispersion than $Mg(OH)_2$ even though both nanofillers had agglomeration. $Mg(OH)_2$ was dispersed in both PLA and PCL, but had crevices (gaps) at the interface with the polymers. APTMS-TiO_2 showed a preferential localization in PLA and it was uniformly distributed.

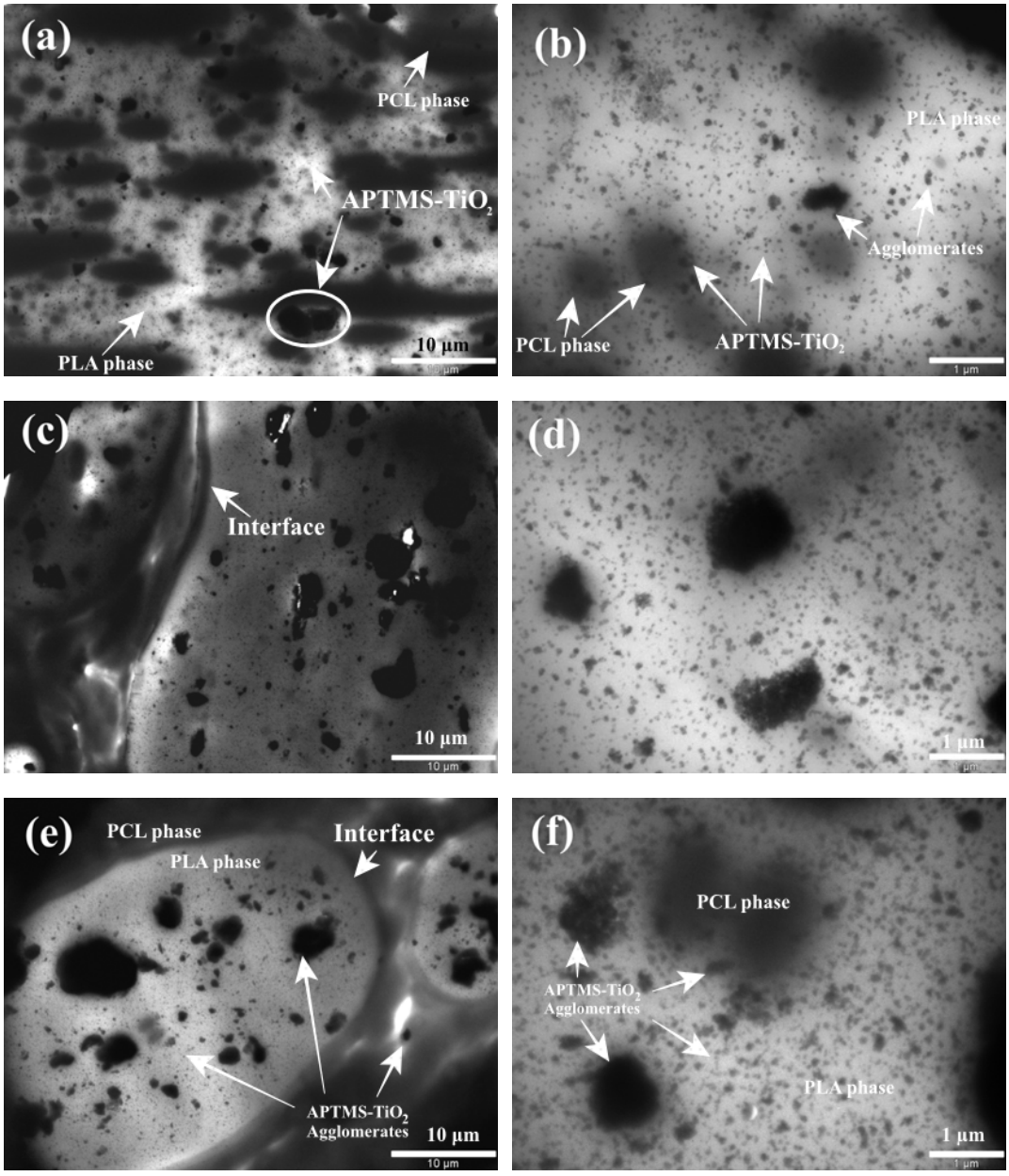

Figure 4.5 TEM images of (a, b) 66.5/28.5/5 w/w PLA/PCL/APTMS-TiO_2, (c, d) 47.5/47.5/5 w/w PLA/PCL/ APTMS-TiO_2 (e, f) 28.5/66.5//5 w/w PLA/PCL/ APTMS-TiO_2 at 1950x and 13500x magnifications

4.2 Differential scanning calorimetry (DSC)

It is essential to understand how polymers in blends influence each other's thermal properties, as well as how the addition of fillers, compatibilizers and additives also influences polymer blends. The glass transition, cold crystallization and melting temperatures of PLA, PCL and their blends and nanocomposites were analysed using differential scanning calorimetry (DSC).

All the results obtained during the analysis were recorded in Figures 4.6 to 4.8 and Tables 4.3 to 4.6. For neat PLA (Figure 4.6), three thermal transitions were observed. The first transition is around 63.1 °C and is attributed to the glass transition temperature (T_g) of PLA. The second temperature transition is observed around 115.7 °C and this is attributed to the cold crystallization temperature (T_{cc}). The third transition, the melting temperature (T_m), is observed around 150.9 °C with the melting enthalpy (ΔH_m) of 14.4 J/g and a degree of crystallinity of 17.7 %. For the neat PCL (Figure 4.6), only the melting temperature was observed at 58.0 °C and had a melting enthalpy (ΔH_m) of 46.4 J/g. The degree of crystallinity (X_c) of PCL was determined to be 33.4 %. Neat PCL was therefore more crystalline than neat PLA. It was noted that some transitions were present but absent in the other polymer. For instance, a cold crystallization temperature was present in PLA, but both the glass transition and cold crystallization temperature were not observed in PCL. The cold crystallization is usually observed when a polymer is cooled at a fast rate, that the chains were not given enough time to pack themselves properly, and then when the polymer is reheated the chains reorganise and recrystallize above its glass transition, but below its melting temperature. The polymer chains start arranging themselves in an ordered manner (stable conformation) to form crystals. Unlike PCL, PLA solidifies very fast when cooled, leading to chains being frozen without proper alignment, therefore slower cooling rates might be a solution, and are necessary to allow proper crystalline packing. So, if PLA is cooled at normal cooling rate (10 ºC/min), crystallisable chains tend to freeze in their random order, but during the reheating, the recrystallization process of those crystallisable chains occurs; hence, the cold crystallization temperature is normally seen for PLA [11, 12]. Initially, when the DSC study was performed, the runs were performed from -90 to 180 ºC in order to allow the observation of the T_g of PCL which typically occurs around -60 ºC. But the T_g did not show, and this might due to the lack of sensitivity of the DSC equipment to the T_g of PCL, therefore, the runs were performed from 0 to 180 ºC, so as to accommodate the other transitions. The glass transition of PCL was therefore studied using dynamic mechanical analysis (DMA) and the results are presented in the next sections.

PLA and PCL were blended together using three different ratios (70/30, 50/50, 30/70 w/w) (Figure 4.6). The melting peaks for both polymers were present in all the polymer blends. This indicated that these two polymers were immiscible. Even though all the other transitions present in the individual polymers were still present in the blends, but the glass transition of PLA could not be seen as it coexisted with the melting peak of PCL as they occur around the same temperature range (60.0 ºC). The PLA cold crystallization temperature of PLA was observed at higher PLA content and disappeared with the increase in PCL content. It was

clearly visible in the neat polymer and in the 70/30 w/w PLA/PCL blend. A shift in the cold crystallization towards higher temperature was observed with the presence of PCL. Neat PLA had a cold crystallization temperature of 115.72 °C while the 70/30 w/w PLA/PCL blend was noted at 125.79 °C. Typically, during the cold crystallization transition, the polymer chains that were in an unstable conformation gain enough mobility to move into desirable conformations [13]. The PCL phase was included in the PLA phase as was seen through morphology studies. This could have therefore restricted segmental motions of the PLA chains resulting in a delay in the temperature at which the transition was observed [11]. There were however no significant changes in the melting temperatures of both polymers in the blends in comparison to the neat polymers.

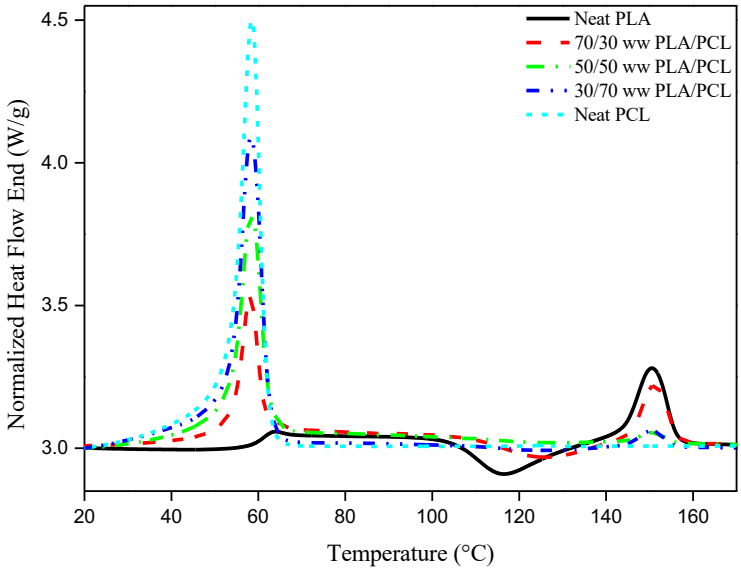

Figure 4.6 DSC curves of the neat polymers and their blends

Interesting observations were made after the addition of $Mg(OH)_2$ and APTMS-TiO_2 nanoparticles to the individual polymers and their polymer blends (Figures 4.7-4.9, and Tables 4.3-4.6). The glass transition temperatures of the PLA/$Mg(OH)_2$ nanocomposites (Figure 4.7 (a), Table 4.3) were lower than that of neat PLA irrespective of the filler content (1, 3, 5 and 10 wt.%). In the presence of $Mg(OH)_2$, the intensity and the broadness (and/or thickness) of the PLA glass transition were increased, and the highest intensity was noted at 1 wt.% $Mg(OH)_2$. This was indicative of an increase the amorphous fractions of the polymer. It is also possible that the $Mg(OH)_2$ nanorods had a plasticizing effect on the PLA at lower filler content, hence a decrease in T_g was observed. For the cold crystallization transition of these nanocomposites, a decrease in temperature was observed at 1 wt.% $Mg(OH)_2$ content. The

decrease indicated that $Mg(OH)_2$ promoted the recrystallization of PLA at low filler content. At 3 and 5 wt.% filler content, an increase in T_g was seen, and this could have been as a result of the $Mg(OH)_2$ nanorods restricting PLA chain movements. Based on the morphology study done for $Mg(OH)_2$ containing nanocomposites (Figure 4.2), the $Mg(OH)_2$ nanorods were arranged in an irregular manner in the polymer matrix. This could have increased the amorphous content of PLA and also restricted PLA chain movement, therefore resulting in an increase in the T_{cc}. The restricted chain movements would have required more energy in order for chain movement to occur, therefore justifying the increase in the temperature at which the cold crystallization transition was observed. However, no particular trend was observed for the intensity and peak thickness of the cold crystallization transitions. The cold crystallization peak intensity was increased at 1 and 5 wt.% $Mg(OH)_2$ filler content but lowered in the 3 wt.%. This irregularity could have been due to the presence of agglomerates which were not consistent in all the nanocomposites and could have possibly restricted polymer chain movement during recrystallization. At 10 wt.% $Mg(OH)_2$ content, the T_{cc} was not observed, and this could have been due to filler content being too high and preventing the crystallization/recrystallization of PLA chains [11]. As for the melting temperature of PLA, a decrease was observed, and the intensity and thickness of the peak began to decrease with the increase in $Mg(OH)_2$ nanoparticle content. This was attributed to the decrease in the crystalline phase due to the $Mg(OH)_2$ nanorods interfering with the cold crystallization process. The only exception was the 99/1 w/w PLA/$Mg(OH)_2$ nanocomposites where an increase in the T_m, melting enthalpies and degree of crystallinity was observed. As mentioned earlier, in the same sample a decrease in the cold crystallization temperature and an increase in the enthalpy was observed. These behaviours could have been due to the inorganic $Mg(OH)_2$ being present in a small amount and effectively acting as a heterogeneous nucleating agent during the cold crystallization process, therefore increasing the amount of crystals that melted during the melting transition. A split in its melting peak was also seen, and this indicated melting of two or more different types of crystals. The lower temperature peak could have been due to the melting of the metastable crystals that were formed during cold crystallization/recrystallization process, and the higher temperature peak could have been melting for the perfected crystals formed during the normal crystallization process. For the PCL/$Mg(OH)_2$ nanocomposites (Figure 4.7 (b)), it was observed that the melting temperature remained the same with the presence of the filler. However, there was a notable increase in the degree of crystallinity of the nanocomposites compared to neat PCL (From 33 to ~ 40 %, Table 4.4). This was attributed to the ability of $Mg(OH)_2$ to act as a nucleating agent for PCL.

Table 4.3 Parameters obtained from DSC analysis for PLA and $Mg(OH)_2$ and APTMS-TiO_2 nanoparticles samples

Sample	T_g / ºC	T_{cc} / ºC	T_m / ºC	ΔH_m / Jg^{-1}	X_c / %	Difference (T_m -T_g)/ºC
Neat PLA	63.1±0.2	115.7±0.6	151.0±0.2	14.4±0.8	17.7	87.9
PLA nanocomposites with $Mg(OH)_2$						
99.0/1.0 w/w PLA/$Mg(OH)_2$	56.5±0.6	115.1±2.8	150.7±4.1	17.7±2.7	19.3	94.2
97.0/3.0 w/w PLA/$Mg(OH)_2$	59.5±2.9	118.5±5.9	146.6±2.6	5.0±0.03	5.5	87.1
95.0/5.0 w/w PLA/$Mg(OH)_2$	59.4±0.7	117.7±7.3	145.5±3.3	3.9±0.2	4.4	86.1
90.0/10.0 w/w PLA/$Mg(OH)_2$	60.1±1.7		145.8±0.9	0.12±0.1	0.1	85.7
PLA nanocomposites with APTMS-TiO_2						
99.0/1.0 w/w PLA/APTMS-TiO_2	63.1±0.1	122.8±0.2	151.6±0.1	17.9±0.1	19.4	88.5
97.0/3.0 w/w PLA/APTMS-TiO_2	62.8±0.2	112.6±0.4	149.0±0.01	25.7±0.3	28.5	86.2
95.0/5.0 w/w PLA/APTMS-TiO_2	62.9±0.3	114.7±0.2	149.9±0.4	23.2±0.2	26.2	87.0

T_g = glass transition temperature, T_{cc} = cold crystallization temperature, T_m = peak temperature of melting, ΔH_m = melting enthalpy, X_c = degree of crystallinity, T_m -T_g = melting temperature – glass transition temperature

With the addition of APTMS-TiO_2 nanoparticles (Figures 4.7 (c) and (d), Table 4.3 and 4.4), the T_g of PLA in the PLA/APTMS-TiO_2 nanocomposites (Figure 4.7 (c), Table 4.3) remained relatively the same. As for the cold crystallization transitions, an increase was observed at 1 wt.% filler content, but as the filler content increased the T_{cc} decreased. The increase for the 99/1 w/w PLA/APTMS-TiO_2 could be as a result of APTMS-TiO_2 nanoparticles being well dispersed in a polymer, as they are low in content, and their effect are seen in being able restrict polymer chain packing and aligning early, therefore shifting the process of reorganization/recrystallization to higher temperature [11]. However, the decrease observed at 3 and 5 wt.% filler content could possibly be attributed to the lower dispersion of the nanoparticles at higher content of APTMS-TiO_2 where its effect might have been compromised. It is possible that the APTMS-TiO_2 nanoparticles plasticized the PLA chains and therefore lowered the temperature at which the transition was observed. Also, the APTMS-TiO_2 might have promoted the cold crystallization process by acting as heterogeneous nucleating agents, and therefore lowered the temperature at which recrystallization was observed. Similarly, for the T_m, a slight increase was observed for the 99/1 w/w PLA/APTMS-TiO_2 but decreases were seen at 3 and 5 wt.% filler content. The slight increase observed for 99/1 w/w PLA/APTMS-TiO_2 could have been due to the fair dispersion of the APTMS-TiO_2 in PLA at low content, which was seen during TEM analysis. This would have effectively restricted polymer chain movement during the melting process, and therefore shift the transition to a higher temperature. However, the decrease observed at 3 and 5 wt.% filler content could have been due to the heteronucleating effect of the APTMS-TiO_2 since an increase in the degree of crystallinity was also observed. The melting transition was broadened to lower temperatures indicating presence of crystals that are imperfect or with thinner lamellar. When the temperature difference between the T_g and T_m of the nanocomposites was compared to that of neat PLA (87.9 ºC), a decrease was observed. This indicated that the filler and the PLA matrix had some level of compatibility. Also, it could have been due to the nanoparticles trying to stabilize the thermal properties of PLA. The only exception was at 1 wt.% filler content, where the temperature difference between the T_g and T_m was found to be 88.5 ºC. This indicated poor compatibility between the PLA and APTMS-TiO_2 at low filler content. An increase in the enthalpy and crystallinity was observed irrespective of the filler content (Table 4.3). At 1, 3 and 5 wt.% APTMS-TiO_2 the degrees of crystallinity were found to be 19.4, 28.5 and 26.2 % respectively, compared with neat PLA which had a degree of crystallinity of 17.7 %. A maximum increase in X_c was observed with 97/3 w/w PLA/APTMS-TiO_2 having the highest X_c (28.5 %). This increase in the degree of crystallinity was attributed to the possible heteronucleating effect of the filler during the cooling process and the cold crystallization

transition. The presence of APTMS on the surface of the nanoparticles might have imparted a rough surface on the nanoparticles making them effective nucleating agents.

In PCL/ APTMS-TiO_2 nanocomposites (Figure 4.7 (d), Table 4.4), the melting temperature of PCL did not change as a result of the presence of the nanoparticles. However, an increase in the enthalpy (46 of neat PCL to 49.9 Jg^{-1} in the composites) and degree of crystallinity (from 33.4 of neat PCL to 36.0 % in the composites) in the presence of APTMS-TiO_2 presence was observed which was attributed to the nucleating effect of the filler. Based on the increase in the degrees of crystallinity experienced for both PLA and PCL, in the presence of the APTMS-TiO_2 nanoparticles, it is an indication that the nanoparticles were effectively acting as nucleating agents. Luo *et al.* [13] observed the same in their investigation of poly(lactic acid) and lactic acid functionalized TiO_2 nanocomposites. They found that presence of TiO_2 (non-functionalized and functionalized) in PLA increased the crystallization rate because of its ability to act as a heterogeneous nucleating agent.

Table 4.4 Parameters obtained from DSC analysis for PCL with $Mg(OH)_2$ and APTMS-TiO_2 nanoparticles samples

Sample	T_m / °C	ΔH_m / Jg^{-1}	X_c / %
PCL	58.0±0.4	46.4±11.2	33.4
PCL nanocomposites with $Mg(OH)_2$			
99.0/1.0 w/w PCL/$Mg(OH)_2$	58.4±0.8	55.3±4.8	40.2
97.0/3.0 w/w PCL/$Mg(OH)_2$	58.1±0.5	54.3±4.1	40.3
95.0/5.0 w/w PCL/$Mg(OH)_2$	58.5±0.5	53.3±0.3	40.3
90.0/10.0 w/w PCL/$Mg(OH)_2$	58.7±0.6	50.6±5.5	40.4
PCL nanocomposites with APTMS-TiO_2			
99.0/1.0 w/w PCL/APTMS-TiO_2	58.5±0.5	49.9±1.1	36.3
97.0/3.0 w/w PCL/APTMS-TiO_2	58.5±0.4	46.3±1.8	34.4
95.0/5.0 w/w PCL/APTMS-TiO_2	59.0±0.9	47.4±1.0	35.9

T_g = glass transition temperature, T_{cc} = cold crystallization temperature, T_m = peak temperature of melting, ΔH_m = melting enthalpy, X_c = degree of crystallinity

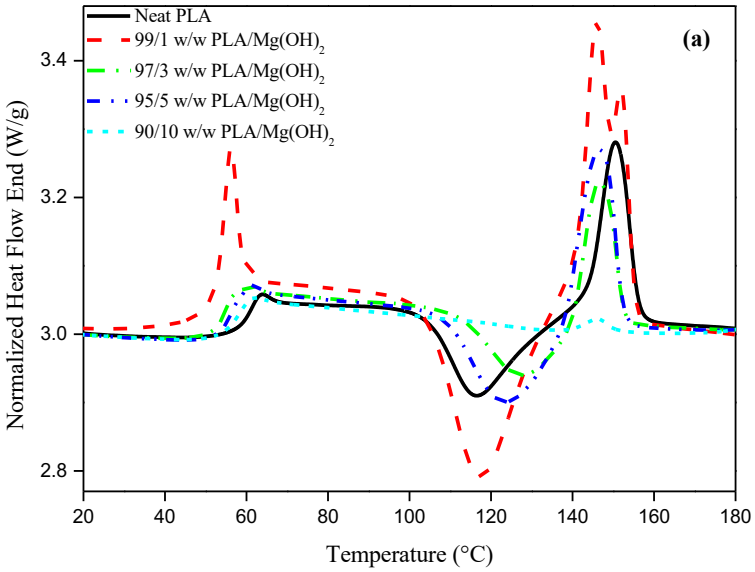
Neat PLA
99/1 w/w PLA/Mg(OH)2
97/3 w/w PLA/Mg(OH)2
95/5 w/w PLA/Mg(OH)2
90/10 w/w PLA/Mg(OH)2
(a)
Normalized Heat Flow End (W/g)
Temperature (°C)

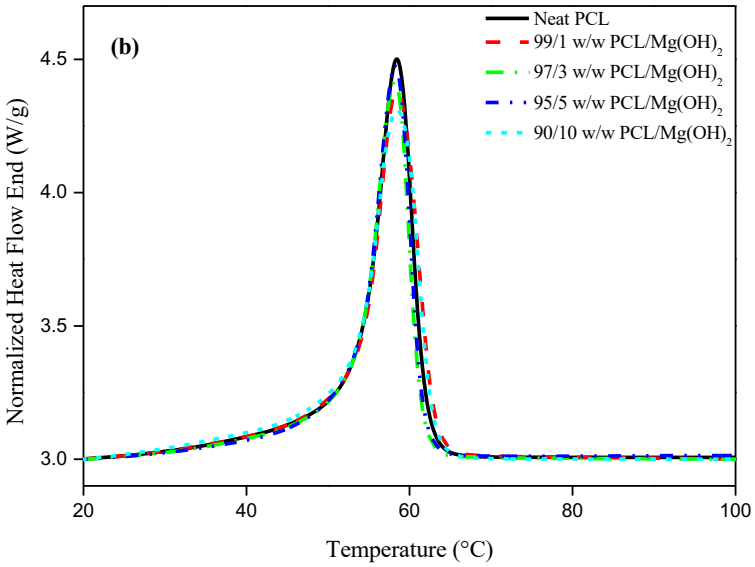
Neat PCL
99/1 w/w PCL/Mg(OH)2
97/3 w/w PCL/Mg(OH)2
95/5 w/w PCL/Mg(OH)2
90/10 w/w PCL/Mg(OH)2
(b)
Normalized Heat Flow End (W/g)
Temperature (°C)

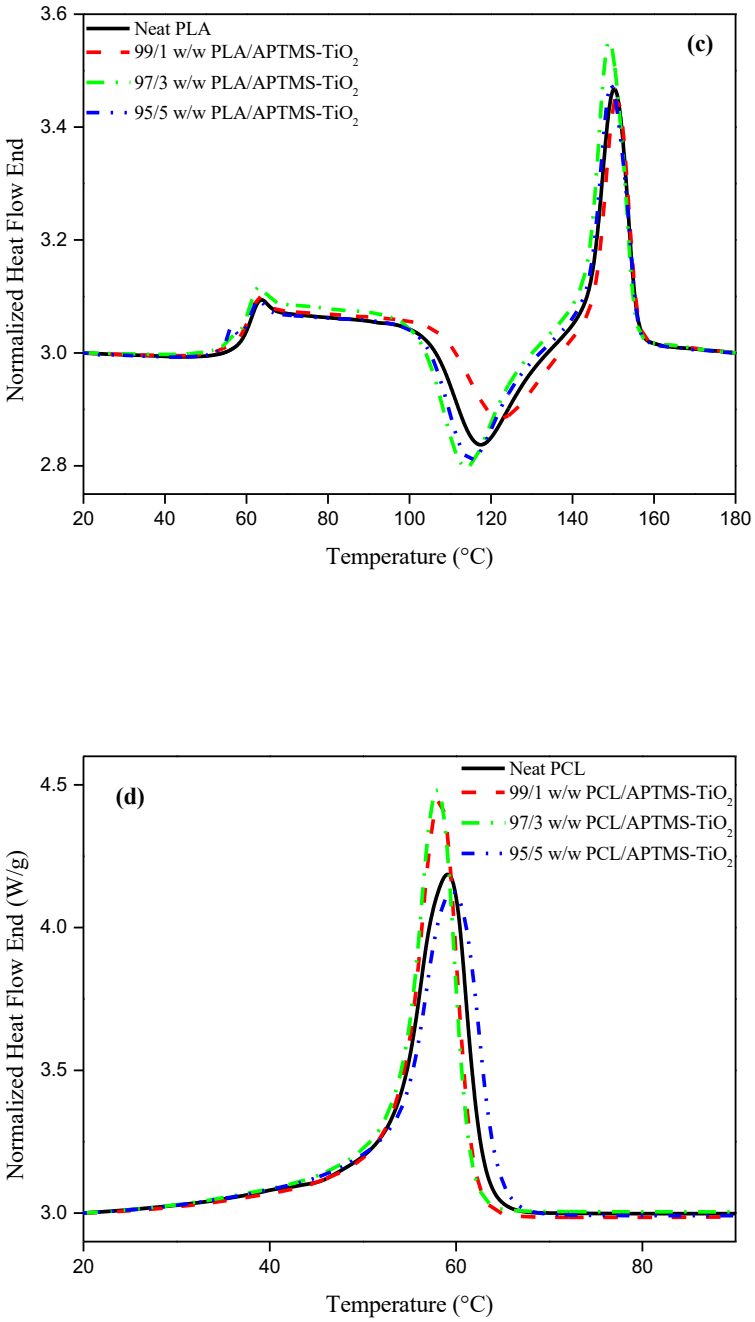

Figure 4.7 DSC curves of the individual polymer nanocomposites with $Mg(OH)_2$ ((a) and (b)) and APTMS-TiO_2 ((c) and (d)) for single polymer composites

For all the $Mg(OH)_2$ blend nanocomposites (Figure 4.8, Table 4.5), the PCL melting transition coexisted with the PLA T_g. The melting temperature of PCL remained relatively the same for the polymer blend nanocomposites with the presence of both PLA and $Mg(OH)_2$ nanorods. The only exception was the 45.0/45.0/10.0 w/w PLA/PCL/$Mg(OH)_2$ where a slight increase by 2 ºC was seen. The increase was attributed to the possibility that restricted chain movements

might have been experienced due to the presence of agglomerates which were seen during SEM and TEM analysis (Figure 4.2 and 4.4). The enthalpy and degree of crystallinity of PCL in all the blend nanocomposites was higher than the PCL in their respective neat polymer blend (Table 4.5). This was attributed to the promotion of crystallization with presence of both PLA and $Mg(OH)_2$ nanorods [13, 14]. A cold crystallization transition (T_{cc}) was observed in some of the $Mg(OH)_2$ blend nanocomposites, especially at a higher PLA content. When the T_{cc} of the $Mg(OH)_2$ blend nanocomposites was compared to the T_{cc} of neat PLA, an increase was observed (Table 4.5). The increase was attributed to possible restricted polymer chain movement due to the presence of the $Mg(OH)_2$ nanorods which were also agglomerated and irregularly arranged as seen through morphology studies using SEM and TEM (Figure 4.2 and 4.4). The only exception was in the 70/30 w/w PLA/PCL blend nanocomposites at 1 wt.% filler where a decrease in the T_{cc} of PLA was seen. The decrease was due to the possible effect of the filler's ability to promote the recrystallization of PLA at a lower temperature, as was seen in the PLA/$Mg(OH)_2$ nanocomposites. The cold crystallization transition was absent in the neat blends (50/50 w/w PLA/PCL and 30/70 w/w PLA/PCL) and when the $Mg(OH)_2$ content increased to 5 and 10 wt.%. The absence of the cold crystallization transition in those samples could have been due to (i) inhibited recrystallization by the large amount of filler since the amount of PLA was low, (ii) the high filler content which led to agglomeration of the filler as seen through SEM and TEM analysis; thus restricted chain mobility required for recrystallization to occur and (iii) the change in the cold crystallization could have been so small that the DSC did not pick it up. The melting temperatures for PLA was a significantly decreased for all the blend nanocomposites. This was clearly noticeable in the 70/30 w/w PLA/PCL blend nanocomposites (Figure 4.8 (a)). For the polymer blend nanocomposites, the above-mentioned observations were attributed to the disturbance of the polymer chain packing from the other polymer as well as the filler. Presence of PCL and $Mg(OH)_2$ disturbed the polymer chain packing of PLA. As mentioned earlier, the $Mg(OH)_2$ nanorods were agglomerated and irregularly arranged, this would have therefore lowered the melting temperature of PLA. The degree of crystallinity of the PLA melting peaks also decreased (from 17.7 % in the neat polymer) in most of the nanocomposites with the exception of a few samples (69.7/29.3/1 w/w PLA/PCL/$Mg(OH)_2$ (30.7 %), 67.9/29.1/3 w/w PLA/PCL/$Mg(OH)_2$ (18.0 %) and the 49.5/49.5/1 w/w PLA/PCL/$Mg(OH)_2$ (18.9 %) blend nanocomposites) (Table 4.5). The decrease in the degree of crystallinity was ascribed to the disturbance of crystallization/recrystallization in the presence of PCL chains and the $Mg(OH)_2$ nanorods in the PLA matrix. The increase in the degree of crystallinity seen for the few samples could have been due to the filler's ability to promote the recrystallization of PLA at lower filler contents

in the presence of a high PLA content. To summarize the effect of the $Mg(OH)_2$ nanorods on the PLA/PCL blend nanocomposites, a slight increase in miscibility between PLA and PCL was achieved by using $Mg(OH)_2$ as a filler and compatibilizer for the different PLA/PCL blend ratios. This was seen with the decrease in the temperature difference between the T_m's of PCL and PLA of the polymer blend nanocomposites compared to that of the neat polymers (93 ºC) or their blends (Table 4.5). The decrease was observed with the presence and increase in content of the $Mg(OH)_2$ nanorods. This was a clear sign that the $Mg(OH)_2$ nanorods acted as a compatibilizer. Carmona *et al.* [14] investigated biodegradable ternary blend of thermoplastic starch (TPS), poly(ε-caprolactone) (PCL) and poly(lactic acid) (PLA) using DSC analysis. It was reported that the presence of TPS resulted in a decrease in the temperature difference between the T_m's of PCL and PLA. They attributed this to the compatibilizing effect of TPS as a result of its amorphous soluble fractions dispersing in both PLA and PCL.

Table 4.5 Parameters obtained from DSC analysis for PLA/PCL blends with $Mg(OH)_2$ nanoparticles as a filler

Samples	PCL			PLA				Difference
	T_{mPCL} /T_{gPLA}/ ºC	ΔH_m / Jg^{-1}	X_c / %	T_{cc} / ºC	T_m / ºC	ΔH_m /Jg^{-1}	X_c /%	($T_{m\ PLA}$-$T_{m\ PCL}$)/ºC
70/30 w/w PLA/PCL	58.2±0.6	12.8±3.4	30.8	126.8±0.7	151.7±0.5	4.5±1.4	6.9	93.5
69.3/29.3/1.0 w/w PLA/PCL/$Mg(OH)_2$	58.0±0.2	19.7±1.3	48.3	111.7±2.9	149.5±3.8	19.8±3.3	30.7	91.5
67.9/29.1/3.0 w/w PLA/PCL/$Mg(OH)_2$	57.2±0.1	18.5±1.1	45.7	116.0±0.5	141.6±0.1	11.4±0.6	18.0	84.4
66.5/28.5/5.0 w/w PLA/PCL/$Mg(OH)_2$	57.9±0.4	18.8±2.3	47.3	126.9±3.2	145.4±1.2	6.4±1.3	10.4	87.5
63.0/27.0/10.0 w/w PLA/PCL/$Mg(OH)_2$	57.3±1.1	15.2±0.4	40.4		144.6	0.0015	0.0017	87.3
50/50 w/w PLA/PCL	58.2±0.2	25.0±4.5	36.0		150.5±0.2	1.6±0.5	3.3	92.3
49.5/49.5/1.0 w/w PLA/PCL/$Mg(OH)_2$	58.4±0.5	30.1±3.6	43.7	119.3±1.0	145.2±0.3	8.7±0.6	18.9	86.8
48.5/48.5/3.0 w/w PLA/PCL/$Mg(OH)_2$	58.7±0.3	27.1±2.3	40.2	128.4	145.1±0.6	1.4±1.4	3.0	86.4
47.5/47.5/5.0 w/w PLA/PCL/$Mg(OH)_2$	58.6±0.3	33.7±2.5	51.1		145.1±0.3	0.7±0.8	1.7	86.5
45.0/45.0/10.0 w/w PLA/PCL/$Mg(OH)_2$	59.5±0.4	21.1±3.5	33.7					
30/70 w/w PLA/PCL	58.2±0.2	45.6±7.1	46.9		150.5±0.2	2.2±0.9	7.9	92.3
29.3/69.7/1.0 w/w PLA/PCL/$Mg(OH)_2$	57.6±0.3	37.1±0.9	38.3	123.3±0.9	144.4±0.3	1.8±0.5	6.6	86.8
29.1/67.9/3.0 w/w PLA/PCL/$Mg(OH)_2$	58.7±0.6	35.6±2.1	37.7		142.2±0.8	0.9±0.5	3.2	83.5
28.5/66.5/5.0 w/w PLA/PCL/$Mg(OH)_2$	59.8±0.2	31.9±2.6	34.6					
27.0/63.0/10.0 w/w PLA/PCL/$Mg(OH)_2$	59.2±0.7	35.5±4.2	40.6					

T_m = peak temperature of melting, $T_{g\ PLA}$ = glass transition temperature of PLA, ΔH_m = melting enthalpy, X_c = degree of crystallinity, T_{cc} = cold crystallization temperature, $T_{m\ PLA}$-$T_{m\ PCL}$ = peak melting temperature of PLA – peak melting temperature of PCL

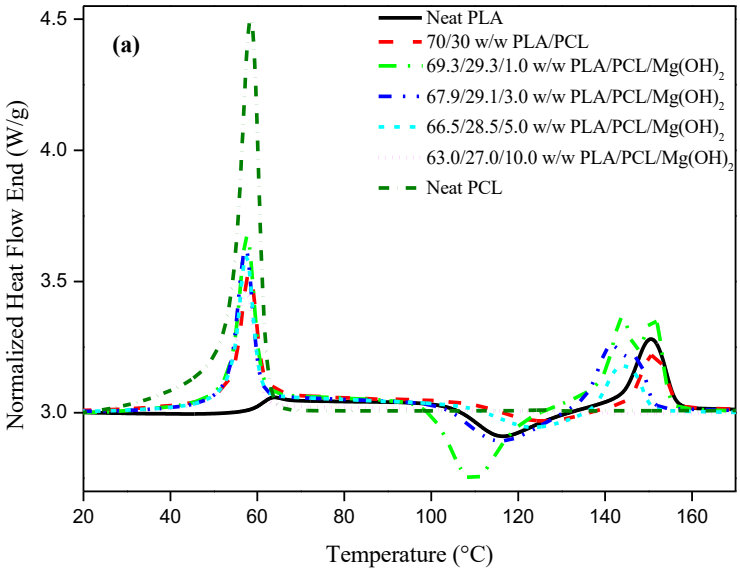
(a)
Neat PLA
70/30 w/w PLA/PCL
69.3/29.3/1.0 w/w PLA/PCL/Mg(OH)2
67.9/29.1/3.0 w/w PLA/PCL/Mg(OH)2
66.5/28.5/5.0 w/w PLA/PCL/Mg(OH)2
63.0/27.0/10.0 w/w PLA/PCL/Mg(OH)2
Neat PCL
Normalized Heat Flow End (W/g)
Temperature (°C)
4.5
4.0
3.5
3.0
20
40
60
80
100
120
140
160

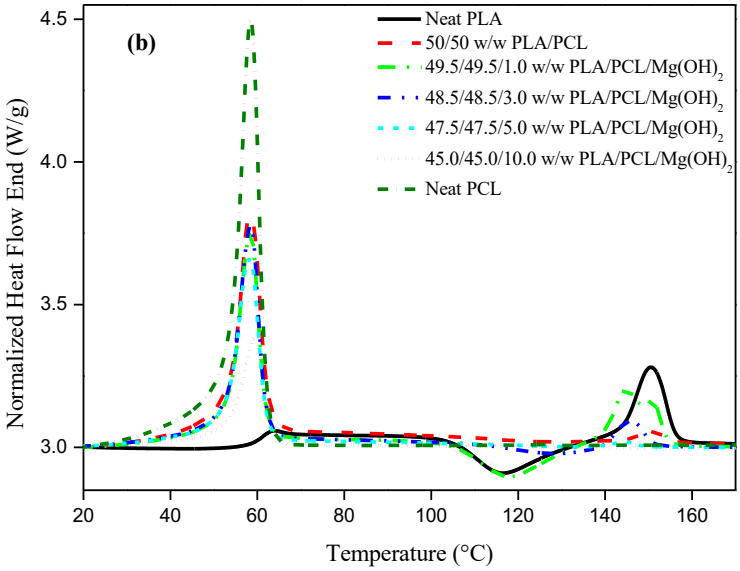
(b)
Neat PLA
50/50 w/w PLA/PCL
49.5/49.5/1.0 w/w PLA/PCL/Mg(OH)2
48.5/48.5/3.0 w/w PLA/PCL/Mg(OH)2
47.5/47.5/5.0 w/w PLA/PCL/Mg(OH)2
45.0/45.0/10.0 w/w PLA/PCL/Mg(OH)2
Neat PCL
Normalized Heat Flow End (W/g)
Temperature (°C)
4.5
4.0
3.5
3.0
20
40
60
80
100
120
140
160

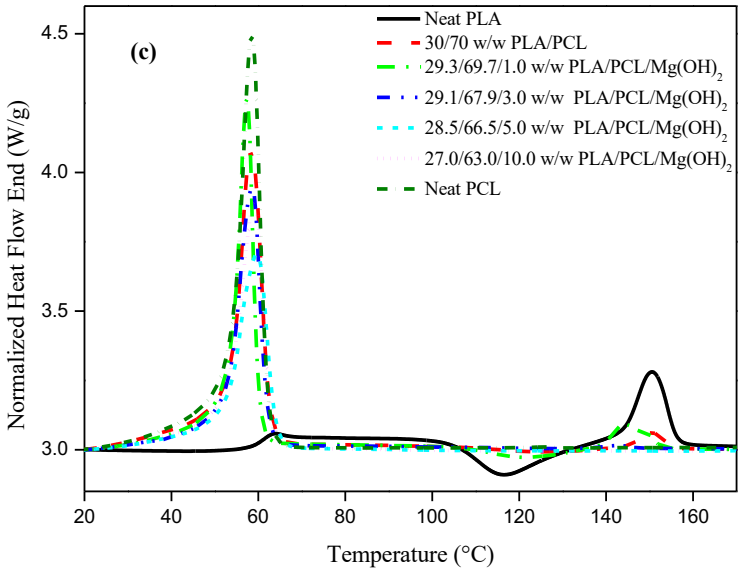

Figure 4.8 DSC curves of the polymer blend nanocomposites with $Mg(OH)_2$ (a) 70/30 w/w PLA/PCL, (b) 50/50 w/w PLA/PCL and (c) 30/70 w/w PLA/PCL.

In the presence of APTMS-TiO_2 nanoparticles, for all the blend nanocomposites (Figure 4.9 and Table 4.6), the position of the melting transition of PCL remained relatively the same and it coexisted with the T_g of PLA. As for the melting enthalpy of PCL, a decrease was seen for 70/30 w/w PLA/PCL (Figure 4.9 (a)) and 30/70 w/w PLA/PCL (Figure 4.8 (c)) nanocomposites. In the 50/50 w/w PLA/PCL (Figure 4.8 (b)) nanocomposites, the presence of APTMS-TiO_2 increased the enthalpy. All the decreases observed for the enthalpy were attributed to the decrease in the crystalline phase due to the presence of PLA which had a lower degree of crystallinity. Also, the presence of APTMS-TiO_2 nanoparticles might have lowered the PCL crystalline phase by disturbing the crystallization process. On the other hand, an increase in enthalpy was however attributed to the good dispersion of the filler which may have heteronucleation effect. An increase in the degree of crystallinity of PLA with the addition of neat TiO_2 and lactic acid functionalized TiO_2 was also reported by Luo *et al.* [13]. They observed that both fillers acted as heteronucleating agents which was seen through increased rates of crystallization and a number of primary nucleation sites which were seen using polarized optical microscope. In all the blends nanocomposites, the glass transition of PLA could not be determined accurately as it coexisted with the PCL melting peak.

Table 4.6 Parameters obtained from DSC analysis for PLA/PCL blends with APTMS-TiO_2 nanoparticles as a filler

Samples	PCL			PLA				Difference
	T_m/T_{gPLA} / °C	ΔH_m/ Jg^{-1}	X_c /%	T_{cc}/ °C	T_m/ °C	ΔH_m/ Jg^{-1}	X_c /%	($T_{m\ PLA}$-$T_{m\ PCL}$)/°C
70/30 w/w PLA/PCL	58.2±0.6	12.8±3.4	30.8	126.8±0.7	151.7±0.5	4.5±1.4	6.9	93.5
69.3/29.3/1.0 w/w PLA/PCL/APTMS-TiO_2	58.0±0.5	14.8±0.7	11.2	124.1±0.4	151.8±0.3	6.7±0.4	7.4	93.8
67.9/29.1/3.0 w/w PLA/PCL/APTMS-TiO_2	57.8±0.3	14.8±1.0	11.7	122.0±0.8	151.5±0.3	9.6±0.8	10.6	93.7
66.5/28.5/5.0 w/w PLA/PCL/APTMS-TiO_2	57.8±0.2	12.4±2.0	10.2	122.0±0.5	151.4±6.0	12.2±0.3	13.5	93.6
50/50 w/w PLA/PCL	58.2±0.2	25.0±4.5	36.0		150.5±0.2	1.6±0.5	3.3	92.3
49.5/49.5/1.0 w/w PLA/PCL/APTMS-TiO_2	57.7±0.4	28.9±3.6	35.9	122.5±0.2	151.0±0.2	1.1±0.1	0.9	93.3
48.5/48.5/3.0 w/w PLA/PCL/APTMS-TiO_2	57.7±0.3	28.0±3.4	35.4	121.8±1.2	150.8±0.7	0.4±0.2	0.4	93.1
47.5/47.5/5.0 w/w PLA/PCL/APTMS-TiO_2	58.1±0.4	30.1±0.4	35.4	121.5±0.7	151.2±0.8	2.5±0.1	2.1	93.1
30/70 w/w PLA/PCL	58.2±0.2	45.6±7.1	46.9		150.5±0.2	2.2±0.9	7.9	92.3
29.3/69.7/1.0 w/w PLA/PCL/APTMS-TiO_2	58.0±0.1	40.4±0.5	70.1	127.4±0.1	150.0±0.3	2.7±0.4	1.3	92.0
29.1/67.9/3.0 w/w PLA/PCL/APTMS-TiO_2	57.7±0.2	43.6±0.4	75.8	124.2±1.4	149.8±0.3	1.6±0.1	0.8	92.1
28.5/66.5/5.0 w/w PLA/PCL/APTMS-TiO_2	57.8±0.2	45.4±0.9	79.8	123.9±0.3	150.0±0.3	2.4±0.1	1.3	92.2

T_m = peak temperature of melting, T_{gPLA} = glass transition temperature of PLA, ΔH_m = melting enthalpy, X_c = degree of crystallinity, T_{cc} = cold crystallization temperature, $T_{m\ PLA}$-$T_{m\ PCL}$ = peak melting temperature of PLA – peak melting temperature of PCL

As for the cold crystallization transition of the PLA phase in the blend nanocomposites (for all the blend ratios), an increase in T_{cc} was observed in comparison to neat PLA and neat polymer blends. The increase was attributed to chain restriction due to the presence of APTMS-TiO_2 nanoparticles in PLA, as it was seen on SEM and TEM results that APTMS-TiO_2 nanoparticles were localized in PLA phase of the blend. For the melting temperature of PLA, it was noted that it also remained relatively the same for all the blend nanocomposites. The melting enthalpies and degrees of crystallinity of the APTMS-TiO_2 polymer blend nanocomposites (Table 4.6) were decreased in comparison to those of neat PLA (14.4 $J.g^{-1}$, 17.7%). This was attributed to a possible disturbance of crystallization/recrystallization of the PLA chain in the presence of both PCL and APTMS-TiO_2. Carmona *et al.* [14] made the same observation in their DSC study. They studied properties of biodegradable ternary blend of thermoplastic starch (TPS), poly(ε-caprolactone) (PCL) and poly(lactic acid) (PLA). During DSC analysis, they observed a decrease in the degree of crystallinity of PCL with the addition of PLA and TPS. They attributed this to PLA and TPS hindering PCL chain mobility therefore reducing the degree of crystallinity. In another study by Nguyen *et al.* [15], they investigated the effect of titanium dioxide on the properties of polyethylene/TiO_2 nanocomposites. During their DSC investigation, they observed that presence of anatase TiO_2 decreased the overall degree of crystallinity of the nanocomposites. It was attributed this to hindrance of the spherulite growth stage by the dispersed TiO_2 nanoparticles. It was stated that the reduction in the bulk crystallization rate and crystal domain sizes may have resulted in a lower degree of crystallinity. In our study, varied observations were made in the enthalpies for each of the polymer blend ratios when compared to their respective polymer blends. For the 70/30 w/w PLA/PCL nanocomposites, an increase in enthalpy and degrees of crystallinity was observed with the presence and increase in content of the APTMS-TiO_2 nanoparticles. In the 50/50 and 30/70 w/w PLA/PCL nanocomposites, no particular trend was observed with regard to the filler content. Any increases observed in the melting enthalpy could have been due to the promotion of the formation of the crystalline phase due to the good dispersion of the filler, as was seen in the TEM and SEM analysis. However, the decreases observed may have been due to a decreased crystalline phase which could have resulted from presence of poor dispersion and/or agglomeration of the APTMS-TiO_2 especially at a higher content. This was similar to what Esteki *et al.* [16] observed in their study of the crystallinity behaviour of polyethylene/clay nanocomposites under the influence of water-assisted melt blending. At low clay contents they observed an increase in the degree of crystallinity. They attributed the increase to the good dispersion of the clay platelets which allows for multiple heterogeneous nucleation sites necessary for the crystallization of the nanocomposites. Buzarovska *et al.* [17] also observed

similar behaviours in their study of PLA nanocomposites with propionic acid functionalized TiO_2 nanoparticles. At lower filler content they observed good dispersion and increases in the degree of crystallinity of the polymer. At higher filler content, where agglomerates were observed, they observed slightly lower degrees of crystallinity. When the temperature difference between the T_m's of PCL and PLA of the 50/50 and 70/30 w/w PLA/PCL blend nanocomposites was compared to that of the neat polymers (93 ºC) or their blends (Table 4.6), a slight increase was observed. This increase was interpreted as an indication of worsened miscibility and compatibility between PLA and PCL with the presence of APTMS-TiO_2 nanoparticles. The only exception was the 30/70 w/w PLA/PCL blend nanocomposites where a slight decrease in the temperature difference was observed with the presence of the APTMS-TiO_2 nanoparticles (Table 4.6). This indicated that the APTMS-TiO_2 nanoparticles, like $Mg(OH)_2$ nanorods, have partially improved the miscibility and compatibility of PLA and PCL, but only in this specific blend composition. To conclude the observations made during DSC analysis, in the single polymer nanocomposites, $Mg(OH)_2$ increased the degrees of crystallinities of PCL at all compositions and in PLA only at low filler content. For the APTMS-TiO_2 single polymer nanocomposites, increases in the degree of crystallinity were observed in both PLA and PCL. There was a slight compatibility between PLA with both $Mg(OH)_2$ and APTMS-TiO_2 at higher filler contents (3, 5 or 10 wt.%). This was shown by the slightly improved difference between the T_m and T_g of PLA. In the polymer blend nanocomposites, both $Mg(OH)_2$ and APTMS-TiO_2 increased the degrees of crystallinities of PCL but decreased the degree of crystallinities of PLA. The only exceptions were the decrease in the crystallinity of PCL in the 70/30 w/w PLA/PCL blend nanocomposites with APTMS-TiO_2. Improved compatibility between PLA and PCL was observed mostly with the presence of $Mg(OH)_2$ in the polymer blend nanocomposites. Addition of APTMS-TiO_2 only improved compatibility of PCL and PLA in the 30/70 w/w PLA/PCL polymer blend nanocomposites This was revealed by the decreased temperature difference between the T_m's of PCL and PLA.

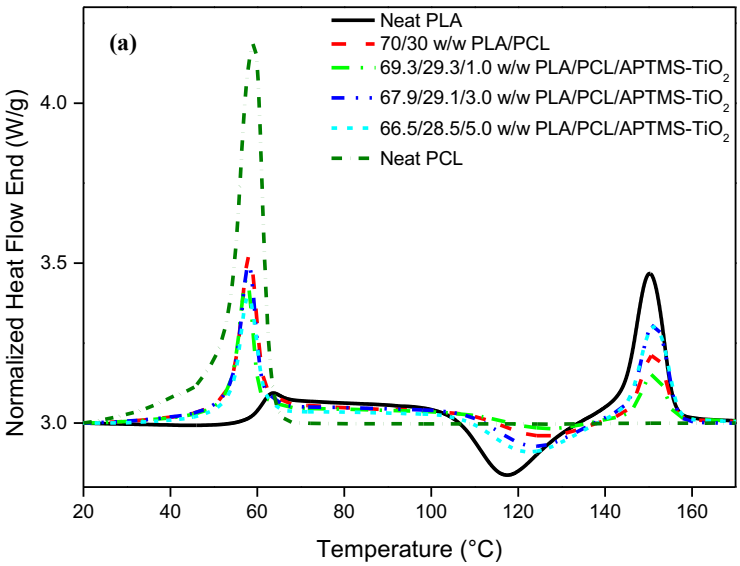
(a)
Neat PLA
70/30 w/w PLA/PCL
69.3/29.3/1.0 w/w PLA/PCL/APTMS-TiO2
67.9/29.1/3.0 w/w PLA/PCL/APTMS-TiO2
66.5/28.5/5.0 w/w PLA/PCL/APTMS-TiO2
Neat PCL
Normalized Heat Flow End (W/g)
4.0
3.5
3.0
20
40
60
80
100
120
140
160
Temperature (°C)

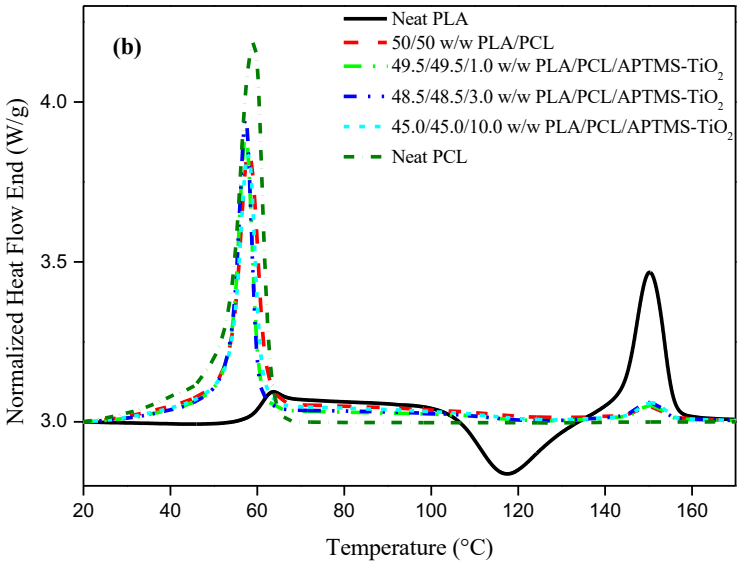
(b)
Neat PLA
50/50 w/w PLA/PCL
49.5/49.5/1.0 w/w PLA/PCL/APTMS-TiO2
48.5/48.5/3.0 w/w PLA/PCL/APTMS-TiO2
45.0/45.0/10.0 w/w PLA/PCL/APTMS-TiO2
Neat PCL
Normalized Heat Flow End (W/g)
4.0
3.5
3.0
20
40
60
80
100
120
140
160
Temperature (°C)

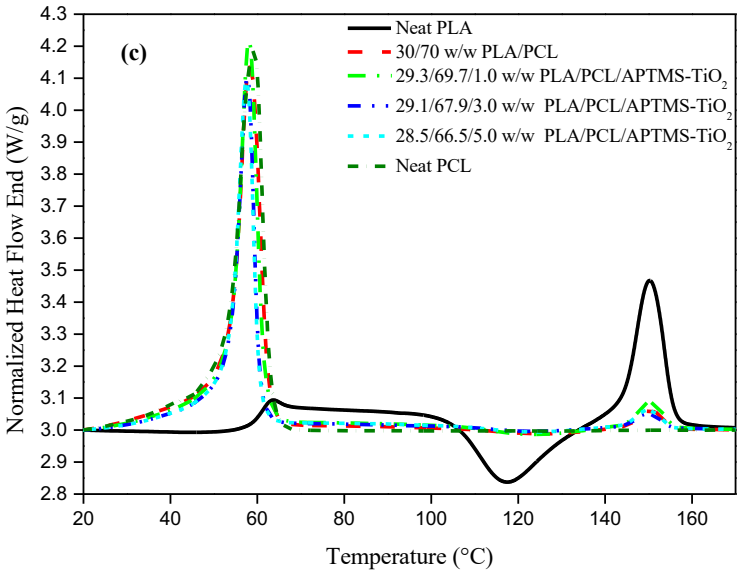

Figure 4.9 DSC curves of the polymer blend nanocomposites with APTMS-TiO_2 (a) 70/30 w/w PLA/PCL, (b) 50/50 w/w PLA/PCL and (c) 30/70 w/w PLA/PCL

4.3 Thermal degradation analysis

4.3.1 Thermogravimetric analysis (TGA)

The thermal stability of materials is important in determining the limit of their working temperature and the environmental conditions for use, which are related to their thermal decomposition temperature and decomposition rate. Figure 4.10 illustrates the TGA results for the thermal degradation studies of the neat polymers (PLA and PCL) and fillers ($Mg(OH)_2$ and APTMS-TiO_2) (Figure 4.10 (a)), and PLA/PCL blends (Figures 4.10 (b)). The degradation of PLA took place in a single step (Figure 4.10 (a)). Maximum degradation occurred around 338 °C with little or no char at 550 °C. PLA is reported to undergo a back-biting ester interchange reactions through a non-radical mechanism involving the -OH chain ends [6]. For PCL, a single step with major degradation occurring around 411 °C was also observed and no char formation was observed as well. The degradation of PCL has been reported to take place via cis-elimination cleavage, followed by the unzipping depolymerisation [6]. For $Mg(OH)_2$ nanorods, a single degradation step was observed with an onset around 100 °C, and major degradation taking place around 357 °C. After complete degradation, a char content of approximately 65

% remained at 550 °C. The mass loss in $Mg(OH)_2$ around 100 °C was as a result of losing bound water, because of its highly hygroscopic properties, water molecules are usually bound on the surface of its nanoparticles. Major degradation was attributed to the dehydration of the $Mg(OH)_2$ to magnesium oxide (MgO), which is much more thermally stable [18-20]. During the degradation of unfunctionalised titania, two degradation steps were observed. Around 600 °C, a char content of 97.6 % remained, indicating very little mass loss. As for functionalized titania, three steps were observed and a char content of 96.0 % remained at 600 °C. The high char content indicated the high thermal stability of TiO_2 at high temperatures. The first steps in both unfunctionalised and functionalised titania around 100 ºC was due to the loss of bound water on the surface of the titania nanoparticles. The mass loss during the second step of both unfunctionalised (between 127.6 and 277.6 °C) and functionalised titania (between 290.4 and 480.4 °C) was attributed to the removal of water molecules which came from the condensation of uncondensed –OH groups on the surface of titania nanoparticles. Zhao *et al.* [1] observed a similar observation. They observed loss of adsorbed water molecules at temperatures between 100 and 160ºC. At higher temperatures, mass loss was attributed to the condensation of the -OH on the surface of the TiO_2 nanoparticles. In the case of functionalised titania, the presence of APTMS molecules could also have contributed because its degradation took place over a wide temperature range. The third step which was only present in functionalised titania (from 480.4 °C till 600 °C), mass loss might be attributed to the oxidative thermal decomposition of APTMS. A comparison between unfunctionalised titania and functionalised titania revealed that there was more mass loss in functionalised titania than there was in unfunctionalised titania. Any additional mass loss observed in the functionalized titania, which was absent in unfunctionalized titania, was attributed to the presence of the APTMS. The difference in mass loss between the two was 1.6 %.

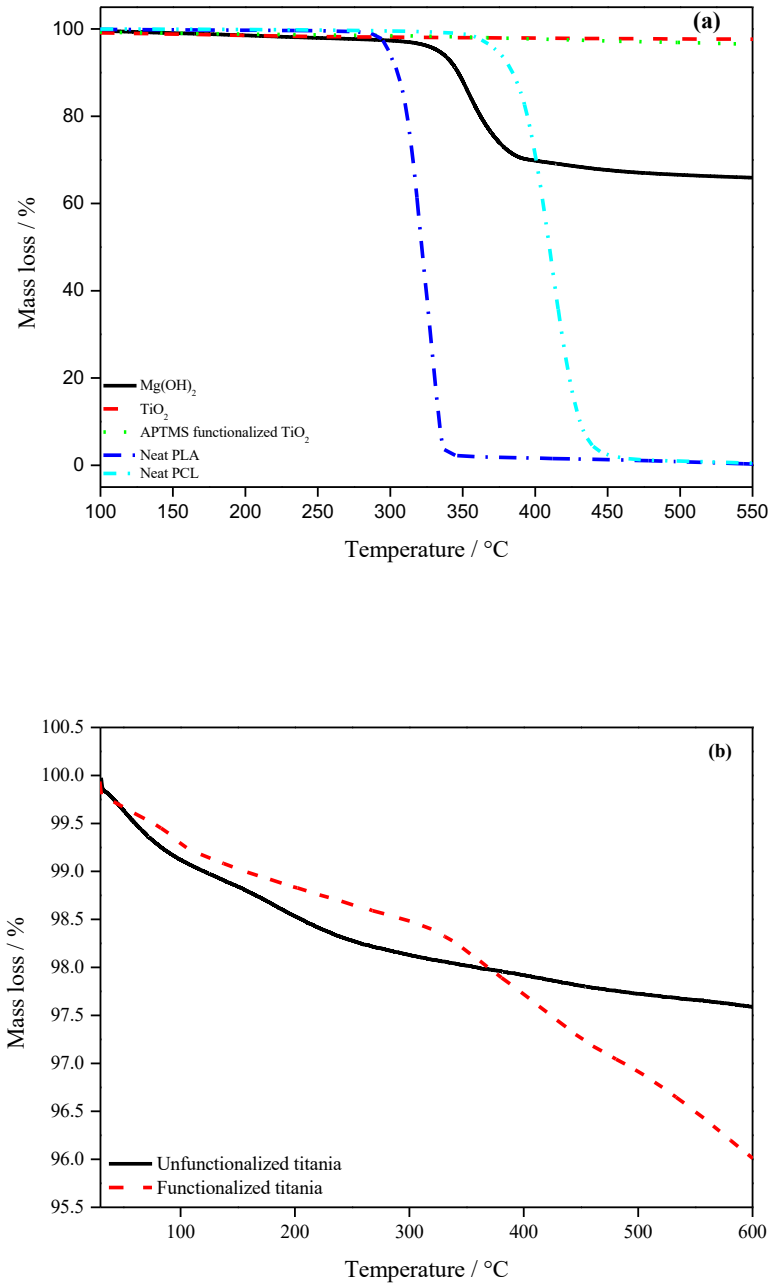

Figure 4.10 The TGA curves for thermal degradation of the (a) nanoparticles and neat polymers (b) unfunctionalised and functionalised TiO_2 nanoparticles

In the polymer blends (Figure 4.11, Table 4.7), two distinct steps were observed, which show the thermal degradation of each component that constitute the blends. This observation clearly indicates that the two polymers are immiscible as seen on morphology by SEM and TEM as well as the transitions on DSC results. The extent of mass loss was directly related to the amount of the constituent polymers in the polymer blends. For instance, in the 70/30 w/w

PLA/PCL blend, around the degradation temperature of PLA (300 ºC), a larger degradation step was observed and a smaller step was observed around the degradation temperature of PCL. The PLA degradation step was therefore more prominent in the blends with more PLA, and PCL step was much more prominent where the PCL content was higher. An increase in the thermal stability of PLA was observed with an increase in PCL content since PCL is much more thermally stable than PLA, and as expected, a decrease in the thermal stability of PCL was observed with the addition of more PLA. When the blends were compared to the neat polymers (PLA and PCL), they had intermediate properties. Neat PCL had the highest thermal stability, followed by 30/70, 50/50, 70/30 w/w PLA/PCL and then neat PLA. Also as expected, no significant char formation was observed for any of the polymer blend ratios at 550 °C. The presence of two thermal degradation steps for blends indicates that the two polymers were indeed immiscible as seen from DSC results. Though they are immiscible, blends having intermediate thermal degradation temperatures when compared to neat components, indicate some degree of compatibility between PLA and PCL. The thermal degradation results of the blends show that PCL was able to improve the low thermal stability of PLA, as all the blends have somehow higher thermal degradation temperatures than the polymer of the lowest thermal stability (PLA). Mofokeng *et al.* [6] saw the same trend in their degradation studies of PLA/PCL blends. They observed an increase in the thermal stability of PLA with the addition and increase in content of PCL.

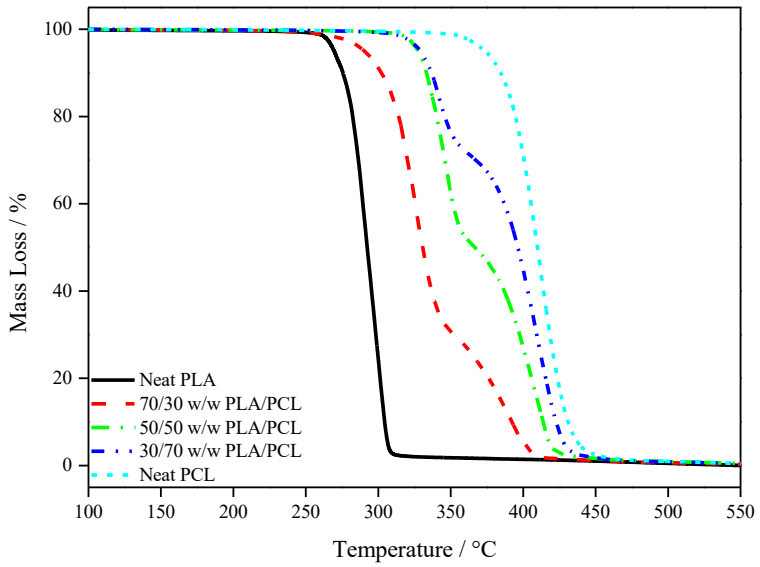

Figure 4.11 The TGA curves for thermal degradation of the neat polymers and their polymer blends

Table 4.7 Thermal degradation temperatures at 20 % (PLA degradation step) and 80 % (PCL degradation step) mass loss for the neat polymers and their blends

Sample	PLA ($T_{20\,\%}$)/ °C	PCL ($T_{80\,\%}$)/°C	Char % @ 550 °C
Neat PLA	326.5	-	0.01
70/30 w/w PLA/PCL	313.7	375.7	0.3
50/50 w/w PLA/PCL	340.5	405.5	0.5
30/70 w/w PLA/PCL	345.8	415.8	0.4
Neat PCL	-	422.9	0.5

$T_{20\,\%}$ and $T_{80\,\%}$ is temperature at 20 % and 80 % mass loss, respectively

The thermal degradation curves of the individual polymers with $Mg(OH)_2$ and APTMS-TiO_2 nanoparticles are presented in Figure 4.12. For the $Mg(OH)_2$ containing samples (Figure 4.12 (a) and (b)), below 300 °C, a decrease in thermal stability of both PLA and PCL in nanocomposites, was observed with the presence and increase in content of $Mg(OH)_2$ (1, 3, 5, 10 wt.%). As expected, the loss of thermal stability at temperatures below 300 °C in the $Mg(OH)_2$ samples was attributed to the low thermal stability of $Mg(OH)_2$ at those temperatures where it loses water bound on its surface. As mentioned earlier, neat $Mg(OH)_2$ nanorods had a low onset of degradation around 100 °C, which is attributed to the loss of water. The presence of water in the biodegradable polymers, prematurely degrades the polymers [20], so the release of water by $Mg(OH)_2$ could have lowered the thermal stabilities of both PLA and PCL. Also another factor to consider would be the dispersion and the compatibility between the filler and polymer matrix [21]. It has been reported that poor compatibility between inorganic fillers and a polymer matrix will result in the metal ions acting as catalysts in the degradation of both PLA and PCL [18-20, 22]. Also, the crevices observed from the SEM images could have been potential catalytic sites for degradation. It is therefore possible that the $Mg(OH)_2$ nanorods could have had a catalytic effect. Above 330 °C it was observed that the samples with higher $Mg(OH)_2$ nanoparticle content became more thermally stable than those with less $Mg(OH)_2$ nanoparticle content. The increase in thermal stability above 300 °C was attributed to the formation of highly thermally stable MgO produced during major degradation of $Mg(OH)_2$. MgO is deposited as layers, absorbing the heat from the polymer matrix. It slows the degradation rate of the constituent polymers and possibly acting as a barrier to the release of volatile degradation products. $Mg(OH)_2$ shows an autocatalytic effect on the thermal

degradation of polymers. At lower temperatures due to the loss of water and other organic materials, it speeds up the rate of thermal degradation of polymer. However at higher temperatures it retards the degradation of polymers. Since it has been reported that biodegradable polymers are susceptible to early thermal degradation in the presence of water [20, 23]. Another interesting observation was the presence of a second degradation peak around the degradation temperature of PCL. This was amplified especially for the 90/10 w/w PCL/$Mg(OH)_2$ sample. This behaviour could be as a results of $Mg(OH)_2$'s autocatalytic effect, whereby it speeds up the degradation at lower temperatures, but at temperatures above 300 ºC, during its second degradation step, insulates the polymers due to the formation of thermally stable MgO. After degradation was complete, char residues in all the samples with the $Mg(OH)_2$ nanorods were observed (Tables 4.8 and 4.9). The higher the $Mg(OH)_2$ nanoparticle content was, the higher the char content which remained after degradation. However, less char was observed than the corresponding $Mg(OH)_2$ content initially added. It is clear that $Mg(OH)_2$ on its own has components in it, that degrade at temperatures below 300 ºC, so it was expected to get an amount of char less than the amount of filler initially added.

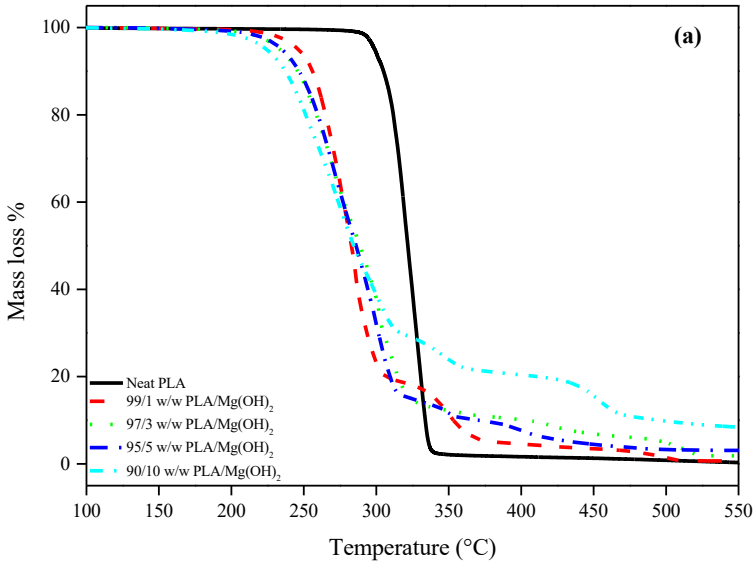

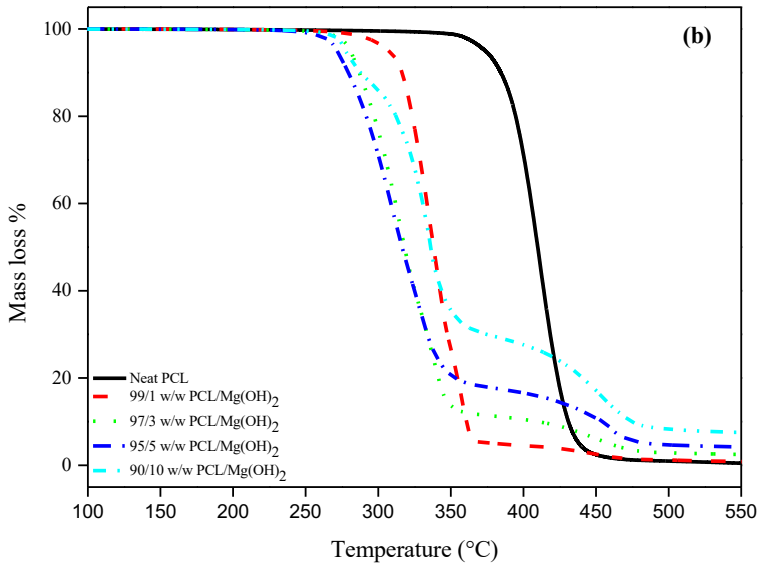
(b)
Mass loss %
Temperature (°C)
Neat PCL
99/1 w/w PCL/Mg(OH)2
97/3 w/w PCL/Mg(OH)2
95/5 w/w PCL/Mg(OH)2
90/10 w/w PCL/Mg(OH)2

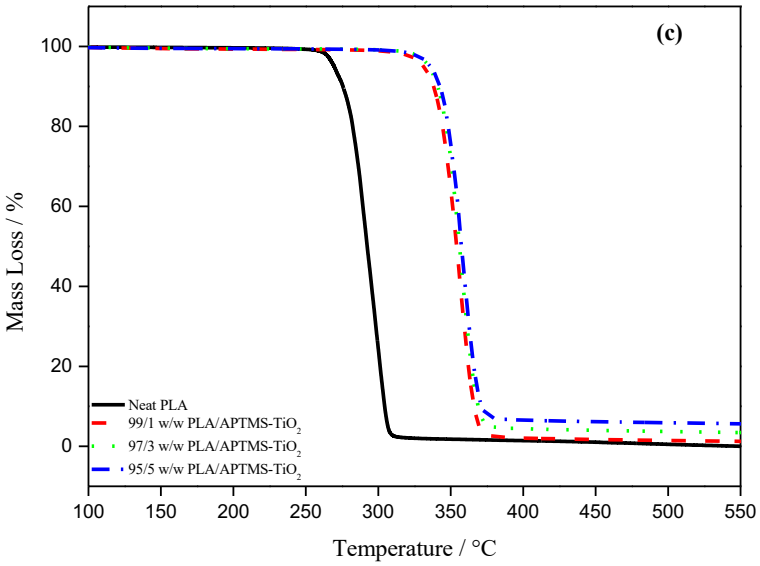
(c)
Mass Loss / %
Temperature / °C
Neat PLA
99/1 w/w PLA/APTMS-TiO2
97/3 w/w PLA/APTMS-TiO2
95/5 w/w PLA/APTMS-TiO2

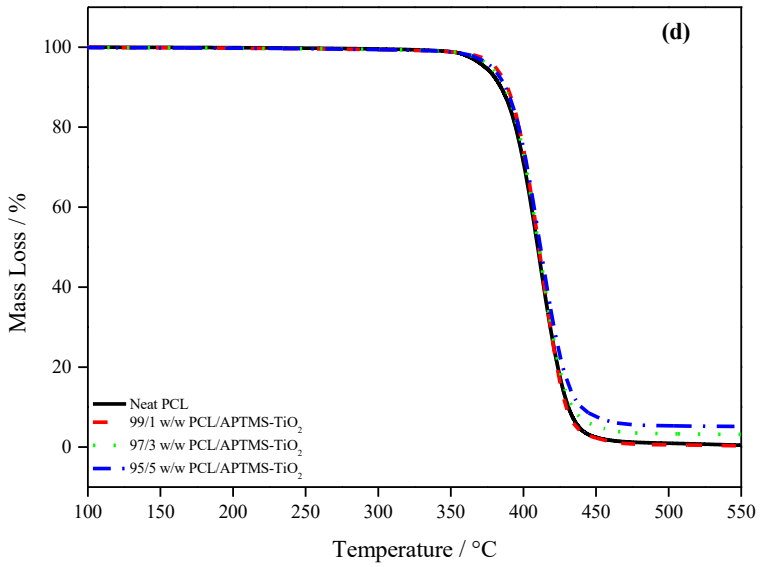

Figure 4.12 TGA curves of the thermal degradation for (a) PLA with $Mg(OH)_2$ (b) PCL with $Mg(OH)_2$ (c) PLA with APTMS-TiO_2 (d) PCL with APTMS-TiO_2

For the APTMS-TiO_2 containing samples (Figure 4.12 (c) and (d), Table 4.8 and 4.9), for both PLA and PCL nanocomposites, it was observed that the thermal stability was increased in the presence and with an increase in content of the APTMS-TiO_2 nanoparticles. The increase in thermal stability was directly proportional to the content of APTMS-TiO_2 added. This was attributed to the higher thermal stability of the TiO_2 nanoparticles. The titania nanoparticles therefore delayed the onset of degradation of the two polymers and possibly acted as an insulant to their polymer chains [6, 21]. After degradation was complete, char residue was also observed in all the samples with the nanoparticles, and its content was directly proportional to the amount of nanoparticles which was used. For the PLA/APTMS-TiO_2 nanocomposites, the amount of char residue which remained was slightly more char than the corresponding nanoparticle content initially added. This was attributed to a better compatibility between the polymer matrix and the nanoparticles, resulting in filler acting as an insulant. Good compatibility between PLA and the APTMS-TiO_2 was observed during SEM analysis. Titania has a high heat capacity allowing it to absorb heat from the polymer matrix. This insulates the polymer chains and therefore increase the degradation temperature of the polymer [24]. But for the PCL/APTMS-TiO_2, less char was observed than the corresponding filler content added (Table 4.9). This was indicative of the loss of organic matter in the nanoparticles. Also, this could also

have been due to the poor insulating properties of the nanoparticles due to poor compatibility. From SEM and TEM analysis (Figure 4.3 and 4.5), it was seen that the APTMS-TiO_2 nanoparticles preferentially located in PLA.

Table 4.8 Thermal degradation temperatures at 20 % (PLA degradation step) mass loss for neat PLA, and their single polymer nanocomposites

Sample	PLA ($T_{20\%}$)/ °C	Char % @ 550 °C
Neat PLA	326.5	0.01
PLA nanocomposites with $Mg(OH)_2$		
99/1 w/w PLA/$Mg(OH)_2$	264.7	0.7
97/3 w/w PLA/$Mg(OH)_2$	258.1	1.8
95/5 w/w PLA/$Mg(OH)_2$	259.3	3.1
90/10 w/w PLA/$Mg(OH)_2$	251.7	8.4
PLA nanocomposites with APTMS-TiO_2		
99/1 w/w PLA/ APTMS-TiO_2	343.9	1.1
97/3 w/w PLA/ APTMS-TiO_2	346.7	3.6
95/5 w/w PLA/ APTMS-TiO_2	348.3	5.6

$T_{20\%}$ is temperature at 20 % mass loss

Table 4.9 Thermal degradation temperatures at 80 % (PCL degradation step) mass loss for neat PCL, and their single polymer nanocomposites

Sample	PCL ($T_{80\%}$)/°C	Char % @ 550 °C
Neat PCL	422.9	0.5
PCL nanocomposites with $Mg(OH)_2$		
99/1 w/w PCL/$Mg(OH)_2$	323.6	0.8
97/3 w/w PCL/$Mg(OH)_2$	297.4	2.5
95/5 w/w PCL/$Mg(OH)_2$	291.1	4.1
90/10 w/w PCL/$Mg(OH)_2$	312.6	7.5
PCL nanocomposites with APTMS-TiO_2		
99/1 w/w PCL/ APTMS-TiO_2	423.0	0.5
97/3 w/w PCL/ APTMS-TiO_2	424.4	3.1
95/5 w/w PCL/ APTMS-TiO_2	427.2	5.0

$T_{80\%}$ is temperature at 80 % mass loss

The polymer nanocomposites at different blend ratios (70/30, 50/50, and 30/70 w/w PLA/PCL) and filler content (1, 3, 5, and 10 wt.%) are illustrated in Figure 4.13. Like in the single polymer nanocomposites with $Mg(OH)_2$ above, the presence of $Mg(OH)_2$ nanoparticle in the blends,

resulted in a loss of thermal stability at lower temperatures (Figure 4.13 (a) to (c)). The higher the $Mg(OH)_2$ content was, the lower the thermal stability. But as it was mentioned earlier, above 330 °C, the opposite was observed, whereby the polymers were insulated to degrade at a bit higher temperatures with remainder of char. Samples with higher $Mg(OH)_2$ nanoparticle content became more thermally stable than those with less $Mg(OH)_2$ nanoparticle content at higher temperatures. Using the nanocomposites with a 30/70 w/w PLA/PCL ratio as an example, an increase in the char content with increase in $Mg(OH)_2$ was observed. From Figure 4.13 (c) and Table 4.10, the following information was observed: (i) With addition of 1 wt.% filler, a char residue of 1.8 wt.% was observed. (ii) With addition of 3.0 wt.% filler, a char residue of 3.2 wt.% was observed. (iii) With addition of 5 wt.% filler, a char residue of 4.7 % was observed and (iv) with the addition of 10 wt.% filler, a char residue of 8.9 % was observed. Clearly, an increase in char residue with increasing $Mg(OH)_2$ content can be seen. Also, at 1 and 3 wt.% filler content, the char content was higher than the amount of filler added. But, at 5 and 10 wt.% filler content, the char was less than the amount of filler added. This was observed for all the nanocomposite ratios. At higher temperatures (<300°C) due to the thermally stable MgO, the Mg(OH) insulates the polymers to degrade at higher temperatures and even leave a char, due to its high heat capacity. This could be that the MgO absorbs heat that was directed to polymers, and this might have shifted the thermal degradation of polymers to higher temperatures. For all the polymer blend nanocomposites containing $Mg(OH)_2$, three distinct steps were observed corresponding to the degradation temperature of the constituent components. The degradation of PLA took place below 250 ºC (around 230 ºC), the one for $Mg(OH)_2$ around 300 ºC, and lastly the one for PCL at temperatures above 300 ºC (around 330 ºC). This indicated a lack of compatibility and immiscibility of the components. This was coherent with observations made during SEM and DSC studies. In SEM analysis, clear phase separation and crevices were observed and during DSC, the constituent components retained the characteristic transition temperatures. In both cases, it pointed towards incompatibility and immiscibility between PLA, PCL and $Mg(OH)_2$.

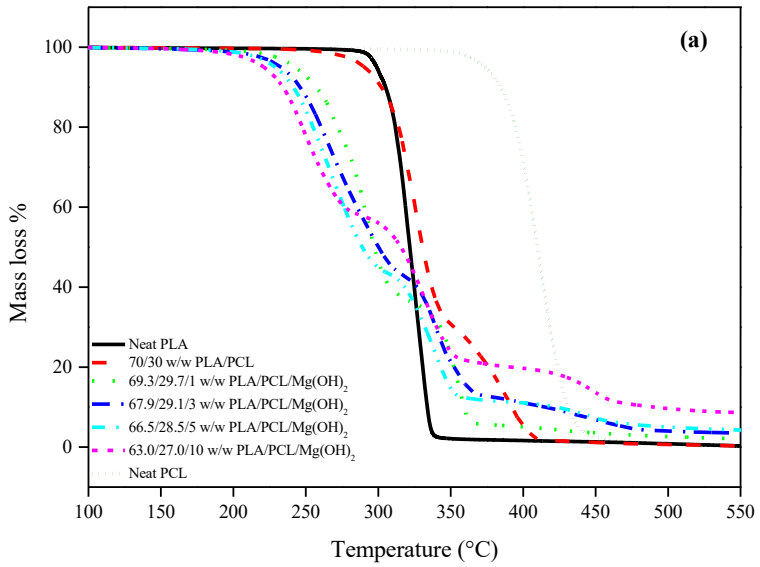
(a)
Mass loss %
Temperature (°C)
Neat PLA
70/30 w/w PLA/PCL
69.3/29.7/1 w/w PLA/PCL/Mg(OH)2
67.9/29.1/3 w/w PLA/PCL/Mg(OH)2
66.5/28.5/5 w/w PLA/PCL/Mg(OH)2
63.0/27.0/10 w/w PLA/PCL/Mg(OH)2
Neat PCL

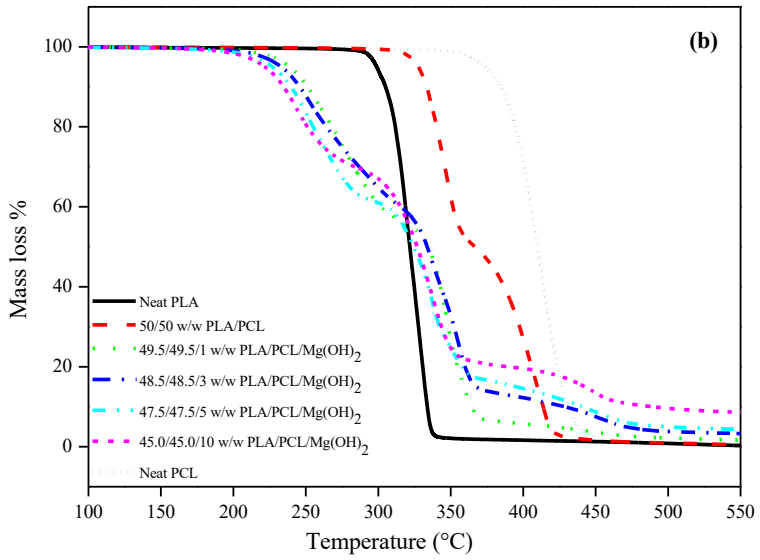
(b)
Mass loss %
Temperature (°C)
Neat PLA
50/50 w/w PLA/PCL
49.5/49.5/1 w/w PLA/PCL/Mg(OH)2
48.5/48.5/3 w/w PLA/PCL/Mg(OH)2
47.5/47.5/5 w/w PLA/PCL/Mg(OH)2
45.0/45.0/10 w/w PLA/PCL/Mg(OH)2
Neat PCL

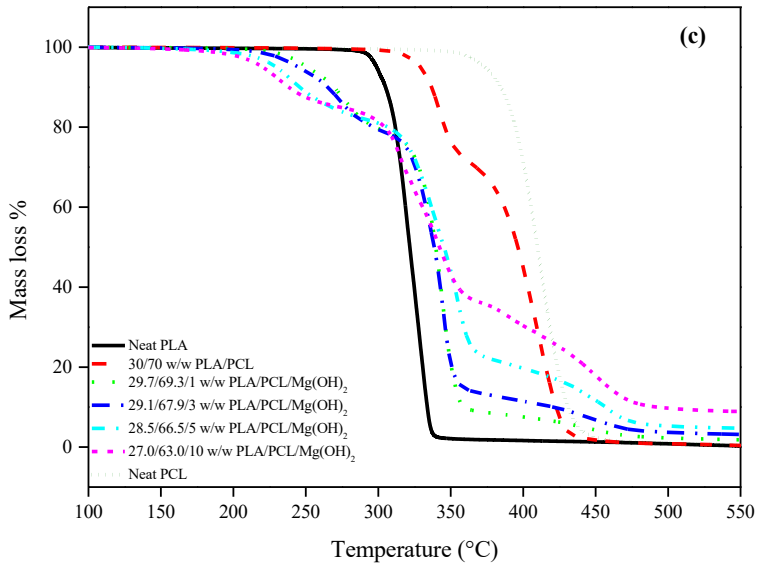

Figure 4.13 Thermal degradation curves for: $Mg(OH)_2$ nanocomposites at three blends ratios (a) 70/30 w/w PLA/PCL (b) 50/50 w/w PLA/PCL (c) 30/70 w/w PLA/PCL

Table 4.10 Thermal degradation temperatures at 20 % (PLA degradation step) and 80 % (PCL degradation step) mass loss for blend nanocomposites with $Mg(OH)_2$

Sample	PLA ($T_{20\%}$)/ °C	PCL ($T_{80\%}$)/ °C	Char % @ 550 °C
70/30 w/w PLA/PCL	313.7	375.7	0.3
69.3/29.7/1 w/w PLA/PCL/$Mg(OH)_2$	271.6	352.6	2.0
67.9/29.1/3 w/w PLA/PCL/$Mg(OH)_2$	260.1	352.1	3.5
66.5/28.5/5 w/w PLA/PCL/$Mg(OH)_2$	254.6	343.6	4.3
63.0/27.0/10w/w PLA/PCL/$Mg(OH)_2$	247.0	392.0	8.6
50/50 w/w PLA/PCL	340.5	405.5	0.5
49.5/49.5/1 w/w PLA/PCL/$Mg(OH)_2$	267.9	354.9	1.7
48.5/48.5/3 w/w PLA/PCL/$Mg(OH)_2$	264.2	360.2	3.3
47.5/47.5/5 w/w PLA/PCL/$Mg(OH)_2$	255.6	358.6	4.4
45.0/45.0/10w/w PLA/PCL/$Mg(OH)_2$	251.5	389.5	8.6
30/70 w/w PLA/PCL	345.8	415.8	0.4
29.7/69.3/1 w/w PLA/PCL/$Mg(OH)_2$	298.4	350.4	1.8
29.1/67.9/3 w/w PLA/PCL/$Mg(OH)_2$	296.6	350.6	3.2
28.5/66.5/5 w/w PLA/PCL/$Mg(OH)_2$	306.1	396.1	4.7
27.0/63.0/10w/w PLA/PCL/$Mg(OH)_2$	304.9	444.9	8.9

$T_{20\%}$ and $T_{80\%}$ is temperature at 20 % and 80 % mass loss, respectively

Figure 4.14 (a)-(c) shows the polymer blend nanocomposites with APTMS-TiO_2, these showed similar trends to those of the single polymer nanocomposites (PLA/APTMS-TiO_2 and PCL/APTMS-TiO_2). The polymer blend nanocomposites had higher thermal degradation temperatures than the pure polymer and their respective blends. An increased thermal stability was observed with the presence of APTMS-TiO_2 nanoparticles. The higher the APTMS-TiO_2 content was, the higher the thermal stability. The formation of char was also observed. This was clearly visible in the nanocomposites with a 30/70 w/w PLA/PCL ratio. Using these composites as an example, an increase in the char content with increase in APTMS-TiO_2 nanoparticles content was observed. From Figure 4.14 (a) and Table 4.11, the following information was observed: (i) With addition of 1 wt.% filler, a char residue of 1.7 % was observed. (ii) With addition of 3 wt.% filler, a char residue of 3.7 % was observed. (iii) With addition of 5 wt.% filler, a char residue of 6 % was observed. Noticeably, an increase in char

residue with increasing filler content can be seen. And also, the remaining char was more than the respective APTMS-TiO_2 content added. This was observed for all the nanocomposite ratios. As stated earlier, the increase in thermal stability was attributed to the high thermal stability of the titania nanoparticles. Also, the increase in thermal stability could have been due to the improved compatibility between the two polymer phases as a result of the functionalised filler acting as a compatibilizer. Following up on the char contents, more char was observed than the corresponding filer added, this revealed that the functionalised titania nanoparticles were a good insulant and prevented early onset of degradation [6]. To summarize observation made during TGA, an improvement in the thermal stability was experienced with $Mg(OH)_2$ only at higher temperatures and was attributed to the formation of MgO. APTMS-TiO_2 nanoparticles were far more effective; an increase in the thermal stability of all its nanocomposites was observed. With both $Mg(OH)_2$ and APTMS-TiO_2, presence of char was seen at 550 ºC indicating that the fillers insulated the polymers and also possibly interacted with the volatile degradation volatiles. The effect of $Mg(OH)_2$ and APTMS-TiO_2 on the degradation volatilization of PLA, PCL and their blends are discussed in the section below.

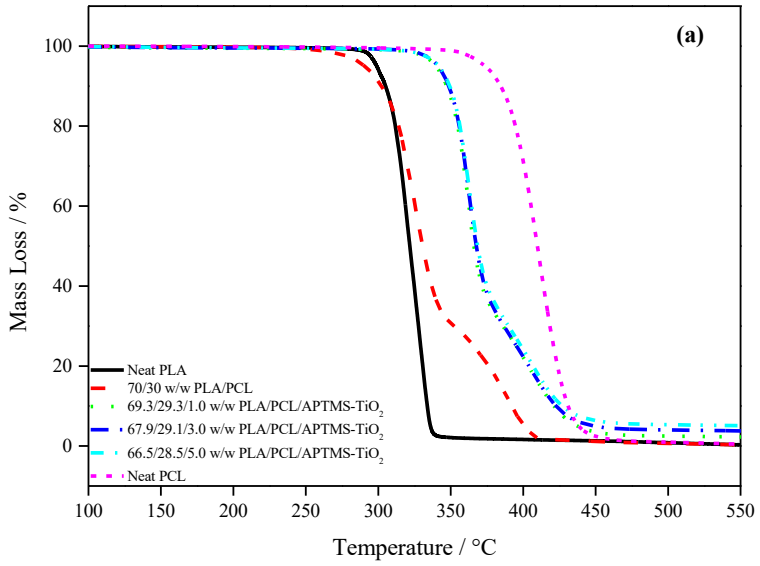

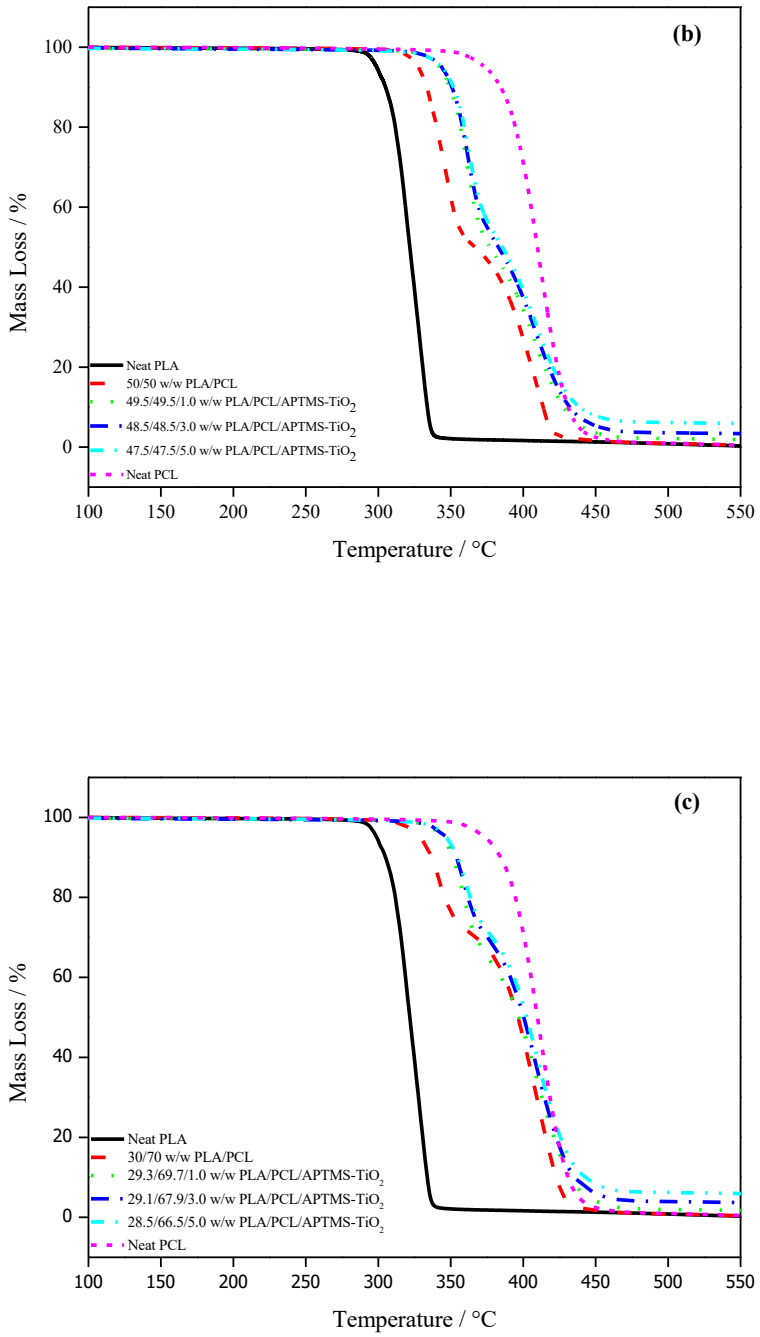

Figure 4.14 Thermal degradation curves for: APTMS-TiO_2 nanocomposites at three blends ratios (a) 70/30 w/w PLA/PCL (b) 50/50 w/w PLA/PCL and (c) 30/70 w/w PLA/PCL

Table 4.11 Thermal degradation temperatures at 20 % (PLA degradation step) and 80 % (PCL degradation step) mass loss for blend nanocomposites with APTMS-TiO_2

Sample	PLA ($T_{20\%}$)/ °C	PCL ($T_{80\%}$)/ °C	Char % @ 550 °C
70/30 w/w PLA/PCL	313.7	375.7	0.3
69.3/29.7/1 w/w PLA/PCL/APTMS-TiO_2	354.8	403.6	2.3
67.9/29.1/3 w/w PLA/PCL/APTMS-TiO_2	355.8	403.8	3.8
66.5/28.5/5 w/w PLA/PCL/APTMS-TiO_2	356.3	407.1	5.1
50/50 w/w PLA/PCL	340.5	405.5	0.5
49.5/49.5/1 w/w PLA/PCL/APTMS-TiO_2	356.8	414.9	1.9
48.5/48.5/3 w/w PLA/PCL/APTMS-TiO_2	358.1	417.5	3.4
47.5/47.5/5 w/w PLA/PCL/APTMS-TiO_2	359.4	420.3	5.9
30/70 w/w PLA/PCL	345.8	415.8	0.4
29.7/69.3/1 w/w PLA/PCL/APTMS-TiO_2	359.2	421.0	1.7
29.1/67.9/3 w/w PLA/PCL/APTMS-TiO_2	361.8	422.7	3.7
28.5/66.5/5 w/w PLA/PCL/APTMS-TiO_2	363.5	425.6	6.0

$T_{20\%}$ and $T_{80\%}$ is temperature at 20 % and 80 % mass loss, respectively

4.3.2 Thermal degradation volatilization studies by thermogravimetric analysis-Fourier transform infrared (TGA-FTIR)

As was mentioned earlier, it is important to study the thermal stability of materials and determining their limits. Knowing the thermal limits is not enough; understanding the volatiles that are released during their degradation is of utmost importance. To address this, thermal degradation of all the samples was performed whilst analysing their volatiles. Figures 4.15 to 4.19 shows the FTIR spectra of all the thermal degradation volatilisation of the prepared samples. During the thermal degradation of neat PLA, an FTIR spectra with peaks at 3581 (O–H stretching), 3007 (C–H stretching and O–H stretching), 2952 (C–H stretching and O–H stretching), 2740 (C–H stretching and O–H stretching), 2706 (C–H stretching and O–H stretching), 2382 (C=O), 2301 (C=O), 2180 (C=C stretching), 2112 (C=C stretching), 1793 (C=O), 1764 (C=O stretching), 1374 (C–H bending), 1240 (C–H bending), 1108 (C–H bending, C-O stretching), and 933 (C–H bending) cm^{-1} was observed. Presence of these peaks was indicative of CO, CO_2, water and compounds containing lactic acid and ester linkages as part of the degradation volatiles. Spectrum with the highest intensity of all the peaks was

observed at 369.43 °C. The spectrum obtained was very similar to one reported by Chen *et al.* [25] for neat PLA.

Neat PCL consists of the monomer units of ε-caprolactone and during its thermal degradation a TGA-FTIR spectra of the degradation volatiles showed peaks at 3538 (O–H stretching), 2979 (O–H stretching), 2944 (C–H stretching and O–H stretching), 2289 (C=O), 2172 (C-O), 2115 (C-O), 1445 (methylene scissoring), 1374 (C–H bending), 1343 (-CH_2-), 1772 (C=O stretching), 1165 (C–O stretching), 1075 (C–H bending), 1014 (C–H bending) and 855 (C–H bending) cm^{-1}. The spectra was indicative of the presence of the typical degradation products of PCL (carboxylic acids (5-hexenoic acid (whose structure contains a carboxyl group, -CH-, -CH_2-, and -CH_3 groups)), ε-caprolactone, carbon dioxide and water) [6, 22, 25]. For both neat PLA and PCL, the temperatures at which their highest intensities of degradation volatiles were seen corresponded to the temperature where the maximum degradation occurred during TGA analysis. The temperature for PCL was higher than that of PLA indicating a higher thermal stability. The spectra of PLA and PCL were however very similar, though the peaks for the volatile products appeared at different wavenumbers. For instance the CO_2 peak in PLA was seen at 2382 and 2301 cm^{-1} but in PCL it was observed at 2384 and 2289 cm^{-1}. Also, the C=O in PLA was seen at 1793 cm^{-1} but in PCL at 1772 cm^{-1}.

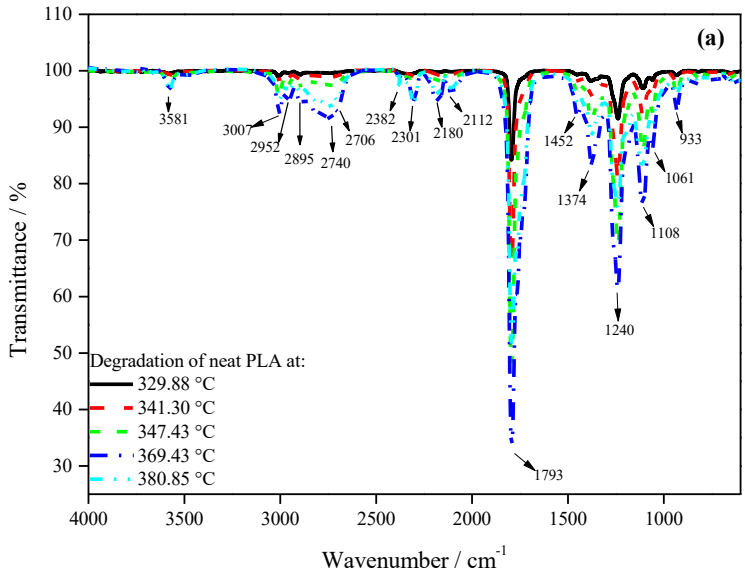

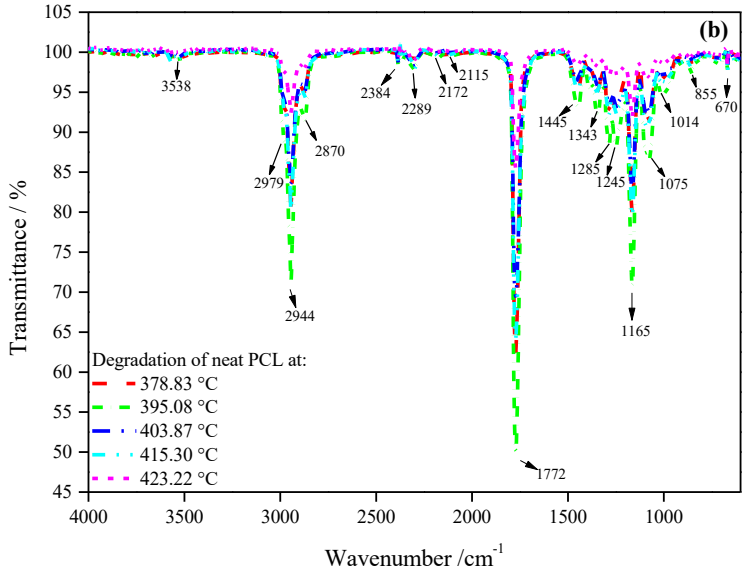

Figure 4.15 FTIR spectra of the degradation products of (a) neat PLA (b) neat PCL

In the polymer blends, the FTIR spectra (Figures 4.16) showed that the degradation products which were observed in both neat PLA and neat PCL were still present. Spectrum with the highest intensity for the degradation volatiles of PLA in the blends was observed at 336.90 °C in 70/30 w/w/ PLA/PCL (Figure 4.16 (a)). Compared with the highest intensity observed in neat PLA (Figure 4.15 (a)) at 369.43 °C, a decrease in the temperature at which the highest thermal degradation volatilization can be seen was observed. It is not clear why, since PCL has a higher thermal stability than PLA. As the content of PCL increased in a blend, the suppression of the degradation volatiles on the PLA phase was observed, as the intensity of the bands became lower. There are two possible reasons here, (i) it could be that the amount of the PLA phase is reduced, as the PCL increases, (ii) the PCL is able to insulate PLA and it is only degrading at temperatures above that of PLA, hence the decrease in the intensities of the bands in PLA phase, and the shift towards higher temperatures of the maximum. [11]. For PLA phase in the 70/30 w/w PLA/PCL blend, maximum intensity was observed at 336.90 °C. In the 50/50 w/w PLA/PCL blend, maximum intensity was observed at 360.03 °C, whilst in the 30/70 w/w PLA/PCL blend it was observed at 367.65 °C. As for the PCL in the blends (Figures 4.16 (b)), a clear decrease in the temperature at which the highest intensity was observed was seen with an increase in PLA content. In the 30/70 w/w PLA/PCL blend, maximum intensity was observed at 417.77 °C. In the 50/50 w/w PLA/PCL blend, maximum intensity was observed at 409.25 °C, whilst in the 70/30 w/w PLA/PCL blend highest intensity was observed at 389.67 °C.

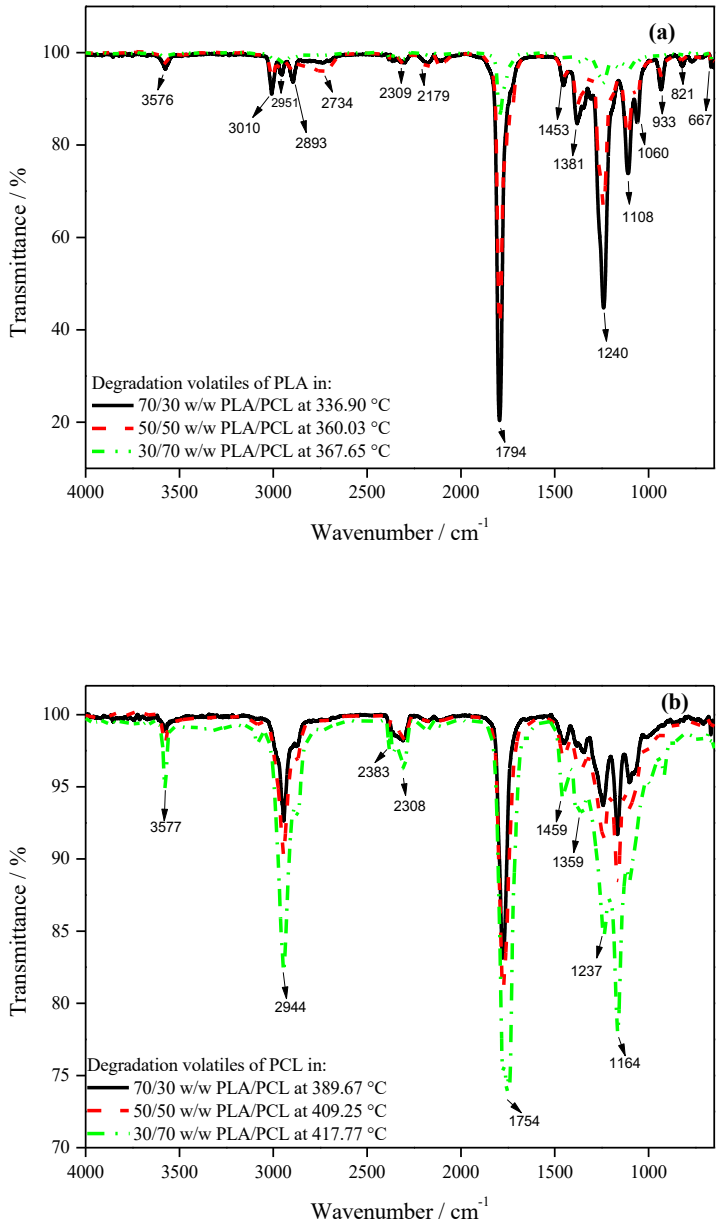

Figure 4.16 FTIR spectra of degradation products of the PLA (a) and PCL (b) in the polymer blends

Addition of fillers, $Mg(OH)_2$ and APTMS-TiO_2 (Figure 4.17), had a significant effect on the degradation of neat PLA and PCL. A decrease in the intensity of the peaks was observed and it was directly proportional to the increase in the amount of the filler. This was observed in all the single polymer nanocomposites. This indicated that the fillers acted as barriers to the release of degradation volatiles of both PLA and PCL. In the PLA/$Mg(OH)_2$ nanocomposites, an

increase in the volatilization degradation temperature by more than 9 ºC at 3 and 10 wt.% $Mg(OH)_2$ content was observed. This was attributed to sufficient suppression of the degradation volatiles by the nanoparticles. However, there was a decrease at 1 and 5 wt.% $Mg(OH)_2$ content, which could have been due to the uneven distribution of $Mg(OH)_2$ in the polymers, seen in the SEM images in Figures 4.2. It is possible that the presence of $Mg(OH)_2$ agglomerates, hindered the $Mg(OH)_2$ nanorods from sufficiently suppressing the release of the degradation volatiles. The decrease could also have been due to an early loss in the thermal stability of the polymers due to the possibility that the $Mg(OH)_2$ catalysed the degradation process due to the release of water at early temperatures (<300ºC). In all the PCL nanocomposites, the presence of $Mg(OH)_2$ resulted in a decrease with the exception of the 95/5 w/w PCL/$Mg(OH)_2$ where a slight increase was observed. So despite $Mg(OH)_2$ reducing the thermal stability of both PLA and PCL, it suppressed the escape of volatiles which was seen with the decrease in the intensities of the peaks of the degradation volatiles. In few single polymer nanocomposites (97/3 w/w PLA/$Mg(OH)_2$, 90/10 w/w PLA/$Mg(OH)_2$ and 95/5 w/w PCL/$Mg(OH)_2$) increases were observed in the temperatures at which the highest intensity (maximum volatilization) were observed. Despite the fillers having a catalytic effect on the degradation of the polymers, their ability to suppress the escape of the degradation volatile could have been greater which led to a delay in temperature which the volatiles would have been observed. This cannot be taken as an improvement in the thermal stability of the polymers, but rather as a measure in the effectiveness of the fillers in suppressing the release of the degradation volatiles (smoke), which is an important attribute for all flame retardants. In the presence of APTMS-TiO_2 in both PLA and PCL, there was a decrease in the intensities on the FTIR peaks as well as a decrease in the temperature at which the highest intensities were observed. The reduced intensities indicated the effectiveness of the nanofiller in blocking the emission of the degradation volatiles. However, the earlier release of the volatiles at lower temperature showed that the nanoparticles possibly increased the rate at which the release of the degradation volatiles of both PLA and PCL was released despite improving their thermal stability which was seen during TGA analysis.

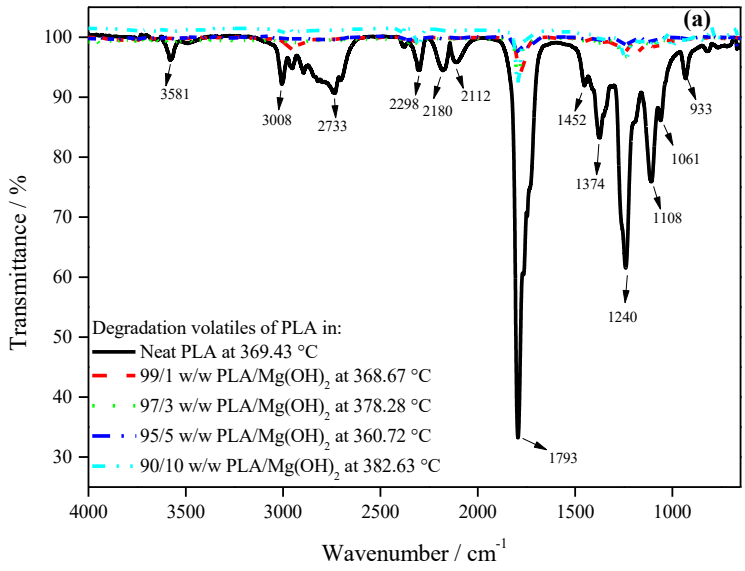
(a)
Transmittance / %
Wavenumber / cm-1
3581
3008
2733
2298
2180
2112
1452
1374
1240
1793
1108
1061
933
Degradation volatiles of PLA in:
Neat PLA at 369.43 °C
99/1 w/w PLA/Mg(OH)2 at 368.67 °C
97/3 w/w PLA/Mg(OH)2 at 378.28 °C
95/5 w/w PLA/Mg(OH)2 at 360.72 °C
90/10 w/w PLA/Mg(OH)2 at 382.63 °C

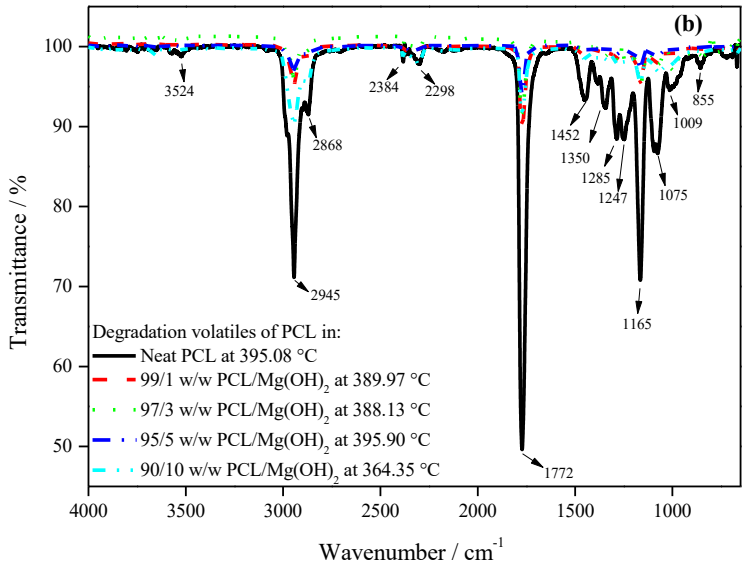
(b)
Transmittance / %
Wavenumber / cm-1
3524
2868
2945
2384
2298
1452
1350
1285
1247
1772
1165
1075
1009
855
Degradation volatiles of PCL in:
Neat PCL at 395.08 °C
99/1 w/w PCL/Mg(OH)2 at 389.97 °C
97/3 w/w PCL/Mg(OH)2 at 388.13 °C
95/5 w/w PCL/Mg(OH)2 at 395.90 °C
90/10 w/w PCL/Mg(OH)2 at 364.35 °C

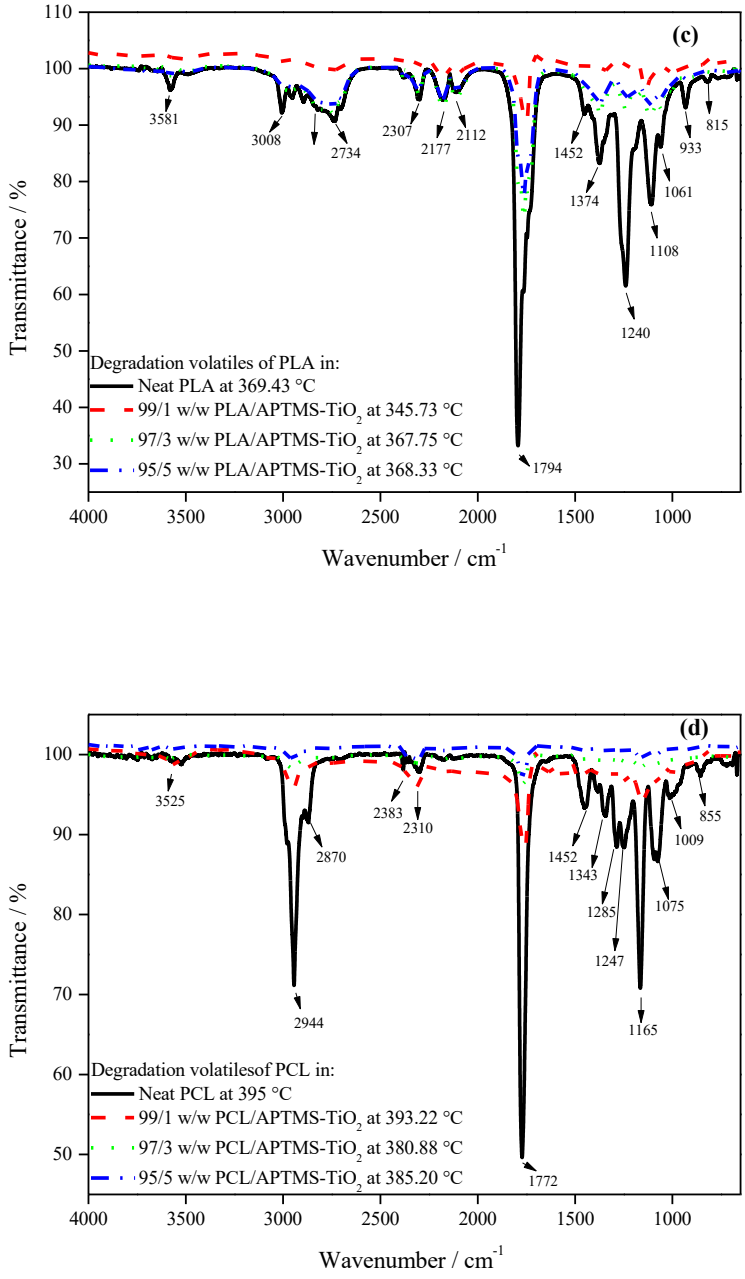

Figure 4.17 FTIR spectra of degradation products of the PLA (a, c) and PCL (b, d) in the single polymer nanocomposites

In the polymer blend nanocomposites (Figures 4.18 and 4.19), with either $Mg(OH)_2$ or APTMS-TiO_2, a decrease in the intensity of the peaks of the degradation volatiles was also observed. Both fillers effectively acted as barriers to the release of the degradation volatiles of both PLA and PCL in the polymer blend nanocomposites. In the $Mg(OH)_2$ nanocomposites, the decrease in the intensities of the peaks were much more pronounced in the 30/70 w/w

PLA/PCL nanocomposites (Figure 4.18 (e) and (f)). From the thermal degradation volatilization of PLA in the $Mg(OH)_2$ polymer blend nanocomposites, varied observations were made for the temperature at which the maximum thermal degradation volatilization was observed in the different polymer blend ratios.

In the 70/30 w/w PLA/PCL blend nanocomposites, at 1 and 3 wt.% $Mg(OH)_2$ content, an increase in the temperature at which the highest intensity was observed. However, when the $Mg(OH)_2$ content was increased to 5 and 10 wt.%, a decrease was seen. This contrast was attributed to the dispersion of the fillers in these nanocomposites. At lower filler content, a fairly good dispersion was achieved. Sufficient interaction between the filler and the polymer matrix was therefore achieved, which resulted in a delay in the temperature at which the maximum thermal degradation volatilization was observed. However, at higher filler content, agglomeration and cracks (see TEM and SEM results, section 4.1.3 and 4.1.4) could possibly have prevented optimum interaction between the $Mg(OH)_2$ nanorods and the polymer matrix. A decrease in the temperature at which the maximum thermal degradation volatilization was therefore observed.

During the degradation of PLA in the 50/50 w/w PLA/PCL blend nanocomposites, an increase in the temperature at which the maximum thermal degradation volatilization occurred was observed compared to the PLA in the neat polymer blend (360.03 ºC). In the presence of 1, 3, 5 and 10 wt.% $Mg(OH)_2$, it was observed at 372.03, 366.80, 366.18 and 365.88 ºC. This was attributed to a possible interaction between the degradation volatiles with the $Mg(OH)_2$ nanorods, therefore suppressing the volatiles to be released at a higher temperature. In the 30/70 w/w PLA/PCL blend nanocomposites, at 1, 3, 5 and 10 wt.% $Mg(OH)_2$ the temperatures at which the PLA maximum thermal degradation volatilization was seen were observed at 366.78, 367.00, 366.77 and 367.00 ºC, respectively. Compared to the highest intensity for the degradation of PLA in the neat polymer blend (367.65 ºC), it remained relatively the same. This indicated that there was possibly no sufficient interaction between the $Mg(OH)_2$ nanorods and the degradation volatiles, so the emission of the degradation volatiles was not retarded to be released at higher temperatures.

Looking at degradation volatiles of PCL in the 30/70 w/w PLA/PCL nanocomposites with $Mg(OH)_2$ (Figure 4.18 (f)), the highest intensities observed decreased with increasing $Mg(OH)_2$ content, as well as the temperature at which they occur. For 29.7/69.3/1 w/w PLA/PCL/$Mg(OH)_2$ the highest intensity was observed at 366.78 °C and had a transmittance intensity of 58.27%. For 29.1/67.9/3 w/w PLA/PCL/$Mg(OH)_2$ it was observed at 359.07 °C

and had a transmittance intensity of 47.98%. For 28.5/66.5/5 w/w PLA/PCL/$Mg(OH)_2$ it was observed at 370.22 °C and had an transmittance intensity of 29.49%. The lowest intensity was observed for 27.0/63.0/10 w/w PLA/PCL/$Mg(OH)_2$ at 350.30 °C and had a transmittance intensity of 21.14%. The decrease in the temperatures at which the highest intensities were observed was coherent with decreases in the thermal stability of the PCL in these polymer blend nanocomposites which was seen during TGA analysis in the presence of $Mg(OH)_2$. The decrease in the intensities of the peaks revealing the ability of $Mg(OH)_2$ in acting as a barrier to the release of the degradation volatiles. There was a shift to the left and an increase in the intensities (maximum thermal degradation volatilization) of the C=O peaks for 70/30 w/w PLA/PCL and 50/50 w/w PLA/PCL nanocomposites with 10 wt.% $Mg(OH)_2$ content. This was an indication that there might have been chemical interaction between the nanoparticles and the volatile degradation products [5].

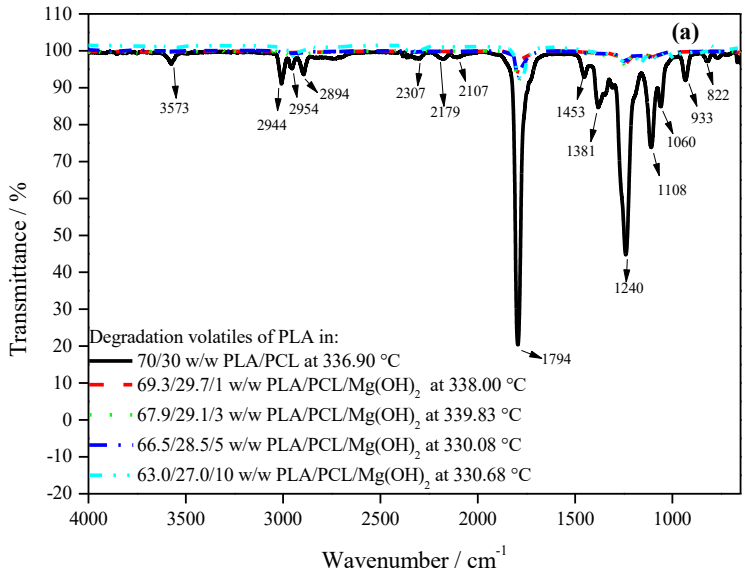

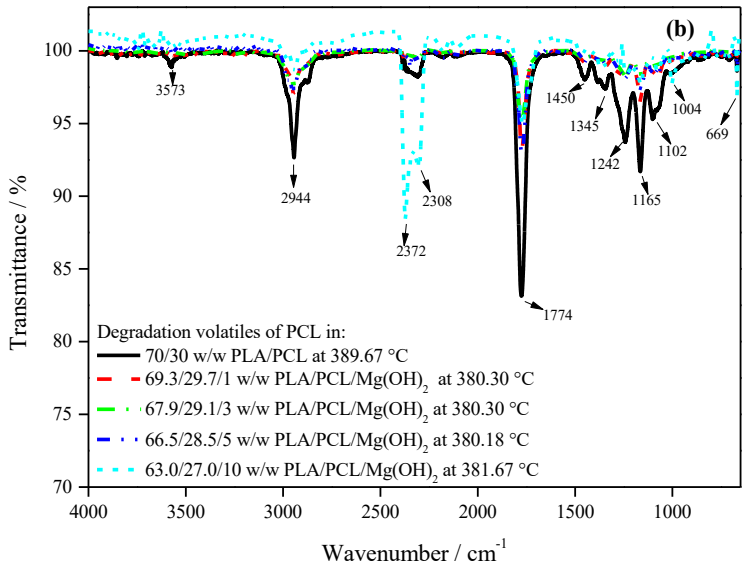
(b)
Transmittance / %
Wavenumber / cm-1
3573
2944
2372
2308
1774
1450
1345
1242
1165
1102
1004
669
Degradation volatiles of PCL in:
70/30 w/w PLA/PCL at 389.67 °C
69.3/29.7/1 w/w PLA/PCL/Mg(OH)2 at 380.30 °C
67.9/29.1/3 w/w PLA/PCL/Mg(OH)2 at 380.30 °C
66.5/28.5/5 w/w PLA/PCL/Mg(OH)2 at 380.18 °C
63.0/27.0/10 w/w PLA/PCL/Mg(OH)2 at 381.67 °C

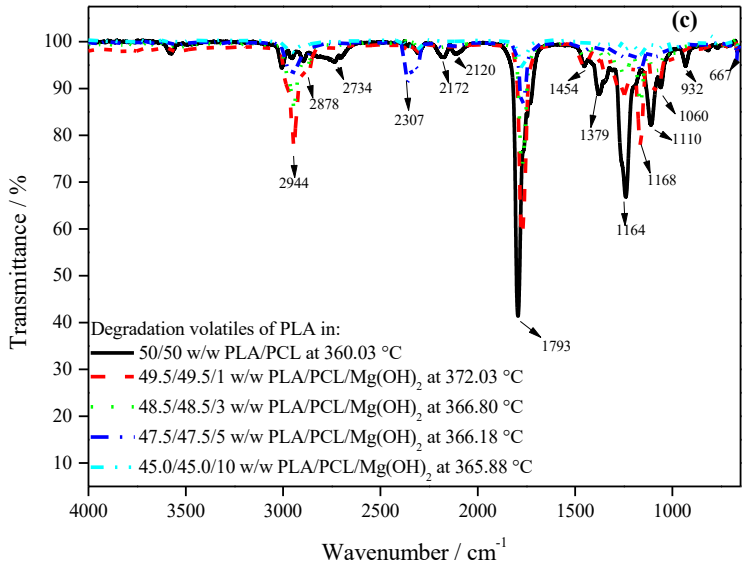
(c)
Transmittance / %
Wavenumber / cm-1
2944
2878
2734
2307
2172
2120
1793
1454
1379
1164
1168
1110
1060
932
667
Degradation volatiles of PLA in:
50/50 w/w PLA/PCL at 360.03 °C
49.5/49.5/1 w/w PLA/PCL/Mg(OH)2 at 372.03 °C
48.5/48.5/3 w/w PLA/PCL/Mg(OH)2 at 366.80 °C
47.5/47.5/5 w/w PLA/PCL/Mg(OH)2 at 366.18 °C
45.0/45.0/10 w/w PLA/PCL/Mg(OH)2 at 365.88 °C

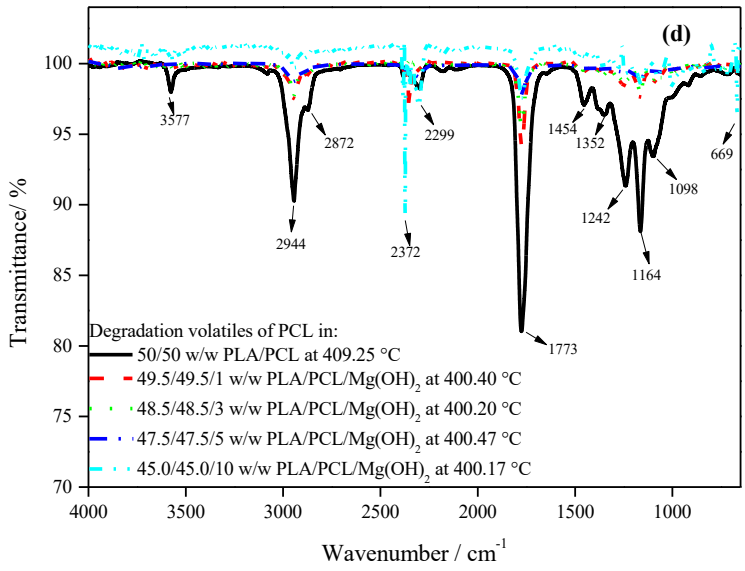
(d)
Transmittance/ %
Wavenumber / cm-1
3577
2944
2872
2372
2299
1773
1454
1352
1242
1164
1098
669
Degradation volatiles of PCL in:
50/50 w/w PLA/PCL at 409.25 °C
49.5/49.5/1 w/w PLA/PCL/Mg(OH)2 at 400.40 °C
48.5/48.5/3 w/w PLA/PCL/Mg(OH)2 at 400.20 °C
47.5/47.5/5 w/w PLA/PCL/Mg(OH)2 at 400.47 °C
45.0/45.0/10 w/w PLA/PCL/Mg(OH)2 at 400.17 °C

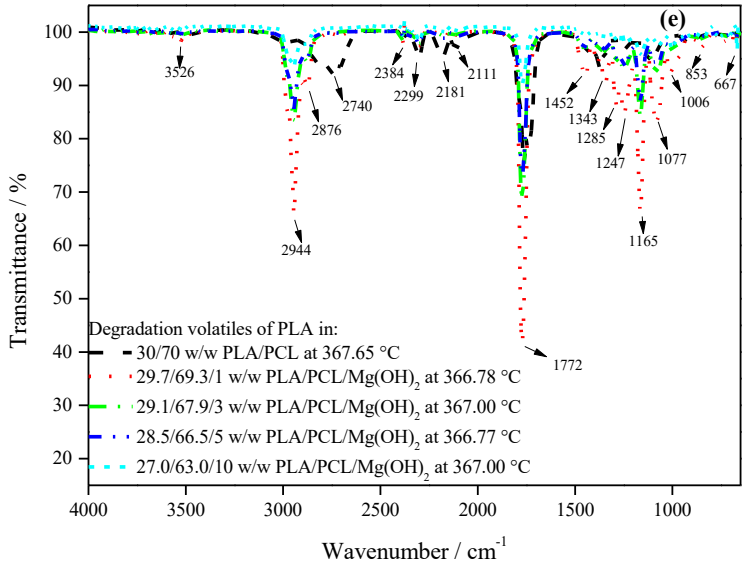
(e)
Transmittance / %
Wavenumber / cm-1
3526
2944
2876
2740
2384
2299
2181
2111
1772
1452
1343
1285
1247
1165
1077
1006
853
667
Degradation volatiles of PLA in:
30/70 w/w PLA/PCL at 367.65 °C
29.7/69.3/1 w/w PLA/PCL/Mg(OH)2 at 366.78 °C
29.1/67.9/3 w/w PLA/PCL/Mg(OH)2 at 367.00 °C
28.5/66.5/5 w/w PLA/PCL/Mg(OH)2 at 366.77 °C
27.0/63.0/10 w/w PLA/PCL/Mg(OH)2 at 367.00 °C

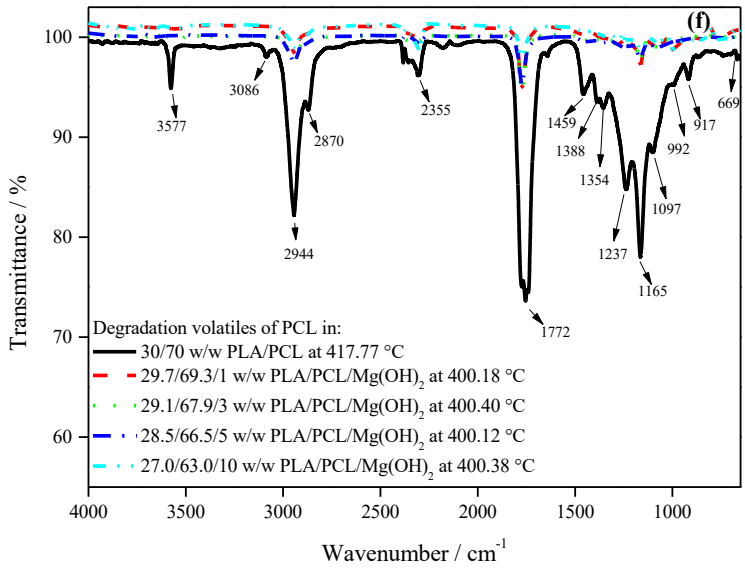

Figure 4.18 FTIR spectra of degradation products of the PLA (a, c, e) and PCL (b, d, f) in the $Mg(OH)_2$ polymer blend nanocomposites

In the APTMS-TiO_2 nanocomposites (Figure 4.19(a) to (f)), a decrease in the intensities of the peaks was also observed during the thermal degradation volatilization of both PLA and PCL. This effect was also much more pronounced in the degradation of PLA in the 70/30 w/w PLA/PCL nanocomposites (Figure 4.19(a)). This was an indication that there was interaction of the APTMS-TiO_2 nanoparticles with the degradation volatiles. The nanoparticles could have acted as a barrier, preventing the escape of the degradation volatiles from PLA. The only exception was during the degradation of PCL in the 70/30 w/w PLA/PCL nanocomposites (Figure 4.19(b)), where an increase in the intensities (maximum thermal degradation volatilization) was observed. In these particular polymer blend nanocomposites, a preferential location of APTMS-TiO_2 in PLA was observed during SEM and TEM analysis. Very few nanoparticles were present in PCL, so it is possible that the nanoparticles present in the PCL were not enough to interact sufficiently with the degradation volatile to shield them from escaping. As for the maximum thermal degradation volatilization temperature for PLA, an increase was seen in the 70/30 w/w PLA/PCL and 50/50 w/w PLA/PCL polymer blend nanocomposites. Using the 70/30 w/w PLA/PCL blend nanocomposites to illustrate this, when 1, 3 and 5 wt.% APTMS-TiO_2 nanoparticle contents were added, their temperatures were found at 339.0, 346.6 and 337.2 ºC, respectively. Compared to the neat polymer blend (70/30 w/w PLA/PCL) which had the highest intensity of the degradation volatiles of PLA at 336.9 ºC, an

improvement was seen. This showed that APTMS-TiO_2 might have interacted with the degradation volatiles and therefore delayed their release at higher temperatures. This also could indicate that the APTMS-TiO_2 increased the thermal stability of PLA. This was supported by the observations made during TGA analysis, where an increase in thermal stability was directly proportional to the content of APTMS-TiO_2 added. Mofokeng *et al.* [23] also observed a similar behaviour. In their study they used unfunctionalised TiO_2 as a nanofiller in poly(lactic acid) (PLA)/poly(hydroxybutyrate-co-valerate) (PHBV) blends. They found that TiO_2 increased the thermal stability of both PHBV and PLA, and the increase was proportional to the content of the filler. They attributed this to the high thermal stability of the filler. In the 30/70 w/w PLA/PCL blend nanocomposites, during the degradation of PLA, there was a decrease in the temperatures at which the maximum thermal degradation volatilization was observed. In the neat polymer blend the spectrum was observed at 367.65 ºC. However, in the presence of the APTMS-TiO_2 nanoparticles at 1, 3 and 5 wt.% contents, the thermal degradation volatilization was seen at 362.42, 360.95 and 365.80 ºC, which was significantly less than the polymer blend. The decrease can be attributed to the observations made in the morphology study; the APTMS-TiO_2 nanoparticles were mostly dispersed in PLA and agglomerates were present. Even though APTMS-TiO_2 nanoparticles could have interacted with the degradation volatiles and decreased the amounts released, the degradation volatiles were released at much lower temperatures. The agglomeration might have prevented the filler from effectively hindering the escape of the degradation volatiles. During the degradation of PCL in the APTMS-TiO_2 nanocomposites, various observations were made in the temperature at which the maximum thermal degradation volatilization was observed. In the 70/30 w/w PLA/PCL, a decrease in the maximum thermal degradation volatilization was observed at 1 wt.%, and remained relatively the same at 3 and 5 wt.% APTMS-TiO_2 content. This also was attributed to dispersion of APTMS-TiO_2 in PLA. It is possible that in PCL there was not a sufficient amount of the nanoparticles to interact with degradation volatile, so they were released at lower temperatures. In the 50/50 w/w PLA/PCL and 30/70 w/w PLA/PCL nanocomposites, a slight increase was seen in the maximum thermal degradation volatilization temperature at 1 wt.% APTMS-TiO_2 content, but significant decreases were seen in both blend ratios at 3 and 5 wt.% filler content. The decreases in the maximum thermal degradation volatilization temperature for PCL phase of the PLA/PCL blends nanocomposites observed in 3 and 5 wt.% APTMS-TiO_2 content, could have been due to the presence of low thermal stability of PLA [6]. And also since the nanoparticles were preferentially located in PLA, during the degradation of PCL, the PCL was not insulated by the APTMS-TiO_2. To summarize the effect of $Mg(OH)_2$ and APTMS-TiO_2, both fillers suppressed the volatile degradation

products which was seen by the reduced intensities in comparison to the neat components. There was a direct correlation between the thermal stability and the maximum thermal degradation volatilization of PLA, PCL and their blends. Also, the maximum thermal degradation volatilization might have also been influenced by the dispersion of the fillers.

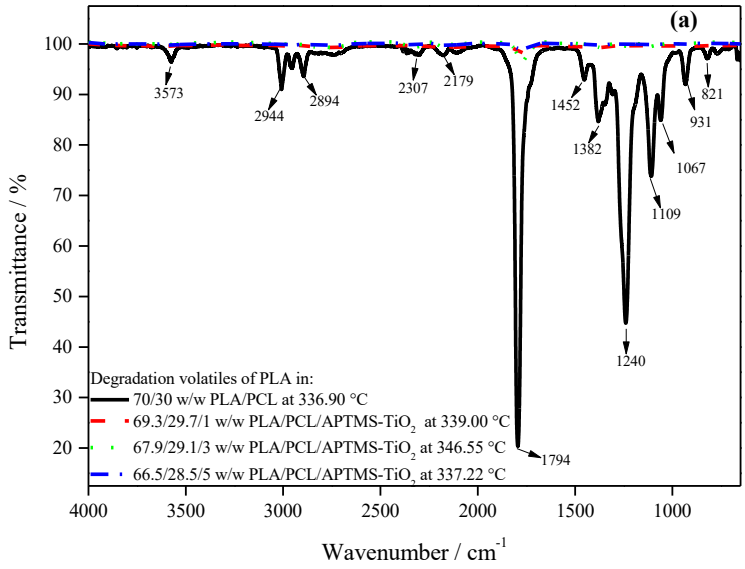

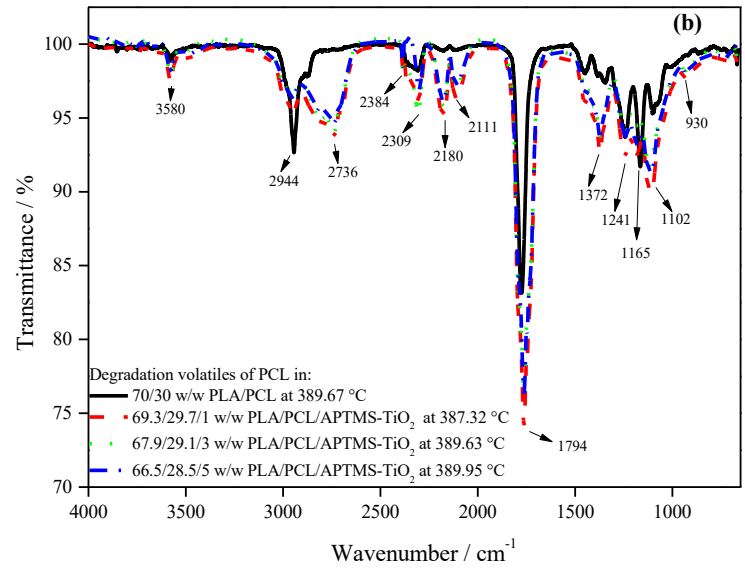

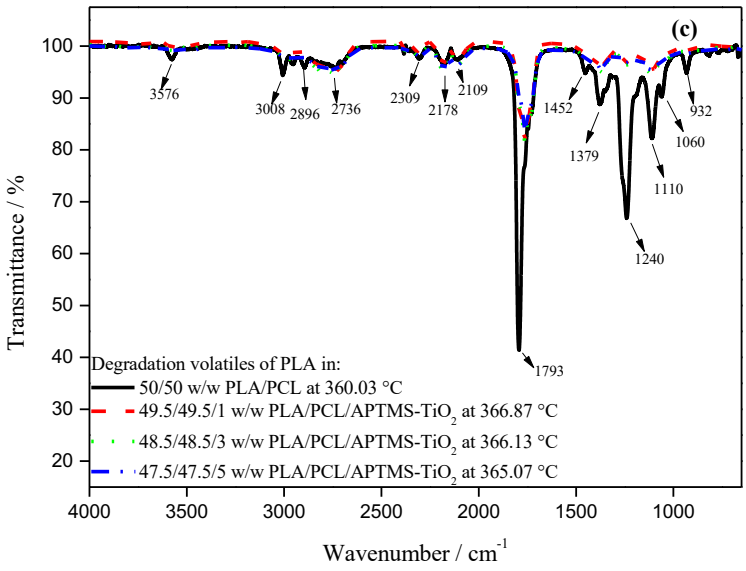
(c)
Transmittance / %
Wavenumber / cm-1
3576
3008
2896
2736
2309
2178
2109
1452
1379
1240
1793
1110
1060
932
Degradation volatiles of PLA in:
50/50 w/w PLA/PCL at 360.03 °C
49.5/49.5/1 w/w PLA/PCL/APTMS-TiO2 at 366.87 °C
48.5/48.5/3 w/w PLA/PCL/APTMS-TiO2 at 366.13 °C
47.5/47.5/5 w/w PLA/PCL/APTMS-TiO2 at 365.07 °C

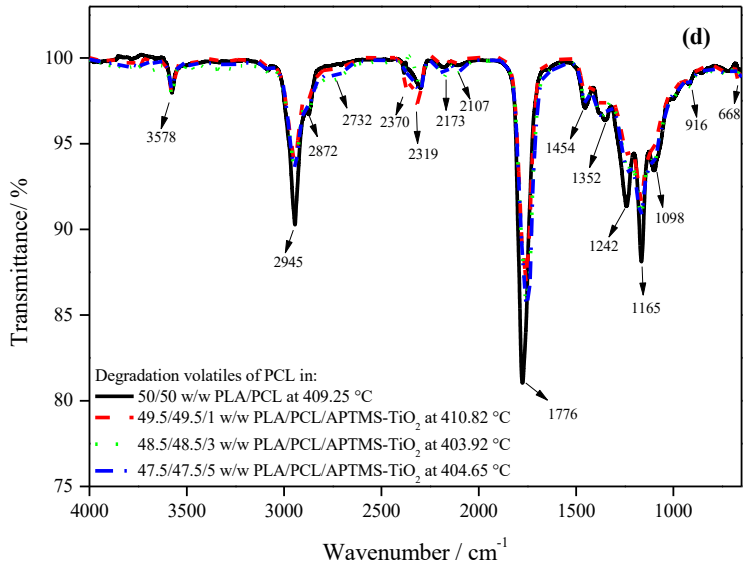
(d)
Transmittance/ %
Wavenumber / cm-1
3578
2945
2872
2732
2370
2319
2173
2107
1776
1454
1352
1242
1165
1098
916
668
Degradation volatiles of PCL in:
50/50 w/w PLA/PCL at 409.25 °C
49.5/49.5/1 w/w PLA/PCL/APTMS-TiO2 at 410.82 °C
48.5/48.5/3 w/w PLA/PCL/APTMS-TiO2 at 403.92 °C
47.5/47.5/5 w/w PLA/PCL/APTMS-TiO2 at 404.65 °C

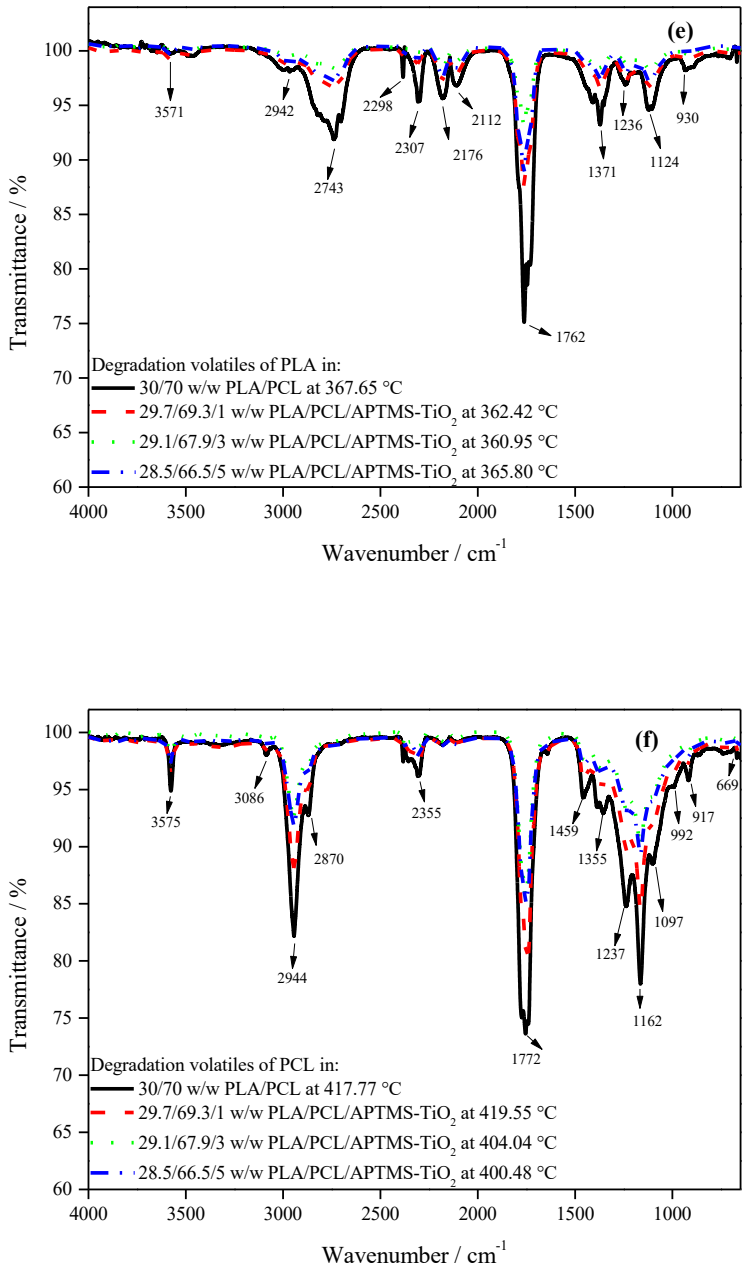

Figure 4.19 FTIR spectra of degradation products of the PLA (a, c, e) and PCL (b, d, f) in the APTMS-TiO_2 polymer blend nanocomposites

4.4 Dynamic mechanical analysis (DMA)

Knowledge of a material's mechanical behaviour as the temperature changes is essential in determining the appropriate usage conditions. Information of relaxation transitions (glass transition), polymer miscibility and filler effectiveness can be obtained through dynamic mechanical analysis. Figures 4.20 to 4.28 show the storage modulus (E'), loss modulus (E'') and tan δ curves for PLA, PCL, blends and their blends nanocomposites with $Mg(OH)_2$ and APTMS-TiO_2 nanoparticles. The storage modulus curves (Figure 4.20) of neat components showed that PLA had a T_g around 58 ºC and a T_{cc} around 90 ºC, and PCL had T_g and T_m around -58 ºC and 59 ºC, respectively. The T_g of PLA and the T_m for PCL occurred around the same temperature range (58-59 ºC). At temperatures between -90 and -58 ºC, neat PLA showed a high storage modulus compared to neat PCL (Figure 4.20). At this temperature, both polymers were below their glass transition and their chains were still frozen. Despite PLA having a lower degree of crystallinity, it showed a higher E' at low temperatures indicating that it is stiffer in nature. PCL had a lower E' even though it had a higher degree of crystallinity, this was due to the presence of CH molecules that made the backbone chain flexible [29]. At temperatures between the glass transitions of both polymers (-58 ºC and 59 ºC) the storage modulus of both polymers decreases as the temperature increased, but PLA still had a higher E' than PCL. Since PCL was at temperatures above its T_g, its polymer chains were much more mobile and free to move than those of PLA which were still frozen. At these temperatures (-58 ºC and 59 ºC), PCL had a larger free volume than PLA, so a lower E' was observed. The effect of blending on the storage modulus of the two polymers will be dealt with later in the discussion, under blends and blends nanocomposites section.

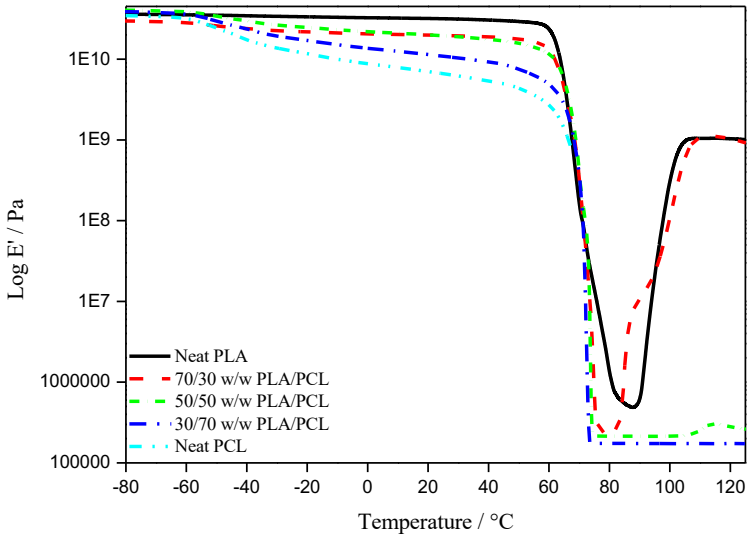

Figure 4.20 Storage modulus curves of neat polymers and their blends

The storage modulus curves for the single polymers nanocomposites are shown in Figure 4.21. For the nanocomposites containing $Mg(OH)_2$, the PLA/$Mg(OH)_2$ were too brittle to test, so only the PCL/$Mg(OH)_2$ were studied. Figure 4.21 (a) shows the storage modulus of neat PCL and its nanocomposites with $Mg(OH)_2$. At temperatures below the glass transition of PCL (-58 ºC), the addition of $Mg(OH)_2$ nanorods to PCL resulted in an increase in the E' at 3 and 10 wt.% content. This trend was also seen at temperatures above the glass transition of PCL, up until -15 ºC. The increase in E' was attributed to reduced free volume of the PCL possibly as a result of being restricted by the $Mg(OH)_2$ nanorods. Also, the increase in the E' might have also been the possibility that, even though the agglomeration was observed by SEM, some $Mg(OH)_2$ nanorods were well dispersed and possibly forming a stiffening physical network. Ostafinska *et al.* [26] observed the same behaviour in their study of the synergistic effects in mechanical properties of PLA/PCL blends filled with TiO_2. They observed a slight increase in the E' and attributed it to formation of a stiffening physical network due to the adhesion between PLA and TiO_2. They also mentioned that the TiO_2 was agglomerated and the adhesion was not perfect, which is why only a slight stiffening effect was observed. As for the decrease in the E' at 1 and 5 wt.% $Mg(OH)_2$ content, this might happen that at 1 wt.% the filler was lower to have had affected E' positively, but at 5 wt.% the agglomeration might have dominated, therefore, both having a plasticizing effect, reducing E'. Cabedo *et al.* [27] also experienced a decrease in E' due to the plasticization effect of clay in PLA/PCL blends clay at 4 wt.% content. No trend could be established in regard to filler content, at 3 and 10 wt.% a

stiffening effect was observed and at 1 and 5 wt.% the plasticization effect was seen. This could be attributed to difference in dispersion in these nanocomposites. It is possible that there was better dispersion in samples where stiffening was observed which allowed better stress transfer from the polymer matrix to the filler. At temperatures from -15 to 60 ºC an increase in the E' was observed irrespective of the filler content. This also was attributed to reduced free volume and restricted polymer chain movement due to the presence of $Mg(OH)_2$ nanorods. This was supported by the DSC results where an increase in the degree of crystallinity was observed for all compositions of PCL/$Mg(OH)_2$. It is clear that the amorphous fractions in these nanocomposites were reduced, less polymer chain movements would therefore be experienced. The increase in the E' might have also been due to restricted chain mobility of PCL therefore increasing the stiffness of the nanocomposites [27]. In the APTMS-TiO_2 containing single polymer nanocomposites (Figure 4.21 (b) and (c)), a decrease in storage modulus at temperature below the T_gs of both PLA and PCL was seen. In the PCL/APTMS-TiO_2 (Figure 4.21 (c)), the reduction in E' was directly proportional to the amount of filler added. For the PLA/APTMS-TiO_2 (Figure 4.21 (b)), the loss in storage modulus did not have any specific trend. The reduction in the storage modulus was attributed to presence of APTMS-TiO_2 which possibly acted as a plasticizing agent, this could have lowered the E' of PLA and PCL. Cabedo *et al.* [27] reported the plasticization effect of clay at low filler content (4 wt.%) in PLA/PCL blends which resulted in a lower E'.

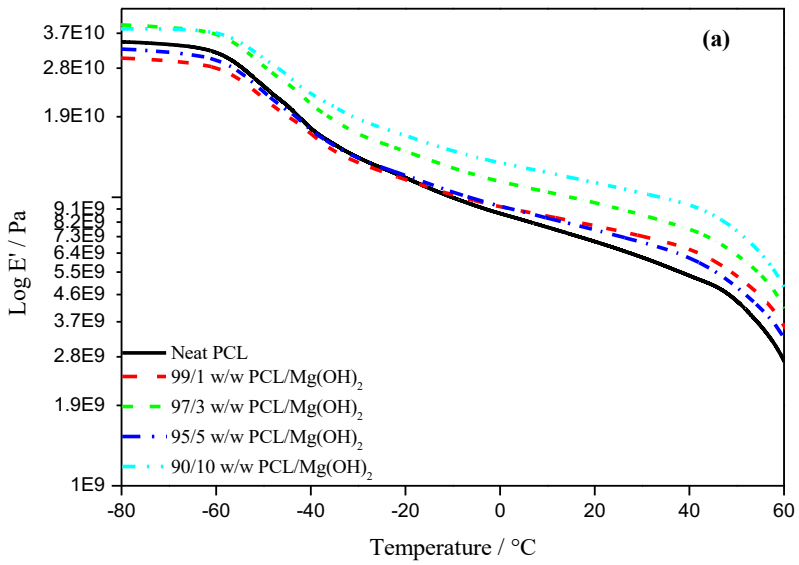

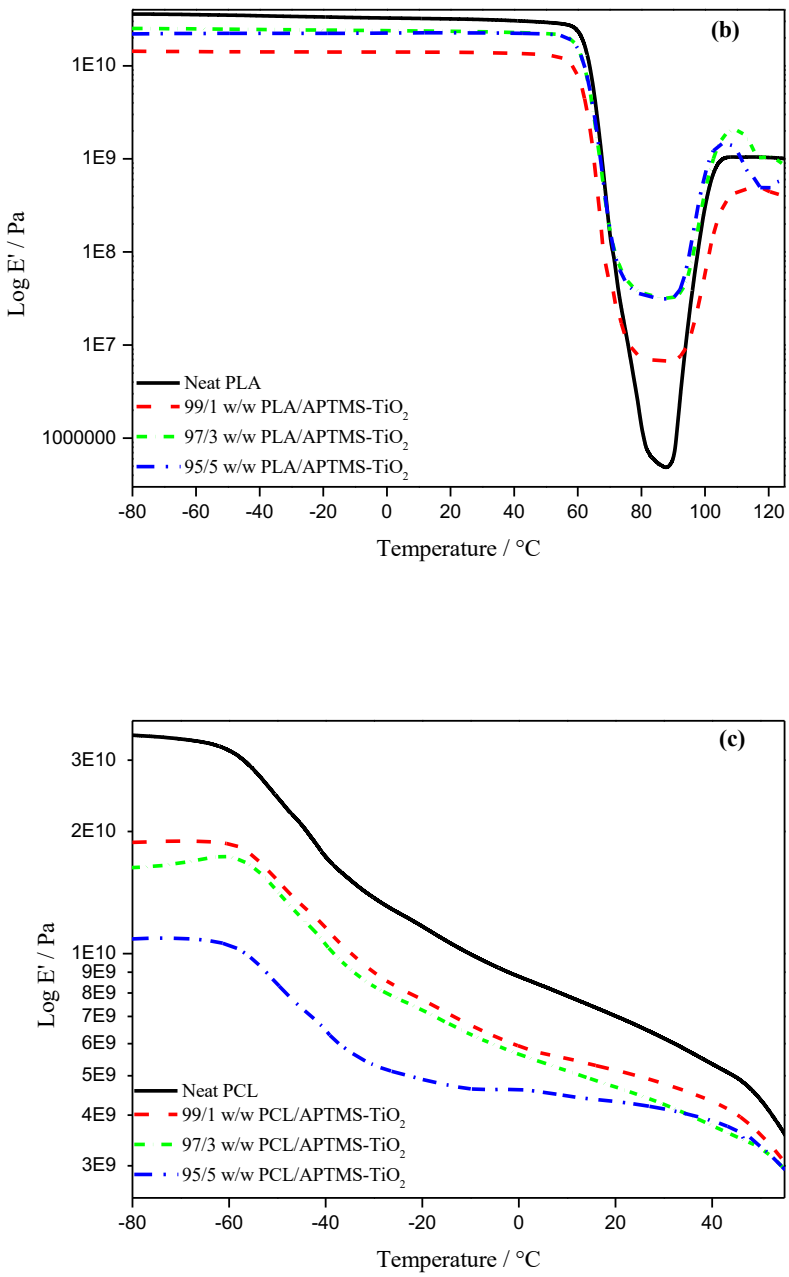

Figure 4.21 Storage modulus curves of (a) neat PCL and its nanocomposites with $Mg(OH)_2$ (b) neat PLA and its nanocomposites with APTMS-TiO_2 (c) neat PCL and its nanocomposites APTMS-TiO_2

PLA and PCL influenced each other's storage modulus when they were blended together. The storage modulus curves of the polymer blends are shown in Figure 4.20. At temperatures below the glass transition of PCL (-58 ºC), the polymer blends had increased storage modulus above that of PLA and PCL. The only exception was the 70/30 w/w PLA/PCL blend which was

significantly lower than the neat polymer and the other blends. The high E' was attributed to the polymers being in a glassy state, where the molecular motion is restricted, due to the lack of free volume to allow rotation of molecules. These observations were coherent with the DSC results, where a decrease in free volume was seen with decrease in the amorphous content (an increase in the degree of crystallinity). The glass transition of PCL in the blends was around -58 ºC and it remained unchanged in comparison to the neat polymer. At temperatures between the glass transition temperatures of PCL (-58 °C) and PLA (58 °C), the polymer blends had intermediate properties to those of the neat polymers. It was seen that adding PLA to PCL improved the storage modulus of PCL, and this was attributed to the stiffness of PLA. The PCL decreased the storage modulus of PLA due to its lower stiffness since the PCL chains are highly mobile at temperatures above its glass transition. This indicated that these two polymers were immiscible. Around 58 ºC, the glass transition of PLA coexisted with the melting temperature of PCL (59 ºC). The polymers blends exhibited intermediate E' of the neat polymers. At temperatures above the glass transition of both polymers (59 ºC), a T_{cc} was observed for the 70/30 w/w PLA/PCL blend around 80 ºC. When compared to the T_{cc} of neat PLA (90 ºC), a decrease was noticed. This was attributed to the plasticizing effect of PCL in PLA, since it has lower T_g due to its flexible chains. In the other blends, the cold crystallization transition was absent or not clearly visible. This could have been due to the absence of the recrystallization of PLA due to the presence of high PCL and filler contents.

The Figure 4.22 (a) to (f) shows the storage modulus curves of polymer blend nanocomposites with $Mg(OH)_2$ and APTMS-TiO_2. In the polymer blend nanocomposites with $Mg(OH)_2$ (Figure 4.22 (a) to (c)), not all the samples could be analysed as some were too brittle to be cut into analysable samples. At temperatures below the T_g of PCL (-58 ºC), the PLA/PCL blend nanocomposites with $Mg(OH)_2$ had E' that is slightly above those of the neat polymers and blends. This was attributed to restricted polymer chain movements with the presence of the $Mg(OH)_2$ nanorods. An increase in E' denotes increased stiffness, meaning that the presence of the filler increased the stiffness. Between the T_gs of the two polymers (-58 and 58 ºC), it was observed that the $Mg(OH)_2$ blend nanocomposites had intermediate properties of the neat polymers. When compared to their respective blends, it was seen that their E' remained the same or increased slightly in the presence of the filler. At temperatures around the T_g of PLA, it was observed that the T_g of PLA coexisted with the melting peak of PCL in these blend nanocomposites. When this transition was compared to the respective blends, a slight decrease was observed in the E'. The E' of the $Mg(OH)_2$ polymer blend nanocomposites did not show any trend in relation to the content of the filler. A decrease in the PLA cold crystallization

temperatures from 90 ºC to around 80 ºC was observed with the presence of $Mg(OH)_2$. This indicated that the nanorods had a plasticization effect on PLA. No trend could be established between the filler content and the decrease in the PLA cold crystallization.

In the APTMS-TiO_2 polymer blend nanocomposites (Figure 4.22 (d) to (f)), at temperature below the T_gs of PLA and PCL (-80 ºC) there was general decrease in the E' in the presence of the nanofiller, when the blends nanocomposites were compared to their respective polymer blends. Presence of APTMS-TiO_2 nanoparticles might have had a plasticization effect on the PLA matrix. This is similar to what was observed for single polymer nanocomposites (PLA/APTMS-TiO_2). Cabedo *et al.* [27] observed a decrease in E' of PLA/PCL blends with the addition of commercially available modified kaolinite ($Al_2Si_2O_5(OH)_4$). They attributed the decrease in E' to the plasticization effect of the kaolinite at 4 wt.%. Presence of APTMS-TiO_2 nanoparticles might have also increased the free volume of the PLA, and therefore lowering the E'. No particular trends could be made in regard to the filler content. A decrease in the PLA cold crystallization temperatures from 90 ºC to about 80 ºC was observed with the presence of APTMS-TiO_2, also this was attributed to the plasticization of PLA by the APTMS-TiO_2 nanoparticles. The polymer blend nanocomposites of both $Mg(OH)_2$ and APTMS-TiO_2 had intermediate E' to those of the neat polymers. Their E' did not differ much from their respective polymer blends, revealing that the fillers had very little influence on the E' of the polymer blends around that temperature range. For all the polymer blend nanocomposites (Figure 4.22), a decrease in the storage modulus was observed with an increase in temperature. This was attributed to an increase in free volume and chain mobility as the temperature increased.

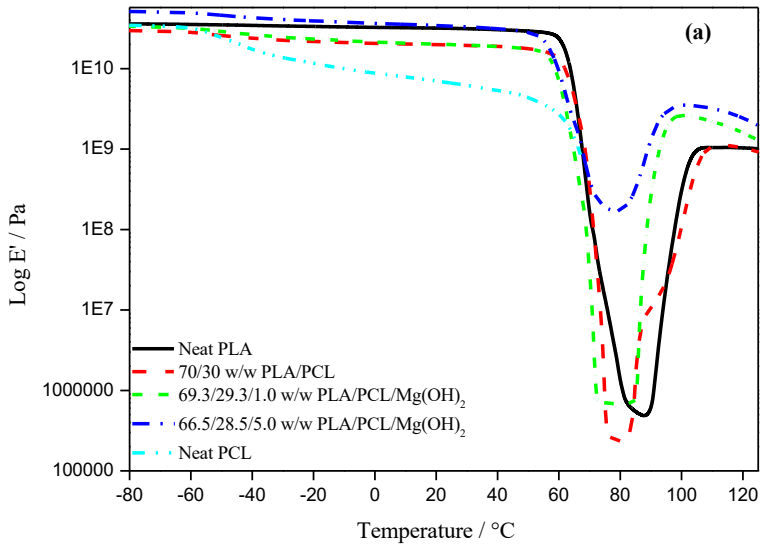
(a)
Log E' / Pa
1E10
1E9
1E8
1E7
1000000
100000
-80
-60
-40
-20
0
20
40
60
80
100
120
Temperature / °C
Neat PLA
70/30 w/w PLA/PCL
69.3/29.3/1.0 w/w PLA/PCL/Mg(OH)2
66.5/28.5/5.0 w/w PLA/PCL/Mg(OH)2
Neat PCL

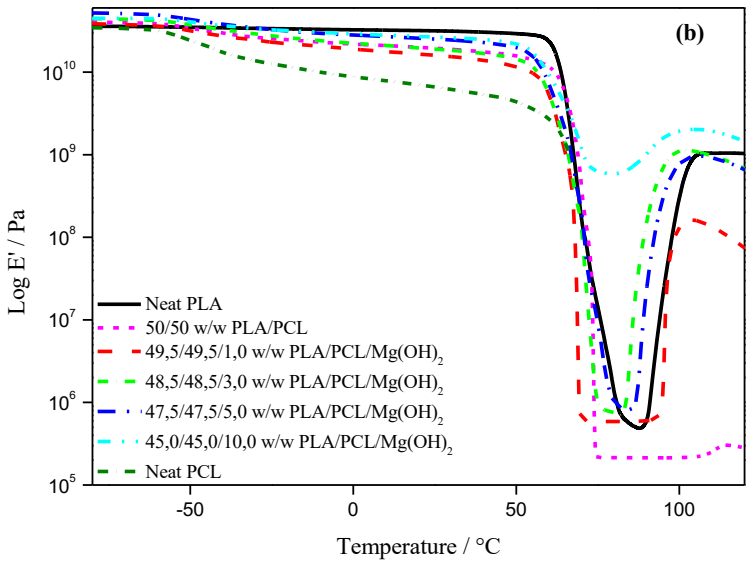
(b)
Log E' / Pa
10^10
10^9
10^8
10^7
10^6
10^5
-50
0
50
100
Temperature / °C
Neat PLA
50/50 w/w PLA/PCL
49,5/49,5/1,0 w/w PLA/PCL/Mg(OH)2
48,5/48,5/3,0 w/w PLA/PCL/Mg(OH)2
47,5/47,5/5,0 w/w PLA/PCL/Mg(OH)2
45,0/45,0/10,0 w/w PLA/PCL/Mg(OH)2
Neat PCL

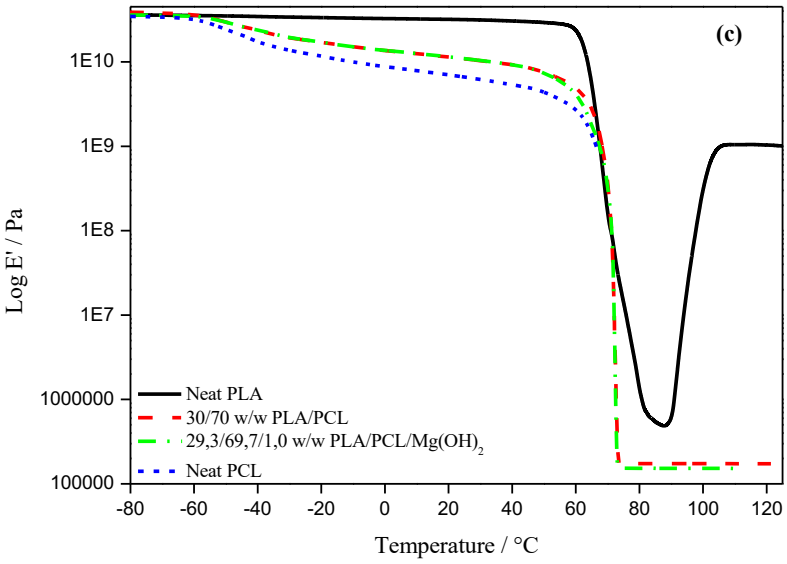
(c)
Log E' / Pa
1E10
1E9
1E8
1E7
1000000
100000
Neat PLA
30/70 w/w PLA/PCL
29,3/69,7/1,0 w/w PLA/PCL/Mg(OH)2
Neat PCL
-80
-60
-40
-20
0
20
40
60
80
100
120
Temperature / °C

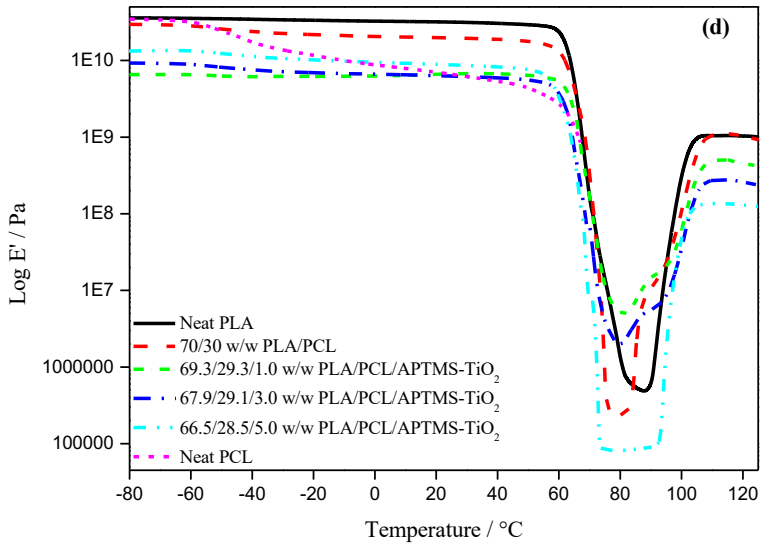
(d)
Log E' / Pa
1E10
1E9
1E8
1E7
1000000
100000
Neat PLA
70/30 w/w PLA/PCL
69.3/29.3/1.0 w/w PLA/PCL/APTMS-TiO2
67.9/29.1/3.0 w/w PLA/PCL/APTMS-TiO2
66.5/28.5/5.0 w/w PLA/PCL/APTMS-TiO2
Neat PCL
-80
-60
-40
-20
0
20
40
60
80
100
120
Temperature / °C

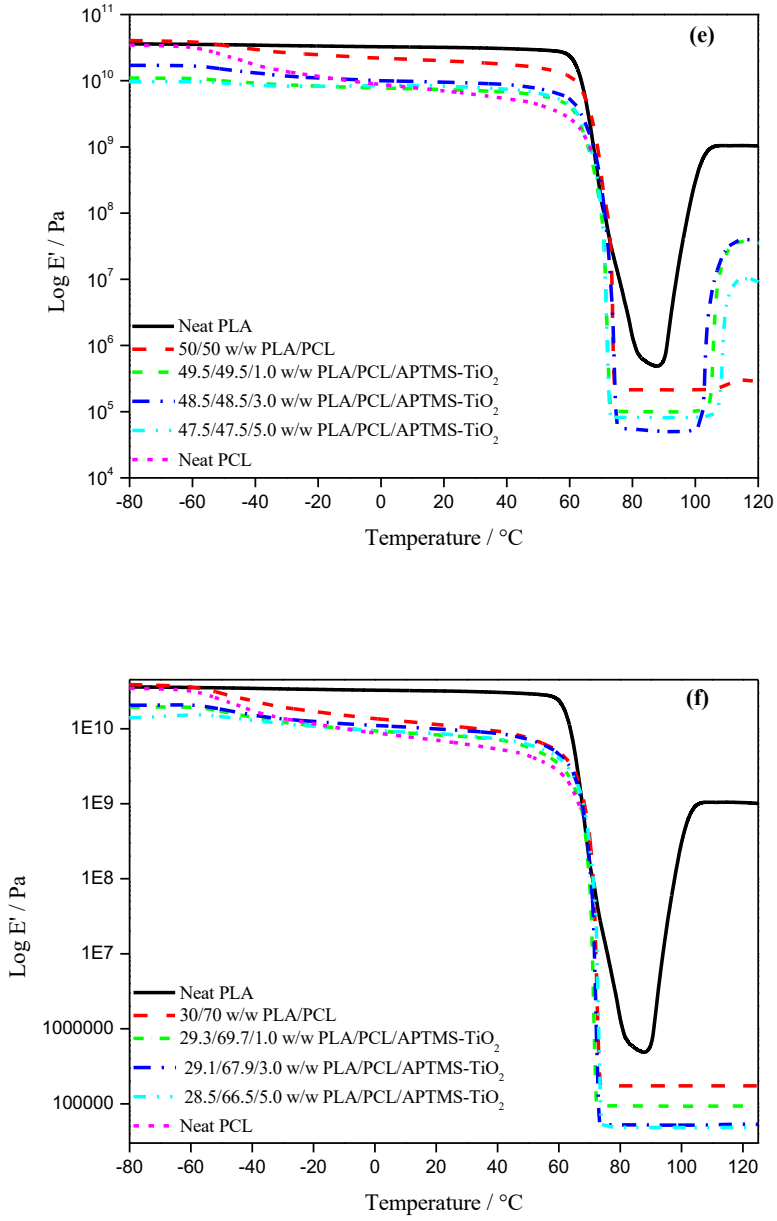

Figure 4.22 Storage modulus curves of (a) 70/30 w/w PLA/PCL and its nanocomposites with $Mg(OH)_2$ (b) 50/50 w/w PLA/PCL and its nanocomposites with $Mg(OH)_2$ (c) 30/70 w/w PLA/PCL and its nanocomposites with $Mg(OH)_2$ (d) 70/30 w/w PLA/PCL and its nanocomposites with APTMS-TiO_2 (e) 50/50 w/w PLA/PCL and its nanocomposites with APTMS-TiO_2 (f) 30/70 w/w PLA/PCL and its nanocomposites with APTMS-TiO_2

Loss modulus is a viscous response of a material to unrecoverable energy dissipation by the material. The glass transition temperatures of constituents in polymer blends or nanocomposites can reveal whether they are miscible or immiscible. A single glass transition reveals full miscibility and presence of two glass transitions shows that the constituents are

either immiscible or partially miscible. If a third component is added, its effects on the miscibility of the constituents can be observed on whether it improves miscibility or not. Figures 4.23-4.25 show the loss modulus curves of PLA, PCL, their blends and their blend nanocomposites with $Mg(OH)_2$ and TiO_2 nanoparticles. The glass transition temperatures of PCL and PLA in these samples are tabulated in Tables 4.12 and Table 4.13. The glass transition temperatures of neat PCL and PLA were determined to be -48.7ºC and 63.0ºC, respectively. The loss modulus of the blends of the two polymers are discussion below under the blends and blends nanocomposites section.

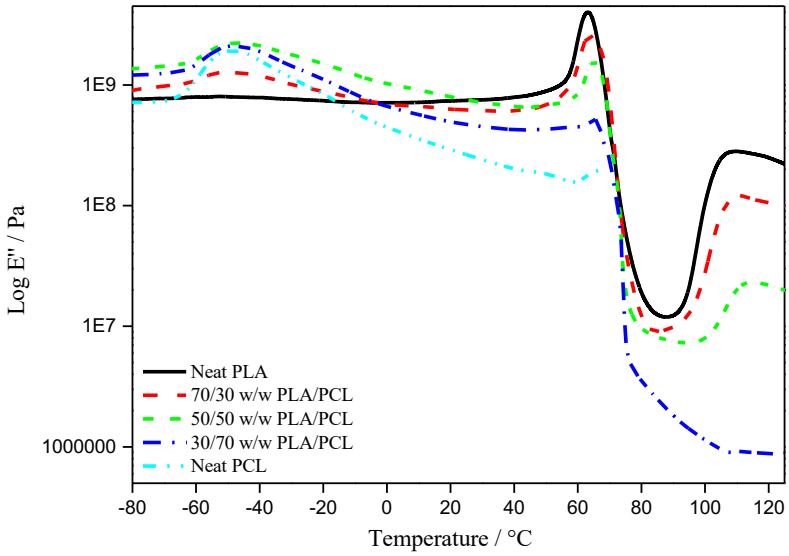

Figure 4.23 Loss modulus curves of neat polymers and their blends

Loss modulus curves of single polymer nanocomposites are shown in Figure 4.24. The PLA/$Mg(OH)_2$ were too brittle to test, so only the PCL/$Mg(OH)_2$ were studied for the $Mg(OH)_2$ single polymer nanocomposites. In the presence of $Mg(OH)_2$ nanorods (Figure 4.24 (a)), a broadening of the PCL T_g peak and a decrease in the glass transition temperature with increasing nanoparticle content was observed. This could have been due to increased mobility of the polymer chains due to the presence of the nanoparticles. It is possible that the $Mg(OH)_2$ nanoparticles acted a plasticizer, since a decrease in the E' was also observed at 1 and 5 wt% filler content. Around 60 ºC, a sharp decrease in the loss modulus was observed and it was attributed to the melting of PCL. When APTMS-TiO_2 was added to both PLA and PCL (Figure 4.24 (b) and (c)), a decrease in the glass transition temperature was observed. It was also noted that in both instances, the peaks narrowed with the presence and increase in content of the

APTMS-TiO_2 nanoparticles. The decrease in T_g was attributed to increased chain mobility of the polymer chains due to interaction with the nanoparticles. When the nanocomposites were compared amongst themselves, a slight increase was observed when the content of the APTMS-TiO_2 nanoparticles was increased. This meant the increased filler content was slightly restricting chain mobility compared to lower filler content.

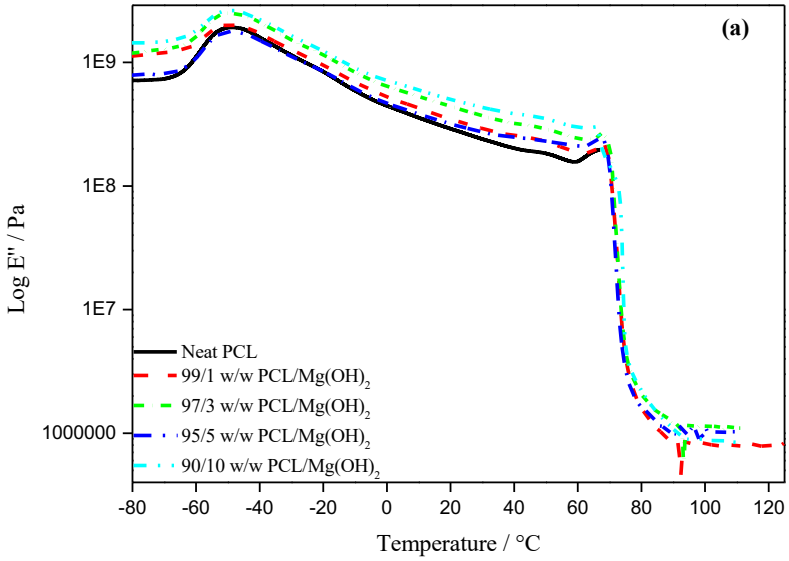

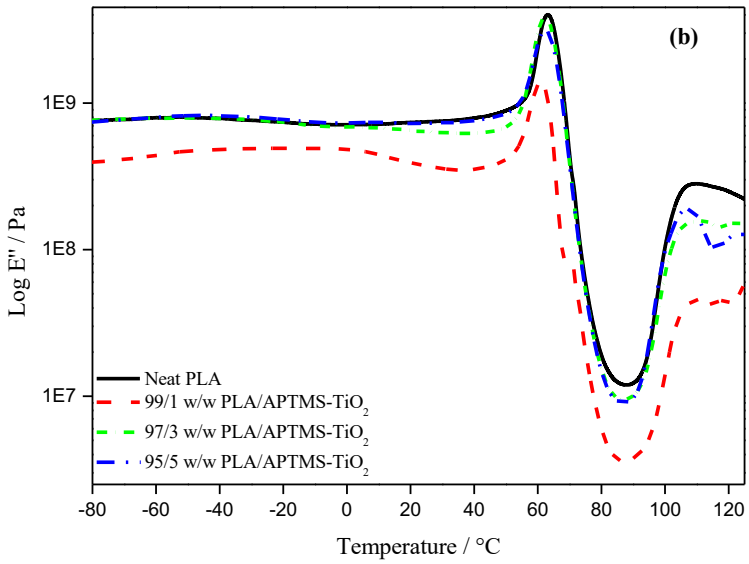

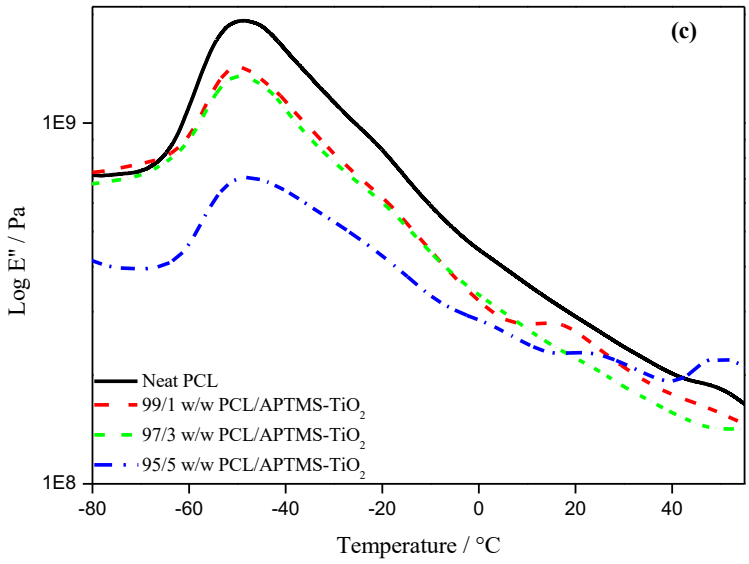

Figure 4.24 Loss modulus curves of (a) neat PCL and its nanocomposites with $Mg(OH)_2$ (b) neat PLA and its nanocomposites with APTMS-TiO_2 (c) neat PCL and its nanocomposites APTMS-TiO_2

In the polymer blends (Figure 4.23), the presence of the one polymer influenced the glass transition of the other polymer. For PCL, an increase in its glass transition temperature was observed with the addition of PLA. The only exception was 70/30 w/w PLA/PCL, where a decrease in the glass transition of PCL was observed. An increase in the T_g of PLA was also observed with the presence and increase in content of PCL content. The increased glass transitions were indicative of restricted chain mobility and the presence of two glass transitions in the blends showed that the two polymers formed immiscible blends and were phase separated.

The loss modulus curves of the polymer blend nanocomposites with $Mg(OH)_2$ and APTMS-TiO_2 are shown in Figure 4.25 (a) to (f). For the $Mg(OH)_2$ nanocomposites (Figure 4.25 (a) to (c), Table 4.12), an increase in the PCL T_g and a decrease in the PLA T_g was observed in the presence of $Mg(OH)_2$. The $Mg(OH)_2$ nanorods restricted chain mobility in PCL but increased the chain mobility of PLA. There was a general decrease in the temperature difference between the glass transition temperatures of PCL and PLA with increasing filler content. This is an indication that the presence of $Mg(OH)_2$ brought some partial miscibility between PCL and PLA. For instance, in the 70/30 w/w PLA/PCL blend, the difference between the T_g of PLA and PCL was 114 ºC, in the presence of 1 wt.% $Mg(OH)_2$ it was 108.8 ºC and at 5 wt.%

$Mg(OH)_2$ it was 105 ºC. This showed that the partial miscibility of PLA and PCL was improved further by increasing the filler content.

In the polymer blend nanocomposites containing APTMS-TiO_2 (Figure 4.25 (d) to (f), Table 4.13), an increase in the T_g of PCL and a decrease in the T_g of PLA was also observed in the presence of APTMS-TiO_2. The APTMS-TiO_2 also restricted the chain mobility in PCL but acted as plasticizer for PLA. This means that even APTMS-TiO_2 nanoparticles like the $Mg(OH)_2$ nanorods seems to have induced the partial miscibility between PLA and PCL. The presence of APTMS-TiO_2 resulted in a decrease in the temperature difference between the glass transition temperatures of PCL and PLA. At all filler contents, there was a smaller difference between the glass transitions of PLA and PCL, indicating an improved partial miscibility between the two polymers with the presence of APTMS-TiO_2. However, the decrease in the temperature difference between the glass transition temperatures of PCL and PLA followed no particular trend with regard to variation in filler content. In the 70/30 w/w PLA/PCL blend the difference between the T_g of PLA and PCL was 114 ºC. When 1 wt.% APTMS-TiO_2 was added it was found to be 104.7 ºC, at 3 wt.% filler content, the difference was 112.7 ºC and at 5 wt.% filler content it was 112.3 ºC. In 50/50 w/w PLA/PCL blend, the temperature difference between the glass transition temperatures of PCL and PLA was 112 ºC. At 1, 3 and 5 wt.% APTMS-TiO_2, the difference was 106.3, 106.4 and 112.9 ºC, respectively. The difference at 5 wt.% filler content (112.9 ºC) was therefore greater than in the respective polymer blends (112.0 ºC). This could be due to poor interaction between the filler and the polymers matrix because of agglomerations as seen in SEM and TEM results. Both $Mg(OH)_2$ and APTMS-TiO_2 generally induced some partial miscibility of PLA and PCL.

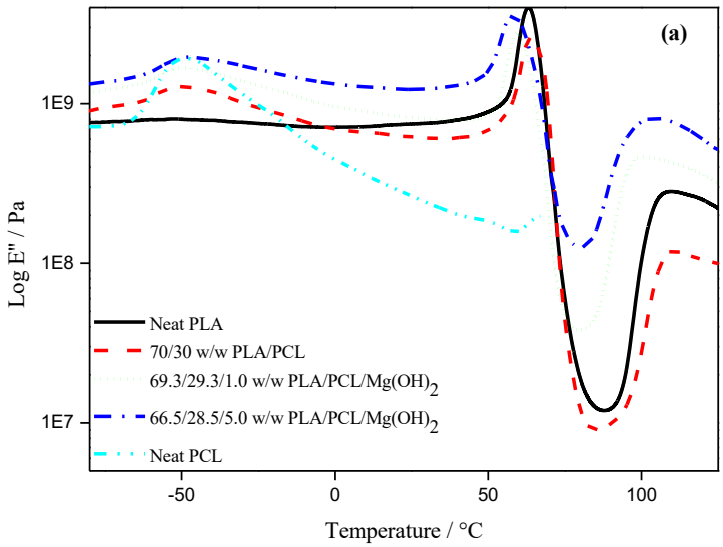
(a)
1E9
1E8
1E7
Log E'' / Pa
Neat PLA
70/30 w/w PLA/PCL
69.3/29.3/1.0 w/w PLA/PCL/Mg(OH)2
66.5/28.5/5.0 w/w PLA/PCL/Mg(OH)2
Neat PCL
-50
0
50
100
Temperature / °C

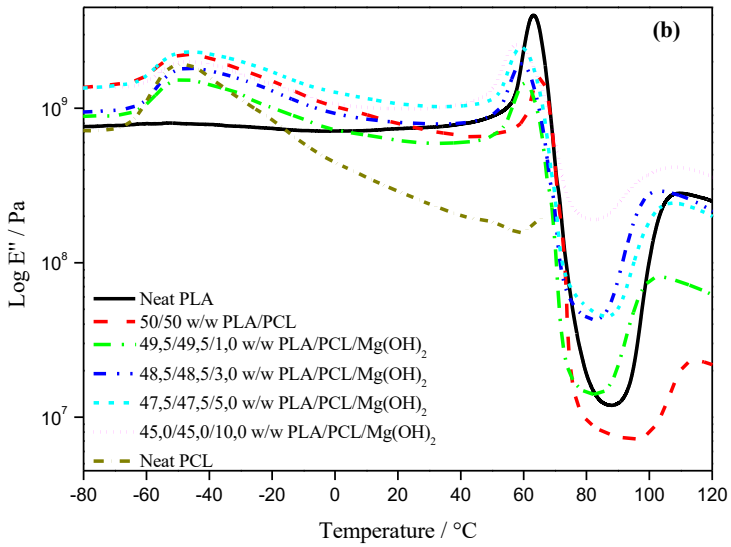
(b)
10^9
10^8
10^7
Log E'' / Pa
Neat PLA
50/50 w/w PLA/PCL
49,5/49,5/1,0 w/w PLA/PCL/Mg(OH)2
48,5/48,5/3,0 w/w PLA/PCL/Mg(OH)2
47,5/47,5/5,0 w/w PLA/PCL/Mg(OH)2
45,0/45,0/10,0 w/w PLA/PCL/Mg(OH)2
Neat PCL
-80
-60
-40
-20
0
20
40
60
80
100
120
Temperature / °C

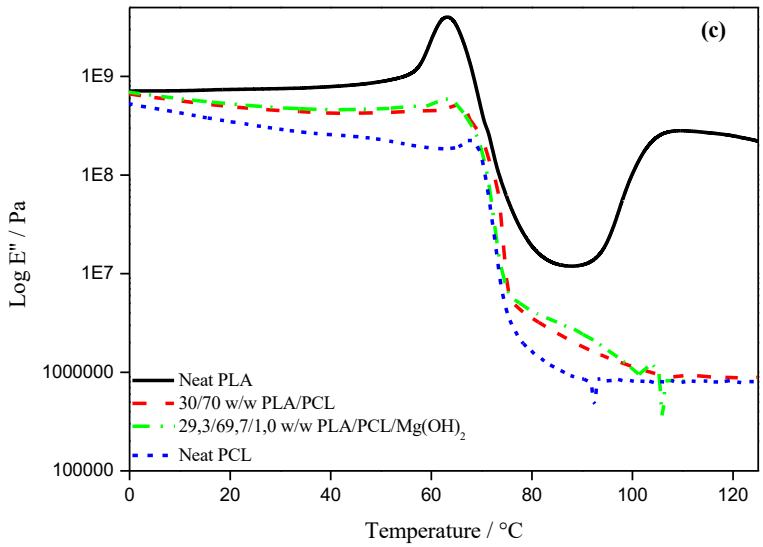
(c)
1E9
1E8
1E7
1000000
100000
Log E'' / Pa
Neat PLA
30/70 w/w PLA/PCL
29,3/69,7/1,0 w/w PLA/PCL/Mg(OH)2
Neat PCL
0
20
40
60
80
100
120
Temperature / °C

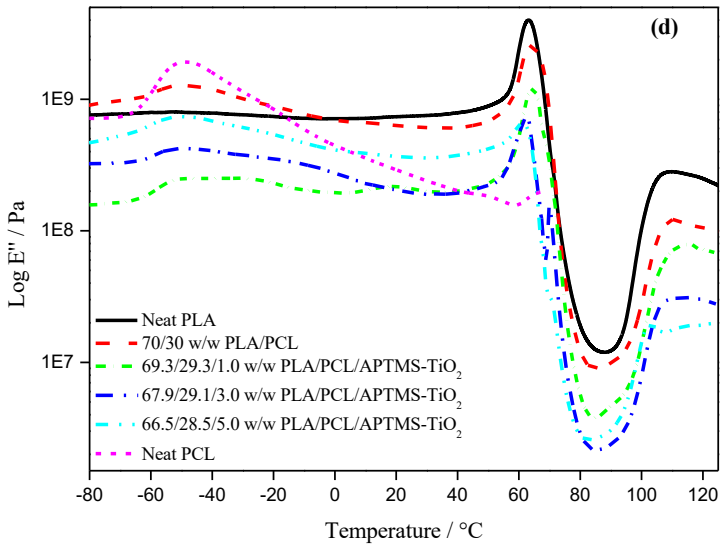
(d)
1E9
1E8
1E7
Log E'' / Pa
Neat PLA
70/30 w/w PLA/PCL
69.3/29.3/1.0 w/w PLA/PCL/APTMS-TiO2
67.9/29.1/3.0 w/w PLA/PCL/APTMS-TiO2
66.5/28.5/5.0 w/w PLA/PCL/APTMS-TiO2
Neat PCL
-80
-60
-40
-20
0
20
40
60
80
100
120
Temperature / °C

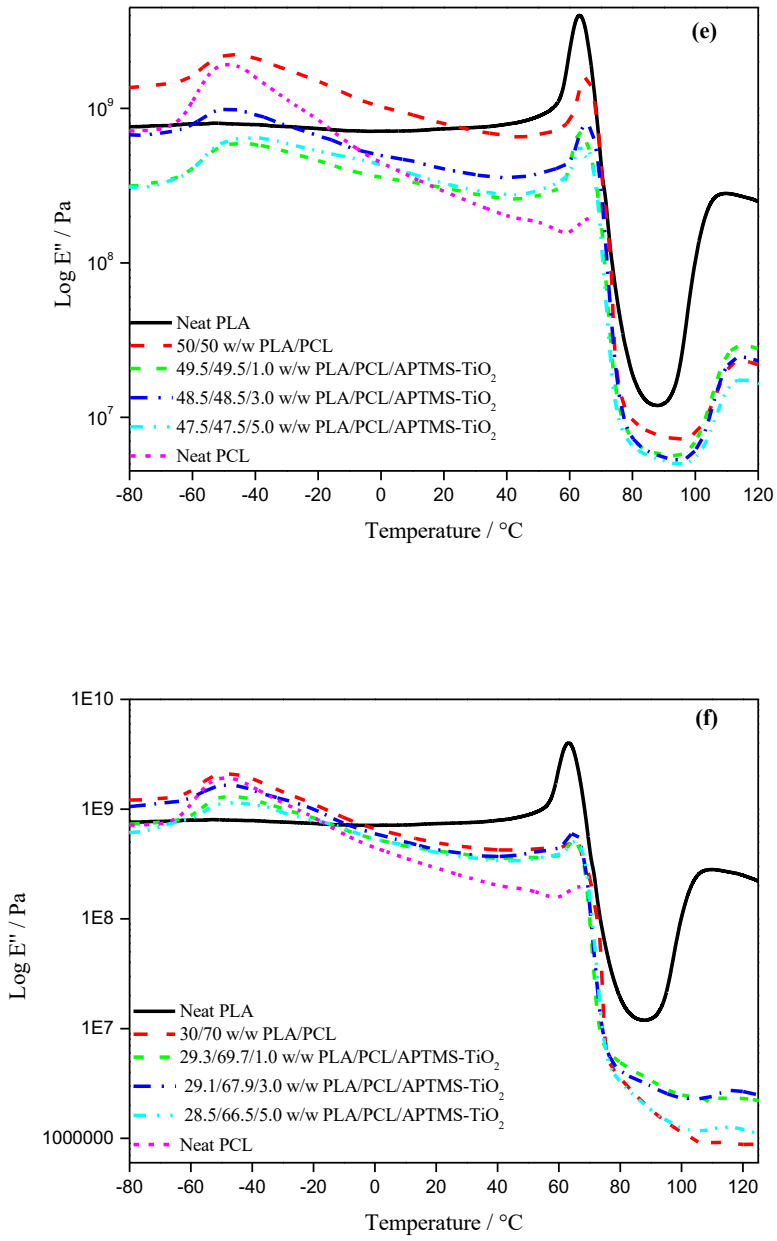

Figure 4.25 Loss modulus curves of (a) 70/30 w/w PLA/PCL and its nanocomposites with $Mg(OH)_2$ (b) 50/50 w/w PLA/PCL and its nanocomposites with $Mg(OH)_2$ (c) 30/70 w/w PLA/PCL and its nanocomposites with $Mg(OH)_2$ (d) 70/30 w/w PLA/PCL and its nanocomposites with APTMS-TiO_2 (e) 50/50 w/w PLA/PCL and its nanocomposites with APTMS-TiO_2 (f) 30/70 w/w PLA/PCL and its nanocomposites with APTMS-TiO_2

Table 4.12 Summary of data obtained from the loss modulus for $Mg(OH)_2$ nanocomposites

Sample	PCL T_g/°C	PLA T_g/°C	Difference ($T_{g,PLA}$-$T_{g,PCL}$)/ºC
70/30 w/w PLA/PCL	-50.0	64.1	114.0
69.3/29.3/1.0 w/w PLA/PCL/$Mg(OH)_2$	-49.3	59.5	108.8
66.5/28.5/5.0 w/w PLA/PCL/$Mg(OH)_2$	-47.8	58.0	105.9
50/50 w/w PLA/PCL	-46.9	65.1	112.0
49.5/49.5/1.0 w/w PLA/PCL/$Mg(OH)_2$	-48.7	60.4	109.1
48.5/48.5/3.0 w/w PLA/PCL/$Mg(OH)_2$	-46.3	59.1	105.4
47.5/47.5/5.0 w/w PLA/PCL/$Mg(OH)_2$	-46.1	59.2	105.3
45.0/45.0/10.0 w/w PLA/PCL/$Mg(OH)_2$	-46.8	57.8	104.6
30/70 w/w PLA/PCL	-48.3	65.3	113.7
29.3/69.7/1.0 w/w PLA/PCL/$Mg(OH)_2$	-44.2	62.9	107.2

Table 4.13 Summary of data obtained from the loss modulus for APTMS-TiO_2 blends and blends nanocomposites

Sample	PCL T_g/°C	PLA T_g/°C	Difference ($T_{g,PLA}$-$T_{g,PCL}$)/ºC
70/30 w/w PLA/PCL	-50.0	64.1	114.0
69.3/29.3/1.0 w/w PLA/PCL/APTMS-TiO_2	-40.4	64.3	104.7
67.9/29.1/3.0 w/w PLA/PCL/APTMS-TiO_2	-50.6	62.1	112.7
66.5/28.5/5.0 w/w PLA/PCL/APTMS-TiO_2	-50.7	61.6	112.3
50/50 w/w PLA/PCL	-46.9	65.1	112.0
49.5/49.5/1.0 w/w PLA/PCL/APTMS-TiO_2	-43.0	63.3	106.3
48.5/48.5/3.0 w/w PLA/PCL/APTMS-TiO_2	-41.2	65.2	106.4
47.5/47.5/5.0 w/w PLA/PCL/APTMS-TiO_2	-49.6	63.3	112.9
30/70 w/w PLA/PCL	-48.3	65.3	113.7
29.3/69.7/1.0 w/w PLA/PCL/APTMS-TiO_2	-46.3	65.8	112.2
29.1/67.9/3.0 w/w PLA/PCL/APTMS-TiO_2	-47.8	64.7	112.5
28.5/66.5/5.0 w/w PLA/PCL/APTMS-TiO_2	-47.1	65.1	112.2

The ability of a material to absorb and dissipate energy is known as the damping ability. For instance, when a material is exposed to vibrations (mechanical energy), they can absorb the vibrations and release it as heat energy. The effectiveness of a material to do so can be studied on tan δ curves [30]. The glass transition peaks on tan δ curves are an indicator of damping abilities of polymers, the higher the peaks the higher the damping ability of a material. Figures 4.26-4.28 shows the tan δ curves of PLA, PCL, their blends, and their nanocomposites and polymer blend nanocomposites with $Mg(OH)_2$ and APTMS-TiO_2 nanoparticles. Figure 4.26 shows the tan δ curves of the neat polymers and their polymer blends. Around -48.7ºC, neat PCL was observed to have a α-relaxation process, and this was attributed to its glass transition temperature. For neat PLA, the glass transition was observed as a α-relaxation process with a peak around 63 ºC. It is important to note that the T_g obtained from tan δ curves differs from one observed in the loss modulus curves. The loss modulus T_g peak correspond to the onset of the T_g on the E' curves whilst the tan δ peak correspond to the midpoint of T_g [30]. A cold crystallization transition was also observed for PLA around 90 ºC.

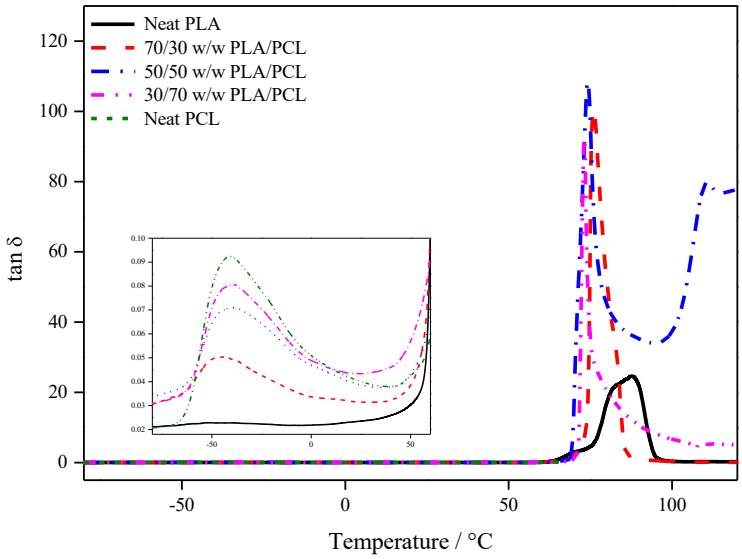

Figure 4.26 Tan δ curves of neat polymers and their blends. The inserted figure shows the magnified tan δ peaks at lower temperatures around the T_g of PCL.

The Figure 4.27 shows the tan δ curves of PLA and PCL and their single polymer nanocomposites with $Mg(OH)_2$ and APTMS-TiO_2 nanoparticles. In the PCL/$Mg(OH)_2$ nanocomposites (Figure 4.27 (a)), an increase in the tan δ peak temperatures was seen which indicated increased chain mobility due to the presence of $Mg(OH)_2$. It could have also been

due to incompatibility between the PCL matrix and the $Mg(OH)_2$ nanoparticles. Then *et al.* [28] observed an increase in the tan δ peaks of poly(butylene succinate) (PBS) with the presence of oil palm mesocarp fibre (OPMF). This was attributed to higher dissipation of energy due to the internal friction of the poor interface between the OPMF and PBS. When 3-aminopropyltrimethoxysilane (APTMS) was added it improved compatibility and interfacial bonding between the PBS and OPMF were reported which resulted in a lower tan δ peak. The tan δ curve of APTMS-TiO_2 nanocomposites are shown in Figure 4.27 (b) and (c). At temperatures below the T_g of PLA (see insert in figure), when the nanoparticles were added an increase in the tan δ maximum values was observed. Around the glass transition of PLA, a decrease in the tan δ maximum values was noted and this was attributed to a decrease in the amorphous content. This was supported by the DSC results where an increase in the degree of crystallinity was observed. When APTMS-TiO_2 nanoparticles were added to PCL (Figure 4.27 (c)), a broadening of the glass transition peak was observed. This was attributed to restricted chain mobility of the PCL by the APTMS-TiO_2. It is clear that APTMS-TiO_2 had better interaction with PLA than PCL. This is coherent with observations seen during SEM and TEM results where APTMS-TiO_2 had a preferential location in PLA.

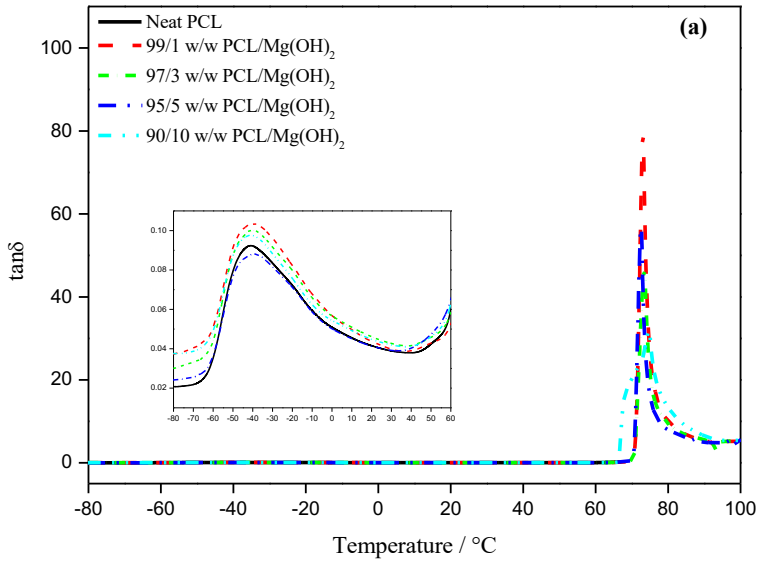

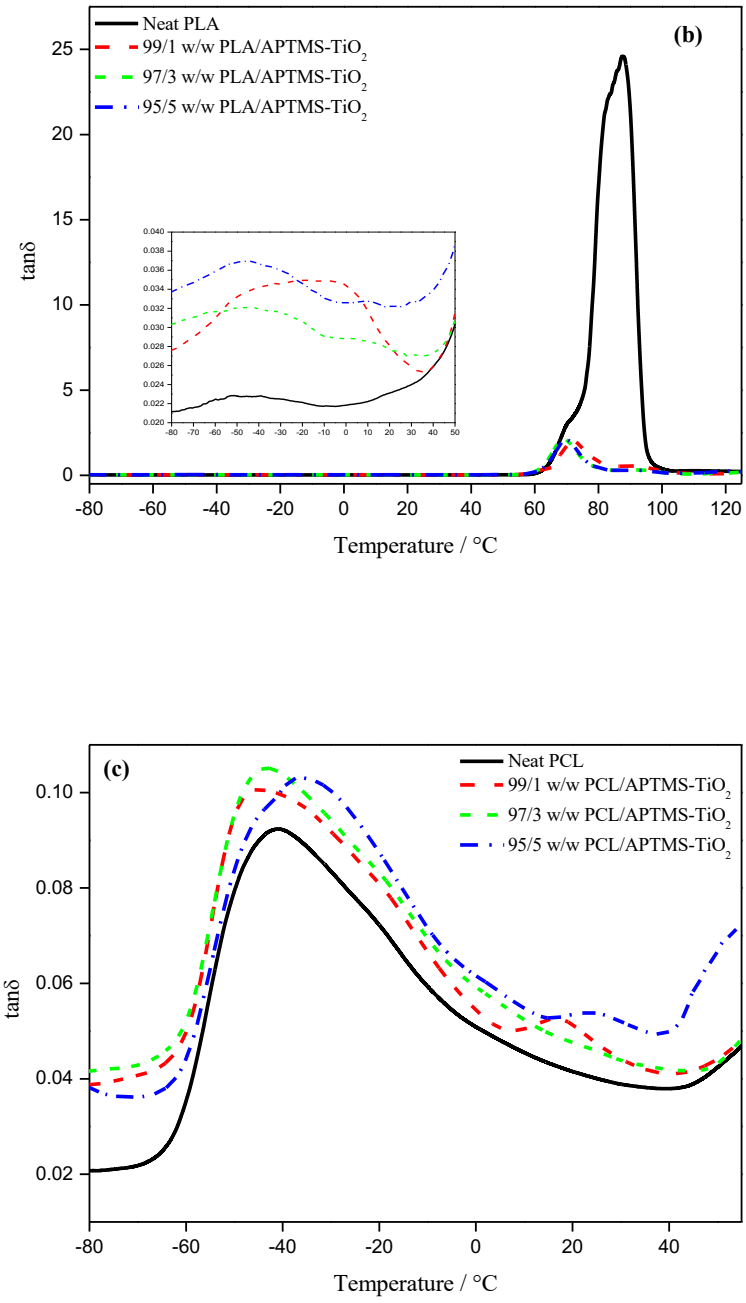

Figure 4.27 Tan δ curves of (a) neat PCL and its nanocomposites with $Mg(OH)_2$ (b) neat PLA and its nanocomposites with APTMS-TiO_2 (c) neat PCL and its nanocomposites APTMS-TiO_2. The inserted figures show the magnified tan δ peaks at lower temperatures around the T_g of PCL.

When PLA was blended with PCL, two relaxation processes were observed around the glass transition temperatures of neat polymers. This indicated the two polymers were immiscible. A decrease in the T_g of both polymers was observed in all the polymer blends revealing increased chain mobility for both polymers. For the α-relaxation process around the T_g of PCL, the intensity of the peaks was proportional to the amount of PCL present. As for the α-relaxation process around the glass transition of PLA, an increase in the peak area, height and intensity was observed with increasing PCL content in the polymer blends. The increase in area and height indicated that PCL increased the damping of PLA. In the 50/50 w/w PLA/PCL blend an additional transition was observed, which was attributed to the cold crystallization peak of PLA.

The Figure 4.28 (a) to (f) show the tan δ curves of polymer blend nanocomposites with $Mg(OH)_2$ and APTMS-TiO_2 nanoparticles. In the polymer blend nanocomposites with $Mg(OH)_2$ nanorods (Figure 4.28 (a) to (c)), there was a general decrease in the tan δ maximum values obtained around the T_g temperatures of PCL with respect to PCL. This indicated a decrease in the damping of PCL with the presence of $Mg(OH)_2$ nanorods. Also, it means there was compatibility between PLA and the $Mg(OH)_2$ nanorods. The only exception was in the 69.7/29.3/1 w/w PLA/PCL/$Mg(OH)_2$ where a slight (though still less than neat PCL) (Figure 4.28(a)) increase was observed in the tan δ maximum values for PCL indicating a slight increase in damping of the PCL. In all the blend nanocomposites, around the T_g of PLA, an increase in the tan δ maximum values was seen at 1 wt.% content, but decreases were observed for the other filler contents (3, 5 and 10 wt.%) when compared to the neat blend. This indicated that at lower $Mg(OH)_2$ content the damping of PLA was increased, the nanoparticles had a plasticizing effect on PLA. At higher filler content, the damping of PLA was decreased which could be attributed to the restriction of chain mobility in the presence of a high $Mg(OH)_2$ content. In a few samples (69.7/29.3/1 and 49.5/49.5/1 w/w PLA/PCL/$Mg(OH)_2$), a double peak above 60 ºC was observed which could be attributed to occurrence of the cold crystallization transition immediately after the T_g of PLA.

In the presence of APTMS-TiO_2 nanoparticles (Figure 4.28 (d) to (f)), for both PCL and PLA, most of the peaks became broader. This indicated that APTMS-TiO_2 amplified their damping. This was particularly visible in the 50/50 and 30/70 w/w PLA/PCL blend nanocomposites. Even though no particular trend could be established in regard to the filler content, it is clear that APTMS-TiO_2 raised the damping of PLA/PCL blends. The high damping indicated the plasticizing effect of the APTMS-TiO_2. The increase in damping, could have also been due to poor adhesion between the APTMS-TiO_2 nanoparticles with both polymers or the filler content was not great enough to have caused the restriction of chain movement at the transition. The only exceptions were at 1 wt.% in the 70/30 and 50/50 w/w PLA/PCL around the T_g of PCL, and at 1 and 3 wt.% in the 70/30 w/w PLA/PCL around the PLA T_g. In these nanocomposites, a decrease in the damping of PCL and PLA was observed. The APTMS-TiO_2 was dispersed well in PLA and on the interface between the two polymers, but not in PCL. This might have had a restricting effect on the chain mobility of PLA. It could have also been due to the compatibility between APTMS-TiO_2 nanoparticles with both PLA and PCL at low filler content. An increase in damping was mostly seen in the nanocomposites which contain APTMS-TiO_2 nanoparticles when compared to those containing $Mg(OH)_2$. So, despite $Mg(OH)_2$ having large agglomerates and voids which were seen during SEM, it is possible that it had better compatibility with PLA/PCL blend than the APTMS-TiO_2 which appeared to be better dispersed. This still needs to be investigated to find out if particles size had anything to do with the observations made in this study.

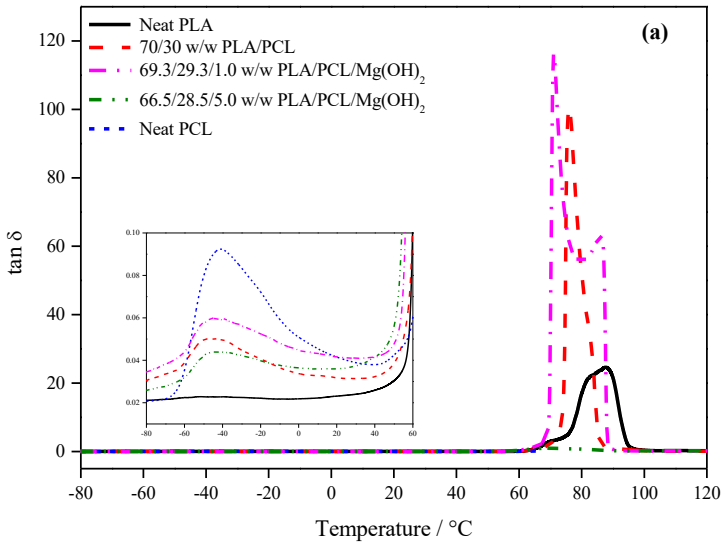

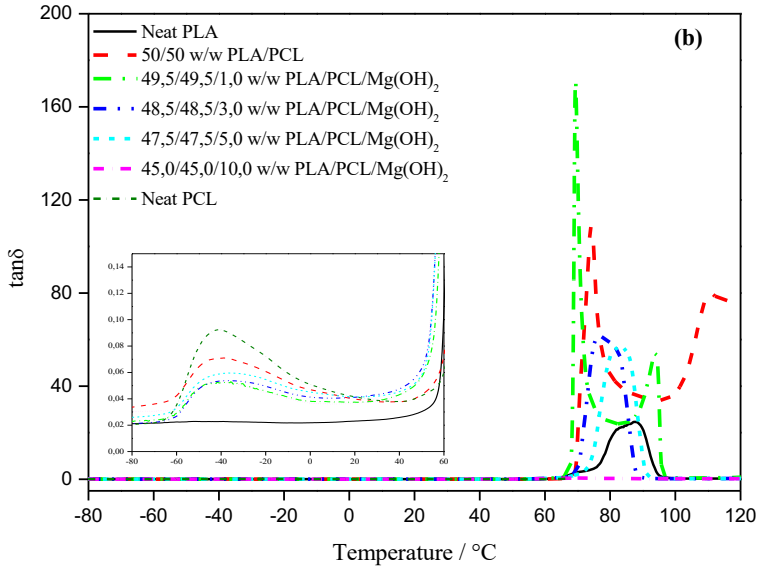
(b)
Neat PLA
50/50 w/w PLA/PCL
49,5/49,5/1,0 w/w PLA/PCL/Mg(OH)2
48,5/48,5/3,0 w/w PLA/PCL/Mg(OH)2
47,5/47,5/5,0 w/w PLA/PCL/Mg(OH)2
45,0/45,0/10,0 w/w PLA/PCL/Mg(OH)2
Neat PCL
tanδ
Temperature / °C

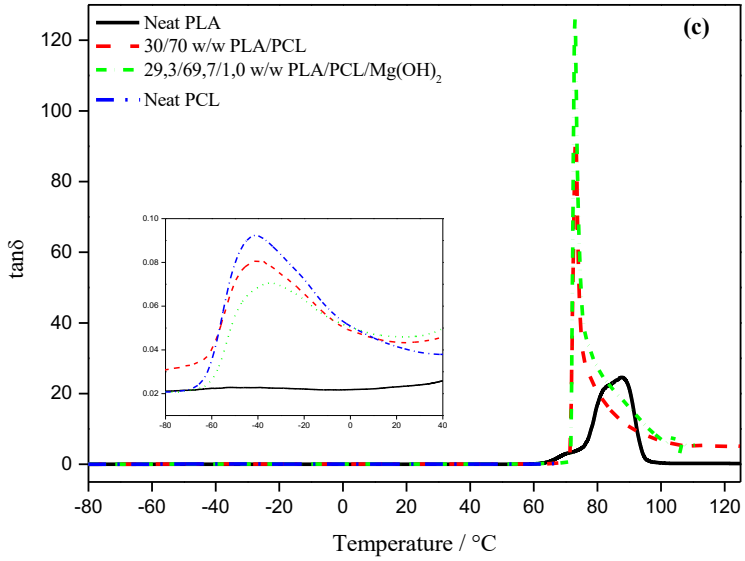
(c)
Neat PLA
30/70 w/w PLA/PCL
29,3/69,7/1,0 w/w PLA/PCL/Mg(OH)2
Neat PCL
tanδ
Temperature / °C

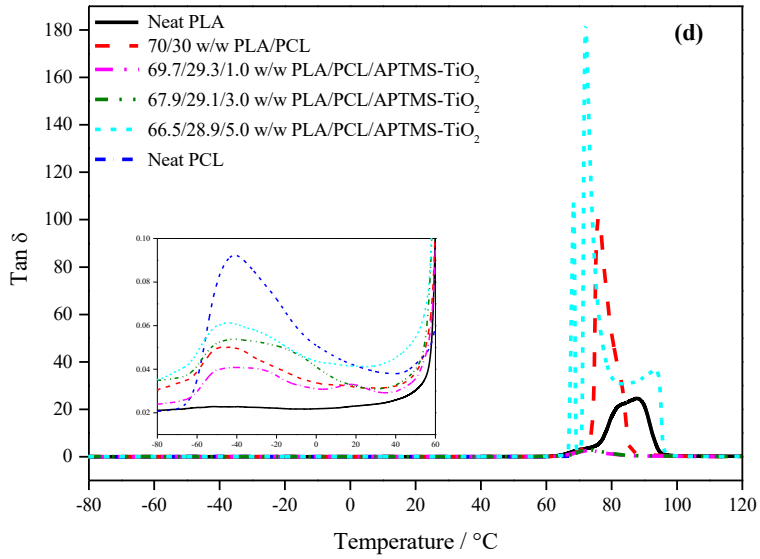
(d)
Neat PLA
70/30 w/w PLA/PCL
69.7/29.3/1.0 w/w PLA/PCL/APTMS-TiO2
67.9/29.1/3.0 w/w PLA/PCL/APTMS-TiO2
66.5/28.9/5.0 w/w PLA/PCL/APTMS-TiO2
Neat PCL
Tan δ
Temperature / °C

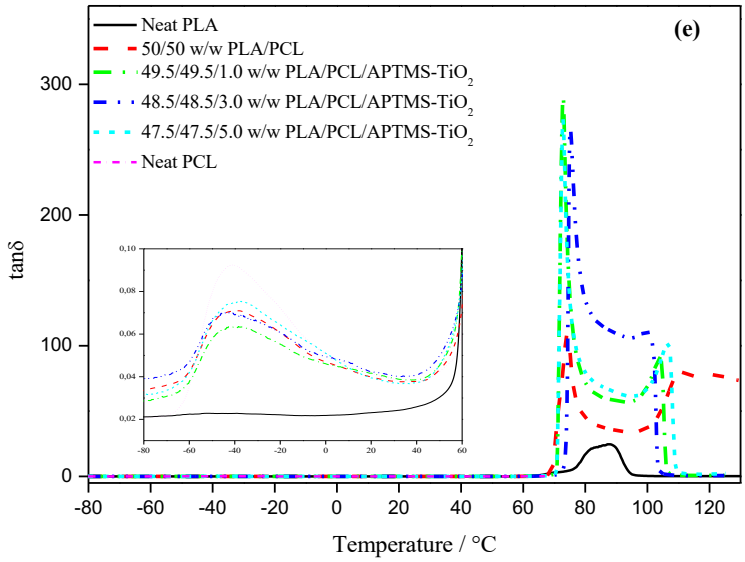
(e)
Neat PLA
50/50 w/w PLA/PCL
49.5/49.5/1.0 w/w PLA/PCL/APTMS-TiO2
48.5/48.5/3.0 w/w PLA/PCL/APTMS-TiO2
47.5/47.5/5.0 w/w PLA/PCL/APTMS-TiO2
Neat PCL
tanδ
Temperature / °C

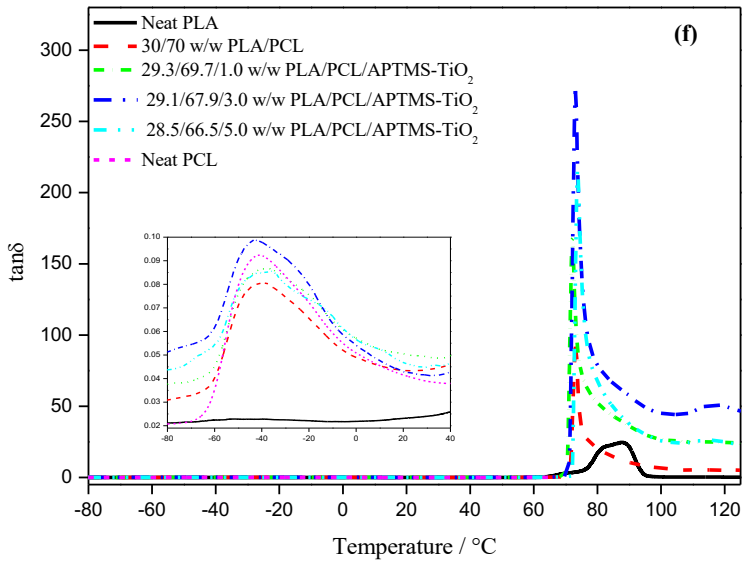

Figure 4.28 Tan δ curves of (a) 70/30 w/w PLA/PCL and its nanocomposites with $Mg(OH)_2$ (b) 50/50 w/w PLA/PCL and its nanocomposites with $Mg(OH)_2$ (c) 30/70 w/w PLA/PCL and its nanocomposites with $Mg(OH)_2$ (d) 70/30 w/w PLA/PCL and its nanocomposites with APTMS-TiO_2 (e) 50/50 w/w PLA/PCL and its nanocomposites with APTMS-TiO_2 (f) 30/70 w/w PLA/PCL and its nanocomposites with APTMS-TiO_2. The inserted figures show the magnified tan δ peaks at lower temperatures around the T_g of PCL.

4.5 References

1. J. Zhao, M. Milanova, M. M. C. G. Warmoeskerken, V. Dutschk. Surface modification of TiO_2 nanoparticles with silane coupling agents. Colloids and Surfaces A: Physicochemical and Engineering Aspects 2012; 413:273– 279.
   DOI: 10.1016/j.colsurfa.2011.11.033
2. D. Pasqui, R. Barbucci. Synthesis, characterization and self-cleaning properties of titania nanoparticles grafted on polyester fabrics. Journal of Photochemistry and Photobiology A: Chemistry 2014; 274:1– 6.
   DOI: 10.1016/j.jphotochem.2013.08.017

3. D. C. L. Vasconcelos, V. C. Costa, E. H. M. Nunes, A. C. S. Sabioni, M. Gasparon, W. L. Vasconcelos. Infrared spectroscopy of titania sol-gel coatings on 316L stainless steel. Materials Sciences and Applications 2011; 2:1375–1382.
DOI: 10.4236/msa.2011.210186
4. K. Nakamoto. Infrared and raman spectra of inorganic and coordination compounds part a: theory and applications in inorganic chemistry; Part B: Application in Coordination, Organometallic, and Bioinorganic Chemistry. John Wiley and Sons: New York (1997).
ISBN 0-471-16394-5
5. B. Stuart. Modern infrared spectroscopy: analytical chemistry by open learning. John Wiley and Sons: New York (1996).
ISBN 0-471-95917-0
6. J. P. Mofokeng, A. S. Luyt. Morphology and thermal degradation studies of melt-mixed poly(lactic acid) (PLA)/poly(ε-caprolactone) (PCL) biodegradable polymer blend nanocomposites with TiO_2 as filler. Polymer Testing 2015; 45:93–100.
DOI: 10.1016/j.polymertesting.2015.05.007
7. R. S. Hebbar, A. M. Isloor, A. F. Ismail. Membrane Characterization. Elsevier: Cambridge (2017).
ISBN: 0444637915, 9780444637918, 978-0-444-63776-5
DOI: http://dx.doi.org/10.1016/B978-0-444-63776-5.00012-7.
8. H. Liu, J. Yi. Polystyrene/magnesium hydroxide nanocomposite particles prepared by surface-initiated in-situ polymerization. Applied Surface Science 2009; 255:5714–5720.
DOI: 10.1016/j.apsusc.2008.12.073
9. C. Carrot, B. Olalla, R. Fulchiron. Relaxation of loose agglomerates of magnesium hydroxide in a polymer melt. Polymer 2012; 53:5560–5567.
DOI: 10.1016/j.polymer.2012.10.004
10. J. J. George and A. K. Bhowmick. Influence of matrix polarity on the properties of ethylene vinyl acetate–carbon nanofiller nanocomposite. Nanoscale Research Letters 2009; 4:655–664.
DOI: 10.1007/s11671-009-9296-8
11. M. Pluta, A. Galeski, M. Alexandre, M. A. Paul, P. Dubois. Polylactide/montmorillonite nanocomposites and microcomposites prepared by melt blending: structure and some physical properties. Journal of Applied Polymer Science 2002; 86:1497–1506.

DOI: 10.1002/app.11309

12. S. Solarski, M. Ferreira, E. Devaux. Characterization of the thermal properties of PLA fibers by modulated differential scanning calorimetry. Polymer 2005; 46:11187–11192. DOI: 10.1016/j.polymer.2005.10.027

13. Y. Luo, W. Li, X. Wang, D. Xu, Y. Wang. Preparation and properties of nanocomposites based on poly(lactic acid) and functionalized TiO_2. Acta Materialia 2009; 57:3182–3191. DOI: 10.1016/j.actamat.2009.03.022

14. V. B. Carmona, A. C. Corrěa, J. M. Marconcini, L. H. C. Mattoso. Properties of a biodegradable ternary blend of thermoplastic starch (TPS), poly(ε-caprolactone) (PCL) and poly(lactic acid) (PLA). Journal of Polymers and the Environment 2015; 23:83–89. DOI: 10.1007/s10924-014-0666-7

15. V. G. Nguyen, H. Thai, D. H. Mai, H. T. Tran, D. L.Tran, M. T. Vu. Effect of titanium dioxide on the properties of polyethylene/TiO_2 nanocomposites. Composites: Part B 2013; 45:1192–1198. DOI: 10.1016/j.compositesb.2012.09.058

16. B. Esteki, H. Garmabi, M. R. Saeb, T. Hoffmann. The crystallinity behavior of polyethylene/clay nanocomposites under the influence of water-assisted melt blending. Polymer-Plastics Technology and Engineering 2013; 52:1–28. DOI: 10.1080/03602559.2013.832853

17. A. Buzarovska. PLA nanocomposites with functionalized TiO_2 nanoparticles. Polymer-Plastics Technology and Engineering 2013; 52: 280–286. DOI: 10.1080/03602559.2012.751411

18. P. R. Hornsby, J. Wang, R. Rothon, G. Jackson, G. Wilkinson, K. Cossick. Thermal decomposition behaviour of polyamide fire-retardant compositions containing magnesium hydroxide filler. Polymer Degradation and Stability 1996; 51:235–249. DOI: 0141-3910(95)00181-6

19. F. Carpentier, S. Bourbigot, M. Le Bras, R. Delobel, M. Foulon. Charring of fire retarded ethylene vinyl acetate copolymer-magnesium hydroxide/zinc borate formulations. Polymer Degradation and Stability 2000; 69:83–92. PII: S0141-3910(00)00044-6

20. T. Su, H. Jiang, H. Gong. Thermal Stabilities and the Thermal Degradation Kinetics of Poly(ε-Caprolactone). Polymer-Plastics Technology and Engineering 2008; 47:398–403. DOI: 10.1080/03602550801897695

21. K. Fukushima, D. Tabuani, G. Camino. Nanocomposites of PLA and PCL based on montmorillonite and sepiolite. Materials Science and Engineering C 2009; 29:1433–1441.
DOI: 10.1016/j.msec.2008.11.005

22. C. Vogel, H. W. Siesler. Thermal degradation of poly(ε-caprolactone), poly(L-lactic acid) and their blends with poly(3-hydroxy-butyrate) studied by TGA/FT-IR spectroscopy. Macromolecular Symposia 2008; 265:183–194.
DOI: 10.1002/masy.200850520

23. J. P. Mofokeng, A. S. Luyt. Morphology and thermal degradation studies of melt-mixed PLA/PHBV biodegradable polymer blend nanocomposites with TiO_2 as filler. Journal of Applied Polymer Science 2015; 132:1–11.
DOI: 10.1002/app.42138

24. J. P. Mofokeng, A. S. Luyt. Morphology and thermal degradation studies of melt-mixed poly(hydroxybutyrate-co-valerate) (PHBV)/poly(ε-caprolactone) (PCL) biodegradable polymer blend nanocomposites with TiO_2 as filler. Journal of Material Science 2015; 50: 3812–3824.
DOI: 10.1007/s10853-015-8950-z

25. X. Chen, J. Zhuo, C. Jiao. Thermal degradation characteristics of flame retardant polylactide using TG-IR. Polymer Degradation and Stability 2012; 97:2143–2147.
DOI: 10.1016/j.polymdegradstab.2012.08.016

26. A. Ostafinska, I. Fortelny, M. Nevaralova, J. Hodan, J. Kredatusova, M. Slouf. Synergistic effects in mechanical properties of PLA/PCL blends with optimized composition, processing, and morphology. Royal Society of Chemistry Advances 2015; 5: 98971–98982.
DOI: 10.1039/c5ra21178f

27. L. Cabedo, J. L. Feijoo, M. P. Villanueva, J. M. Lagaron, E. Gimenez. Optimization of biodegradable nanocomposites based on aPLA/PCL blends for food packaging applications. Macromolecular Symposia 2006; 233:191–197.
DOI: 10.1002/masy.200650124

28. Y. Y. Then, N. A. Ibrahim, N. Zainuddin, B. W. Chieng, H. Ariffin, and W. M. Z. W. Yunus. Effect of 3-aminopropyltrimethoxysilane on chemically modified oil palm mesocarp fiber/poly(butylene succinate) biocomposite. BioResources 2015; 10:3577–3601.
DOI: 10.15376/biores.10.2.3577-3601

29. J. P. Mofokeng, A. S. Luyt. Dynamic mechanical properties of PLA/PHBV, PLA/PCL, PHBV/PCL blends and their nanocomposites with TiO_2 as nanofiller. Thermochimica Acta 2015; 613:41–53.
DOI: 10.1016/j.tca.2015.05.019

30. R. P. Chartoff, J. D. Menczel, S. H. Dillman. Dynamic mechanical analysis (DMA). In: J. D. Menczel, R. B. Prime. Thermal analysis of polymers fundamentals and applications. John Wiley and Sons: New York City (2009).
ISBN 978-0-471-76917-0

Chapter 5

Conclusions

PLA, PCL and PLA/PCL blend nanocomposites were prepared via melt mixing in the presence of two nanofillers (magnesium hydroxide ($Mg(OH)_2$ and 3-aminopropyltrimethoxysilane functionalised titania (APTMS-TiO_2)). This was done to enhance the morphology and thermal properties of PLA, PCL and their blends for short shelf application materials, in order to create a competitive alternative to non-biodegradable oil-based plastics which are currently causing environmental pollution. The efficiency of the two fillers' ($Mg(OH)_2$, and APTMS-TiO_2) on the properties of each polymer and their blends were compared using different techniques to determine the most effective filler for various potential applications.

The functionalization of TiO_2 was confirmed with the presence of a Si-O-Ti stretching vibration band at 919 cm^{-1} on an FTIR spectrum which was absent in neat TiO_2 and the APTMS functionalizing agent. This band indicated that there was a new bond formed between the TiO_2 and APTMS. During thermal degradation of the APTMS-TiO_2, an additional degradation step between 480.4 and 600 °C which was absent in neat TiO_2 indicated that the TiO_2 nanoparticles were successfully functionalized. There was ~1.6 wt.% APTMS in the functionalized TiO_2. In the polymer blends, the APTMS-TiO_2 nanoparticles had a preferential location in PLA and were well dispersed with few agglomerates. Perhaps, if the amount of functionalizing agent had been higher, the dispersion could have been even better in APTM-TiO_2 nanocomposites and blend nanocomposites. Modifying the method used for functionalization by increasing the reaction time from 4 to 16 hours could possibly double the amount of APTMS grafted onto TiO_2. This would allow the TiO_2 to maintain its high thermal stability and photocatalytic properties whilst improving the interaction of the nanoparticles with the polymer matrix.

The $Mg(OH)_2$ nanorods showed a dispersion in both polymers, but large agglomerates (>10 μm) and crevices within the agglomerates and at the interface with the PLA and PCL polymer matrix were observed. In the $Mg(OH)_2$ nanocomposites, if the particle size had been smaller (<25 nm like the TiO_2 nanoparticles), the wetting surface between the filler and polymers could have been improved. In future studies, the ultrasonication of the $Mg(OH)_2$ would be recommended to achieve better dispersion. Also, another way of combating the agglomeration could be surface modification of $Mg(OH)_2$ using fatty acids, oleic acid, silanes, silicone oil, sodium oleate, stearic acid, titanates and zinc stearate. These would be options to consider,

since most of them have been reported to improve the dispersion of $Mg(OH)_2$ in non-biodegradable polymers.

Both $Mg(OH)_2$ and APTMS-TiO_2 nanoparticles effectively acted as heteronucleating agents and partially improved miscibility between the PLA and PCL as a result of their dispersion in the polymer matrices even though it was not perfect.

In the $Mg(OH)_2$ single and polymer blend nanocomposites, an autocatalytic effect of the filler on the rate of thermal degradation of the polymers was observed. An earlier onset of the thermal degradation was observed at lower temperatures (below 300 ºC) due to the loss of water which is known to catalyse the thermal degradation of biodegradable polyesters. At temperatures above 300 ºC, MgO which is a by-product during thermal degradation of $Mg(OH)_2$ was present and this resulted in improvements in the thermal stabilities of the polymers. In contrast, the presence of APTMS-TiO_2 nanoparticles in both single and blend nanocomposites resulted in an increase in thermal stabilities of all the nanocomposites. The thermal stability of $Mg(OH)_2$ at lower temperatures could possibly be improved by functionalization as well. Functionalization would make less -OH groups available for condensation, preventing the release of water at lower temperatures which catalyses the thermal degradation of biodegradable polyesters. Also, the functionalizing agents could possibly increase the adhesion of the $Mg(OH)_2$ and polymer matrix, therefore improving the insulation of the polymers. And again, if the functionalizing agent has high thermal stability, that would improve the thermal properties of the $Mg(OH)_2$ nanoparticles and the polymer matrix.

A decrease in the intensity of the degradation volatiles was observed using both $Mg(OH)_2$ and APTMS-TiO_2 nanoparticles. This revealed that there was some level of smoke suppression due to a possible interaction between the fillers and the degradation volatiles. A general increase in the maximum thermal degradation volatilization temperatures for both PLA and PCL with the presence of both $Mg(OH)_2$ and APTMS-TiO_2 nanoparticles was also seen. This pointed towards a possible interaction between the degradation volatiles and the fillers resulting in a delay in the temperature at which the degradation volatiles were emitted. However in some cases the volatiles were released earlier than in the neat polymers or blends pointing towards a possible catalytic effect of the fillers in the degradation of PLA and PCL. Improving dispersion of these nanocomposites could be key in achieving better smoke suppression.

$Mg(OH)_2$ single and blend nanocomposites had higher storage modulus compared to APTMS-TiO_2 nanocomposites. The increase in E' of the polymers in the presence of $Mg(OH)_2$ is an

indication that the stiffness was increased, but it was not really clear if the stiffness was due to increase in the degree in crystallinity or not. Though the DSC results showed that $Mg(OH)_2$ acted as heterogenous nucleating agent, but most of the properties were not strongly affected by the increase in crystallinity in the presence of this filler. This could be due to the fact that $Mg(OH)_2$ did not interact well with the polymers in the blends, and there were lot of gaps on the interface between the polymers and the nanorods as seen on the SEM figures. In the loss modulus curves, there was generally an increase in the T_g of PCL and a decrease in the T_g of PLA with both $Mg(OH)_2$ and APTMS-TiO_2 nanoparticles. The temperature difference between the glass transition temperatures of PCL and PLA decreased with increasing filler content. This indicated that the partial miscibility between PLA and PCL had been increased.

Presence of $Mg(OH)_2$ generally increased the tan δ maximum values in the single nanocomposites, and a decrease was observed in the polymer blends. In the APTMS-TiO_2 nanocomposites, a general increase in tan δ maximum values obtained around the T_g of PCL and PLA in the single and blend nanocomposites was seen. The damping was generally lower in the $Mg(OH)_2$ nanocomposites, when compared to APTMS-TiO_2 nanocomposites. This indicated that $Mg(OH)_2$ nanorods had a better stiffening effect than the APTMS-TiO_2 nanoparticles which mostly had a plasticizing effect on the chains of the polymers. Improving the dispersion of $Mg(OH)_2$ nanoparticles could possibly improve the stiffening ability of $Mg(OH)_2$ of which will increase the degree of crystallinity of the polymers, and ultimately the thermomechanical properties of PLA and PCL. Also, the changes in the tan δ maximum values could have been due to differences in compatibility between both fillers with PLA and PCL. The high tan δ maximum values in the presence of APTMS-TiO_2 nanoparticles with both PLA and PCL indicated poor adhesion of the nanoparticles with both polymers. The lower damping seen with $Mg(OH)_2$ nanoparticles could have been due to compatibility between the polymer matrix with the filler. From the SEM images of the $Mg(OH)_2$ nanocomposites, the nanoparticles were dispersed in both polymers, even though large agglomerates and voids were present. The voids could have been due to the large particle size of the filler, the $Mg(OH)_2$ nanorods had a particles size <100 nm and some their agglomerates were greater than 10 μm. Decreasing the size of the $Mg(OH)_2$ nanoparticles (to <25 nm like the TiO_2 nanoparticles) could possibly increase the surface area for interaction with the polymer and therefore help clear this uncertainty. $Mg(OH)_2$ and APTMS-TiO_2 nanoparticles increased the PCL peak temperatures and decreased PLA peak temperatures in both single and blend nanocomposites. This also indicated increased partial miscibility between the PLA and PCL.

In conclusion, the objective of the study was achieved, as blending helped overcome some of the poorer properties of the single polymers and their nanocomposites. The addition of PCL to PLA and vice versa, had a positive effect on the properties. A slight improvement in the miscibility of PLA and PCL was achieved with both $Mg(OH)_2$ and APTMS-TiO_2 nanoparticles as fillers. No significant changes were observed in the melting temperatures of PCL in the presence of PLA. It is known that the low melting temperature of PCL is its limiting factor in some applications, though thermomechanical analysis results indicated improved miscibility through their glass transition temperatures in the presence of both nanofillers. In future melting temperature of PCL in blends with PLA can be improved with a successful functionalisation of inorganic nanofiller as indicated above. Whereby the dispersion of the nanofiller will be of high priority, in the polymers and on their interface, and that will lead into improved important properties, including the good adhesion between the two polymers. In that case the melting temperature of PCL will also improve, and the resulting materials can be used on applications where PCL melting temperature was a limiting factor.

The thermal stability results indicated that blending averaged the properties of these two polymers, as all the blends had intermediate thermal degradation temperatures to those of PLA and PCL. The presence of high thermally stable PCL improved the thermal stability of PLA, while its thermal stability was compromised due to the presence and increase in content of low thermally stable PLA. The presence of APTMS-TiO_2 nanoparticles had a positive effect on both the thermal stabilities of the PLA and PCL, as the degradation temperatures increased further on the PLA phase, and the PCL ones picked up as well in the process. It was seen that both fillers could be used as smoke suppressants, as the thermal degradation volatiles release were slower in the presence of both nanofillers. When compared to the intensities of the FTIR spectra and release temperatures in neat polymers and blends, the nanocomposites and blends nanocomposites had lower intensities, and a shift towards higher temperatures on maximum release of the degradation products. It could be interesting in the future to do thermal degradation kinetics in order to see the degradation mechanisms, and flame tests in the future in order to investigate and see properly the effect of these nanofillers on the thermal properties of both PLA and PCL in details.

Recommendations for future work:

- Investigate the surface energy properties of APTMS-TiO_2
- Investigate the influence of functionalizing $Mg(OH)_2$ on the properties of PLA/PCL
- Investigate the influence of $Mg(OH)_2$ and APTMS-TiO_2 particle size on the properties of PLA/PCL
- Investigate the degradation kinetics of $Mg(OH)_2$ and APTMS-TiO_2 nanocomposites with PLA/PCL polymer blends
- Investigate the biodegradability of PLA/PCL polymer blend nanocomposites with $Mg(OH)_2$ and APTMS-TiO_2 nanoparticles

Acknowledgements

First and foremost, I would like to thank God for the opportunity He granted me to undertake this project.

Secondly, my heartfelt appreciations go to my supervisor **Dr Julia Puseletso Mofokeng** for her unending support and faith in me. She was always present and willing to help me through all challenges with patience and kindness. She taught me valuable academic and life lessons that I will value forever.

I acknowledge the University of the Free State (UFS) for the resources (internet, library, financial support, laboratories, workshops etc.) they provided that made it possible for me to successfully complete my studies. This work is based on the research supported in part by the National Research Foundation South Africa (Grant Numbers 105588, 109781 and AEMD170601235957).

I would like to acknowledge Ms. Hanlie Grobler from the University of the Free State (Bloemfontein campus) for analysing my SEM and TEM samples.

A special thanks to my parents, **Professor Geofrey Mukwada and Mrs Ester Mukwada** for being my inspiration and role models. I thank you for your unconditional love and support for all my dreams.

I would like to thank my siblings **Geoffrey Tavonga Mukwada and Thandanani Brandon Mukwada** for their support and encouragement. I love you guys, you can do anything!!!

I would like to thank the Faculty of Natural and Agricultural Sciences and the Chemistry Department (Ms Palesa Leeche, Mrs Cheryl-Ann König, Mrs Moipone Malimabe, Dr Mfiso Mngomezulu, Dr Nomampondomise Molefe, Mr Rantoa Moji, Mr Tyson Mosoabisane, Mr Khotso Mpitso and Mr Tsietsi Tsotetsi) for their support.

I would like to express my gratitude to the Polymer Research Group of UFS (Qwaqwa campus) (Dr. Dusko Dudić, Ms. Thandi Gumede, Ms. Nomvula Kokozela, Ms. Tholwana Motloung, Mrs. Mothepane Mbongo, Mr. James Selemakoro, Mr. Tebello Tsotetsi, Ms. Tshilidzi Athalia Matshavha, Mr. Ziphozonke Zikode, Mr. Lesia Mokoena, Mr. Mbongeni Ngwenya, Mr. Thabo Mdletshe and Mr. Xolani Blom). I would also like to thank them for their emotional support, constant encouragement and for the many laughs we shared.

"As the morning sun rises
I rise with it
And the birds sing songs of joy
Songs of a morning glory
My dreams awake with me
And as I rise, I live them everyday

A journey, a journey of a thousand steps
A journey we have all began
A journey of hope and a better life
We stand in grace and walk in boldness.

A few mountains to climb
A few valleys to overcome
And a few rivers to cross
We will surely overcome

We lay with satisfaction as the sun goes down
Strive when others are asleep
And we begin our race all over again
In the rain, wind, cold, storms, and throbbing sun
We will remain standing."

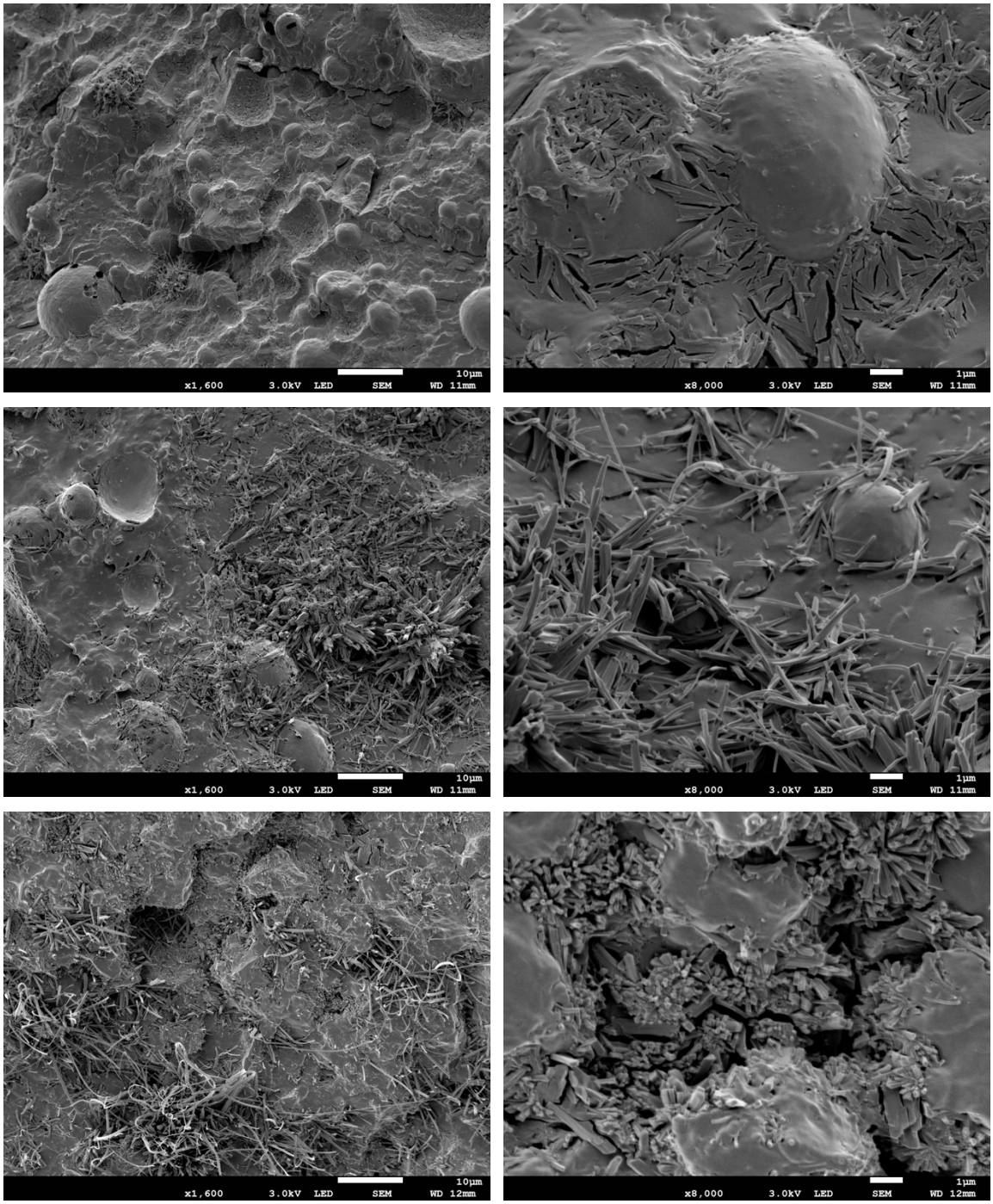

Figure A.1 SEM micrographs of the fracture surfaces of (a, b) 69.3/29.3/1 w/w PLA/PCL/$Mg(OH)_2$, (c, d) 49.5/49.5/1 w/w PLA/PCL/$Mg(OH)_2$, (e, f) 29.3/69.7/1 w/w PLA/PCL/$Mg(OH)_2$ blend nanocomposites at 1600x and at 8000x magnification

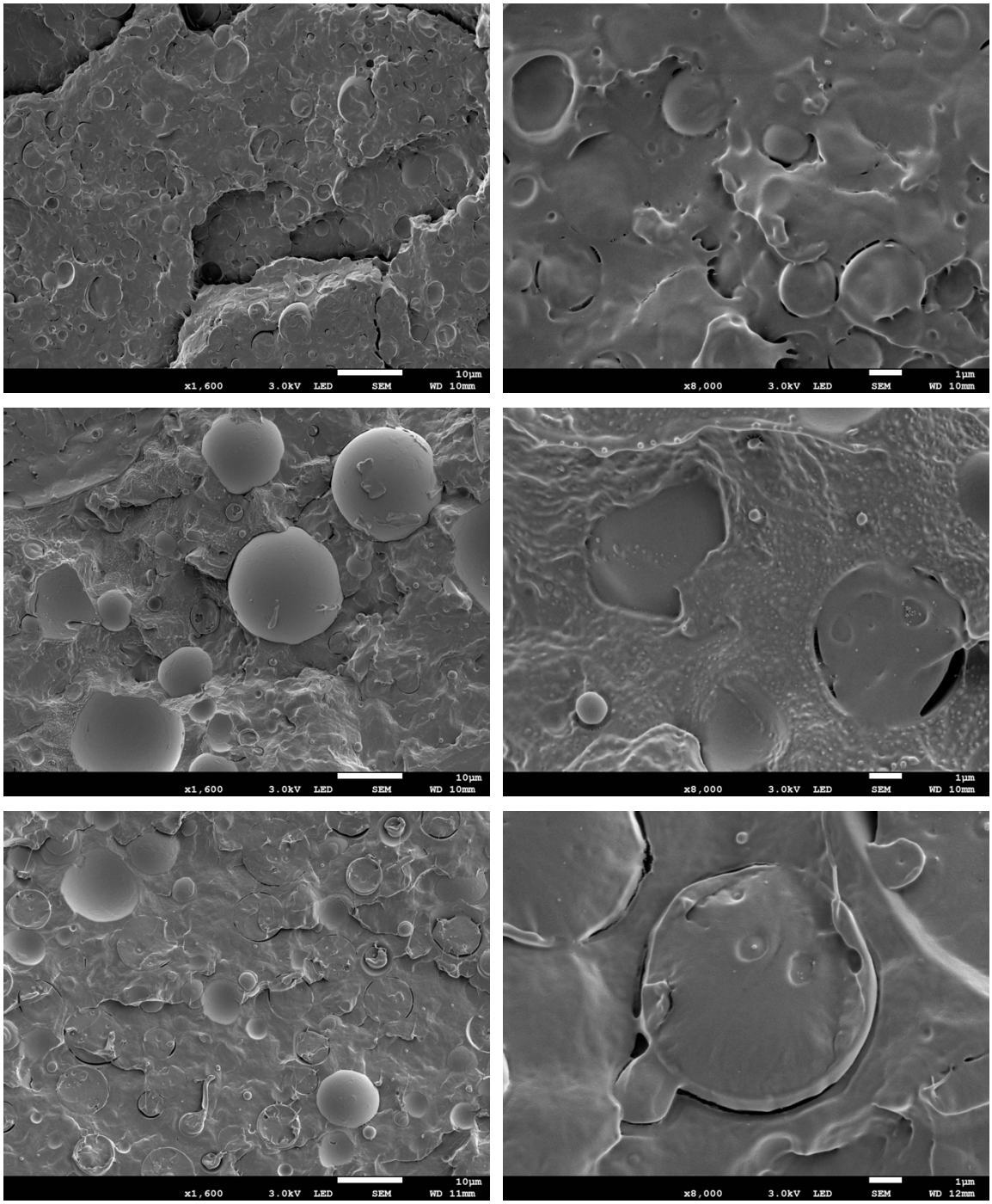

Figure A.2 SEM micrographs of the fracture surfaces of (a, b) 69.3/29.3/1 w/w PLA/PCL/APTMS-TiO_2, (c, d) 49.5/49.5/1 w/w PLA/PCL/ APTMS-TiO_2, (e, f) 29.3/69.7/1 w/w PLA/PCL/ APTMS-TiO_2 blend nanocomposites at 1600x and at 8000x magnification

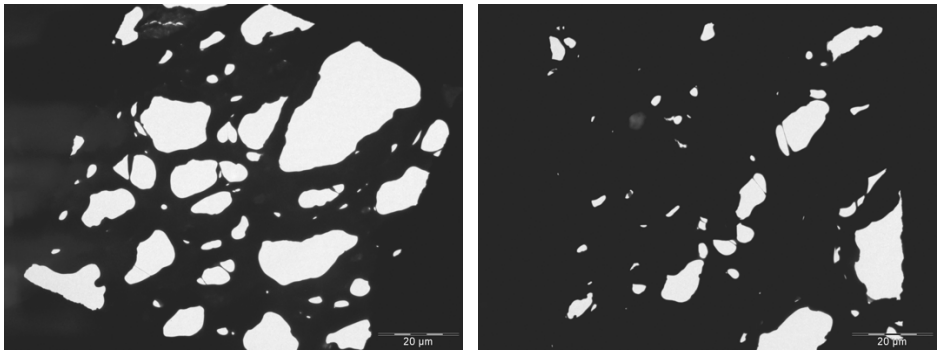

Fgure A.3 TEM images of (a) 66.5/28.5/5 w/w PLA/PCL/$Mg(OH)_2$ (b) 47.5/47.5/5 w/w PLA/PCL/$Mg(OH)_2$ at 800x magnifications

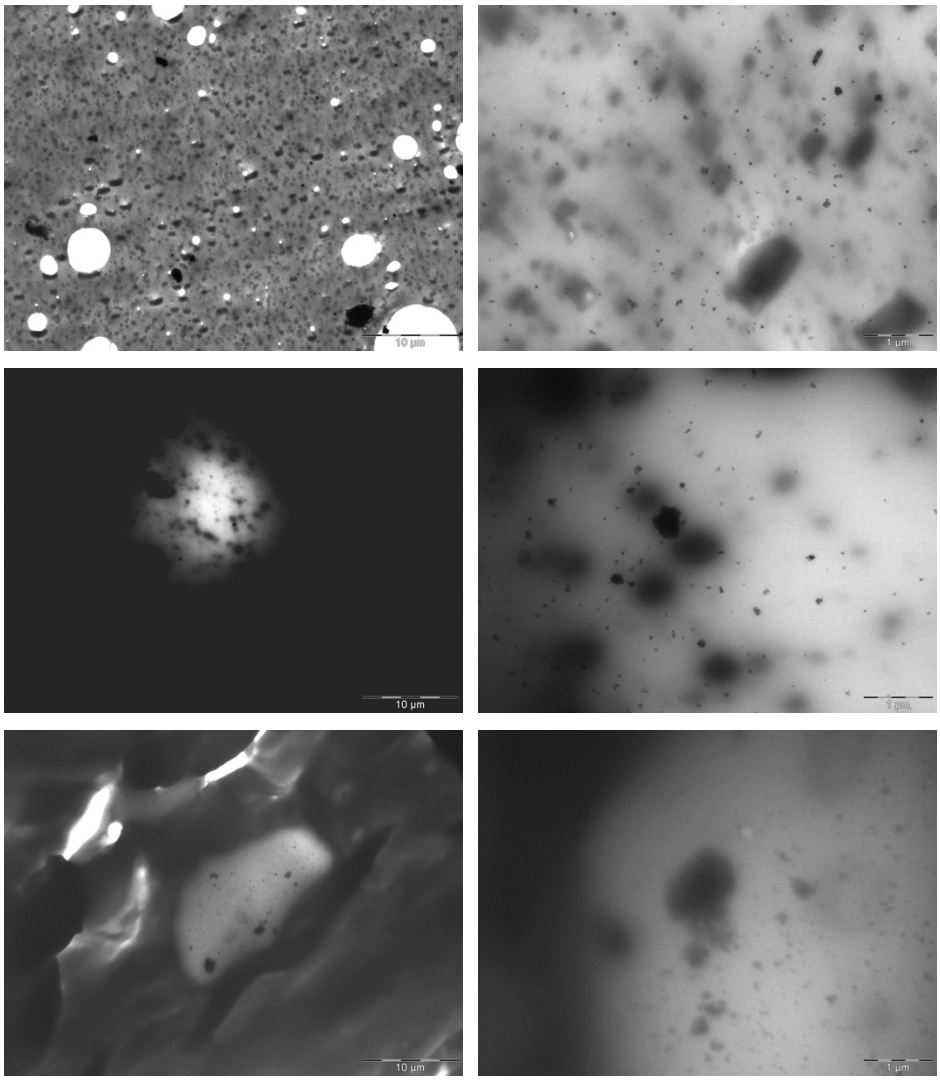

Figure A.4 TEM images of (a, b) 69.3/29.3/1 w/w PLA/PCL/APTMS-TiO_2, (c, d) 49.5/49.5/1 w/w PLA/PCL/ APTMS-TiO_2 (e, f) 29.3/69.7/1 w/w PLA/PCL/ APTMS-TiO_2 at 1950x and 13500x magnifications

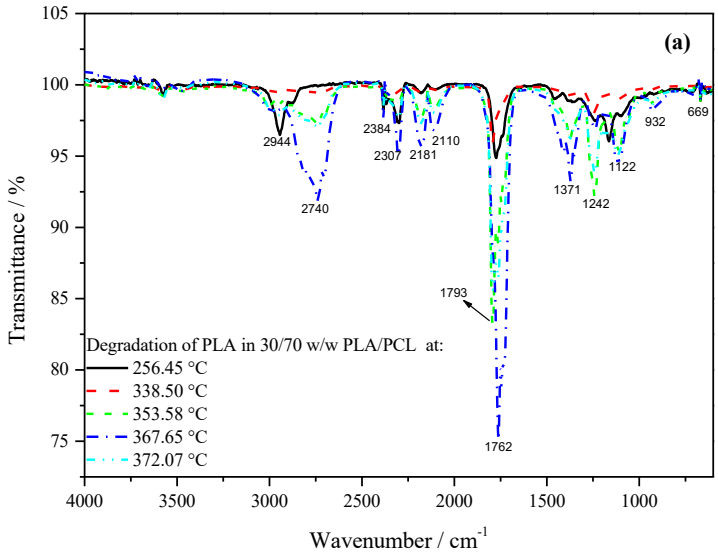
(a)
Transmittance / %
Wavenumber / cm-1
Degradation of PLA in 30/70 w/w PLA/PCL at:
256.45 °C
338.50 °C
353.58 °C
367.65 °C
372.07 °C
2944
2740
2384
2307
2181
2110
1793
1762
1371
1242
1122
932
669

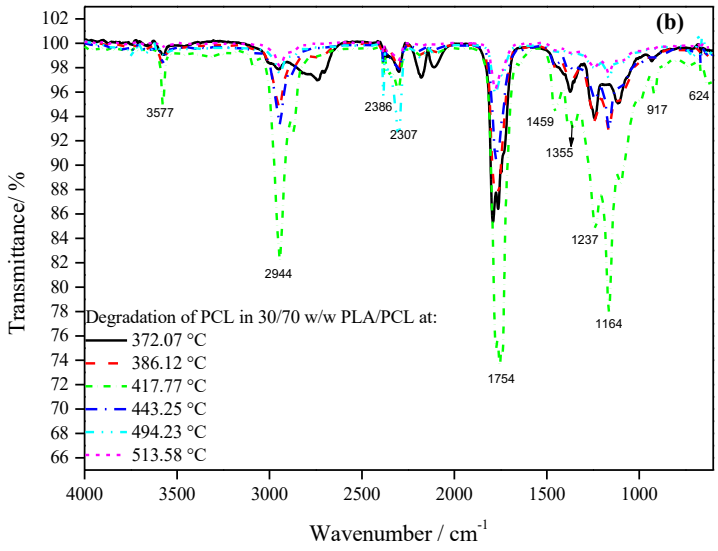
(b)
Transmittance/ %
Wavenumber / cm-1
Degradation of PCL in 30/70 w/w PLA/PCL at:
372.07 °C
386.12 °C
417.77 °C
443.25 °C
494.23 °C
513.58 °C
3577
2944
2386
2307
1754
1459
1355
1237
1164
917
624

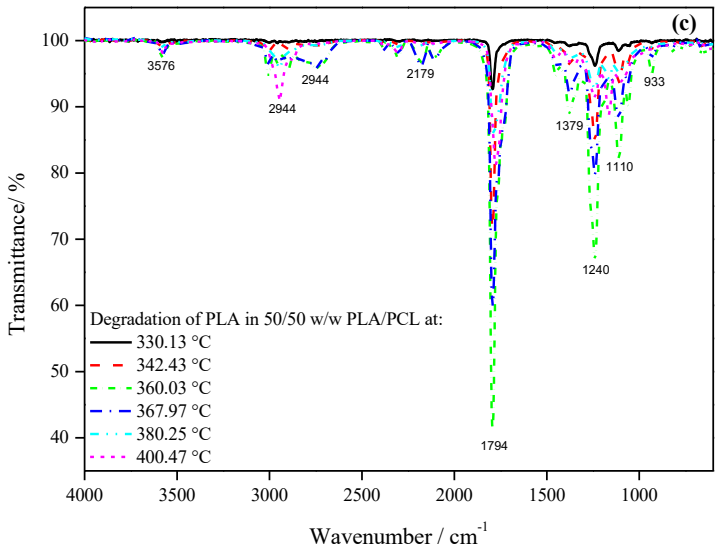
(c)
Transmittance/ %
Wavenumber / cm-1
3576
2944
2944
2179
1794
1379
1110
1240
933
Degradation of PLA in 50/50 w/w PLA/PCL at:
330.13 °C
342.43 °C
360.03 °C
367.97 °C
380.25 °C
400.47 °C

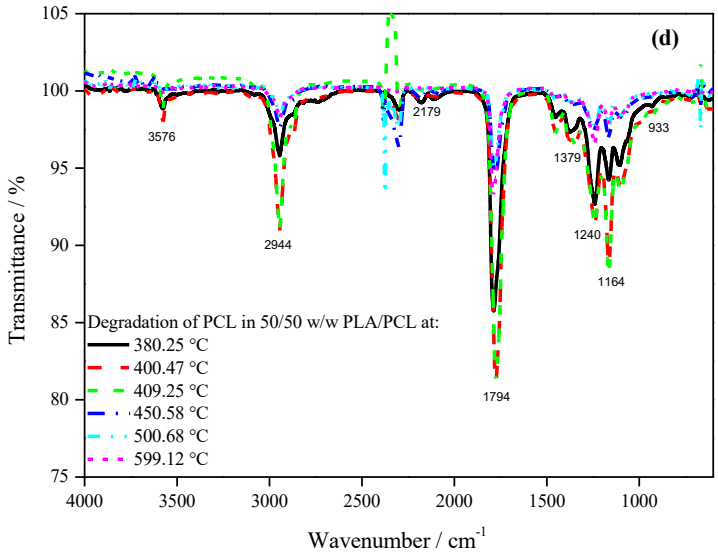
(d)
Transmittance / %
Wavenumber / cm-1
3576
2944
2179
1794
1379
1240
1164
933
Degradation of PCL in 50/50 w/w PLA/PCL at:
380.25 °C
400.47 °C
409.25 °C
450.58 °C
500.68 °C
599.12 °C

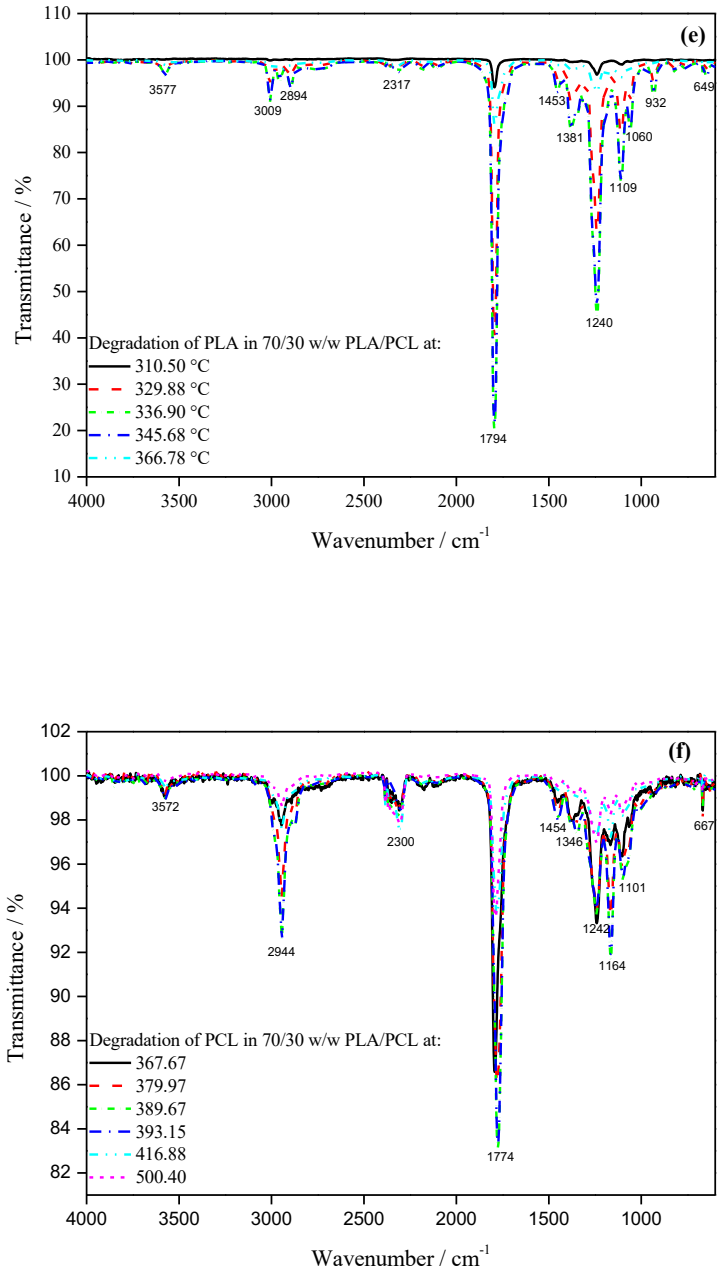

Figure A.5 FTIR spectra of degradation products of the PLA (a, c, e) and PCL (b, d, f) in the polymer blends

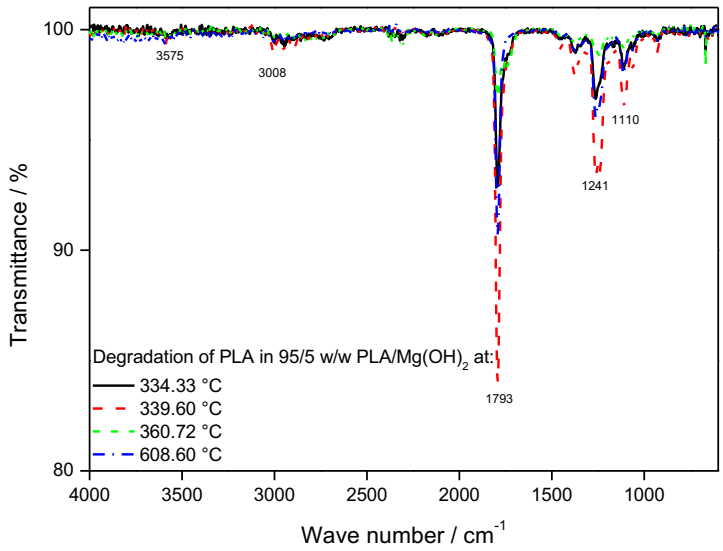

Figure A.6 FTIR spectra of degradation products of PLA with 5 wt.% $Mg(OH)_2$ nanoparticles

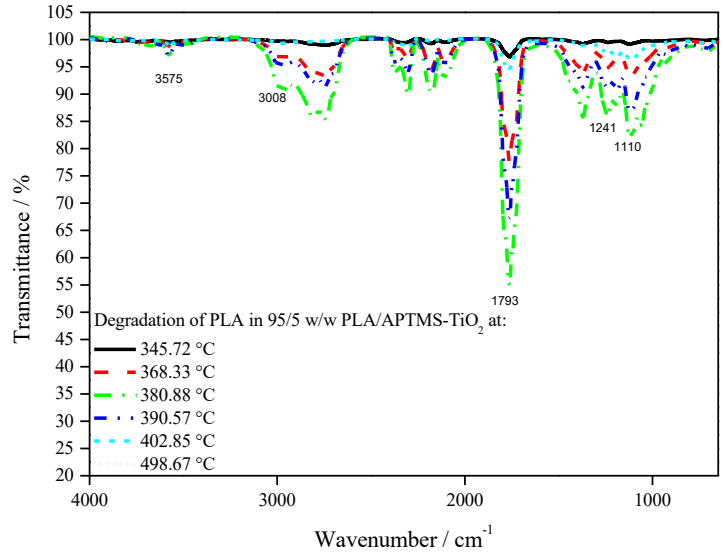

Figure A.7 FTIR spectra of degradation products of PLA with 5 wt.% APTMS-TiO_2 nanoparticles

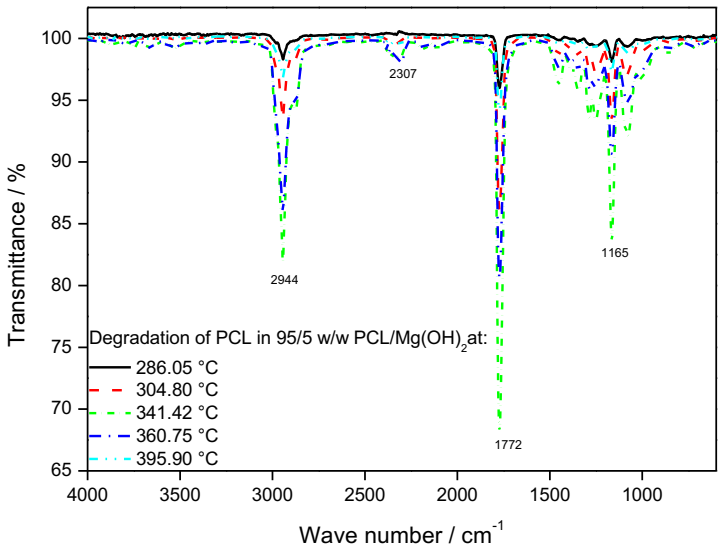

Figure A.8 FTIR spectra of degradation products of PCL with 5 wt.% $Mg(OH)_2$ nanoparticles

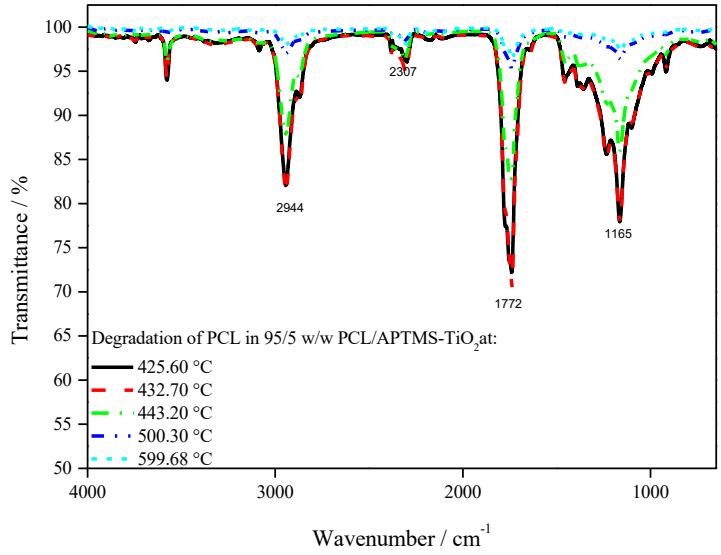

Figure A.9 FTIR spectra of degradation products of PCL with 5 wt.% APTMS-TiO_2 nanoparticles

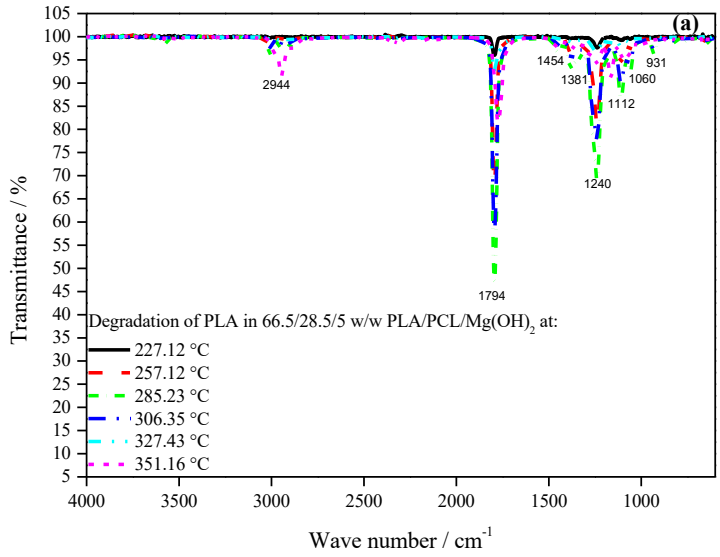

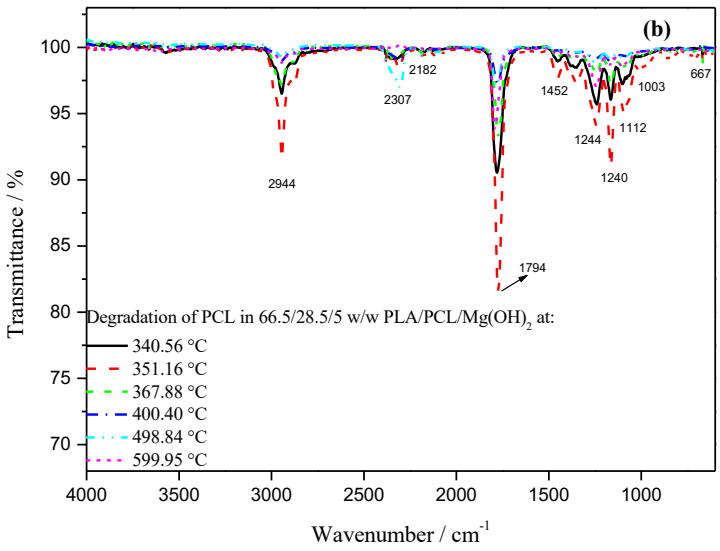

Figure A.10 FTIR spectra of degradation products of (a) PLA and (b) PCL in 66.5/28.5/5 w/w PLA/PCL/$Mg(OH)_2$

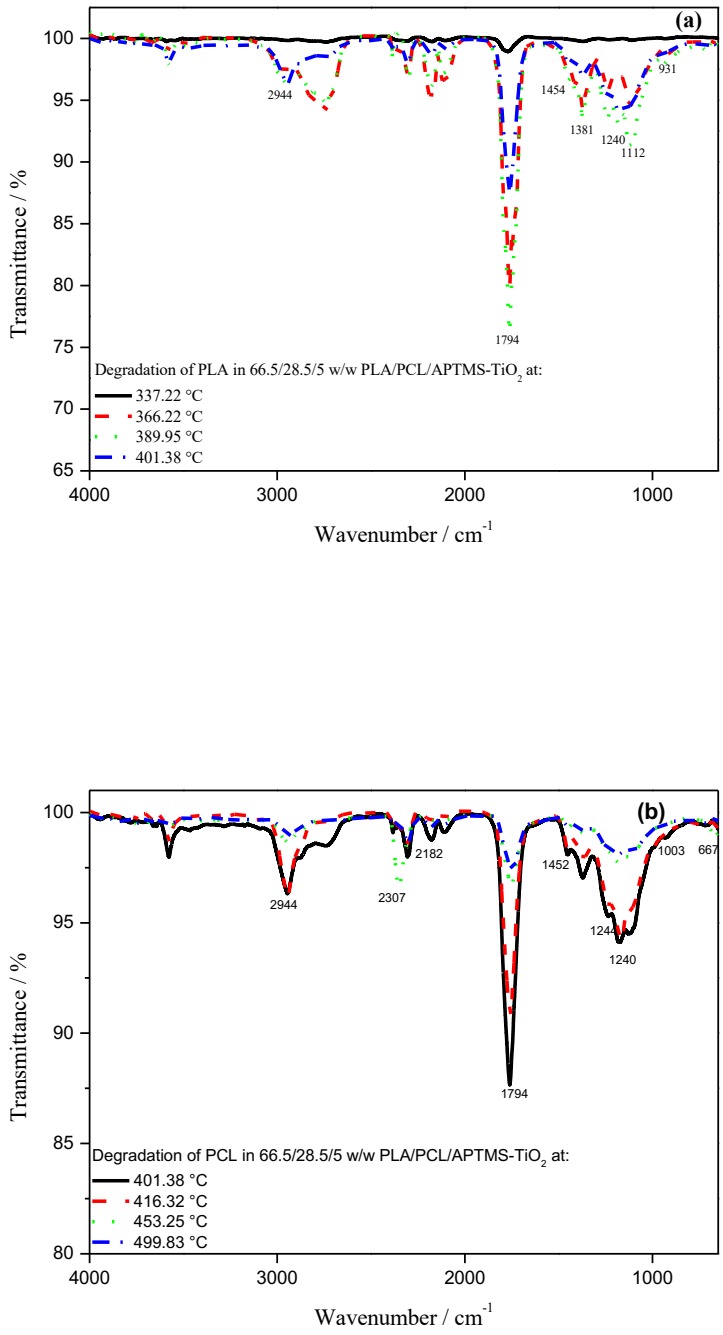

Figure A.11 FTIR spectra of degradation products of (a) PLA and (b) PCL in 66.5/28.5/5 w/w PLA/PCL/APTMS-TiO_2

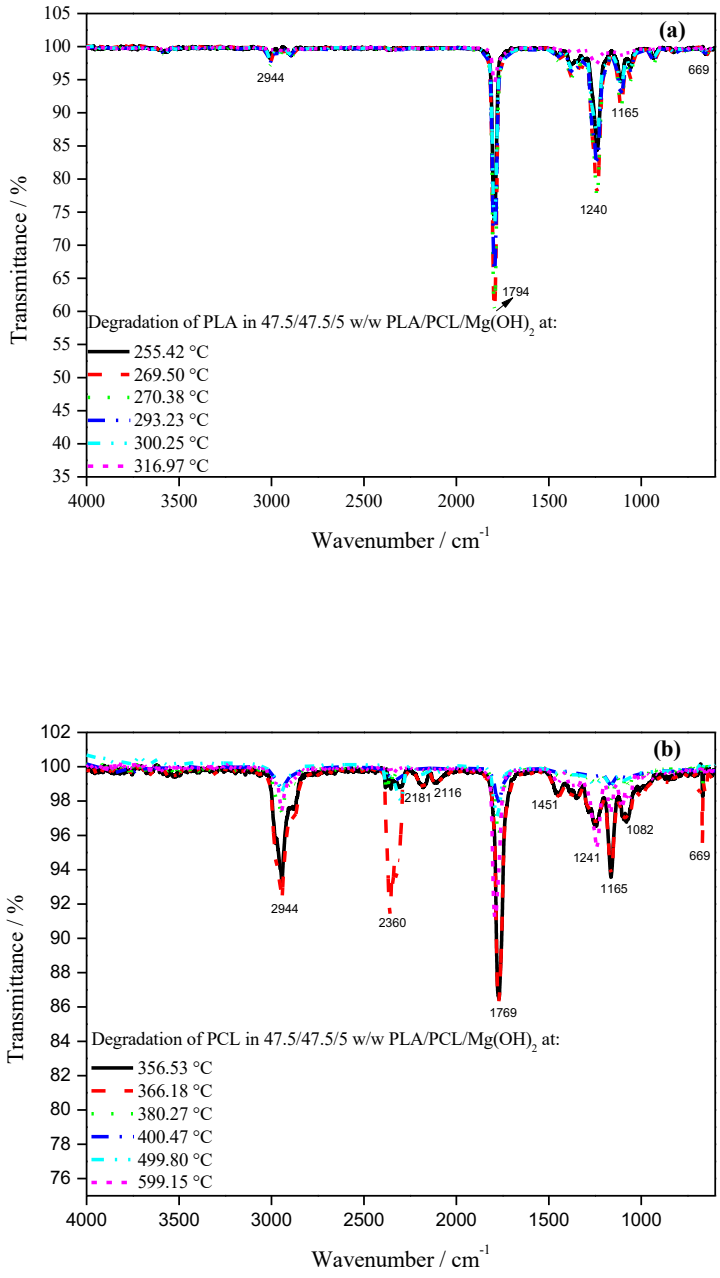

Figure A.12 FTIR spectra of degradation products of (a) PLA and (b) PCL in 47.5/47.5/5 w/w PLA/PCL/$Mg(OH)_2$

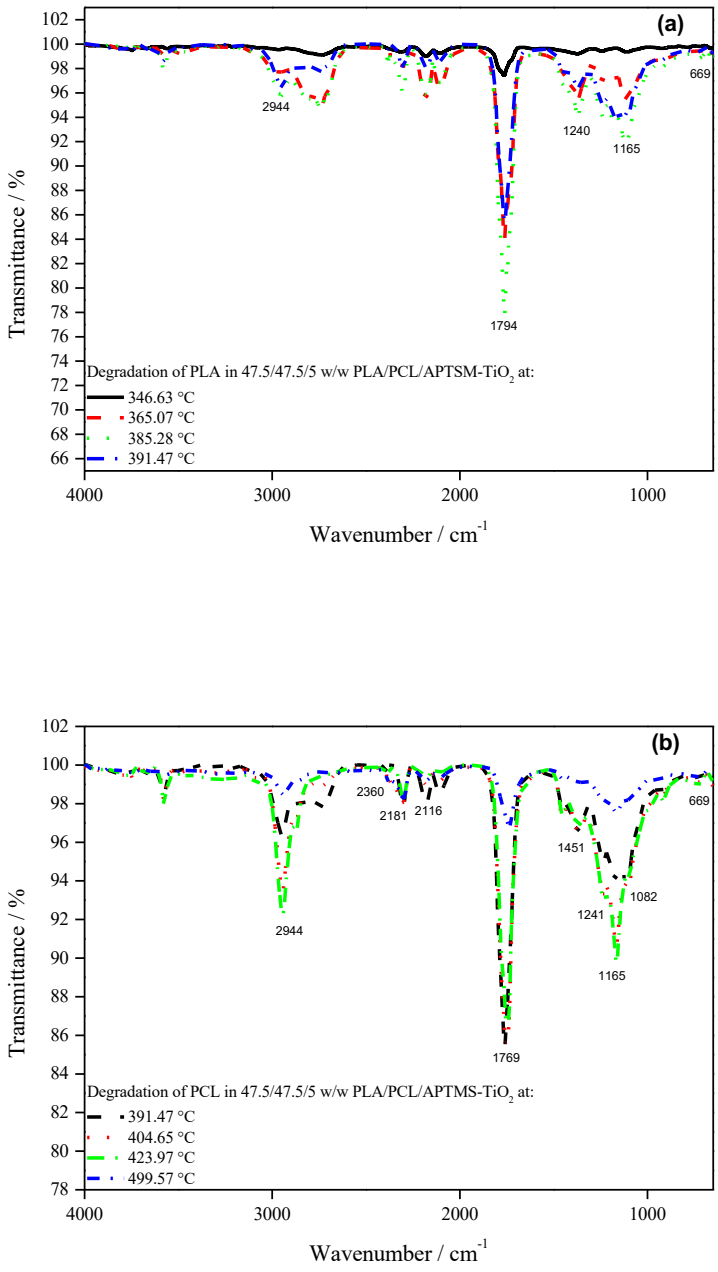

Figure A.13 FTIR spectra of degradation products of (a) PLA and (b) PCL in 47.5/47.5/5 w/w PLA/PCL/APTMS-TiO_2

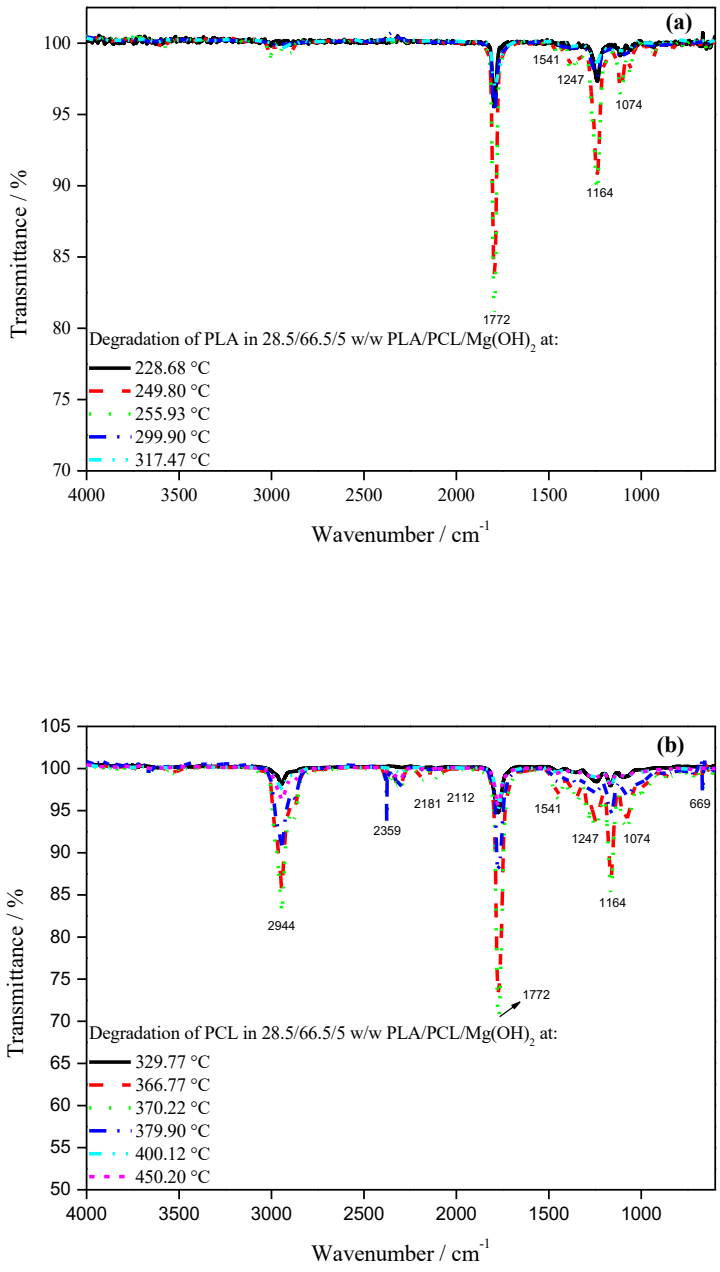

Figure A.14 FTIR spectra of degradation products of (a) PLA and (b) PCL in 28.5/66.5/5 w/w PLA/PCL/$Mg(OH)_2$

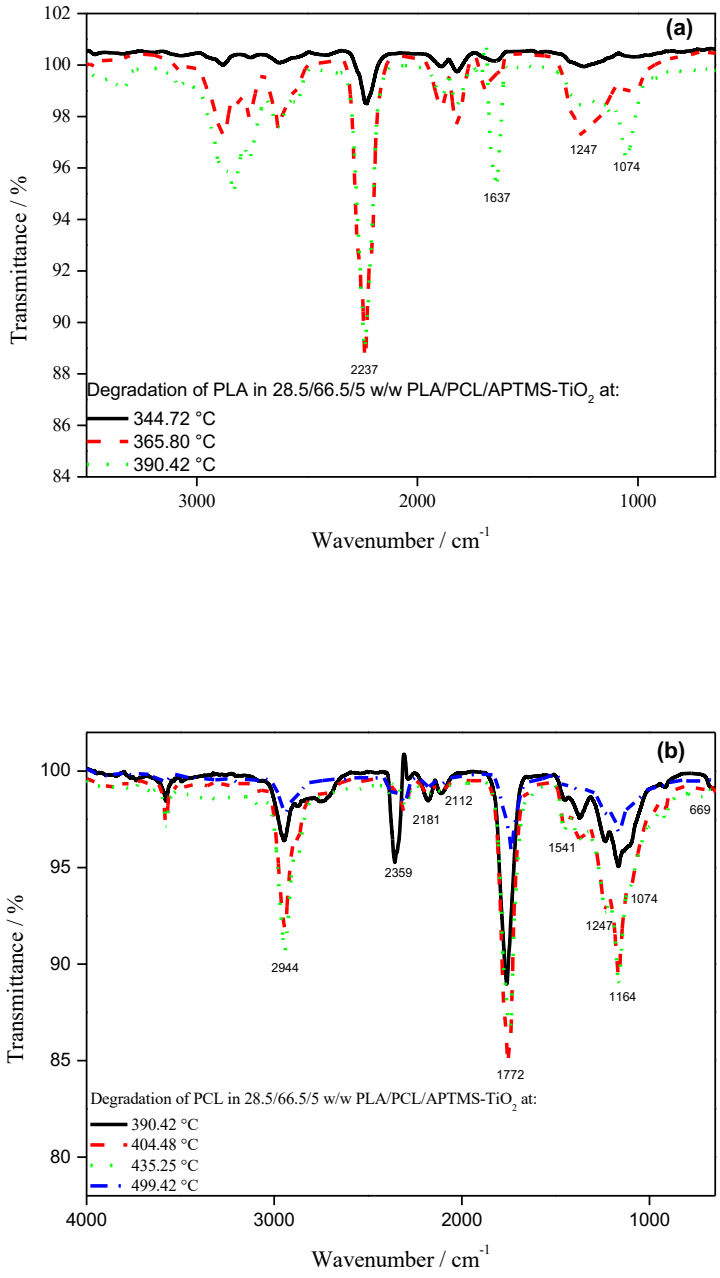

Figure A.15 FTIR spectra of degradation products of (a) PLA and (b) PCL in 28.5/66.5/5 w/w PLA/PCL/APTMS-TiO_2